PhD Thesis

Acute respiratory and skeletal muscle wasting in critical illness

Sunil Patel

CID: 00988900

Section of Anaesthetics, Pain Medicine and Intensive Care

Department of Surgery and Cancer

Imperial College London

Submitted for the degree of PhD – 3rd July 2023

Final submission – 14th December 2023

Supervisors: **Dr Brijesh Patel, Prof. Suveer Singh, Prof. Masao Takata**

Contents

Statement of originality *1*

Copyright declaration *1*

Acknowledgements *2*

Abstract *5*

List of figures *7*

List of tables *12*

Abbreviations *14*

Chapter 1: Introduction *17*

1.1 Intensive care: a resource in demand **17**

1.2 Surviving critical illness **18**

1.3 Intensive care unit acquired weakness: a difficult diagnosis **19**

1.3.1 Gold standard diagnostics for ICUAW 20

1.3.2 Electrophysiological assessment in ICUAW 21

1.4 Skeletal and respiratory muscle in health **22**

1.4.1 Basic skeletal muscle structure and molecular function 22

1.4.2 Peripheral skeletal muscle 23

1.4.3 Respiratory muscles 24

1.4.3.1 The diaphragm 24

1.4.3.2 Intercostal muscles 25

1.5 Muscle wasting during critical illness **25**

1.5.1 Clinical risk factors for critical illness associated muscle wasting 26

1.5.2 Neuromuscular blockade 26
1.5.3 Sedation 27
1.5.4 Steroid administration 28
1.5.5 Immobility 28
1.5.6 COVID19 and muscle wasting 29
1.6 Impact of mechanical ventilation on respiratory muscle 31
1.7 Peripheral versus respiratory muscle wasting in critical illness 32
1.8 Quantifying muscle wasting in critical illness 33
1.8.1 Ultrasonography 33
1.8.1.1 Musculoskeletal ultrasound in the ICU – the challenges 34
1.8.1.2 Echogenicity in musculoskeletal ultrasound 35
1.8.1.3 Parasternal muscle ultrasound – a muscle with promise? 36
1.8.2 Muscle strain in critical illness 36
1.8.3 Computed tomography imaging 38
1.9 Inflammation and critical illness 39
1.9.1 Inflammation in critical illness associated muscle wasting 41
1.9.2 TNF-α induced skeletal muscle wasting 41
1.10 Critical illness associated myonecrosis 42
1.10.1 Programmed necrosis – necroptosis 44
1.10.1.1 TNFα induced necroptosis 44
1.10.1.2 Necroptosis activation and necro-inflammation 45
1.10.1.3 Biomarkers of necroptosis 46
1.11 Summary, aims and hypotheses 48
Chapter 2: Methods 49
2.1 Clinical studies 49
2.1.1 MUSCLE-ICU study 50

2.1.1.1 Screening and preparation of CT images 51
2.1.1.2 Skeletal muscle groups in L3 axial sections 52
2.1.1.3 Tissue density recognition and quantification 53
2.1.1.4 Reliability study of body composition analysis 54
2.1.2 WAVE and DeVENT studies 55
2.1.2.1 Disruption to patient recruitment in prospective trials 55
2.2 Clinical procedures 55
2.2.1 Venepuncture and blood processing 56
2.2.2 Respiratory and skeletal muscle ultrasound 57
2.2.2.1 Diaphragm ultrasound 58
2.2.2.2 Parasternal muscle ultrasound 60
2.2.2.3 Parasternal muscle strain 61
2.2.2.4 Rectus femoris muscle ultrasound 64
2.2.2.5 Echogenicity analysis 65
2.2.2.6 Musculoskeletal ultrasound training and competency 68
2.2.2.7 Ultrasound reproducibility and reliability studies 68
2.2.3 Defining significant changes in muscle mass 69
2.3 Molecular techniques 69
2.3.1 Enzyme-linked immunosorbent assays (ELISA) 69
2.3.1.1 Multiplex ELISA assay system 69
2.4 MUSCLE-UK study samples 71
2.4.1 MUSCLE-UK serum 72
2.4.2 Human skeletal muscle experiments 72
2.4.2.1 Protein extraction from human skeletal muscle 72
2.4.2.2 Protein quantification in human skeletal muscle 73
2.4.3 Western blotting 74
2.4.3.1 Western blotting controls 77
2.4.4 Immunohistochemistry of human skeletal muscle 77

2.4.4.1 Preparing tissue sections of human skeletal muscle 77
2.4.4.2 Fluorescence microscopy 78
2.4.4.3 Widefield microscopy 79
2.4.4.4 Confocal microscopy 80
2.5 Data handling 80
2.6 Statistical analysis 80
Chapter 3: Assessment of skeletal muscle wasting in critical illness using computed tomography imaging 82
3.1 Background 82
3.1.1 The Coronavirus Disease 2019 pandemic 84
3.2 Aims 85
3.3 Hypotheses 85
3.4 Methods 85
3.4.1 MUSCLE-ICU Study 85
3.4.2 Computed tomography image acquisition 86
3.4.3 Software selection and image analysis 86
3.4.4 CT assessed skeletal muscle wasting – a pilot study 87
3.5 Statistical analysis 88
3.6 Results 89
3.6.1 Skeletal muscle wasting pilot study cohort 89
3.6.1.1 High intra- and inter-observer reliability achieved using ImageJ CT muscle analysis 89
3.6.2 Investigating inter-software variability in CT imaging muscle analysis 91
3.6.3 MUSCLE-ICU Study 95
3.6.4 Clinical characteristics of critically ill patients with low muscle mass 96
3.6.5 Baseline skeletal muscle bulk and quality are only weakly correlated 99

3.6.6 Muscle bulk and quality decline continuously in severe ARDS 100
3.6.6.1 Low muscle states are common in patients with severe ARDS 101
3.6.7 Skeletal muscle density and pre-ICU length of stay are associated with ICU mortality 102
3.6.8 Factors predicting longitudinal change in skeletal muscle mass 104
3.6.9 Clinical characteristics in COVID19 ARDS 107
3.6.9.1 COVID19 ARDS patients had a longer time to first CT study 109
3.6.10 Skeletal muscle bulk, but not quality was lower in COVID19 ARDS patients 109
3.6.11 Acute skeletal muscle wasting is higher in patients with COVID19 111
3.6.11.1 ICU mortality is similar in COVID19 and non-COVID19 patients 112
3.6.12 Inflammation in COVID19 associated muscle wasting 113

3.7 Discussion 114

Chapter 4: Longitudinal evaluation of skeletal and respiratory muscle wasting in critical illness using ultrasound 119

4.1 Background 119

4.2 Aims 120

4.3 Hypotheses 121

4.4 Methods 121

4.4.1 Study cohorts 121
4.4.2 Quantitative measurements of skeletal and respiratory muscle 121
4.4.3 Reproducibility study protocol 122
4.4.4 Statistical analysis 123

4.5 Results 124

4.5.1 Reliability and reproducibility study 124
4.5.1.1 Intra- and inter-observer agreement 129
4.5.2 Protocol amendments for main clinical study 131
4.5.3 Clinical study cohort 131

4.5.4 Number of suitable imaging studies 133
4.5.4.1 Peripheral skeletal muscle wasting occurred acutely and continuously 134
4.5.4.2 Parasternal muscle cross-sectional area and end-inspiratory thickness 135
4.5.4.3 Diaphragm end-expiratory thickness 138
4.5.5 Peripheral versus respiratory muscle wasting 139
4.5.6 Diaphragm and parasternal muscle changes 141
4.5.7 Defining high and low muscle wasting groups 142
4.5.7.1 Associations with rate of muscle wasting 143
4.5.8 Clinical associations and risk factors for muscle wasting 145
4.5.8.1 Differences in muscle wasting patterns by admission diagnosis 145
4.5.8.2 Muscle wasting in COVID19 ARDS 146
4.5.9 Echogenicity and muscle mass 147
4.5.10 Inflammation in acute muscle wasting 149
4.5.11 Predicting muscle wasting status 153
4.5.11.1 Pro-inflammatory cytokine profiles in acute muscle wasting 154
4.5.11.2 Programmed necrosis signals in critical illness associated muscle wasting 162

4.6 Discussion 162

Chapter 5: Non-invasive assessment of parasternal muscle in critical illness 169

5.1 Background 169

5.2 Chapter contributions 171

5.3 Aims 172

5.4 Hypotheses 172

5.5 Methods 172

5.5.1 Additional study cohort data 172
5.5.2 Clinical data 173
5.5.3 Ultrasonography of parasternal, diaphragm and rectus femoris muscle 173

5.5.4 Parasternal function measurements 174
5.5.5 Rectus femoris and diaphragm ultrasound 174
5.5.6 Statistical analysis 174
5.6 Results 175
5.6.1 Study cohort 175
5.6.2 Baseline parasternal muscle mass measurement 177
5.6.2.1 Longitudinal variation in PSM thickness and cross-sectional area measurement 179
5.6.3 Parasternal muscle activity studies 181
5.6.4 Parasternal muscle strain measurement reliability 182
5.6.5 Parasternal muscle strain in critical illness 183
5.6.6 Parasternal muscle characteristics by admission aetiology 183
5.6.7 Parasternal muscle strain changes during ICU admission 184
5.6.8 Change in parasternal muscle activity during different ventilation modes 185
5.6.9 Changes in parasternal muscle activity and parasternal muscle atrophy 187
5.6.10 Parasternal muscle strain and ventilation 188
5.6.10.1 Determinants of change in parasternal muscle thickness 188
5.6.11 Changes in parasternal muscle mass compared to other muscle groups 189
5.6.11.1 Changes in parasternal and rectus femoris muscle 189
5.6.11.2 Changes in parasternal and diaphragm muscle 190
5.6.12 Impact of ventilation on parasternal muscle contractile activity 192
5.6.12.1 Ultra-protective ventilation and effect on parasternal and other muscle groups 193
5.7 Discussion 195
Chapter 6: Programmed necrosis in critical illness associated muscle wasting 203
6.1 Background 203
6.2 Aims 204
6.3 Hypotheses 204

6.4 Methods 205

6.4.1 Sample acquisition 205

6.4.2 Defining myonecrosis 205

6.4.3 Systemic markers of inflammation and necrosis 206

6.4.4 Quantitative and qualitative measurement of necroptosis machinery 206

6.4.4.1 pMLKL protein quantification 207

6.4.4.2 pMLKL confirmation with immunohistochemistry 207

6.5 Statistical analyses 207

6.6 Results 208

6.6.1 Clinical cohort 208

6.6.2 Prevalence of pMLKL in skeletal muscle during critical illness 211

6.6.3 Protein expression of pMLKL is upregulated in necrotic tissue 214

6.6.4 Programmed necrosis immunohistochemistry of healthy skeletal muscle 218

6.6.4.1 Absence of pMLKL in non-necrotic skeletal muscle during critical illness 219

6.6.5 Upregulation of pMLKL in necrotic skeletal muscle during critical illness 221

6.6.5.1 Distribution of pMLKL in necrotic muscle 223

6.6.5.2 Translocation of pMLKL during critical illness 227

6.6.5.3 RIPK3 co-localises with pMLKL in necrotic muscle 227

6.6.6 Systemic inflammation as predictors of myonecrosis 228

6.6.6.1 Serum cytokines do not reliably predict underlying myonecrosis 229

6.6.7 Intramuscular inflammatory mediators do not differentiate underlying myonecrosis 231

6.6.7.1 Systemic markers of necrosis do not differentiate patients with myonecrosis 233

6.7 Discussion 235

Chapter 7: Discussion 242

7.1 Overview 242

7.2 Summary of main findings 243

7.3 Limitations 247

7.4 Future work and direction 248

7.4.1 Formalising methodology of musculoskeletal ultrasound in the ICU 248

7.4.2 Developing parasternal strain protocol and clinical application 248

7.4.3 Long-term effect of PSM atrophy on physical function 249

7.4.4 Confirming activation of programmed myonecrosis 249

7.4.5 Developing in-vitro models of programmed necrosis in human skeletal muscle 250

Chapter 8: References 251

Chapter 9: Appendix 265

Appendix 9-1. Permission to use MUSCLE-UK samples in thesis 265

Appendix 9-2. Raw data from musculoskeletal ultrasound reliability studies 266

Appendix 9-3. Ultrasonographic changes in respiratory and skeletal muscle 270

Appendix 9-4. Systemic inflammatory mediators in high and low wasting patients 271

Appendix 9-5. Systemic inflammatory mediators in ARDS and non-ARDS patients 272

Appendix 9-6. Systemic inflammatory mediators in COVID19 and non-COVID19 patients 273

Appendix 9-7. Linear mixed effects models of parasternal muscle thickness 274

Appendix 9-8. Linear mixed effects models of parasternal contractile activity 275

Appendix 9-9. Linear mixed effects models of diaphragm end-expiratory thickness 276

Appendix 9-10. Linear mixed effects modelling: PSM thickness over ICU admission 277

Appendix 9-11. PSM thickness over ICU admission and effect of PSM thickening fraction 278

Appendix 9-12. PSM thickness over ICU admission and effect of PSM strain 279

Appendix 9-13. Parasternal muscle thickness and rectus femoris cross-sectional area 280

Appendix 9-14. PSM thickness and association with diaphragm thickness over ICU admission 281

Appendix 9-15. Diaphragm thickening fraction over ICU admission 282

Appendix 9-16. Diaphragm thickness and association with diaphragm thickening fraction..... 283

Appendix 9-17. PSM thickness and association with diaphragm thickening fraction..... 284

Appendix 9-18. Diaphragm thickness and association with PSM strain and thickening fraction285

Appendix 9-19. Parasternal muscle thickening fraction and strain and ventilation strategy..... 286

Appendix 9-20. Effect of vvECMO on parasternal, diaphragm, and rectus femoris muscle 287

Appendix 9-21. Original Western blots from MUSCLE-UK skeletal muscle protein 288

Appendix 9-22. Acquiring healthy human skeletal muscle biopsies 290

Appendix 9-23. Immunohistochemistry of health human skeletal muscle 291

Appendix 9-24. Serum concentration of inflammatory cytokines and circulating markers of necrosis in necrotic and non-necrotic patients 292

Appendix 9-25. Intramuscular concentration of inflammatory cytokines in necrotic and non-necrotic patients 293

Appendix 9-26. Parasternal muscle strain reliability study 294

Appendix 9-27. Clinical and ultrasound data from RWH study..... 295

Statement of originality

I declare that the work presented in this thesis is my own. Any data that has been acquired from other sources has been appropriately referenced. Collaborative projects with other research groups are also clearly referenced and contributions from individuals are cleared stated.

Copyright declaration

The copyright of this thesis rests with the author. Unless otherwise indicated, its contents are licensed under a Creative Commons Attribution-Non Commercial 4.0 International Licence (CC BY-NC). Under this licence, you may copy and redistribute the material in any medium or format. You may also create and distribute modified versions of the work. This is on the condition that: you credit the author and do not use it, or any derivative works, for a commercial purpose. When reusing or sharing this work, ensure you make the licence terms clear to others by naming the licence and linking to the licence text. Where a work has been adapted, you should indicate that the work has been changed and describe those changes. Please seek permission from the copyright holder for uses of this work that are not included in this licence or permitted under UK Copyright Law.

Acknowledgements

This work would not have been possible without the support of so many influential and understanding people.

Firstly, to my wife Anisha, who is always by my side and understanding of the challenges I faced and often brought home. She never complained or questioned me and was always a shoulder to lean on. Without her, none of this would have been possible. To my wonderful children, Ria and Rowan, who kept me smiling and grounded. They were my escape from the stresses of research when it was needed. Thanks to my mum and brother for eternal support and encouragement in everything I do.

To my supervisor, Dr Brijesh Patel, an ever-present beacon of support, knowledge and understanding. Thank you for giving me the autonomy to develop myself and my research ideas as well as steering me back to reality! I have always said that without Brij as my supervisor, I am certain I would have ventured away from formal research. His drive and enthusiasm were always there even in challenging times of the pandemic. He is not only my academic supervisor but a great friend. Thank you also to Professors Suveer Singh and Masao Takata for their invaluable experience and direction in delivering critical care research.

Thank you to the division of anaesthetics, pain medicine and intensive care at Chelsea and Westminster Hospital for welcoming me to the group with a new direction of research and to everyone who passed through the department between 2018 and 2021 and helped develop my laboratory skills. Special thanks to Dr Sharon Mumby for providing desk space(!) as well as endless lab, logistic and planning advice for multiple aspects of my research.

To my ‘research brother’, Rhodri Handslip, who was there for support, advice and most importantly lunch! Thanks for the dry research banter to make the day fun but above all, thanks for being a friend. Thanks to Dr Danielle Bear and Dr Rebecca D’Cruz for providing 24/7 moral support. Their own research experiences and challenges provided a much need forum. Thanks for your honesty and opinions to address day to day challenges but above all thank you for the frequent meetups and absorbing my frustrations!

Conducting clinical research is always challenging but the expert support from The Royal Brompton research team was immense. Thanks to all team members for putting up with my countless spreadsheets and requests for sample and data collection.

Research has taught me the importance of team working and collaboration. Thanks to Dr Zudin Puthucheary not only for providing his expertise, but also on-demand advice and support in a challenging area of critical care research. Thank you to Professor Steve Harridge for inviting me to his research group and providing laboratory space for exciting collaborative work. Notable thanks to Dr Thomas Francis for his countless hours of enthusiasm and microscopy expertise. I like to think I triggered an interest in critical illness research! Thanks to Professor Sam Orde for collaborating on an international scale and pushing forward concepts of muscle strain in critical illness.

Finally, none of this research would have been possible without the patients on the ICU. Thank you to every one of you, and your families who endured a time of sadness and hardship but were always open and understanding of clinical research opportunities.

For Anisha, Ria and Rowan

Abstract

Acute skeletal muscle wasting in critical illness is common and contributes to ICU acquired weakness, which negatively impacts quality of life in survivors. There is no gold-standard for describing muscle wasting and longitudinal descriptions in multiple muscle groups are lacking. Understanding the pathophysiology of myonecrosis, a common histological description during critical illness, also requires exploration.

At ICU admission, 27% of ICU patients had a low muscle mass state and lost 10% of muscle bulk on a second CT study (12 days (IQR 6-19). Furthermore, muscle quality significantly declined in parallel and was associated with underlying inflammation. Prospective assessment of peripheral and respiratory muscle in the first 14 days of critical illness showed significant loss in diaphragm, parasternal and rectus femoris muscle bulk as early as day 3. Severity of wasting between respiratory and non-respiratory muscle was not significantly different. Severe COVID-19 infection did not significantly affect the extent of wasting, High rates of wasting were associated with inflammation, but distinct phenotypes were not identified on cytokine analysis. Non-invasive assessment of parasternal muscle strain was reliable and reproducible and longitudinal modelling showed association with mechanical ventilation strategy and increased muscle atrophy.

Protein and immunohistochemical analysis of necrotic skeletal muscle showed an upregulation of pMLKL, and co-localisation and translocation with RIPK3 at day 7-10 – providing the first description of necroptosis activation in skeletal muscle during critical illness.

Ultrasound reliably described longitudinal quantitative and qualitative changes in skeletal muscle. When compared to CT imaging, the extent of loss in peripheral and respiratory muscle was similar. Muscle atrophy in COVID-19 patients was not significantly different to other aetiologies of ARDS.

Parasternal muscle strain assessment may serve as a useful non-invasive measure of respiratory muscle loading. Finally, the evidence to support activation of programmed necrosis warrant further investigation.

List of figures

Figure 2-1. Skeletal muscle groups at the L3 vertebral level 53

Figure 2-2. Hounsfield unit densities of tissue at the L3 vertebral level 54

Figure 2-3. Surface anatomy of respiratory and peripheral skeletal muscle ultrasound 58

Figure 2-4. B-mode ultrasound of the diaphragm 59

Figure 2-5. M-mode ultrasound of the diaphragm 60

Figure 2-6. B-mode ultrasound of parasternal muscle 61

Figure 2-7. Parasternal muscle strain analysis 63

Figure 2-8. Rectus femoris ultrasound 65

Figure 2-9. Parasternal muscle echogenicity analysis 67

Figure 2-10. Correlation and reliability between methods for echogenicity calculation 67

Figure 2-11. Principle and mechanism of the Meso-Scale Discovery® multiplex assay system. 71

Figure 2-12. Human skeletal muscle samples for homogenisation and protein extraction 73

Figure 2-13. Relationship between skeletal muscle mass and protein concentration 73

Figure 2-14. Protein loading for target protein detection in skeletal muscle homogenate 76

Figure 2-15. Western blotting controls 77

Figure 3-1. Muscle quantification using CT imaging and ImageJ software 87

Figure 3-2. Intra and inter-rater correlation and reliability for skeletal muscle cross-sectional area using ImageJ 90

Figure 3-3. Intra and inter-rater correlation and reliability for skeletal muscle cross-sectional area using ImageJ in MUSCLE-ICU patients 92

Figure 3-4. Bland-Altman and correlation plots of skeletal muscle cross-sectional area data using sliceOmatic in MUSCLE-ICU patients. 93

Figure 3-5. Bland-Altman and correlation plots comparing skeletal muscle cross-sectional area data using ImageJ and sliceOmatic. 94

Figure 3-6. Consort diagram for the MUSCLE-ICU study 96
Figure 3-7. Correlation between admission skeletal muscle index and density 99
Figure 3-8. Correlation between patient demographics and skeletal muscle index and density 100
Figure 3-9. Longitudinal changes in skeletal muscle during critical illness 101
Figure 3-10. Change in incidence of low muscle state during critical illness 102
Figure 3-11. L3 level muscle data in patients with COVID19 and non-COVID19 ARDS on admission to the ICU 110
Figure 3-12. Skeletal muscle cross-sectional area and density change in COVID19 and non-COVID19 patients 111
Figure 3-13. Kaplan-Meier plot for ICU survival at 60 days in COVID19 and non-COVID19 patients. 112
Figure 3-14. Daily C-reactive protein trend in COVID19 and non-COVID19 ARDS. 113
Figure 4-1. Bland-Altman plots for diaphragm measurements for healthy volunteers and ICU patients in ultrasound reliability study 125
Figure 4-2. Bland-Altman plots for parasternal muscle measurements for healthy volunteers and ICU patients in ultrasound reliability study 126
Figure 4-3. Bland-Altman plots for rectus femoris muscle measurements for healthy volunteers and ICU patients in ultrasound reliability study 127
Figure 4-4. Change in rectus femoris cross-sectional area during critical illness 134
Figure 4-5. Longitudinal changes in rectus femoris cross-sectional area during critical illness 135
Figure 4-6. Parasternal muscle ultrasound changes in critical illness 136
Figure 4-7. Change in parasternal muscle during critical illness 137
Figure 4-8. Diaphragm thickness assessment using ultrasound 138
Figure 4-9. Change in diaphragm thickness during critical illness 139
Figure 4-10. Longitudinal patient changes in respiratory and peripheral skeletal muscle 140
Figure 4-11. Comparison of changes in peripheral and respiratory muscle during critical illness 141
Figure 4-12. Comparison of respiratory muscle thickness and contraction 142

Figure 4-13. High- and low-waster groups by daily loss of rectus femoris cross-sectional area 143
Figure 4-14. High- and low-waster groups and clinical risk factors 144
Figure 4-15. Comparison of muscle mass changes by ARDS diagnosis status 145
Figure 4-16. Comparison of muscle changes in COVID19 and non-COVID19 critical illness 146
Figure 4-17. Change in muscle echogenicity during critical illness 148
Figure 4-18. Comparison of echogenicity changes and wasting status in rectus femoris and parasternal muscle 148
Figure 4-19. Relationship between change in muscle mass and echogenicity 149
Figure 4-20. C-reactive protein levels in patients with high and low daily rate of muscle wasting ... 150
Figure 4-21. Baseline CRP levels by admission diagnosis 151
Figure 4-22. Longitudinal trends in CRP levels during ICU admission. 151
Figure 4-23. Association between CRP levels over the first 7 days and change in respiratory and peripheral skeletal muscle bulk 152
Figure 4-24. Correlation between baseline pro-inflammatory mediators and extent of rectus femoris muscle atrophy 155
Figure 4-25. Correlation between baseline pro-inflammatory mediators and extent of parasternal muscle atrophy at day 3 156
Figure 4-26. Correlation between baseline pro-inflammatory mediators and extent of diaphragm muscle atrophy at day 3 157
Figure 4-27. Pro-inflammatory cytokine profiles for high and low muscle wasting status 159
Figure 4-28. Pro-inflammatory cytokine profiles in ARDS and non-ARDS critical illness 160
Figure 4-29. Pro-inflammatory cytokine profiles by in COVID19 and non-COVID19 critical illness ... 161
Figure 5-1. Consort diagram of parasternal muscle study 176
Figure 5-2. Baseline parasternal muscle measurements 178
Figure 5-3. Longitudinal changes in parasternal muscle during critical illness. 179
Figure 5-4. Longitudinal change in coefficient of variation of parasternal muscle measurements ... 180

Figure 5-5. Longitudinal changes in parasternal muscle thickness in critical illness 180

Figure 5-6. Effect of early mandatory ventilation on parasternal muscle..... 181

Figure 5-7. Bland-Altman plots of parasternal muscle strain measurements. 182

Figure 5-8. Change in parasternal muscle strain during critical illness. 184

Figure 5-9. Parasternal muscle activity during mechanical ventilation..... 186

Figure 5-10. Longitudinal change in parasternal muscle strain during mechanical ventilation 186

Figure 5-11. Parasternal muscle activity in critical illness 187

Figure 5-12. Parasternal muscle strain and observed effects on tidal volume 188

Figure 5-13. Changes in parasternal muscle thickness and rectus femoris cross-sectional area 190

Figure 5-14. Parallel changes in parasternal muscle and diaphragm 191

Figure 5-15. Changes in parasternal muscle and diaphragm activity..... 192

Figure 5-16. Longitudinal changes in parasternal, diaphragm and rectus femoris muscle during extracorporeal support 194

Figure 6-1. Consort diagram for inclusion of patients from MUSCLE-UK study 209

Figure 6-2. Prevalence of pMLKL in necrotic skeletal muscle during critical illness..... 212

Figure 6-3. Prevalence of pMLKL in non-necrotic skeletal muscle during critical illness 213

Figure 6-4. Expression of pMLKL in skeletal muscle of critically patients and healthy volunteers 214

Figure 6-5. Western blotting of non-necrotic and necrotic human skeletal muscle 215

Figure 6-6. pMLKL changes between T1 and T2 in NEC and NONEC groups..... 216

Figure 6-7. pMLKL expression compared to admission in non-necrotic and necrotic patients 217

Figure 6-8. pMLKL expression in non-necrotic human skeletal muscle using Western blotting..... 218

Figure 6-9. Immunohistochemistry of pMLKL expression in healthy human skeletal muscle 219

Figure 6-10. Immunohistochemistry of non-necrotic skeletal muscle 220

Figure 6-11. Spinning disc microscopy of non-necrotic skeletal muscle at day 7 221

Figure 6-12. pMLKL expression in necrotic human skeletal muscle during critical illness 222

Figure 6-13. Presence of pMLKL in human skeletal muscle during critical illness..... 223

Figure 6-14. Distribution of pMLKL within necrotic skeletal muscle 224

Figure 6-15. Multi-focal pMLKL in necrotic skeletal muscle 225

Figure 6-16. Distribution of pMLKL in necrotic skeletal muscle. 226

Figure 6-17. Wide field microscopy of necrotic human skeletal muscle during critical illness. 226

Figure 6-18. Translocation of pMLKL in human skeletal muscle during critical illness. 227

Figure 6-19. Co-localisation of RIPK3 and pMLKL in necrotic human skeletal muscle. 228

Figure 6-20. Baseline levels of systemic cytokines in non-necrotic and necrotic patients 229

Figure 6-21. Systemic inflammatory mediators in non-necrotic patients. 230

Figure 6-22. Systemic inflammatory mediators in necrotic patients. 231

Figure 6-23. Baseline levels of intramuscular cytokines in non-necrotic and necrotic patients 232

Figure 6-24. Intramuscular concentration of inflammatory cytokines in non-necrotic muscle. 232

Figure 6-25. Intramuscular concentration of inflammatory cytokines in necrotic muscle. 233

Figure 6-26. Systemic markers of necrosis in non-necrotic and necrotic patients 234

List of tables

Table 1-1. Intensive care unit admissions in the United Kingdom 18

Table 2-1. Summary of clinical studies in this thesis 49

Table 2-2. Inclusion and exclusion criteria for patients recruited in clinical studies 50

Table 2-3. Clinical, physiological and outcome data collection in MUSCLE-ICU study 51

Table 2-4. Time points for venesection and clinical ultrasound in WAVE and DeVENT studies 56

Table 2-5. Serum analytes used in the Meso-Scale Discovery® multiplex ELISA assay 70

Table 2-6. Materials and reagents used in Western blotting experiments 75

Table 2-7. Primary and secondary antibodies used in Western blot experiments 76

Table 2-8. Primary and secondary antibodies used in immunohistochemistry 78

Table 3-1. Admission and CT measurements of skeletal muscle pilot study cohort. 91

Table 3-2. Intra-class correlation coefficients for quantitative analysis using two software packages 94

Table 3-3. Patient cohort data in the MUSCLE-ICU study 98

Table 3-4. Univariate/multivariate logistic regression model of factors associated with ICU survival 104

Table 3-5. Univariate/multivariate linear regression model of factors associated with skeletal muscle change at follow-up CT imaging 106

Table 3-6. Patient characteristics and ICU admission detail in MUSCLE-ICU study 108

Table 3-7. Quantitative analysis of skeletal muscle in COVID19 and non-COVID19 patients on admission to the ICU 110

Table 4-1. Basic baseline demographics of ICU patients in the ultrasound reliability study 124

Table 4-2. Clinical details for ICU patients included in reliability study 128

Table 4-3. Intra- and inter-observer agreement in respiratory and peripheral skeletal muscle ultrasound in healthy volunteers and ICU patients 130

Table 4-4. Patient demographics and clinical characteristics of patients recruited to prospective clinical studies 133
Table 4-5. Changes in parasternal muscle during critical illness 137
Table 4-6. Clinical characteristics of high- and low-wasting rate patients 144
Table 4-7. Longitudinal changes in echogenicity in rectus femoris and parasternal muscles 147
Table 4-8. Binomial logistic regression of muscle wasting status 154
Table 5-1. Cohort data of parasternal muscle study 177
Table 5-2. Clinical characteristics of patients included in parasternal muscle activity study 183
Table 6-1. Clinical characteristics of MUSCLE-UK study patients 210
Table 6-2. Clinical characteristics of MUSCLE-UK patients with serum and muscle tissue 210
Table 6-3. Systemic markers of necrosis in non-necrotic and necrotic patients. 234

Abbreviations

ε	Strain
ΔEG	Change in echogenicity
ΔPSM_{EG}	Change in parasternal echogenicity
ΔRF_{EG}	Change in rectus femoris echogenicity
$\%\Delta PSM_{EG}$	Percentage change in parasternal echogenicity
$\%\Delta RF_{EG}$	Percentage change in rectus femoris echogenicity
6MWT	Six-minute walk test
ANOVA	Analysis of variance
APACHE II	Acute physiology and chronic health evaluation score
ARDS	Acute respiratory distress syndrome
AUC	Area under the curve
BMI	Body mass index
BSA	Bovine serum albumin
CCK-18	Cleaved cytokeratin 18
CI	Confidence interval
cIAP	Cellular inhibitors of apoptosis
CIM	Critical illness myopathy
CIN	Critical illness neuropathy
COV	Patient ID label for MUSCLE-ICU study with coronavirus 2019 disease
CoV	Coefficient of variation
COVID19	Coronavirus disease 2019
CPAx	Chelsea Critical Care Physical Assessment tool
CRP	C-reactive protein
CSA	Cross-sectional area
CT	Computed tomography
CT1	Computed tomography scan 1
CT2	Computed tomography scan 2
CT3	Computed tomography scan 3
CT3	Computed tomography scan 4
CT5	Computed tomography scan 5
DAMP	Damage associated molecular patterns
DAPI	4',6-Diamidino-2-Phenylindole, Dihydrochloride
DeVENT	Decision Support System to Evaluate VENTilation in ARDS
DIA	Diaphragm
DIA_{EXP}	Diaphragm end-expiratory thickness
DIA_{INSP}	Diaphragm end-inspiratory thickness
DIA_{TF}	Diaphragm thickening fraction
DICOM	Digital Imaging and Communications in Medicine
DISC	Death-initiating signalling complex
DMD	Duchenne's muscular dystrophy
DMD	Duchenne's muscular dystrophy
ECMO	Extracorporeal membrane oxygenation
EDTA	Ethylenediaminetetraacetic acid
EG	Echogenicity
EIM	External intercostal muscle
ELISA	Enzyme-linked immunosorbent assay
EMG	Electromyography
GCSF	Granulocyte colony stimulating factor
H&E	Haemotoxylin and eosin
HU	Hounsfield units
HV	Healthy volunteers
ICC	Intraclass correlation coefficient
ICM	Intercostal muscle
ICS	Intercostal space

ICU	Intensive care unit
ICUAW	Intensive care unit acquired weakness
IFNγ	Interferon gamma
IIM	Internal intercostal muscle
IL-1β	Interleukin-1 beta
IL-10	Interleukin-10
IL-2	Interleukin-2
IL-6	Interleukin-6
IL-8	Interleukin-8
IMAT	Intramuscular adipose tissue
IQR	Inter-quartile range
L3-SkM_{CSA}	3rd lumbar vertebral level skeletal muscle cross-sectional area
L3-SkM_{SMD}	3rd lumbar vertebral level skeletal muscle density
LBM	Lean body mass
MAND	Mandatory mode of mechanical ventilation
MAPK	Mitogen-activated protein kinase
MCP-1	Monocyte chemoattractant protein 1
MLKL	Mixed lineage kinase domain like pseudokinase
MRC	Medical Research Council
mSv	Milli-Sievert
MUSCLE-ICU	Acute muscle wasting in the ICU
MV	Mechanical ventilation
NCOV	Patient ID label for MUSCLE-ICU study without coronavirus 2019 disease
NEC	Patients with histological evidence of necrosis
NMB	Neuromuscular blockade
NONEC	Patients without histological evidence of necrosis
OR	Odds ratio
PAMP	Pathogen associated molecular patterns
P_aO_2/F_iO_2	Ratio of partial pressure of oxygen in arterial blood to fractional of inspired oxygen
PBS	Phosphate buffered saline
PEEP	Positive end-expiratory pressure
PFA	Paraformaldehyde
pMLKL	Phosphorylated mixed lineage kinase domain like pseudokinase
PPV	Positive pressure ventilation
PRR	Pathogen recognition receptors
PSM	Parasternal muscle
PSM_{ε}	Parasternal muscle strain
PSM_{CSA}	Parasternal muscle cross-sectional area
PSM_{EG}	Parasternal muscle echogenicity
PSM_{EXP}	Parasternal muscle end-expiratory thickness
PSM_{INSP}	Parasternal muscle end-inspiratory thickness
PSM_{TF}	Parasternal muscle thickening fraction
RASS	Richmond agitation and sedation score
RF	Rectus femoris
RF_{CSA}	Rectus femoris cross-sectional area
RF_{EG}	Rectus femoris muscle echogenicity
RIPK1	Receptor-interacting serine/threonine-protein kinase 1
RIPK3	Receptor-interacting serine/threonine-protein kinase 3
ROI	Region of interest
Rpm	Revolutions per minute
RRT	Renal replacement therapy
SARF	Severe acute respiratory failure
SARS-COV2	Severe acute respiratory syndrome coronavirus 2
SAT	Subcutaneous adipose tissue
SBT	Spontaneous breathing trial
SkM	Skeletal muscle
SMD	Skeletal muscle density

SMI	Skeletal muscle index
SOFA	Sequential organ failure assessment
SPONT	Spontaneous mode of mechanical ventilation
SV	Self-ventilating
T1	Time point 1 (=ICU admission)
T2	Time point 2 (=day 7-10 of ICU admission)
TNFα	Tumour necrosis factor alpha
TRAF2	TNF receptor-associated factor 2
TRAIL	TNF-related apoptosis-inducing ligand
UK	United Kingdom
UPP	Ubiquitin proteasome pathway
VAT	Visceral adipose tissue
VEGF	Vascular endothelial growth factor
VIDD	Ventilator induced diaphragm dysfunction
vvECMO	Veno-venous extracorporeal membrane oxygenation
WAVE	Weaning Algorithm for Mechanical Ventilation
WAVE-RMU	Weaning Algorithm for Mechanical Ventilation Respiratory Muscle Ultrasound
WCC	White cell count

Chapter 1: Introduction

1.1 Intensive care: a resource in demand

Intensive care units (ICU) provide complex medical support and treatment for patients with severe illness, life-threatening injury or after routine/high-risk complex surgery.[1] This often involves invasive monitoring, multiple drug therapies and periods of prolonged immobilization compared to the individual's baseline. The number of admissions to the ICU in the United Kingdom (UK) is rising (Table 1-1).[2] In the 10 year period from 2008 to 2018, there was a 82% increase in UK ICU admissions (89,682 in 2008 vs. 163,340 in 2018)[3]. This is expected to continue owing to an ageing population, advances in treatment and utilisation of healthcare services. The latter has been crudely tested by the devastating and unprecedented impact of the COVID19 global pandemic which caused significant strain on critical care services across the world. The COVID19 pandemic has however highlighted the progression in modern day medicine through rapid development of the COVID19 vaccine and utilisation of existing therapeutics[4,5]. This builds on the development and application of novel treatments, as well as developing technology and strategies in delivering critical care. For example, the delivery of invasive mechanical ventilation in patients with acute respiratory distress syndrome (ARDS) that improve ICU outcomes (low tidal volume ventilation[6], use of neuromuscular blockade[7], prone positioning[8] and extra-corporeal membrane oxygenation (ECMO)[9] in the pre-pandemic era.

	2012	2017	2018	2019	COVID19**
Number of admissions	133,682	162,244	163,340	161,729	37,503
Age – years	61.1 (18.2)	60.7 (17.9)	60.5 (17.8)	60.6 (17.7)	58.9 (13.1)
Male – No. (%)	74,268 (55.6)	94,105 (55.5)	95,367 (55.7)	94,490 (56.0)	25,066 (66.0)
APACHE II score	##	15.3 (6.8)	15.2 (6.7)	15.2 (6.6)	14.8 (5.3)
Length of stay pre-ICU – days	##	0 (0-1)	0 (0-1)	0 (0-2)	1 (0-3)
ICU length of stay – days	2.2 (1.0-5.1)	2.5 (1.1-5.2)	2.4 (1.0-5.1)	2.6 (1.1-5.4)	10 (5-22)§
Total hospital length of stay – days	12 (6-26)	11 (5-22)	11 (5-22)	11 (5-22)	17 (9-32) §
ICU Mortality – No. (%)	20,342 (15.2)	22,407 (13.8)	21,325 (13.1)	22,525 (13.9)	14,269 (38.0)
Hospital mortality after ICU – No. (%)	28,248 (22.2)	31,588 (19.5)	30,195 (18.5)	31,673 (19.6)	10,872 (40.1)
Mechanically ventilated – No. (%)	54,902 (41.1)	60,664 (35.7)	60,252 (35.2)	60,593 (35.9)	13,845 (36.0)

Table 1-1. Intensive care unit admissions in the United Kingdom

Table constructed using data from ICNARC summary statistics *(available as open access at: https://www.icnarc.org/Our-Audit/Audits/Cmp/Reports/Summary-Statistics)*. Data from each year is from 1st April to the following 31st March unless otherwise specified. **COVID19 admissions only in the period 1st February 2020 to 1st July 2021. ## not reported, § data only available from 1st February 2020 to 31st August 2020.

1.2 Surviving critical illness

Despite modernisation and advancement of critical care services and resources, long term physical restriction and psychological morbidity in survivors of critical illness has been shown to persist for up to 5 years.[10,11] This was described in two landmark studies by Herridge *et al.,*[10,11] that looked at the adverse effects on physical function, mental wellbeing and quality of life in 109 survivors of critical illness secondary to ARDS at 1 and 5 years post ICU admission. They found that at 1 year, survivors self-reported physical restriction, or more specifically, muscle wasting and weakness as the cause to their limitation – objectively determined by a lower 6 minute walk test distance (6MWT) than predicted (achieving only a mean of 66% predicted distance at 1 year).[11] Muscle weakness was again highlighted as a cause for impairment in a separate study by Poulsen *et al.,* in a non-ARDS cohort at 1 year[12]. Finally, Herridge *et al.,* also found that only 49% of survivors returned to work at 1 year[10] (rising

to 77% at 5 years[11]) and utilised healthcare services more in the same period with muscle weakness described as an underlying factor.

Despite these striking statistics, current guidance concerning rehabilitation following critical care lacks an evidence base[13], and one such reason is likely due to the complex and poorly understood pathophysiology of critical care associated muscle weakness and ICU-acquired weakness (ICUAW). In fact, the guidance published by the National Institute of Health and Care Excellence acknowledges the lack of evidence and recommends research to focus on effective methods of identifying patients at risk of critical illness associated physical morbidity and methods of monitoring.[13] What is clear, is that muscle weakness, begins early in critical illness[14,15] and muscle mass declines (i.e. wastes, or atrophies) sharply within seven days and is associated with disease severity[14]. Muscle weakness has also been shown to be an independent predictor of mortality, associated with prolonged mechanical ventilation and hospital length of stay.[16,17] Therefore, there is a clear need to develop tools that help identify muscle wasting early so that intervention can be prompt and serve to prevent adverse sequelae both during critical illness and in the those that survive.

1.3 Intensive care unit acquired weakness: a difficult diagnosis

Intensive care unit acquired weakness (ICUAW) is common in critical illness and carries significant morbidity and mortality.[11,18,19] The prevalence of ICUAW varies, and this may be due to a heterogenous patient population in the ICU and multiple contributing risk factors[20]. A median incidence of 43% (IQR 25-75%) has been reported in a systematic review of 31 studies[21] which is in stark contrast to the proportion of patients with primary neuromuscular disorders (Guillain-Barre syndrome, moto-neurone disease, myasthenia gravis etc) admitted to the ICU.[22] Furthermore, there is no global consensus on when the diagnosis can be made and this affects timing of currently accepted assessments. ICUAW is a diagnosis of exclusion, caused by critical illness and its treatments, and conventionally confirmed following a combination of clinical examination, functional assessment and

neurophysiological testing.[23] There is no consistent presentation of ICUAW and it is often suspected when there is delayed recovery or failure to progress.

The observed weakness is a combination of neurogenic and myogenic pathway disruption, leading to critical illness neuropathy (CIN) and critical illness myopathy (CIM) respectively.[24] The clinical picture is often one of a symmetrical weakness. Myopathy tends adopt a flaccid, symmetrical pattern affecting the proximal muscle groups more so than the distal ones.[20] However, the clinical picture is complicated as there is often superimposed neuropathy. CIN tends to affect distal limbs more than proximal but also causes a flaccid, symmetrical weakness, with lower limbs more affected than upper limbs. Respiratory muscles are also affected acutely[15] and there is emerging evidence to suggest it occurs earlier than proximal limb weakness.[25] This may present as prolonged or difficult weaning from mechanical ventilation.[26,27] ICUAW is a well described syndrome in the literature but has multiple associated mechanisms.[19,20,28–30] The diagnosis is commonly made late as a significant proportion of patients are deeply sedated whilst receiving MV, therefore, the volitional components of assessment become redundant[31] and clinical suspicion dominates. What is clear from ICUAW is that muscle mass falls significantly across the ICU admission irrespective of when the baseline measurement was taken, but the greatest rate of change is seen in the first 7-10 days.[14,32–34] Multiple studies report that a 10% decline in muscle bulk over the first week of ICU admission, given by the rectus femoris cross-sectional area, can result in clinical weakness.[32,35,36]

1.3.1 Gold standard diagnostics for ICUAW

A diagnosis of ICUAW relies on a multi-modal approach and assessment. Early diagnosis is severely restricted as volitional tests assume patient compliance and participation – this requires not only motor function but neurological stability to understand specific instructions – pre-requisites that are rarely achieved in the early stages of critical illness due to deep sedation with or without neuromuscular blockade, severity of disease, physiological lability and commonly delirium. A simple

and widely adopted measure of motor function in ICUAW is the Medical Research Council (MRC) score[21] – an ordinal scaled score that measures motor function in six muscle groups and is often considered the gold standard of the bedside tests. It is however limited in cases of isolated limb injuries, indwelling devices etc. There is also a poor correlation with physical function after critical illness[37] however it is frequently incorporated into ICUAW diagnosis. The assessment scores muscle strength in a range of muscle groups in the upper and lower limb from 0 to 5. The summative score ranges from 0 to 60 and a score of <48 is suggestive of ICUAW. It should be noted that the non-linearity of the score means that differences between scores are not comparable. For example, the difference between a score of 1 and 2 is not the same as the difference between 3 and 4. Furthermore, there is of course inter-rater variation. Frequently coupled with MRC score is hand-held dynamometry. This measures handgrip strength against pre-set weights but is limited in its ability to make assumptions about global muscle strength and also has a significant floor effect.[38] A more recently derived scoring system is the Chelsea Critical Care Physical Assessment Tool (CPAx). CPAx is numerical score composed of 10 physical function domains which are individually graded from 0 to 5, thus giving a maximum total score of 50 (which represents full independence, and 0 equivalent to the most dependent). It has advantages over the aforementioned methods in that it incorporates respiratory function assessments in the form of ventilator dependence. CPAx has a limited floor and ceiling effect when assessed in validity studies.[39]

1.3.2 Electrophysiological assessment in ICUAW

Electrophysiology constitutes an important part of the ICUAW diagnosis and often confirms the clinical suspicion rather than disproving it. CIM is characterised by limb and respiratory muscle weakness with preservation of sensory function[40], which is quantified by the compound motor action potentials across different muscle groups of the limb.[40,41] Similarly, CIN is characterised by a symmetrical, distal sensory-motor axonal polyneuropathy of the sensory and autonomic nerves.[40,41] A reduction in sensory nerve actional potentials is often combined with abnormal, or reduced, nerve conduction.[19]

These diagnostic tools are very rarely performed in early critical illness. When they are utilised, the weakness is often established and failure to progress is often already present. There needs to be a focus on earlier recognition of weakness and contemporaneous assessment to identify those likely to develop ICUAW.

1.4 Skeletal and respiratory muscle in health

1.4.1 Basic skeletal muscle structure and molecular function

Human skeletal muscle accounts for approximately 40% of total body weight and has a hierarchal structure that enables coordinated contraction of muscle fibres and generation of variable force and movement.[42] Apart from locomotion, skeletal muscle is crucial in human metabolism and accounts for 50-75% of total body protein,[42] serving as a rich store of energy during exercise as well as during starvation where protein metabolism occurs to produce glucose. Thus, in times of extreme stress and illness, reduced skeletal muscle mass contributes to impaired recovery and host response.

Skeletal muscle architecture begins with arrangement of the basic structural unit - the myofibre (or muscle cell). These are variable sized, multi-nucleated cells are long (up to 100μm), cylindrical in shape and wrapped in connective tissue called the endomysium. At a cellular level, the plasma membrane of the myofibre is called the sarcolemma. It is here where satellite cells (the stem cell of skeletal muscle) are found. Satellite cells are vital in growth, repair and regeneration for the skeletal muscle.[43,44] Within each myofibre are myofibrils – thread like structures which serve as contractile elements of the muscle. Within these are the sarcomeres, which are the fundamental unit of contraction. Sarcomeres are composed of two main types of proteins – thick filament myosin and thin filament actin. A collection of myofibres form a fascicle, which are in turn surrounded by the perimysium for structural support and provision of blood and nerve supply. Whole muscle is formed from a collection of fascicles and is also encased by the epimysium for additional support and association with tendons.

Force generation and muscle movement is the product of a coordinated process consisting of neuromuscular signalling, excitation-contraction coupling and movement of the sarcomere filaments.[44] The sliding filament theory is the widely regarded molecular description of muscle contraction. Following a neuromuscular stimulus, calcium ion influx occurs in the sarcoplasmic reticulum which binds to troponin on actin. This leads to tropomyosin movement away from active binding sites on actin. Myosin binding sites are now exposed, and actin-myosin cross-bridge links are formed with increasing overlap leading to shortening of the sarcomere and the resultant forces are transmitted ailing the myofibre leading to contraction. When the stimulus is removed, calcium ions are actively transported back to the sarcoplasmic reticulum and covering of the binding sites by tropomyosin and inhibition of cross-bridge linking and restoration of sarcomere length. Adenosine triphosphate is the crucial energy to coordinate this contraction. Thus, in critical illness, during marked inflammatory states and organ dysfunction, exhaustion of energy stores may impair muscle activity early.

1.4.2 Peripheral skeletal muscle

There are multiple muscle groups in the upper and lower limbs as well as the torso, all of which have unique roles in stabilisation, resistance, weight bearing and load bearing. The quadriceps represent the largest muscle group in the lower limb and are frequently active in health as they are crucial in weight bearing, locomotion, and exercise. They form the anterior compartment of the thigh and are made up of *vastus medialis, vastus lateralis, vastus intermedius and rectus femoris*. The rectus femoris is superficially located, easily identified and its cross-sectional area is easily measured[45–47], making it a commonly studied muscle in critical illness, particularly when using ultrasonography. Evaluation of changes of quadriceps thickness in critical illness shows that the rate of change was greatest for rectus femoris compared to other quadriceps muscles in the first 3 days of ICU admission.[47] This may be due to the rectus femoris being involved in high-power movement requiring higher composition of type 2 muscle fibres which are more prone to fatigue than type 1 fibres.[47]

1.4.3 Respiratory muscles

Respiratory muscles are skeletal muscles that are involved in movement of the chest wall during the active process of inspiration – the net effect of which is to generate tidal volume and facilitate gas exchange.[48] The diaphragm is the principle respiratory muscle but there are several other muscle groups that support respiration, particularly during acute illness and physiological decompensation. These include sternocleidomastoid, scalene, pectoralis major, intercostals (internal and external) and the anterior abdominal muscles (rectus abdominus, external oblique, internal oblique, transversus abdominis).

1.4.3.1 The diaphragm

During normal spontaneous breathing, the right and left hemi-diaphragms contract and move inferiorly during the active process of inspiration. Neural innervation, specifically motor function, is served by the right and left phrenic nerve which arises from the ventral rami of the third, fourth and fifth cervical spine roots[49] and can be particularly susceptible to damage during cardiothoracic surgery.[50–52] When the diaphragm contracts, there is an outwards displacement of the anterior abdominal wall and an increase in intrathoracic volume through concurrent contraction of the external intercostal muscle and lifting of the ribs upwards and outwards. This creates a negative pressure gradient and allows inward air flow. Study of mechanical activity and movement of the diaphragm is facilitated by its attachment to the lateral chest wall and lower rib cage.[53,54] The point at which the diaphragm opposes the lower rib cage and chest wall is called *the zone of apposition*.[55,56] It is at this point most non-invasive ultrasonography is performed. Diaphragm muscle bulk and activity are the two most important quantitative measures. The former is often inferred by end-expiratory thickness at functional residual capacity and ranges from 1.8-3 mm (millimetres).[57] A thickness of less than 2 mm often used to define atrophy.[53] Diaphragmatic thickening fraction provides an indication of inspiratory capacity.[58]

1.4.3.2 Intercostal muscles

Two distinct muscle fibre layers comprise the intercostal muscles (ICM). The fibres of the outermost layer, the *external intercostal muscle (EIM)*, are obliquely positioned between the ribs and their fibres run infero-anteriorly, from the inferior border of the rib above to the superior border of the rib below. EIMs are active during inspiration and interact with the diaphragm and accessory muscles to support inspiration.[59] The inner muscle layer, the *internal intercostal muscles (IIM)*, are positioned ventrally and their fibres run in an opposite direction to the EIM – obliquely, but infero-posteriorly. As a result, lateral ICM has two layers composing the ICM and a single layer in the ventral aspect. The thickest portion of the sole ventrally positioned IIM are often referred to as the *parasternal intercostals*. The IIM are active during expiration. The role of PSM in respiration was investigated by De Troyer *et al.,* who undertook a complex physiological study utilising the concept mechanical advantage of the muscle, which was defined as the fractional change in muscle length per unit volume increase of the relaxed chest wall[60]. They used this concept to investigate changes in maximum airway pressure and the relationship to the PSM mechanical advantage. A notable finding during passive inflation was that there was PSM shortening in all intercostal spaces but the absolute decline reduced from the second to the fifth ICS.[59] They found a PSM mechanical advantage of 0.6-2.2% per litre and during maximum contraction a change in airway pressure in the region of 1-3 cmH_2O was achieved, therefore deduced that PSM has an inspiratory action on the lung.

1.5 Muscle wasting during critical illness

Muscle homeostasis is delicately balanced between complex catabolic and anabolic pathways[61–63], and atrophy ensues when there is a stimulus which perturbs this balance. Atrophy can be secondary to either specific disease (i.e. neuromuscular disease, chronic lung disease[64,65] or a consequence of an acute insult such as sepsis.[66] Muscle wasting was classically described in patients with cancer (and described as cancer-associated cachexia) and largely accepted as an inevitable consequence of progressive disease.[67,68] This also seems the unfortunate reality in severe critical illness where an

imbalance in protein homeostasis driven by increased catabolism[14] and compounded by other aspects such as delivery of adequate nutrition[69,70] and immobility (see below). Muscle atrophy leads to a reduction in lean body mass (LBM),[36] where losses can be as high as 1 kg LBM per day and predominantly occurring in the first week of admission to the ICU.[71,72] In those that survive their critical illness, an improvement in weight may be seen from a gain of fat mass rather than LBM[10] and this may be crucial in understanding why many patients require prolonged rehabilitation and continue to experience physical restriction in the period after critical illness.

1.5.1 Clinical risk factors for critical illness associated muscle wasting

Even after accounting for patient heterogeneity, varying disease aetiology and treatments in the ICU present additional causes for ICUAW and muscle wasting.[73,74] Some of the most important clinical risk factors for muscle wasting in ICUAW and are discussed in detail below.

1.5.2 Neuromuscular blockade

Neuromuscular blockade (NMB) and subsequent skeletal muscle paralysis is achieved by using non-depolarising (atracurium, rocuronium, vecuronium) and depolarising agents (succinylcholine). These agents bind to nicotinic receptors at the motor end plate. NMB facilitates endotracheal intubation but there is data supporting avoidance of prolonged in many critical care settings, for example in traumatic brain injury.[75] However, more recently, the early administration of NMB in patients with severe ARDS improved 90 day survival and was associated with increased ventilator-free days without increasing muscle weakness.[7] Furthermore, smaller studies have also shown a reduction in pro-inflammatory cytokines in BAL fluid following NMB administration in severe ARDS.[76] Despite, the lack of supporting literature, prolonged use of NMB in critical illness is common place in the context of mechanical ventilation dysynchrony, refractory respiratory failure and therapeutic hypothermia following cardiac arrest.[77] Most of the literature for NMB in critical illness is compiled from retrospective and observational studies, which in turn have heterogenous patient populations and thus concluding

causal relationship between NMB and muscle weakness is difficult. Puthucheary *et al.,* reviewed observation studies looking at NMB use and ICUAW. They reported that only 5 out of 16 studies found an association between NMB and ICUAW. In addition, the majority of studies include patients receiving concurrent corticosteroids, (particularly those with near-fatal asthma where steroid use is a mainstay of treatment[78,79]) which in itself is a predisposing factor for muscle weakness and atrophy. There is however more recent data to suggest that short-term use of NMB does not increase the incidence of ICUAW. Firstly, the use of NMB in severe ARDS was investigated by Papazian *et al.,*,[7] they showed that short-term use of cisatracurium was associated with a reduced 90 day mortality and no difference in ICUAW (NMB; 29% vs. no NMB 32%, p=0.49. Secondly, Forel *et al.,* had similar incidence of ICUAW after 48-hours of NMB administration or placebo.[76] In addition, most of the current literature arises from studies performed in the era before lung-protective ventilation strategies and ventilator modes that allow intermittent-mandatory breaths and more intuitive spontaneous modes of breathing which in turn avoid disuse atrophy and favour liberation from mechanical ventilation. Thus, previous causal relationships between NMB and ICUAW were likely to be heavily confounded by these factors.

1.5.3 Sedation

Sedation facilitates the delivery of mechanical ventilation, assists procedures as well as reducing pain and anxiety during critical illness. There is no universal approach to delivering sedation in the ICU and the subject area has been the focus of many randomised controlled trials involving more novel agents.[80–83] Of course, NMB cannot be administered without appropriate sedation and general anaesthesia. Thus, in this scenario, immobilisation may be prolonged or worsened. A pathophysiological consequence is an increase protein catabolism, decreased protein synthesis, loss of muscle mass and microvascular dysfunction.[84,85] For over 20 years, it has been known that formal, daily sedation holds leads to reduced MV duration and ICU length of stay, which in turn is likely to be associated with reduced incidence of ICUAW. Furthermore, Strom *et al.*, demonstrated that a 'no

sedation' strategy for patients receiving MV led to increase ventilator-free days when compared to those receiving propofol and midazolam.[86] These findings have not yet been reproduced.

1.5.4 Steroid administration

Corticosteroid-induced myopathy was first described in 1977 by MacFarlane and Rosenthal in a case of near-fatal asthma[87] and is also a frequently suspected cause of myopathy and atrophy in critical illness.[88] Corticosteroid administration is common and often indicated in a variety of conditions that are managed on the ICU. For example, in those with refractory septic shock[89], where steroid administration has been shown to reduce the duration of shock, reduce the duration of vasopressor use and reduce organ-failure days,[90] which in turn are all risk factors for muscle wasting. With respect to muscle, there is a degree of equipoise towards steroids and the relationship to CIM, some studies finding an independent association with neuromyopathy[31], and most others not.[91,92] Some would argue the use in the context of down-regulating inflammation associated with CIM[93] - a process commonly encountered in the ICU. On the other hand, steroid-induced hyperglycaemia poses an additional risk factor for the development of CIM and muscle atrophy.[72,94]

1.5.5 Immobility

Critical illness is often associated with immobility, more so, in the early phases where there is a reduction in active physical movement, dependence on passive rehabilitation which in turn is often compounded by the need for deep sedation to maintain physiological stability.[95–97] However, the impact of immobility on physiological stability and skeletal muscle architecture is well described [98] and muscle wasting is worse in the context of immobility and critical illness than in immobility alone.[99,100] This led to investigation of assistance technologies such as supine ergometry and artificial stimulation of skeletal muscle to improve muscle function and reduce the incidence of ICUAW and muscle wasting in the immobile, critically ill patient.[101–103] To-date, none of these interventions have led to a reduction

in ICUAW incidence and this highlights the need for earlier recognition of weakness in early critical illness.

1.5.6 COVID19 and muscle wasting

SARS-CoV2, causes Coronavirus Disease 2019 (COVID19), and led to a global pandemic in humans in 2020. The pandemic significantly increased healthcare utilisation across the world and notably raised the need and strained current resource for MV in critical care services. Between 1st February 2020 and 31st August 2020 there were 338,804 confirmed cases of COVID19[104] which contributed to a spike in ICU admissions in March-April 2020.[105] In the same period of 1st February 2020 and 31st August 2020, there were 10,953 admissions to ICU representing 3.2% of all documented cases.[105] Of these, 7668 (70%) were male and the median hospital stay was 1 day (IQR 0-3). COVID19 is pro-inflammatory, pro-thrombotic and commonly presents as severe acute respiratory failure.[106,107] Most notably 5,868 (54%) required MV due to severe COVID19 pneumonia/acute respiratory distress syndrome alone. Strikingly, 85% had at least moderate ARDS. Furthermore, 4240 (39%) died in the ICU and 4554 (42%) died whilst still hospitalised despite surviving ICU. Finally, the median ICU LoS was 10 days (IQR 5-22) and the median duration of MV was 13 days (IQR 7-23 days). Collectively, these data suggest that the negative sequelae of prolonged MV, specifically muscle wasting and weakness, is likely to be greater. This therefore raised the possibility of significant functional restriction in survivors of critical illness secondary to severe COVID19.

Pre-pandemic data demonstrates that severity of illness is associated with discharge outcomes of function, psychological state and quality of life, long after leaving the ICU. An epidemiological study of the UK COVID19 ICU data between 1st February 2020 and 31st August 2020 found that the acute physiology and chronic health evaluation score (APACHE II) score did not adequately reflect the acute severity of critically ill patients with COVID19 – as illustrated by lower P_aO_2/F_iO_2 ratios and higher than expected mortality.[108] There is currently no longitudinal data describing the onset, severity and

trajectory of muscle wasting in severe COVID19 infection. It is therefore important that the degree of muscle wasting is described as this may help support provision of healthcare services for patients requiring long-term support and likely to utilise such services for a prolonged period.

Follow-up studies of patients hospitalised with COVID19 in 2020 demonstrated 288/1077 (26%) patients were admitted for MV and/or higher organ support. Of the whole cohort, 92% had at least one persistent symptom of which muscle ache, physical slowing, limb weakness and breathlessness were four of the top ten responses[109]. This early data suggests that the impact of hospitalisation with COVID19 carries significant impact in those that survive, and thus further highlights the importance of early diagnostics to identify those at risk.

In severe COVID19 infection, high body mass index (BMI) of critically ill patients was commonly seen. This may render some imaging techniques such as ultrasound less sensitive to detect change. Thus, computed tomography (CT) imaging analysis may be preferred in oedematous or obese patients where available. There is a paucity of data describing muscle changes in severe COVID19. In a small Italian study, paraspinal muscle density at the level of T12 in 150 patients admitted to hospital with COVID19 was found to predict admission to the ICU. However, there was no longitudinal imaging data and this group used muscle density <30HU to define a low muscle mass state.[110] Aerde *et al.,* quantified the incidence of ICUAW using MRC-sum score (MRC<48 indicating ICUAW) in a single-centre retrospective observational study of critically ill patients with COVID19.[111] In their study, 486 patients were hospitalised (114 requiring ICU, of which 74 (65%) required MV, 11/174 ICU patients died). They found at the point of waking in the ICU, ICUAW was present in 72% of patients, falling to 52% at ICU discharge and 27% at hospital discharge). They also found that those with clinical weakness had longer duration of MV and longer ICU stay. There was no quantification of muscle bulk alongside these data. A prospective study of 32 ICU patients in Brazil with severe COVID19 infection found that at day 10 of admission, rectus femoris cross-sectional area declined by 30% (95% CI -26% to -34%)

which was in turn associated with a reduction in handgrip strength (-22% (95% -4% to -40%). The muscle loss seen in this study exceeds that Puthucheary *et al.,* demonstrated in a general, non-COVID19 ICU population (-30% at day 10 vs. 17% at day 10) and may suggest a more severe trajectory of muscle loss in COVID19 patients. However, to-date there is a dearth of data to describe changes in muscle bulk and muscle quality in critically ill COVID19 patients.

1.6 Impact of mechanical ventilation on respiratory muscle

The diaphragm serves as the principle respiratory muscle, and in critical illness it is susceptible to wasting and subsequent weakness like other skeletal muscle, particularly during MV.[112] During mechanical ventilation, the mechanics of breathing are significantly altered. Positive-pressure ventilation (PPV) drives gas into the lungs targeting pre-defined pressures or volumes. Whilst acute MV support provides a state of lung rest and respiratory muscle unloading, excessive or prolonged support leads to muscle atrophy and proteolysis.[15,113] This ventilatory "over-assistance" can be as high as 50% of the time on MV[114] and may lead to ventilator-induced diaphragm dysfunction (VIDD) – defined as the loss of diaphragmatic force generating capacity associated with MV.[112] As VIDD is a diagnosis of exclusion, its incidence is probably underestimated.[115] On a molecular level, VIDD leads to myofibre atrophy, intracellular lipid accumulation and mitochondrial dysfunction.[15,116,117] With 36% of ICU admissions in 2017 receiving MV,[2] MV-associated sequelae, specifically VIDD, prolonged weaning and muscle weakness are likely to be common but underdiagnosed. It is reported that approximately 40% of the total time spent on MV is during the weaning process[118,119] and difficulties in complete separation are encountered in around 25%.[120] Thus, the recognition of diaphragm dysfunction is imperative as it is associated with prolonged MV and longer periods of weaning.[58,121] With respect to accessory muscles, changes during MV are poorly described. A recent study by Dres *et al.,* studied the relationship of diaphragmatic and parasternal muscle thickening fraction during a SBT showed that an inverse relationship between the two exists.[122] This agrees with established

findings that diaphragm dysfunction is partially compensated during critical illness via an increase in extra-diaphragmatic muscle activity.[123]

In health, the diaphragm is the principle respiratory muscle during the active process of inspiration. Expiration relies on elastic recoil of the respiratory muscle group. In critical illness, there is frequent disruption to the load of the respiratory muscle pump, with respiratory failure a common consequence. The diaphragm is often dysfunctional in severe acute illness[124,125] (i.e. in severe pneumonia, ARDS and during exacerbations of chronic lung disease). Initiation of MV aims to re-balance the respiratory muscle loading. The principle being to counterbalance excessive loading and prevention of atrophy through 'over-resting'. It is now well documented that respiratory muscle dysfunction occurs early and is associated with adverse outcomes such as increased function dependence at 6 months post ICU discharge and increased ICU mortality.[16,116] In this light, easily available, dynamic and repeatable methods of assessing respiratory muscle activity are lacking.

The acuity in diaphragmatic atrophy was described in Levine *et al.,* who described myofibre atrophy as early as 18 hours after MV initiation in brain-dead organ donors[15]. The cross-sectional area reduction was greater in these patients compared to those undergoing elective surgery for thoracic malignancy but requiring MV. In this landmark paper, there was also evidence to suggest that the pectoralis muscle groups, an accessory respiratory muscle, were less atrophic. Whether this is due to greater activity (rather than prolonged atrophy) of accessory respiratory muscles is unclear.

1.7 Peripheral versus respiratory muscle wasting in critical illness

Studies in chronic respiratory disease have also shown that loss of muscle mass through ultrasonographic assessment is related to loss of physical function and reduction in activity long-term.[64,126] There was an initial thought that peripheral muscle weakness observed in ICUAW and any subsequent or concurrent VIDD/diaphragm dysfunction was simply an extension of the same process.

However, studies have shown that diaphragm dysfunction may be more prevalent than limb weakness in patients undergoing active weaning from MV.[25] Dres *et al.,* found that in a general ICU cohort, the prevalence of diaphragmatic dysfunction, measured by tracheal twitch measurement, was twice as high as the prevalence of ICUAW.[25] Furthermore, the group reported a lower prevalence of ICUAW that was correlated with weaning failure but not with diaphragm dysfunction, suggesting that ventilator-induced effects mainly impact respiratory muscle.[15] However, the assessment of respiratory muscle utilised specialist invasive techniques and peripheral skeletal muscle weakness utilised only clinical assessment of strength. Those with ICUAW did however have a longer duration of MV and overall ICU length of stay. Whilst, underlying mechanisms were not studied, this clinical study raises the question that peripheral and respiratory muscle behave differently during MV and may lead to negative patient outcomes.

1.8 Quantifying muscle wasting in critical illness

1.8.1 Ultrasonography

Ultrasonography has become a corner stone of medical practice since the mid-20th century after Wild and Neal first described its application in characterising human tissues.[127] In modern medicine, the application of ultrasound has exploded with uses in most medical and surgical disciplines. It's use in muscle was first described in the 1980s by Heckmatt *et al.,*, who studied the thigh muscles of 10 paediatric patients with Duchenne's musculoskeletal dystrophy (DMD) and noticed ultrasonographic differences between DMD muscle and those of adult muscle controls.[128] As technology has vastly developed, ultrasound is now considered cheap, reproducible and non-invasive that can be used to assess both respiratory[129–131] and skeletal muscle.[126,132,133]

Skeletal muscle has distinctive features.[134,135] Healthy muscle is relatively anechoic, however, perimysial connective tissue within the muscle gives a 'speckled' appearance. When viewed in a longitudinal plane (along the long axis of the muscle), fascicular anatomy is visible and when viewed

in cross-sectional view, fascial planes are evident and help to differentiate individual muscles within groups. A notable example is of the quadriceps muscle group composed of the *rectus femoris, vastus intermedius, vastus lateralis and vastus medialis*. Using the example of the quadriceps, the femur represents a reliable structure to gauge depth and further differentiae the muscle groups. Subcutaneous fat also has low echo intensity but septae of the fat layer can mimic that seen within muscle if the operator is not familiar with the overall anatomy of the muscle in question.[136,137]

1.8.1.1 Musculoskeletal ultrasound in the ICU – the challenges

Respiratory muscle ultrasound has been extensively validated in healthy volunteers[54,56,138] and found to be highly reproducible in the setting of clinical studies within the ICU.[55,58,121,139]. Despite this, there is a lack of robust standards and evidence-based guidelines relating to the application of point of care ultrasound in critical illness associated muscle wasting despite numerous published studies utilising quantitative measurements as a primary outcome.[137,140] In this respect, there are a wide range of quantitative and qualitative data that can be acquired from musculoskeletal ultrasound in the ICU. For example, observational studies have reported a variety of muscle groups of the upper and lower limb, and within these changes in muscle thickness, cross-sectional area and echogenicity have been described.[46,47,141,142] The challenges and controversy arise from either technical and methodological factors or from patient factors. From a technical perspective, there are inconsistencies in the quality of reporting methods, and sometimes a complete lack of reporting, when ultrasound is used to assess muscle changes in the ICU. Therefore, universal application of technique is yet to be adopted (unlike in the use of echocardiography) and as such, comparing data between studies can be difficult. Experts in the field suggest transparency of training protocols, reliability testing (intra- and inter) and disclosure of measures taken to reduce inaccuracies.[35,137,143] In the ICU, there can be a variety of patient factors that can lead to inaccuracies in quantitative and qualitative measurement of muscle. Obesity is commonly encountered in the ICU, and fascial boundaries in these individuals may be difficult to delineate as they often require a greater depth of scan which leads to reduced resolution.

Furthermore, patients are often oedematous but there is a degree of equipoise as to whether this affects quality of image and quantitative measurements of muscle.[46,133] Muscle and fat are highly compressible, therefore, over application of pressure coupled with subcutaneous oedema can lead to distortion of the muscle structure and alter appearance thus reducing the overall quality of the image. Patient position (supine vs. semi-erect) and the presence of overlying various paraphernalia of critical illness (central venous catheters, extra-corporeal catheters, drains, dressings etc) may impact on whether repeated measurements can be taken in the identical location each time.

1.8.1.2 Echogenicity in musculoskeletal ultrasound

Echogenicity (EG) relates to the differential acoustic impedance of tissue with ultrasound.[144] Normal muscle will have a low EG due to the low fibrous and fat content of the tissue.[145] This radiological principle has been used to detect differences in muscle appearance across a range of ages, neuromuscular disorders[46,135,145,146] and in critical illness secondary to severe sepsis.[147] In critical illness, muscle EG has been found to be a marker of muscle quality and strongly associated to the presence of myofibre necrosis[133] and may offer a completely non-invasive tool to assess myonecrosis in critical illness alongside measurement of change in RF_{CSA}. A study by Puthucheary *et al.,* investigated the changes in muscle EG (ΔEG) in 30 critically ill patients between day 1 and day 10 of ICU admission. ΔEG was significantly associated with histologically confirmed muscle necrosis in the same patient and served as a good predictor for myonecrosis with an area under the curve (AUC) of 0.85. However, ΔEG was only between day 1 and day 10 and therefore the exact rate of decline is unknown. In addition, the study size was limited due to incomparable images between patients as the ultrasound images require identical settings for gain and depth. Finally, the group compared rectus femoris cross-sectional area with vastus lateralis muscle biopsies. Whilst this offers a pragmatic solution of studying the critically ill patient owing to minimal disruption in patient position and avoiding biopsy of muscle near large vascular structures (and creating avoidable risk), the muscles compared are two distinct

muscles within the quadriceps. Despite these limitations, echogenicity represents a useful analytical tool for the qualitative assessment of muscle.

1.8.1.3 Parasternal muscle ultrasound – a muscle with promise?

Normal respiratory mechanics of the thorax and particularly intercostal and parasternal muscles are well described.[131,148] Furthermore, accessory respiratory muscles such as the intercostals are often activated to a greater extent than the diaphragm in assisted ventilation.[149] However, it is only recently that the assessment of parasternal muscle activity in critical illness has developed as a potential tool in the assessment of breathing during MV and in weaning failure.[150,151] Respiratory muscle ultrasound has largely been dominated by study of the diaphragm and there is established literature relating to techniques.[139,152,153] Despite detailed literature on respiratory muscle mechanics and function,[48,59,60] there is a paucity of clinical studies concerning quantitative assessment of the parasternal muscles during critical illness. Yoshida *et al.,*, demonstrated in 12 healthy male volunteers that parasternal muscle thickness increased significantly during maximal inspiration when measured anteriorly, but not when measured laterally or posteriorly.[150] Nakanishi *et al.,*, then showed that excessive inspiratory pressure (incrementing pressure support) leads to parasternal muscle atrophy (ascertained by changes in muscle thickness) in the first 7 days of critical illness, and that changes in thickness are associated with longer ICU stay and duration of MV.[154] More recent studies have since showed that parasternal muscle ultrasound, specifically measurement of thickening fraction, may be able to identify those with high inspiratory efforts (indicated by high PSM thickening fraction) in the presence of underlying diaphragm dysfunction[155] and perhaps those who will fail a spontaneous breathing trial (SBT) during weaning attempts.[151,156]

1.8.2 Muscle strain in critical illness

In addition to assessment of muscle bulk, assessment of muscle strain (ε) can provide insights into respiratory muscle loading.[122,151,155] Strain is the fractional deformation experienced by a structure

when a force (or a stress) is applied, i.e. the relative movement of muscle fibres during contraction. The fundamental relationship between stress and strain in musculoskeletal physiology is dictated by the limits of stretch and elasticity of the muscle in question (Hooke's law: strain of a material is proportional to the applied stress within the elastic limit of the material). Low levels of muscle stress imply adequate muscle load (and therefore less strain) but conversely, high levels of stress lead to high strain and load imbalance on the myofibre. If the degree of stress exceeds a threshold, then there is a risk of contractile failure and dysfunction. Mathematically, stress (σ) = force/area. Therefore, when contractile force is kept constant, muscles with low cross-sectional area will experience greater levels of stress compared to larger ones. Muscle strain measurements have already been widely employed in the myocardium using echocardiography[157] but only in a small number of conceptual studies of the diaphragm,[158–160] and none involving PSM. EMG measures the sum of active motor units at the point of the electrode position and is not a direct measure of muscle strain.[161] In the context of mechanical ventilation, it is unclear how the institution of invasive ventilation affects parasternal muscle bulk and function.

To-date, non-invasive measurement of muscle activity, or more accurately described as contractility, has been confined to changes in thickness of muscle during inspiration and expiration. The concept of muscle strain has been widely utilised in myocardium and echocardiography.[162,163] Strain simply measures the deformational change in a structure and carries no unit of measure.[157] The technique utilises specific foci in the image called speckles that are generated from interaction of the ultrasound wave and the tissue. These speckles can then be tracked during a defined period (usually a respiratory cycle or cardiac cycle) and their displacement measured relative to a starting state (i.e. in end expiration). Quantitative strain measurements can then be used to accurately describe activity along a muscle structure. Thickening fraction and displacement measures are indirect[159] and do not assess the longitudinal muscle activity which corresponds to muscle fibre motion.

Currently, there are no validation studies of muscle strain in critically-ill patients although small pilot studies have been described to demonstrate utility in muscle with increasing load of upper limb muscles in healthy volunteers.[141,160] However, strain is likely to be effort and muscle dependent and thus normal ranges may not be required. There have been pilot studies in healthy volunteers to assess relationship between conventional measures of diaphragmatic thickening fraction and displacement with diaphragmatic strain.[158,159] However, there is a need to better understand small respiratory muscle activity in critical illness, specifically during mechanical ventilation, and to develop reliable, reproducible methods – of which strain calculation may serve as a measure of ventilatory loading.

1.8.3 Computed tomography imaging

Skeletal muscle quantification using computed tomography imaging provides an additional approach of quantifying and describing skeletal muscle changes in critical illness. It does have some unique advantages over musculoskeletal ultrasound. For example, cross-sectional area of deep lying skeletal muscle can be quantified in their entirety either using free-hand software tools and a region of interest (with minimal anatomical knowledge of muscle groups). Most notably, more advanced software packages allow tissue compartmentalisation for skeletal muscle and intra-muscular fat densities by applying well published Hounsfield units of density.[164,165] Hounsfield unit ranges of interest are: skeletal muscle (SkM) [-29 to +150], intra-muscular adipose tissue (IMAT) [-190 to -30], visceral adipose tissue (VAT) [-150 to -50] and subcutaneous adipose tissue (SAT) [-190 to -30][166,167]. CT imaging is considered the gold standard for the assessment of body composition in clinical studies. Furthermore, using a single CT slice of the abdomen, whole body muscle index can then be calculated to provide indices of low muscle mass states (i.e. sarcopenia).[168] This is particularly useful tool as low and high muscle mass states is poorly predicted from body mass index alone, and muscle index can vary amongst individuals with identical BMI.[169,170] In a critical care cohort, patients with low skeletal muscle index at admission have higher 6-month mortality and higher morbidity.[171,172] In addition, CT imaging of muscle also allows assessment of muscle quality through measurement of tissue density.

Higher density muscle (as indicated by a greater number of image pixels corresponding to skeletal muscle HU) is associated with a lower ICU mortality, duration of MV and duration of extracorporeal support in severe respiratory failure.[173,174] Studies utilising CT imaging in critically ill patients are largely confined to utilisation of an admission CT image to predict clinical outcomes[165,171,174] and in some cases, an initial CT image may not be available until days or weeks after the onset of critical illness. However, if early imaging and longitudinal studies are available then considerable amounts of quantitative data can be ascertained in critically ill patients.

Pragmatically, CT imaging carries risks associated with ionising radiation. To provide context, the ionising radiation associated with a single chest x-ray is in the region of 0.02mSv (milli-Sievert), in stark contrast, a CT study of the chest, abdomen and pelvis is equal to around 28mSv (or 1,400 chest x-rays).[175] Furthermore, CT imaging in the critically ill require logistical planning of moving critically ill patients to the imaging department, thus repeated prospective measurements are not always feasible. Conversely, repeated studies at multiple time points are more often feasible with ultrasound and allow intra- and inter-observer reliability to be assessed with ease.

1.9 Inflammation and critical illness

Inflammation is classically defined as a combination of redness *(rubor)*, warmth *(calor)*, pain *(dolor)* and swelling *(tumor)* by Celsus in 30 BC. Loss of function was later added to this description, and collectively this is still regarded as the definition. Inflammation is first and foremost a protective mechanism against pathogenic stimuli and endogenous signals, with the ultimate aim to eradicate said stimulus, clear cellular debris, repair tissue and restore function.[176] Inflammation begins when pattern-recognition receptors (PRRs) on the host cell interacts with specific sites on presenting pathogens (pathogen-associated molecular patterns, PAMPs), or from endogenously generated signalling (danger associated molecular patterns, DAMPs). Downstream effects of this interaction lead

to release of proinflammatory cytokines and signalling cascades. Ultimately, inflammation causes an imbalance in anabolic and catabolic processes, often impairing the former and favouring the latter.

There is no doubt that pro-inflammatory processes frequently occur in critical illness. However, the varying aetiology of disease, heterogenous patient population and initiation of mechanical ventilation may mean that multiple inflammatory cascades overlap and are activated concurrently.[177] Cytokines are ubiquitously expressed, small pleiotropic molecules (<40kDa) that regulate and influence the host immune response in health and disease. In health, their expression is low at the translational level,[178] and it is a pathological and/or noxious stimulus that triggers the cascade of events leading to upregulation of a plethora of pro-inflammatory mediators.

Characterising inflammation in critical illness can be difficult, and there is often variation in inflammatory 'phenotypes' amongst patients for the reasons eluded to above. For example, a large clinical study of 1,655 patients in two surgical ICUs, found that amongst those who died with infectious aetiology as the reason for admission had higher median admission levels of interleukin-2 (IL-2), interleukin-8 (IL-8), interleukin-10 (IL-10) and granulocyte colony stimulating factor (GCSF).[179] In contrast, amongst those who died from trauma had higher median admission levels of interleukin-4 (IL-4), IL-6, IL-8 and tumour necrosis factor α (TNFα). It is important to note that amongst those that died (from any aetiology), the APACHE II score was higher (21.8 vs. 15.4, $p<0.01$) and there was a greater prevalence of coronary artery disease, cerebrovascular disease and chronic renal impairment. A sepsis specific study by Mera *et al.*, , investigated a broad inflammatory cytokine panel in the first 7 days of ICU admission.[180] This group found higher levels of IL-8 and monocyte chemoattractant protein 1 (MCP-1) soon after admission in non-survivors, with the former most predictive of mortality. MCP-1 has a crucial role in migration and infiltration of monocytes and macrophages leading to marked pro-inflammatory response.[181] Furthermore, there was a persistent elevation of interleukin-1β (IL-1β), IL-6, IL-8, interleukin-12 (IL-12), interferon-γ (IFNγ), GCSF and TNFα in those that died. There is

therefore some suggestion that identification of soluble pro-inflammatory mediators in early critical illness may provide insight into outcomes on the ICU.

1.9.1 Inflammation in critical illness associated muscle wasting

Skeletal muscle is able to synthesise and release pro-inflammatory and anti-inflammatory cytokines to maintain homeostasis and in response to pathogenic stimuli.[182] Pro-inflammatory cytokines, have been implicated in skeletal muscle wasting in range of diseases[66,183,184] as well during mechanical ventilation[185]. TNF, IL-1β and IL-6 are commonly associated in human and animal models,[66,186,187] either through stimulation of downstream mediators of proteolysis or through further activation of cytokines. There is an extensive evidence base for these mediators as upstream stimuli for protein catabolism, commonly through activation of nuclear factor kappa-light-chain-enhancer of activated B cells (NF-κB). Furthermore, TNF-α triggers multiple cell death cascades independent of proteolytic pathways and may present novel mechanisms for the pathophysiology underlying muscle necrosis in critically ill patients. What is interesting is that direct blockade of TNF-α or IL-6 has not been shown to prevent significant muscle wasting, albeit in non-critical care cohorts[188,189]. This may suggest that despite elevated levels of pro-inflammatory cytokines, early activation of other distal pathways via these mediators may occur. For example, Lang and colleagues demonstrated that injection of a non-lethal dose of LPS in male rats induced expression of TNF-α, IL-1β and IL-6 as early as 1, 2 and 4 hours respectively.[183] However, circulating levels of these proinflammatory cytokines may not accurately reflect the events occurring at the muscle level[187] but may help identify those at risk. Thus, the study of TNF-α, IL-1β, IL-6, IL-8 (and IL-10 as a key anti-inflammatory cytokine) as markers of underlying inflammatory burden is well supported.

1.9.2 TNF-α induced skeletal muscle wasting

TNFα is a pro-inflammatory cytokine that has been most extensively studied in skeletal muscle. It causes a plethora of changes within the micro- and macrostructure of skeletal muscle. TNFα effects

on muscle tissue can be broadly dichotomised into those that promote atrophy or those that cause contractile dysfunction.[20] *In vitro* studies have conclusively shown that clinically relevant doses of TNFα causes induction of muscle-specific catabolic proteins, reduction in protein content and myofibre diameter over several days.[190] These findings were all later confirmed in a landmark clinical study by Puthucheary *et al.,*. TNFα triggers catabolic, proteolytic pathways after binding to its type 1 TNF receptor (TNFR1), causing downstream stimulation of NFκB – a transcription factor that is pivotal in cell differentiation, apoptosis and in the coordination of inflammatory responses. Subsequent activation of the inhibitor of NF-κB kinase (IKK) complex which causes phosphorylation of the otherwise quiescent inhibitor (in non-stimulated cells), IkB. This leads to NFκB activation and subsequent upregulation of proteins specific to striated muscle and associated with skeletal muscle atrophy – MURF1 and MAFBX (atrogin-1).[191,192] This downstream signalling stimulates the ubiquitin-proteasome pathway[193] (UPP) leading to breakdown of the dominant muscle proteins – actin and myosin.[194] TNF-α is an important upstream stimulus for muscle breakdown via the UPP. Proteasomes are protein complexes that serve to breakdown proteins, regulating protein turnover and thus protein homeostasis.[195] The targeting of proteins for breakdown by the UPP system stems from "labelling" of a target protein with a ubiquitin molecule.[66,196] This initial label results in further addition of ubiquitin, through the action of E1 (ubiquitin activating) and E2 (ubiquitin conjugating) enzymes, forming a poly-ubiquitin chain bound to the proteasome. Next, the rate-limiting step of E3 enzymes (ubiquitin ligases) binding and breaking down the protein substrate into short length polypeptides occurs.[194] Lastly, TNFα alters resting calcium levels in myotubes[197] which can lead to reduced force of contraction and tetanic force production in limb and diaphragm muscle.[198]

1.10 Critical illness associated myonecrosis

Myonecrosis has been found to occur in up to 54% of critically ill patients receiving MV.[14,199] Whilst the occurrence of a necrosis-associated muscle wasting seems to occur in patients with a higher number of organ failures and higher APACHE II scores,[14] the pathophysiology is poorly understood,

yet it carries a significantly worse prognosis than muscle wasting in the absence of necrosis in critically ill patients.[24] Myonecrosis appears to be a significant contributor to a decline in muscle quality,[133] and has been demonstrated in a significant proportion of patients in critical illness.[3,6] The specific mechanisms of how myonecrosis is executed remains uncertain. Helliwell and colleagues found that 48% (15 out of 31) of critically ill patients had histological evidence of myonecrosis from biopsies of the tibilias anterior, quadriceps and forearm muscles. This group also showed 5 of the 12 (41%) patients who had serial biopsies performed also showed progressive necrosis as given by the proportion of myofibres affected. An interesting finding in the histology was that the necrosis was non-homogenous and did not favour areas near vessels or those in central locations. In a more recent study, Puthucheary *et al.,* found that 20 patients out of 37 (54%) had histological evidence of necrosis by day 10 of their ICU admission.[14] Interestingly, all those that had evidence of necrosis demonstrated positive immunostaining for CD68, a known marker of M1 macrophages – a finding also noted in Helliwell's study. Furthermore, clinical parameters including chronic illness was not found to be a significant factor. These two studies have both demonstrated that degree of muscle atrophy may not predict those who develop necrosis. Both studies did however find an association with atrophy and number of failing organs.

Three distinct histological entities of myopathy during critical illness have been described.[199–201] In addition to acute necrotising myopathy, myopathy with selective loss of myosin filaments and CIM have different biochemical and physiological characteristics. For example, in CIM, whilst there is muscle fibre atrophy and variation in fibre size, there can be single fibre necrosis and fatty degeneration of fibres. What is notable in this sub-type, is that inflammatory changes are often absent.[200] Necrotising myopathy has more prominent features of necrosis with vacuolisation and phagocytosis of fibres. Myopathy with selective loss of myosin filaments is rare and often associated with corticosteroid use with or without neuromuscular blockade and this may ultimately progress to more familiar necrotising myopathy. Currently it is unclear whether these histopathological

descriptions represent different myopathy syndromes or are simply manifestations of the same process, ultimately leading to widespread myonecrosis. The chronology of this process is poorly understood.

1.10.1 Programmed necrosis – necroptosis

Historically necrosis was thought to be an unregulated process, leading to the destruction of a cell triggered by a physical stress.[202] However, it is now well established that necrosis can be accidental, secondary, or follow a programmed pathway. A distinguishing feature of necrosis from apoptosis, another programmed cellular death process, is the release of intracellular contents preceded by a period of "cell swelling" (oncosis), plasma membrane permeability and organelle swelling before rupture of the cell membrane.[203] Secondly, a differentiating microscopic feature is the absence of nuclear fragmentation and chromatin condensation.[202,204] The difficulty in distinguishing accidental, secondary and programmed necrosis highlights the importance of identifying biochemical markers of the underlying process. Programmed necrosis, known as necroptosis, has been implicated in a range of disease states including ARDS, myocardial infarction[205] and ischaemic-reperfusion injury.[206,207] Existing literature of necroptosis mechanisms have largely focussed on TNF-receptor activation since its discovery that it can induce both apoptosis and necrotic cell death.[202,208] Other death receptors (and their respective activating ligands) that are important initiators of necroptosis include FAS, TRAIL1 and TRAIL2.[208–210] However, the pleiotropic activity of TNFR1 highlights an important role in both inflammation and necroptosis.

1.10.1.1 TNFα induced necroptosis

Whether the myonecrotic process is triggered by an inflammatory insult which then follows a dysregulated pattern versus a more coordinated pathway is currently not known. Understanding the mechanism may explain why some patients have varying severity of weakness in the years that follow critical illness. To-date, clinical studies investigating acute muscle wasting have focused on catabolic

protein pathways triggered by TNFα (as outlined above) and other proteolytic pathways triggered by TNFα. However, programmed cell-death cascades remain relatively unexplored. TNFα binds to TNFR1 leading to a change in the cytosolic portion of the receptor and recruits an array of proteins including TRADD, RIPK1, cIAP1, cIAP2 and TRAF2[202] to form complex 1. Receptor-interacting serine/threonine-protein kinase 1 (RIPK1) is polyubiquitylated in complex 1 which favours NFκB[211,212] and MAPK pathway activity and promotes cell survival.[213] However, if this complex is destabilised, usually through deubiquitylation of RIPK1, a programmed cell-death pathway is favoured through the formation of a death-initiating signalling complex (DISC) – complex IIa.[214,215] At this point, if inhibitors of apoptosis and NF-κB essential modulator (NEMO) are non-functional or blocked, then a further complex, termed complex IIb, is formed. It is at this point that if caspase activity is inhibited, then there is a 'switch' from pro-apoptosis to pro-necroptosis through formation of the 'necrosome'.[210] RIPK1 is therefore an important protein involved in both the apoptotic and necroptotic pathways and also fundamental in the formation of the DISC.

1.10.1.2 Necroptosis activation and necro-inflammation

Necroptosis is archetypally activated by ligation of tumour necrosis factor receptor 1 (TNFR1) by tumour necrosis alpha (TNFα).[216,217] A crucial step in this signalling is the blockade of caspase activation and the formation of a RIPK1 and RIPK3 complex[218–221] with subsequent RIPK3-dependent phosphorylation of mixed-lineage kinase domain-like (MLKL) – a terminal effector protein.[222,223] Oligomerisation of phosphorylated-MLKL (pMLKL) leads to formation of pores in the cell membrane inducing sodium influx, cellular oncosis and eventually lysis.[224,225] Lysis of the cell causes systemic exposure to a number of damage-associated molecular patterns (DAMPs) (such as HMGB-1, IL-1β, IL-1α, IL-33 and nucleic acids)[216,226–228] which promotes further inflammation coined 'necro-inflammation'.

1.10.1.3 Biomarkers of necroptosis

Reliable biomarkers of necroptosis are lacking in clinical studies.[229,230] Few prospective human studies have shown that higher RIPK3 levels within 3 days of ICU admission are associated with mortality across a variety of ICU presentations[231–233]. Furthermore, plasma RIPK3 (but not RIPK1 or MLKL) has been found to be associated with the need for MV, the occurrence of ARDS and also serves as an independent predictor for ventilator-induced lung injury in experimental models.[234] *Ma et al.,* sought to investigate associations of systemic RIPK3 levels in critical illness. This group prospectively looked at 953 patients across 5 ICUs in North America and Korea (47% with a diagnosis of sepsis)[233] and the plasma levels of RIPK3 on day 1 of ICU admission. They found that RIPK3 was associated with in-hospital mortality and organ dysfunction, however, further mechanistic evidence to conclusively support underlying necroptosis activation was not studied and there was significant variation in sample collection across hospital sites which may have affected measured levels. RIPK3 can be regarded as pleiotropic, and it should be noted that elevated RIPK3 in isolation, may suggest, but does not prove an underlying programmed necrotic pathway is upregulated.[235,236] For example, RIPK3 can activate caspase-8-dependent apoptosis independent of its kinase activity[237] and activate other inflammatory complexes such as the NLRP3 inflammasome with downstream release of IL-1β in the absence of necroptosis activity.[238] Therefore, high levels of RIPK3 in isolation, whilst suggestive, do not confirm downstream activation of necroptosis.

Human studies focussing on necroptosis in peripheral skeletal muscle are lacking. However, *Szobi et al.,*[239] demonstrated significant expression of phosphorylated RIPK3 in human myocardium of 16 patients with either ischaemic or dilated cardiomyopathy causes of cardiac failure (versus 4 healthy controls). Furthermore, in the same cohort, caspase-8 expression (indicating apoptosis activity) was downregulated indicating pro-necroptotic signalling was upregulated. To-date, there is only one study of necroptosis activation in human peripheral skeletal muscle. In this notable study, Morgan *et al.,* examined skeletal muscle of dystrophin-deficient patients (Duchenne's muscular dystrophy (DMD),

an inherited disorder), and found that myofibre death was associated with significant upregulation of RIPK3 and pMLKL – crucial machinery of necroptosis activation, in DMD patients (n=6 vs n=5 control).[8] The same group also demomnstrated, through an *in vitro* model, that C2C12 murine skeletal muscle cells undergo necroptosis following TNFα stimulation. A primary human skeletal muscle model has not been described. Thus, analysis of plasma and skeletal muscle of critically ill patients may provide initial insights to whether the observed myonecrosis demonstrate biomarkers of necroptosis.

1.11 Summary, aims and hypotheses

There is a need for robust guidelines and agreed methodology in musculoskeletal ultrasound in critical illness. Routinely collected CT images are commonly not used to assess musculoskeletal sequelae of critical illness and there are few prospective clinical studies utilising ultrasound to assess changes in peripheral skeletal and respiratory muscle in parallel during critical illness. Most notably, non-invasive measurement of parasternal muscle activity has only recently emerged as a bedside method of assessing respiratory muscle function during invasive mechanical ventilation and longitudinal descriptions are lacking. The rapid rise in critical care utilisation during the COVID19 pandemic has also raised concerns over long-term effects of surviving critical illness – of which muscle wasting and weakness is frequently reported. There is little description of muscle wasting in critically ill patients during the height of the COVID19 pandemic. Identification of risk factors and trajectory of wasting is vital to assist in predicting those who are likely to experience physical restriction. Finally, the high incidence of myonecrosis during critical illness warrants investigation of potential inflammatory phenotypes, underlying mechanisms and biomarkers. This PhD will aim to develop understanding of peripheral and respiratory muscle wasting during critical illness. The main hypotheses of this thesis are:

1. Computed tomography and ultrasound imaging are reliable and comparable methods of assessing acute respiratory and skeletal muscle wasting and changes in quality.
2. Parasternal muscle wasting and dynamic strain assessment can assist with respiratory muscle loading during invasive mechanical ventilation.
3. There is upregulation of necroptosis machinery in skeletal muscle during critical illness associated muscle wasting.

Chapter 2: Methods

2.1 Clinical studies

Patients were prospectively recruited from three ethically approved clinical studies (Table 2-1). Eligibility and inclusion criteria for the clinical studies are summarised in Table 2-2. Personal consultees provided consent in person or via telephone given that patients were sedated and ventilated. During the COVID19 pandemic, consent was obtained via telephone only. Retrospective consent from patients was sought when capacity was regained.

Trial	Details
WAVE	Primary aim: To compare the duration of mechanical ventilation and the weaning period between patients managed with standard care or with mechanical ventilation adjusted according to the Beacon Caresystem. Ethical approval granted by local Research and Ethics Committee (REC) (Ref. 18/LO/0282) and the synopsis registered on clinicaltrials.gov (NCT03697785). The study was sponsored by The Royal Brompton Hospital.
DeVENT	Primary aim: (1) To evaluate whether an open-loop physiologic model-based decision support system reduces driving pressure during mechanical ventilation in patients with ARDS. (2) characterize ARDS patients in terms of clinical features, physiological measurements and non-invasive measurement of biomarkers. Ethical approval granted by local Research and Ethics Committee (REC) (Ref. 19/LO/1606) and the synopsis registered on clinicaltrials.gov (NCT04115709). The study was sponsored by Imperial College London.
MUSCLE-ICU	Primary aim: To investigate the quantitative and qualitative changes of skeletal muscle during critical illness. The study was registered with the Health Regulatory Authority (HRA) (IRAS project ID: 285418 and ethical approval was granted by the Research and Ethics Committee (REC) (reference: 20/HRA/4756). The study was sponsored by Imperial College London (Ref. 20IC6279).

Table 2-1. Summary of clinical studies in this thesis

WAVE; Weaning Algorithm for Mechanical Ventilation, DeVENT; Decision Support System to Evaluate VENTilation in ARDS, MUSCLE-ICU; Acute muscle wasting in critical illness.

Trial	Inclusion	Exclusion
WAVE	• Mechanically ventilated at 24 hours following intubation • Age > 18 years	• The absence of an arterial catheter for blood sampling at study start. • Mechanical ventilation initiated for more than 48 hours. • Likely not to survive or withdrawal of care within 48 hours of ICU admission. • Medical history of home mechanical ventilation, long term oxygen therapy and non-invasive ventilation • Respiratory failure likely to require extracorporeal support. • Severe cardiogenic shock likely to require extracorporeal support. • Severe isolated right heart failure. • Head trauma or other conditions where intra-cranial pressure may be elevated. • Primary (non-overdose related) neurological patients (Glasgow coma score <10, neurologic damage with limited prognosis, stroke hemiplegia). • End stage liver disease. • Repeated ICU admission within same hospital admission and/or likely to have prolonged ICU stay with cumulative mechanical ventilation (>21 days) • Pregnancy.
DeVENT	• Invasive mechanical ventilation. • Within 1 week of a known clinical insult or new or worsening respiratory symptoms. • Chest radiograph with bilateral infiltrates consistent with evidence of pulmonary oedema but not fully explained by cardiac failure. • Hypoxaemia as defined by PaO_2/FiO_2 of ≤ 300mmHg (or ≤ 40kPa) (pre-ECMO PaO_2/FiO_2 will be used should patient be placed on extracorporeal support).	• Age < 18 years old. • The absence of an arterial catheter for blood sampling at study start. • Consent declined. • Over 7 days of mechanical ventilation. • Treatment withdrawal imminent within 24 hours. • Do Not Attempt Resuscitation order in place. • Severe chronic respiratory disease requiring domiciliary ventilation (except for sleep disordered breathing) • Veno-Arterial ECMO
MUSCLE-ICU	• Patients aged >18-years • Diagnosis of SARF/ARDS of any aetiology (primary group) (and control groups: critical illness of any other cause including non-SARF/ARDS) • Appropriate CT imaging of the chest and abdomen following quality check	• Patients aged less than 18-years old • No suitable chest or abdominal CT imaging available

Table 2-2. Inclusion and exclusion criteria for patients recruited in clinical studies

Patients in WAVE were peri- or post-operative cardiac surgery patients, whereas patients in DeVENT all had diagnosis of acute respiratory syndrome. Patients in MUSCLE-ICU consisted of general, cardiac and severe respiratory failure patients. *WAVE; Weaning Algorithm for Mechanical Ventilation, DeVENT; Decision Support System to Evaluate VENTilation in ARDS, MUSCLE-ICU; Acute muscle wasting in critical illness.*

2.1.1 MUSCLE-ICU study

The primary objective of this retrospective study was to describe the extent of acute muscle wasting using computed tomography imaging collected as part of routine care in patients with critical illness,

more specifically, severe acute respiratory failure (SARF) of any aetiology (with or without extracorporeal support). Retrospective interrogation of the hospital's patient registration systems was performed to identify patients admitted to the ICU and then stratified according to admission diagnosis. Clinical and radiological data collected is summarised in Table 2-3. Patients included in this study were >18-years old, had a diagnosis of SARF of any cause and had appropriate CT imaging of the chest and abdomen following quality checks (see 2.1.1.1)

Admission • Age • Gender • Body mass index • Admission diagnosis • Co-morbidities • APACHEII and SOFA score • MV days pre-admission • Hospital LoS pre-admission • Intubation date • Primary hospital admission date • Use of ECMO	Respiratory • PEEP • p/F ratio • Peak inspiratory pressure • Tidal volume Critical care support • Medications (not limited to neuromuscular paralytics, vasopressors, sedatives, corticosteroids etc) • Daily sedation drug doses • Sedation days (per drug) • Neuromuscular blockade days	Laboratory • CRP • WCC • Bilirubin, platelets, creatinine (the biochemical markers of pro-inflammatory phenotype) • Albumin Outcome • ECMO days • ICU mortality
Renal • Creatinine • Urea • RRT days • Daily fluid net fluid balance	Radiological • All CT imaging from admission	

Table 2-3. Clinical, physiological and outcome data collection in MUSCLE-ICU study

APACHE II; acute physiology and chronic health evaluation score, SOFA; sequential organ failure assessment score, MV; mechanical ventilation, LoS; length of stay, ECMO; extracorporeal membrane oxygenation, RRT; renal replacement therapy, ICU; intensive care unit, PEEP; positive end-expiratory pressure, p/F; P_aO_2:FiO_2 ratio, CT; computed tomography, CRP; C-reactive protein, WCC; white cell count.

2.1.1.1 Screening and preparation of CT images

After identification of patients, completed CT studies were studied for suitability. Studies were suitable if there was complete visualisation of muscle groups at the level of interest and an axial slice

was available. Studies were excluded if there was partial/complete obscuration or exclusion of any muscle group at the level of interest and/or significant artefact causing difficulty quantifying muscle groups.

CT imaging studies were performed by staff within the department of radiology at The Royal Brompton Hospital, London as per their departmental standard operating procedures. Contrast and non-contrast CT studies were included. CT studies were viewed using IMPAX software (Agfa-Gevaert, Mortsel, Belgium). Coronal and sagittal views were linked at the mid-point of the L3 vertebral body. This anatomical point was then viewed in an axial view after soft-tissue reconstruction. Five millimetre (mm) thick axial slices were used. If 5 mm sections were not available, then the next thickest slice was used. If sagittal or coronal views were not available, then manual identification of the vertebral level was performed by counting down cranial to caudal. Axial images were anonymised and stored offline as DICOM files for analysis in two software packages: ImageJ (National Institute of Health (NIH), Bethesda, MD, USA) and Slice-O-Matic version 5.0 (TomoVision, Montreal, QC, Canada).

2.1.1.2 Skeletal muscle groups in L3 axial sections

The distinct muscle groups at the third lumbar vertebral level (L3) when viewed in an axial view are illustrated in Figure 2-1. These muscle groups were quantified and summed to give the total muscle area at this level, L3-SkM_{CSA}.

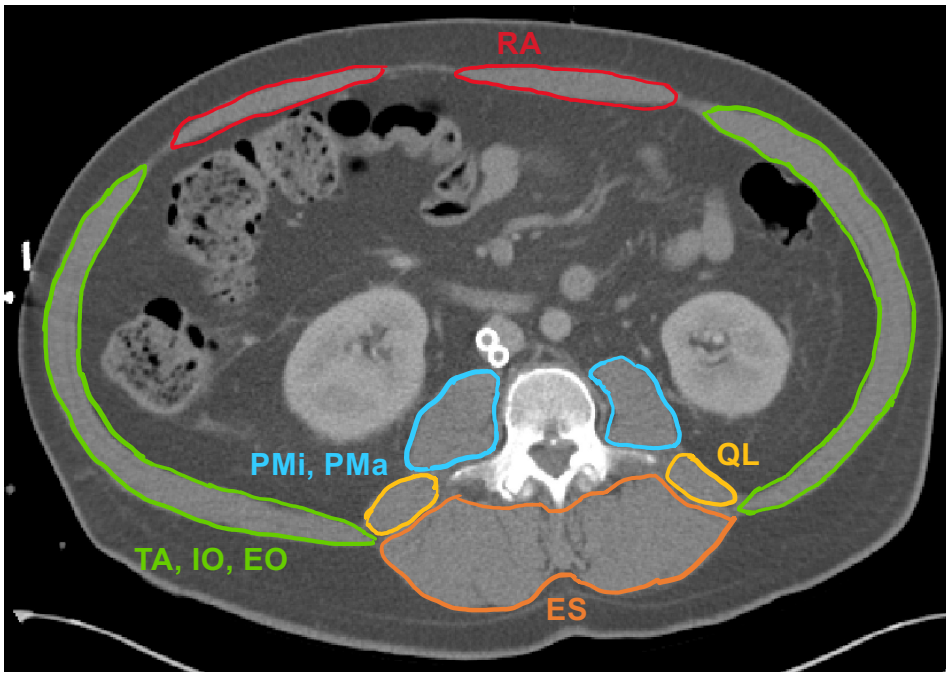


Figure 2-1. Skeletal muscle groups at the L3 vertebral level

Axial view at the mid-L3 vertebral level and five muscle groups: *rectus abdominis (RA, red outline), transverse abdominis (TA), internal oblique (IO) and external oblique (EO) (all green outline), psoas minor (PMi) and psoas major (PMa) (both blue outline), quadratus lumborum (QL, yellow outline) and erector spinae (ES, orange outline)*. The sum of these groups gives the total cross-sectional area of skeletal muscle at the L3 level, L3-SkM_{CSA}.

2.1.1.3 Tissue density recognition and quantification

Tissue densities were identified using published Hounsfield unit (HU) ranges (–29 to +150 HU for muscle, –190 to –30 HU for intermuscular adipose tissue (IMAT) and subcutaneous adipose tissue (SAT) and –150 to –50 HU for visceral adipose tissue (VAT)[165] (Figure 2-2). In Slice-O-Matic, cross-sectional area of skeletal muscle at the L3 level ($SkM_{L3\text{-}CSA}$) and muscle density (an indicator of muscle quality) (in Hounsfield units) (SMD) was obtained by selecting the appropriate tissue window and manually shading the tissue structures in the axial view as per the Alberta protocol described by Mourtzakis *et al.,*.[240] The software computes the L3-SkM_{CSA} and SMD in centimetres squared and mean Hounsfield units respectively. L3-SkM_{CSA} is calculated by summing the pixels for the tissue regions and multiplying by the pixel surface area. The ImageJ method is well described,[166] but requires more

manual processes to differentiate tissue densities. In a preliminary study, I found that one single axial image takes between 6-10 minutes using Slice-O-Matic and 12-15 minutes using ImageJ (data not shown). Skeletal muscle index (SMI) is used as a measure of total body skeletal muscle and allows between patient comparisons. SMI was calculated by dividing L3-SkM_{CSA} by height (in metres) squared. Clinical thresholds for 'low SMI' and 'normal SMI' were taken from a large healthy population study and stratified by age, gender and BMI.[168]

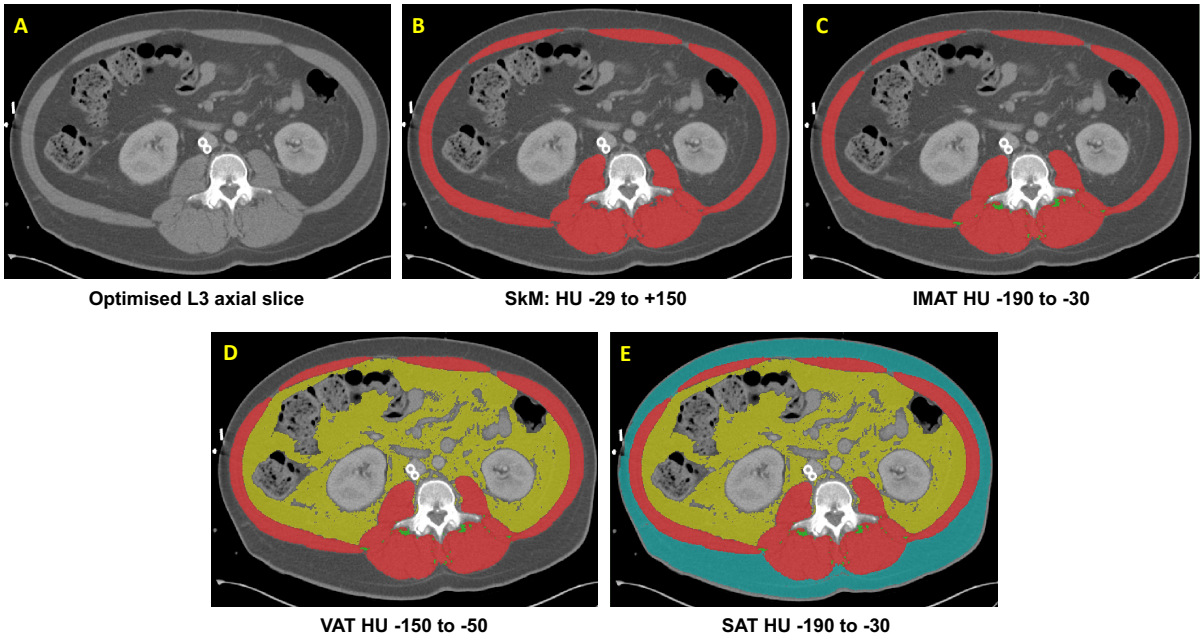


Figure 2-2. Hounsfield unit densities of tissue at the L3 vertebral level

(A) an example of a suitable axial L3 CT slice for analysis. (B) Identification of skeletal muscle tissue (red) using -29 to +150 HU, (C) identification of intra-muscular adipose tissue (C, green) and visceral adipose tissue (D, yellow) using -150 to -50 HU) and subcutaneous adipose tissue (E, cyan).

2.1.1.4 Reliability study of body composition analysis

To demonstrate validity of quantitative measurements, a reliability study of 30 patients was performed to ensure operators can accurately quantify muscle groups using two software packages. Operators were blinded to all clinical information and each other's measurements until the study was completed. Scans were analysed and then re-analysed with an interval of at least 7 days by the same

examiner to reduce recall bias. Measurements are reported as an average from three assessments alongside a coefficient of variation (CoV).

For the measurement reliability study, an a priori power calculation determined that to compare two observations a minimum of 12 participants were required, anticipating intra-class correlation coefficients (ICC) between 0.6 and 0.9[20] and using a significance level of 0.05 and power of 80%. The sample size for all other determinants of the study will be determined by the number of available CT scans. Agreement will also be visually represented by Bland-Altman graphs and quantitatively reported using the intra-class correlation coefficient (ICC).

2.1.2 WAVE and DeVENT studies

Prospective, longitudinal respiratory and skeletal muscle ultrasound was performed on patients recruited to sub-studies of the WAVE and DeVENT trials. Blood sampling was also performed in these patients only.

2.1.2.1 Disruption to patient recruitment in prospective trials

The COVID19 pandemic led to temporary suspension of non-essential research activity within the recruiting hospitals and throughout the United Kingdom in general. This meant that between March 2020 and August 2020, recruitment to the WAVE study did not take place. The DeVENT study began recruitment in March 2020.

2.2 Clinical procedures

Patients recruited to WAVE and DeVENT studies underwent prospective blood sampling and ultrasound imaging on pre-defined study days (Table 2-4). Venesection (2.2.1) and ultrasound imaging (2.2.2) was performed on day 0 (study randomisation), day 1 (if not able to obtain day 0), day 3, day 7, day 14, day 21 and ICU discharge (or date as close to as possible). When a study day fell

on weekends or holidays, or when the research team were not available, investigations were taken on most appropriate day as agreed by the research team (Table 2.2).

Study Day	Range for study procedure
Baseline	Day 0 or Day 1
Day 3	Day 3, 4 or 5
Day 7	Day 6, 7 or 8
Day 14	Day 12, 13, 14 or 15
Day 21	Day 19, 20, 21 or 22
ICU discharge (D)	D, D-1, D+1, D+2

Table 2-4. Time points for venesection and clinical ultrasound in WAVE and DeVENT studies

Baseline studies were performed on the first day of admission to our tertiary severe respiratory failure centre. Follow-up ultrasound studies were performed within a range to accommodate for patient needs, weekends and operator availability.

2.2.1 Venepuncture and blood processing

Blood was collected from the patient by trained personnel via an indwelling arterial catheter. Blood was collected in ethylenediaminetetraacetic acid (EDTA), serum separator tubes (SST) and lithium heparin (LiHep) anti-coagulated tubes. Samples were kept on ice until processed and all samples were processed within 2 hours of collection. Plasma was isolated from EDTA and LiH tubes by centrifugation of the whole blood at 2000g for 10 minutes at 4^{o}C, before removal, aliquoting and storage at -80^{o}C until required. SST tubes were kept at room temperature for 30 to 45 minutes before centrifugation at 2000g for 10 minutes at room temperature before removal of serum, aliquoting and storage at -80^{o}C until required.

2.2.2 Respiratory and skeletal muscle ultrasound

Respiratory (diaphragm and parasternal muscle) and peripheral skeletal muscle (rectus femoris) was prospectively studied using ultrasound. Muscle mass (cross-sectional area and/or thickness) was quantified for all muscle groups. Dynamic measurements (thickening fraction, longitudinal strain) were assessed for respiratory muscle only.

An ultrasound protocol for the clinical studies was developed using high-impact peer reviewed publications and discussion with experts in the field.[54,57,138,152] Approximately 60 hours of private study and practice was undertaken over a three month period prior to formal study. Images were obtained using a Philips Sparq or Philips EPIQ 7 ultrasound machine (Philips Healthcare, Andover, Massachusetts, USA). A high-frequency 12 MHz linear probe was used for all anatomical sites as able. Selection of probe can vary depending on the anatomical site (detailed below) and body habitus of the patient. Frequency, gain and depth were kept constant for each patient where able. Images were recorded as Digital Imaging and Communications in Medicine (DICOM) files and analysed offline using a dedicated analysis package (McKesson Cardiology, v13.1.2, McKesson Ltd., Israel). A single operator (SP) analysed all images in a random order after blinding of all identifiable information. Intra-rater reliability was assessed for all patient studies.

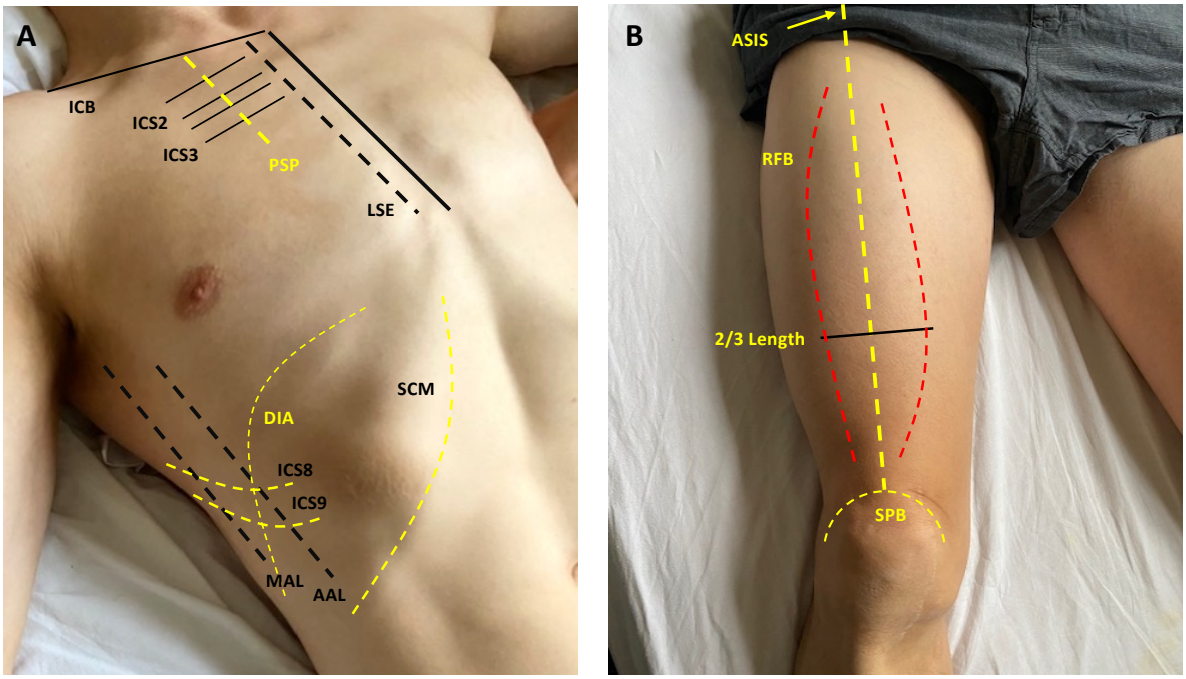


Figure 2-3. Surface anatomy of respiratory and peripheral skeletal muscle ultrasound

Diaphragm and parasternal surface anatomy (A), Lower limb anatomy for quadriceps ultrasound (B). Ultrasound probe positioned perpendicular to the relevant anatomical landmark. Patients were positioned 30 degrees head up with the knee in gentle knee flexion. *ICB = inferior clavicular border, ICS2 = 2nd inter-costal/parasternal space, ICS3 = 3rd inter-costal/parasternal space, ICS8 = 8th inter-costal space, ICS9 = 9th inter-costal space PSP = parasternal muscle imaging point, LSE = lateral sternal edge, DIA = diaphragm, SCM = sub-costal margin, MAL = mid-axillary line, AAL = anterior axillary line, ASIS = anterior superior iliac spine, SPB = superior border of patella, 2/3 length = between ASIS and SPB. RFB = red dotted line outlining the rectus femoris muscle bulk.* This image has also been published in Chapter 27 of *Point-of-Care Ultrasound in Critical Care: a practical guide to POCUS (Scion Publishing Ltd, 2022).*[241]

2.2.2.1 Diaphragm ultrasound

A 12 MHz, high-frequency ultrasound probe was placed in the 8th or 9th intercostal space (ICS8 and ICS9 respectively) between the anterior and mid-axillary line on the right side. This site represents the zone of apposition – where the abdominal contents meet the chest wall.[53] At this point, the diaphragm appears as a non-echogenic structure bounded by the echogenic pleura superiorly and the echogenic peritoneum inferiorly (Figure 2-4). Diaphragm thickness was dynamically assessed during tidal breathing using brightness mode (B-mode) ultrasound and thickness measurements calculated using

motion mode (M-mode) (Figure 2-5). A slow sweep (scrolling) speed of 10 millimetres per second was adopted to obtain three consecutive and visually consistent breaths.[242] Inspiratory and expiratory thickness was calculated by drawing a vertical line at the appropriate respiratory phase (Figure 2-5). End-expiratory thickness was calculated as late as possible before the next respiratory cycle. The mean of three consecutive breaths were used in subsequent analyses. Diaphragm thickening fraction was calculated by: [(mean DIA_{INSP} – mean DIA_{EXP}) / mean DIA_{EXP}]*100.

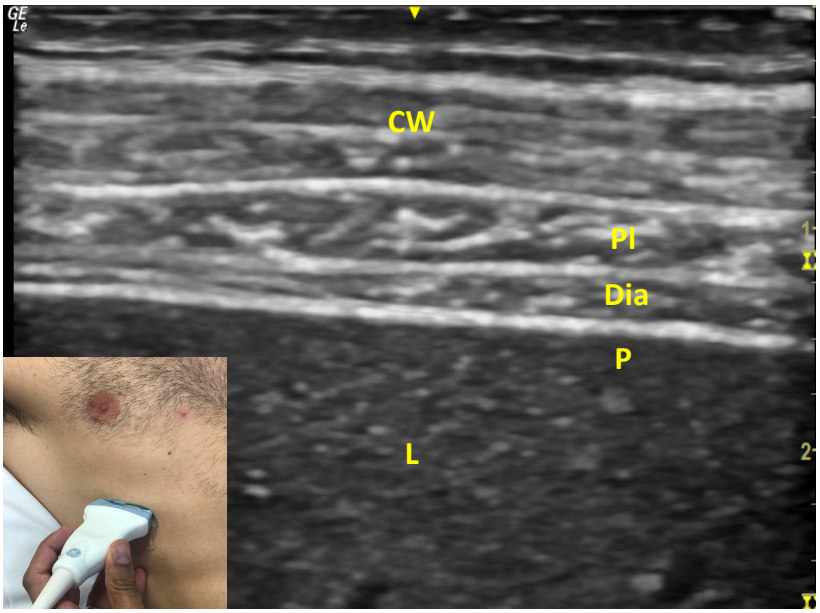


Figure 2-4. B-mode ultrasound of the diaphragm

The anatomical location and orientation of ultrasound probe in the 8th intercostal space is shown in the inset. The diaphragm (Dia) is a non-echogenic structure, bound superiorly by the pleura (Pl) and inferiorly by the peritoneum (P). The liver (L) is the most inferior structure and the chest wall (CW) musculature and subcutaneous tissue lie superior to the pleura. The ultrasound image shown was captured using a 12 MHz linear probe.

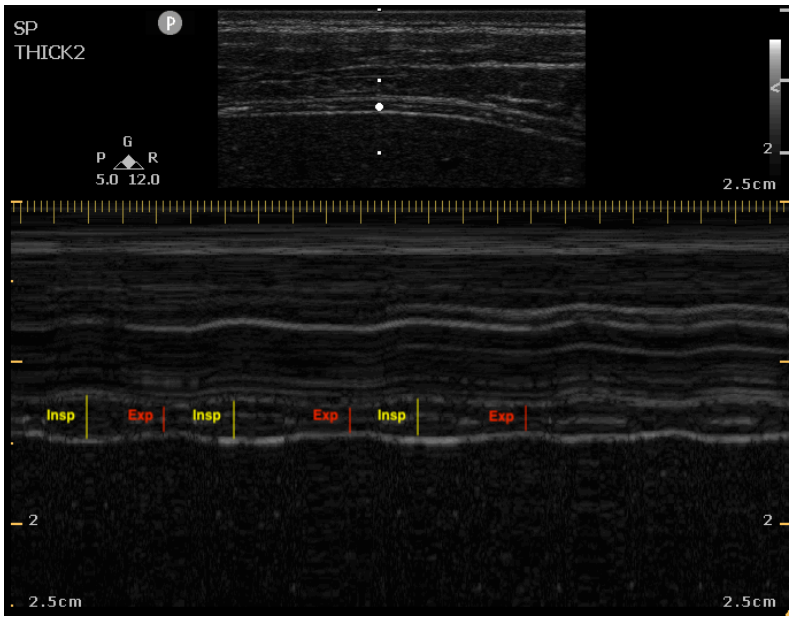


Figure 2-5. M-mode ultrasound of the diaphragm

M-mode ultrasound of the diaphragm performed following B-mode image visualization. The B-mode representation (upper image) depicts the trajectory of the M-mode line. The generated M-mode image below shows four consecutive respiratory cycles (inspiration: yellow, expiration: red). End-expiratory thickness (Exp) and end-inspiratory thickness (Insp) are then used to calculate thickening fraction. Four complete breaths are shown in this figure.

2.2.2.2 Parasternal muscle ultrasound

A 12 MHz high-frequency probe was placed in the 3rd intercostal space approximately 3cm lateral to the sternal edge.[131,243] In practice sessions, this space was the most reliably identified and demonstrated greater muscle bulk when compared with ICS2. In addition, no other muscle groups lie superficially (i.e. pectoral muscles) and ICS below ICS3 were more likely to have monitoring leads obscuring the anatomical site. The sternal edge was best found using the ultrasound where a continuous echogenic line is seen traversing the image view horizontally. When this echogenic structure disappears, the sternal edge was marked, and the probe placed 3cm lateral to this point (Figure 2-3 and Figure 2-6). During image acquisition, 20-30 second video files were recorded of the PSM, to ensure at least three complete tidal breaths. End-inspiratory and end-expiratory points were noted from the ventilator flow-volume curves and the time on the image acquisition when

inspiration/expiration was not clear. Inspiratory and expiratory thickness was calculated by drawing a vertical line at the appropriate respiratory phase. End-expiratory thickness was calculated as late as possible before the next respiratory cycle. The mean of three consecutive breaths were used in subsequent analyses. Parasternal thickening fraction was calculated by: [(mean PSM_{INSP} – mean PSM_{EXP}) / mean PSM_{EXP}]*100. Three measurements for parasternal muscle end-expiratory thickness (PSM_{EXP}), parasternal muscle end-inspiratory thickness (PSM_{INSP}), parasternal muscle cross-sectional area (PSM_{CSA}) and parasternal muscle strain (PSM_{ε}) were calculated and the mean used in subsequent analyses.

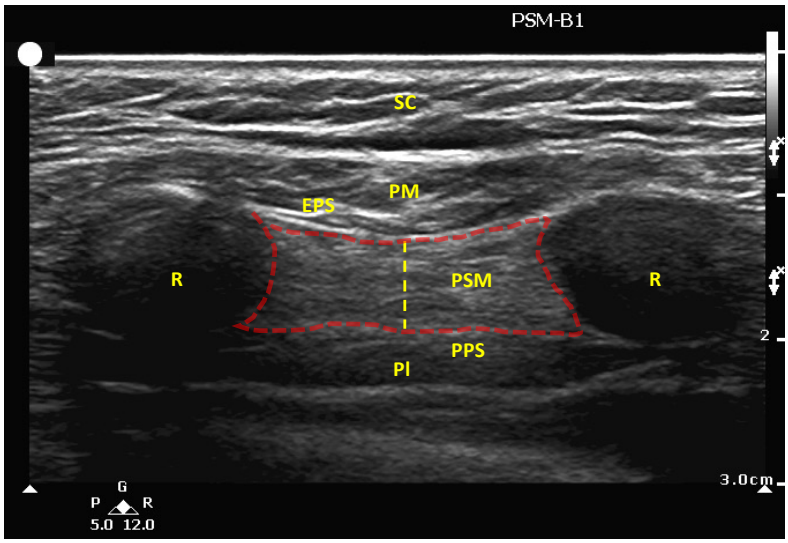


Figure 2-6. B-mode ultrasound of parasternal muscle

Parasternal muscle ultrasound in the third intercostal space. The subcutaneous tissue (SC) lies superficially and above the pectoralis major (PM) muscle. The parasternal muscle (PSM) is a biconcave structure bound by the external parasternal surface superficially, the pleural parasternal surface (PPS) inferiorly and the ribs (R) bilaterally. The cross-sectional area (dashed red line) is the area bounded by these four structures. The parasternal muscle thickness (vertical dashed line) is from the centre of the PSM and from the inner EPS to the inner PPS. The pleura (PI) is often the deepest structure seen.

2.2.2.3 Parasternal muscle strain

To perform parasternal muscle strain analysis, video files were transferred to a workstation running TomTec Image Arena workstation (TomTec, Unterschleissheim, Germany). A single respiratory cycle

period was chosen from the clip with the use of the 'anatomical M-mode' function (Figure 2-7). The centre of the parasternal muscle was manually traced from one rib to the other with 4 to 5 points and tracking enabled. Accuracy of tracking was initially assessed visually then by review of the strain curves looking for timing with respiratory effort, smoothness and time to peak. All images were analysed three times to ensure accuracy of results and the mean used for subsequent analyses. Strain values are negative values assessing deformation. Therefore, the more negative a value, the more deformation that has occurred or, the more negative the strain the greater the degree of contraction of the parasternal muscle. A random selection of 12 patient images from the studies were selected for blinded inter- and intra-rater analysis.

All PSM strain analysis was performed by Professor Sam Orde (Clinical Associate Professor, University of Sydney, Australia) who also helped construct the analysis methodology. Furthermore, Professor Orde analysed all pseudonymised B-mode video files that I supplied. Professor Orde acted as a blinded rater in the reliability study along with Dr Emma Bowcock (ICU specialist/echocardiography fellow, Intensive Care Unit, Nepean Hospital, Sydney, Australia). Professor Ordes had performed more than 1000 hours of analysis and holds formal accreditation in echocardiography and strain analysis and performed more than 100 hours in respiratory musculoskeletal strain analysis prior to commencing this study.

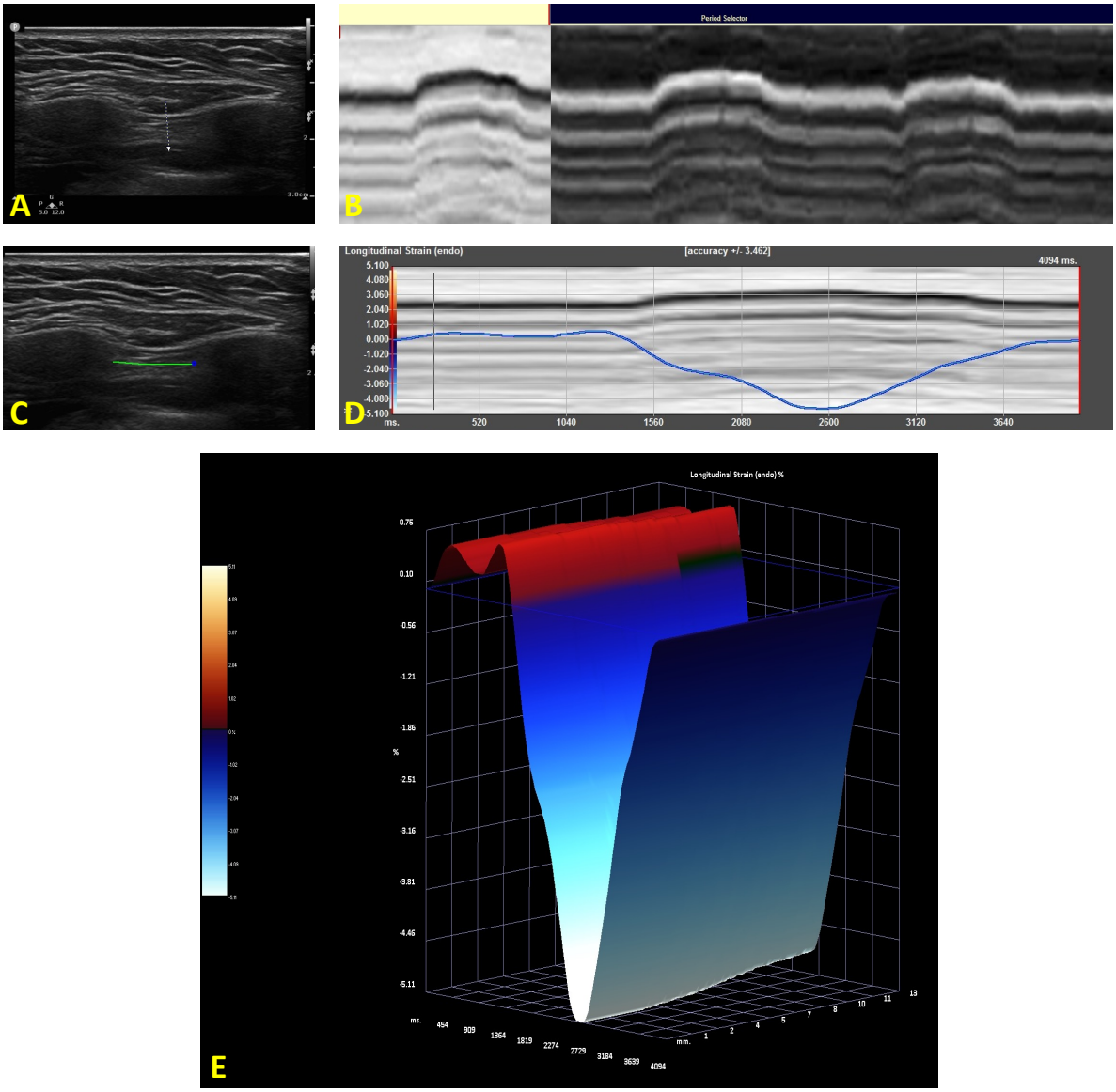


Figure 2-7. Parasternal muscle strain analysis

Parasternal muscle strain analysis from a single study time point. B-mode ultrasound of the parasternal muscle is performed (A), followed by M-mode by directing the analysis line through the middle of the muscle. From the subsequent M-mode output, a single respiratory cycle is selected (B, grey shading). Speckle tracking is then applied longitudinally across the muscle using 4 to 5 points (C, green line) and the corresponding strain trace during the respiratory cycle is produced (D). On this plot, the y-axis represents degree of strain (more negative value = greater strain), and the x-axis is time (milliseconds). Panel E represents a 3D plot of time (x-axis), strain (y-axis) and distance (in mm) (z-axis). Colour scale highlights greater strain from red (low) to blue (mild) to white (high).

2.2.2.4 Rectus femoris muscle ultrasound

The rectus femoris muscle is the most superficial muscle of the quadriceps group in the anterior thigh. To perform rectus femoris ultrasound, the patient is positioned at 30 degrees on an examination couch or bed (using the integrated measure on the bed when available). The knee was relaxed to avoid artificial contraction and rotation of the muscle. The ultrasound probe was placed on a marked position of two thirds the distance from the anterior superior iliac spine to the superior patellar point (Figure 2-3). The transducer is placed perpendicular to this skin at this point and ensuring that no angle is created in any other plane. A minimal compressive technique was adopted using an excess of ultrasound gel to reduce artificial compression. An adequate depth was when a layer of ultrasound gel was seen superiorly and the femur inferiorly (Figure 2-8). If the width of the visualised muscle cannot be reliably included one screen width, a curvilinear probe (6 MHz) was used for all scans for that patient. Three separate images were acquired twice, at least five minutes apart to assess intra-operator reliability. The rectus femoris cross-sectional area (RF_{CSA}) was calculated by drawing a line on the inner most aspect of the fascia.[126] Gain and depth settings were kept consistent for each patient as able.

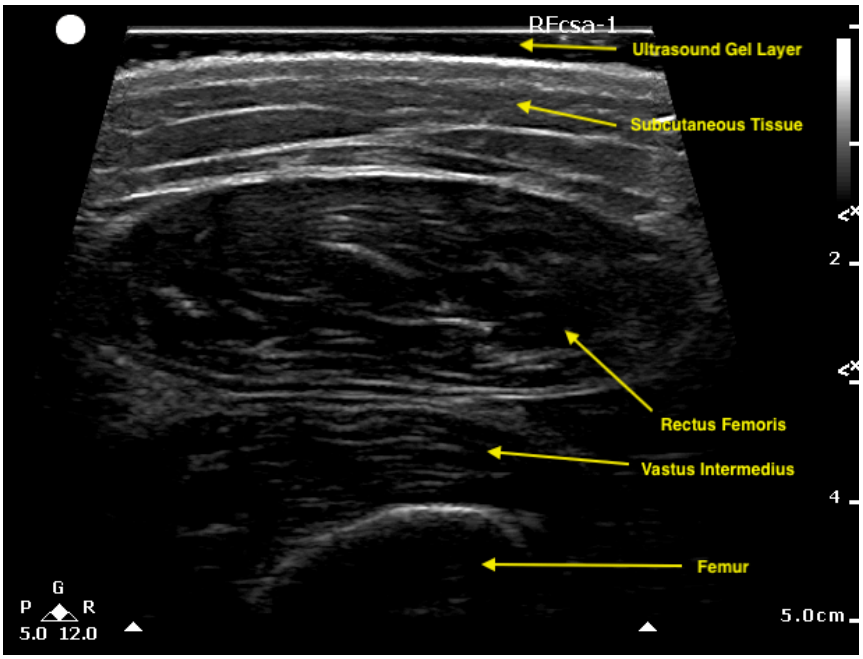


Figure 2-8. Rectus femoris ultrasound

Ultrasound image of the right quadriceps at a point two-thirds the distance from the anterior-superior iliac spine to the supra-patellar border. Minimal compression technique, with visualisation of the ultrasound gel superiorly and the femur inferiorly. The entire circumference of the muscle can be seen for delineation of the cross-sectional area which is calculated offline.

2.2.2.5 Echogenicity analysis

Echogenicity (EG) relates to the differential acoustic impedance of tissue with ultrasound.[144] Normal muscle will have a low EG due to the low fibrous and fat content of the tissue.[145] This radiological principle has been used to detect differences in muscle appearance across a range of ages and neuromuscular disorders.[46,135,145,146] In numerous diseases, this healthy tissue with low echogenicity is replaced with fibrous or fatty tissue, thus increasing EG.[244] Skeletal muscle EG has been found to increase in critical illness[46,147] and is also associated with the presence of myofibre necrosis when directly compared to histological specimens[133] and may offer a completely non-invasive tool to assess myonecrosis in critical illness.

EG will be assessed by grey-scale histogram analysis using open access software ImageJ (NIH, Bethesda, MD, USA). EG is calculated by grayscale analysis of pixels in a region of interest (i.e. the muscle cross-sectional area or, a selected portion of the muscle ('square method')). The mean EG of the RF_{CSA} (RF_{EG}) was calculated using the trace method[143] – where all visible muscle perimeter (excluding artefact and bordering fascia) will be used as the region of interest (ROI).[245] Parasternal muscle echogenicity (PSM_{EG}) was calculated using a rectangular shaped ROI which was adapted from the 'square technique'[46,143,243]. In the ROI, pixels are analysed on grayscale distribution using the histogram function on most imaging software packages. An 80 x 30 pixel rectangle was drawn on the central most area of the PSM that best avoided any significant artefact and/or fascia and/or pleural lines. When analysing a sub-set of preliminary echogenicity data, acoustic shadowing from the ribs in the parasternal muscle area reduced the EG significantly and produced wide limits of agreement following reliability analysis (Figure 2-10).[243] Only images with standardised gain and depth settings were analysed for EG. Images were again assessed at two time points and intra-operator coefficients were calculated. To assess intra-observer reproducibility, images and/or video are required at each time point for each operator. Patients were excluded from the analysis if they did not satisfy these criteria. PSM_{EG} was measured three times at end-expiration and the average used for analysis.

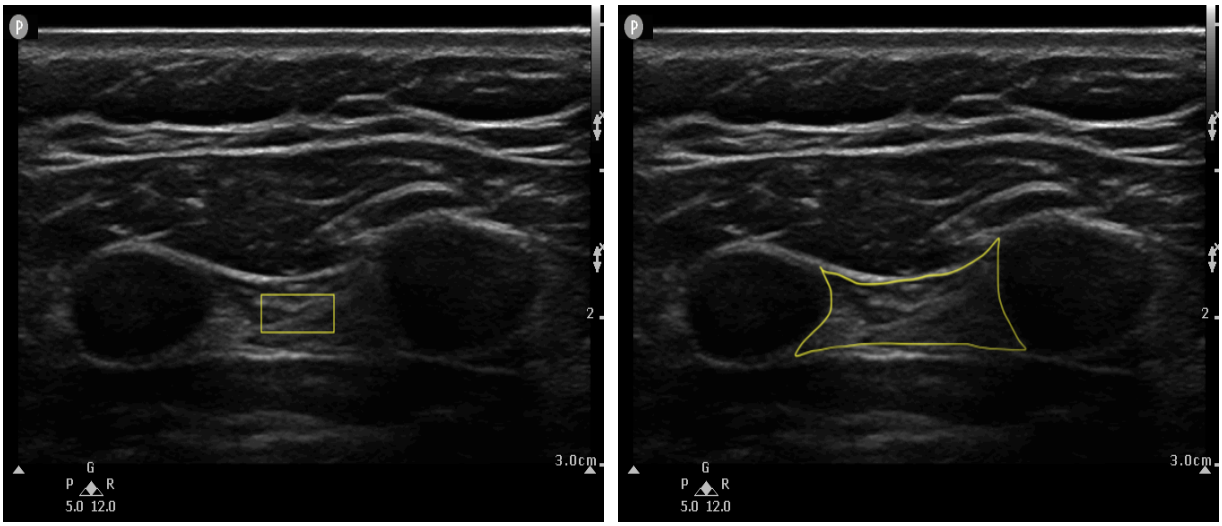


Figure 2-9. Parasternal muscle echogenicity analysis

The left panel illustrates the 'square technique' using a set pixel area and reduces the impact of acoustic shadowing from the ribs on the calculated echogenicity value when compared to the cross-sectional area method in right panel. The image on the right shows that in the bottom right corner, there is a significant acoustic shadow causing underestimation of calculated echogenicity.

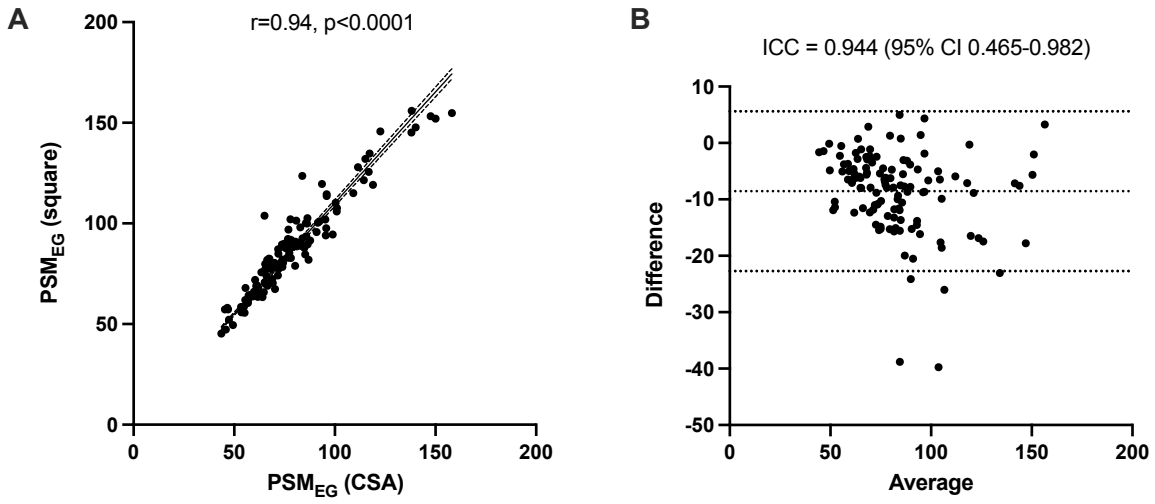


Figure 2-10. Correlation and reliability between methods for echogenicity calculation

Excellent correlation of parasternal muscle echogenicity (PSM_{EG}) between square and cross-sectional area methods (A). (B) Bland-Altman plot of the two techniques showing wide limits of agreement despite high intra-class correlation coefficient.

2.2.2.6 Musculoskeletal ultrasound training and competency

Prior to using the ultrasound protocol in clinical studies, I sought to demonstrate reliability data. Ultrasound training for rectus femoris ultrasound was provided by an expert clinician in the field (Dr Zudin Puthucheary, ZP) on two separate occasions. Demonstration of the learned technique to ZP was conducted prior to utilisation in a formal study. Approximately 60 hours of independent training time was conducted by SP to optimise the full protocol. In this study, myself (SP) and two other clinicians (SS and RH) were enlisted as operators for the clinical ultrasound protocol. SP taught SS and RH all clinical aspects of the technique including image acquisition.

2.2.2.7 Ultrasound reproducibility and reliability studies

To ensure a robust and reliable technique, a reproducibility study was performed in two cohorts: (1) 12 healthy volunteers and (2) 12 ICU patients receiving mechanical ventilation on the ICU. Ethical approval was sought under the WAVE trail as a separate study (WAVE-RMU – WAVE **R**espiratory **M**uscle **U**ltrasound). Operator 1 (SP), who has formal training in thoracic ultrasound, led and developed the respiratory and peripheral muscle ultrasound technique. Two additional operators (SS and RH), who were experienced with ultrasound in critical care but with no prior experience with the mentioned anatomical sites, were provided with a study manual and received training by SP on three occasions in order to demonstrate operational ability of the ultrasound equipment and application at the bedside before being allowed to participate in the studies – this is similar to methodology in previous studies[152]. The reliability study using healthy volunteers was performed by SP and RH. The reliability study using critical care patients was performed by SP and SS. Operators performed each scan at the three sites. A mean of three measurements (per time point) for each operator will be used to determine the intra-observer and inter-observer agreement via calculation of the intra-class correlation coefficient (ICC). An acceptable agreement was an ICC >0.9 and a coefficient of <7.5%.[246] To reduce any potential bias, the ultrasound machine will be individually set up by each operator at each time point. Images/video was recorded by the operator and analysed offline using a dedicated

analysis package (McKesson Cardiology, v13.1.2, McKesson Ltd., Israel). A single operator (SP) analysed all images in a random order after anonymisation for operator and patient details, before unblinding and recording results.

2.2.3 Defining significant changes in muscle mass

Previous clinical studies demonstrated that 32 patients were required to detect a 10% reduction in RF_{CSA} over 10 days (α=0.05, β=0.10)[126] and is often used a clinical cut-off in ICU and non-ICU clinical studies.[14,126] Puthucheary *et al.,* found a 10% loss of RF_{CSA} within 7 days of ICU admission (equating to a daily loss of 1.4%). In respiratory muscle, there is a lack of normative data and defining significant loss using pre-defined cut-offs is not transferrable from data in peripheral muscle. I therefore defined 'high wasters' as those with $\geq$1.4% loss per day of RF_{CSA} when compared to their baseline measurement.

2.3 Molecular techniques

2.3.1 Enzyme-linked immunosorbent assays (ELISA)

Plasma and serum pro-inflammatory cytokines and soluble mediators related to systemic necrosis were quantified using standalone or multi-panel enzyme-linked immunosorbent assays (ELISA). Tumour necrosis factor receptor 1 (TNFR1) (R&D Systems, Minnesota, USA), Receptor-interacting serine/threonine-protein kinase 3 (RIPK3) (Cusabio, Wuhan, China) and cleaved cytokeratin 18 (CCK-18) (VLVbio, Stockholm, Sweden) were measured using standalone ELISA kits according to the manufacturer's instructions.

2.3.1.1 Multiplex ELISA assay system

A multi-analyte panel was designed using concepts like those in conventional ELISA techniques. A 14-analyte panel was designed in concordance with the manufacturer's instructions (Meso Scale

Discovery, Maryland, USA). The analytes used in the multi-panel assay are summarised in Table 2-5. The maximum number of analytes that can be analysed on a single well in a 96-well format using this assay is 10, therefore, four further analytes (VEGF, RAGE, Ang2 and FasL were included in a separate multiplex assay plate using an identical approach.

Analyte Abbreviation	Full name
TNF-α	Tumour necrosis factor alpha
IL-1α	Interleukin 1 alpha
IL-1β	Interleukin 1 beta
IL-6	Interleukin 6
IL-8	Interleukin 8
IL-10	Interleukin 10
IL-18	Interleukin 18
MCP-1	Monocyte chemoattractant protein 1
IFN-γ	Interferon gamma
TRAIL	Tumour necrosis factor related apoptosis inducing ligand
VEGF	Vascular endothelial growth factor
RAGE	Receptor for advanced glycation end-products
FasL	FS-7 associated surface ligand
Ang2	Angiopoietin 2

Table 2-5. Serum analytes used in the Meso-Scale Discovery® multiplex ELISA assay

The bespoke multiplex plates are constructed in a series of steps. The 96-well plates are specifically designed such that within each well are 10 'spots' to which manufacturer designed 'linkers' specifically bind to (Figure 2-11). Biotinylated capture antibodies, specific to an analyte, are then coupled to appropriate linker (as advised by the manufacturer. This linker-biotinylated capture antibody complex is then applied to the plate for 1 hour. A record is made of which analyte is bound to which linker and spot – as this is important in the analysis phase of the plate using dedicated software. After washing the plate, samples were then added at two-fold dilution and incubated for 1 hour. The plate is washed a further three times before capture reagents (detection antibodies conjugated with electro-chemiluminescent labels) are added. To read, a manufacturer specific instrument is used (Meso Scale

Discovery, Maryland, USA). A voltage is applied to the plate electrodes on the bottom of the plate under each well. The effect is that the captured ECL labels emit light, and the instrument measures the emitted light which is proportional to the amount of analyte present in the sample. Data is exported from the instrument as a text file and processed in Discovery Work Bench (v4.0, Meso Scale Discovery, Maryland, USA) on a personal computer. The reagents of the assay are listed in Table 2.6.

Some human plasma samples required deactivation in a category 3 laboratory facility. These samples were deactivated using Triton 0.1%. Assay standards were tested with and without Triton 0.1% with no effect on subsequent concentration.

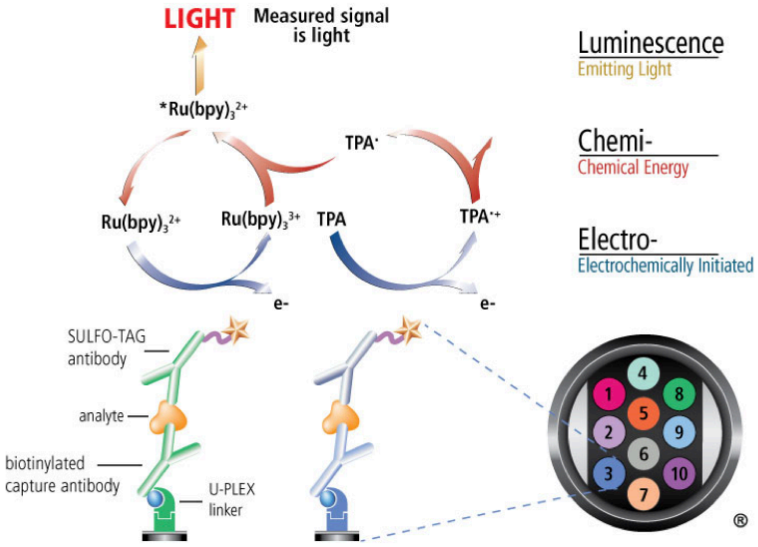


Figure 2-11. Principle and mechanism of the Meso-Scale Discovery® multiplex assay system.

Reproduced from https://www.mesoscale.com/~/media/files/product%20inserts/u-plex%20development%20pack.pdf

2.4 MUSCLE-UK study samples

Human plasma, serum and skeletal muscle tissue samples and specimens were collected as part of a prospective observational cohort study (UK-MUSCLE; NCT01106300). A consortium agreement was in

place for exchange of specimens across sites including utilisation in this thesis. Clinical and other relevant study data are detailed in the appropriate chapter.

2.4.1 MUSCLE-UK serum

Whole blood was pre-processed by the MUSCLE-UK study group and serum was stored at -80^{o}C until required for ELISA assays.

2.4.2 Human skeletal muscle experiments

2.4.2.1 Protein extraction from human skeletal muscle

Human skeletal muscle biopsies of the vastus lateralis were kindly provided by Dr Zudin Puthucheary and the UK-MUSCLE study consortium. The conchotome technique[247] was used and whole tissue specimens were snap frozen in liquid nitrogen and stored at -80^{o}C. When required, 8-20mm^{3} samples (Figure 2-12) were thawed on ice before weighing in a 2ml reinforced tube containing 2.4mm steel beads (Bertin Corp., MD, USA). 300µl of ice-cold lysis solution (RIPA buffer (Merck Life Science, UK) with 1% protease/phosphatase inhibitors and 0.5M EDTA (Thermo Fisher Scientific, MA, USA)). Samples were homogenised using high frequency homogenisation (Precellys 24, Bertin Instruments, France) at 6000 rpm for 15 second. Homogenisation was repeated if necessary. The homogenisation tube was then centrifuged at 12,000 rpm for 5 minutes at 4^{o}C to pellet debris. The supernatant was removed and aliquoted before storing at -80^{o}C before use.

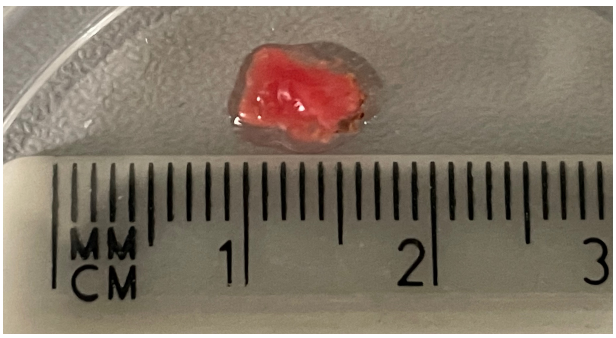


Figure 2-12. Human skeletal muscle samples for homogenisation and protein extraction

Thawed human skeletal muscle tissue of up to 20mm^3 was homogenised using steel beads for protein extraction. Samples were weighed pre-homogenisation to determine mass to protein ratio.

2.4.2.2 Protein quantification in human skeletal muscle

Protein concentration was calculated using the Bradford assay method.[248] Muscle homogenate samples were diluted 1:10 with deionised water and then a further 1:10 dilution to a final volume of 100µl in a 96 well plate. 200µl of Bradford reagent (diluted 1:4 with deionised water) was then added to each sample well before gentle agitation and measuring absorbance at 600nm for 30 seconds. The absorbance of the samples was compared to the generated standard curve of serially diluted standards of bovine serum albumin (Merck Life Science, UK). Muscle mass was positively correlated with protein concentration (µg/µl) (Figure 2-13) and consistent with published concentrations.[249]

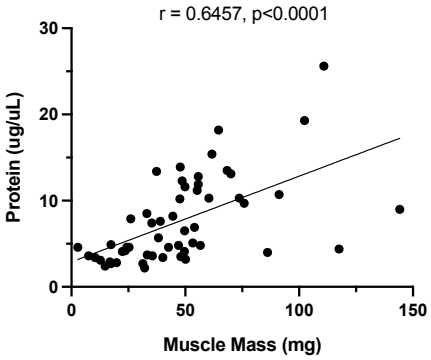


Figure 2-13. Relationship between skeletal muscle mass and protein concentration

Mass of human skeletal muscle was positively correlated with protein concentration (r=0.6457, p<0.0001) (Spearman's correlation test).

2.4.3 Western blotting

Proteins of interest in human skeletal muscle were studied using Western blotting. Materials, solutions and antibodies used for Western blotting are listed in Table 2-6Table 2-7. Target proteins identified in specimens using immunohistochemistry but thought to be present in low concentrations were selected as a positive control and immunoblotted against increasing protein loads to determine appropriate loading quantity of muscle homogenate in subsequent experiments (Figure 2-14). To balance against the appearance of non-specific bands, a loading protein mass of 50µg was chosen. To 50µg of protein, sample loading buffer (with 2.5% 2-mercaptoethanol as a reducing agent) and phosphate buffered saline were added to achieve a final loading volume of 20µl and 4x overall dilution of the loading buffer. Samples were then heated for 5 minutes at 90^{o}C.

Pre-made gels were immersed into an electrophoresis tank (XCell SureLock™, Thermofisher) (which was placed in an ice slurry) containing running buffer such that the level is above the wells of the gel. Prior to sample loading, a protein standard ladder was added to the first well to ascertain protein weight in the sample. Up to 25µL of sample, prepared as above, was carefully loaded into the well and electrophoresis was performed at a constant 200V/110mA for 60-80 minutes. The endpoint was when the sample dye reached the lower end of the gel. When complete, the gel was removed under water from the plastic casing using a spatula and placed into the transfer sandwich as described. The nitrocellulose membrane was carefully removed and cropped. The membrane was then blocked in 5% BSA for 1 hour before washing with TBST for 5 minutes for a total of 3 washes. Primary antibodies were applied overnight at 4^{o}C with gentle rocking. The membrane was then washed as above before incubating with the appropriate HRP-conjugated secondary antibody for 1 hour. A further wash was performed before the blot was developed. Excess wash was removed and ECL solution was applied to the membrane as per the manufacturer's instructions and incubated for 5 minutes. To develop the blot, chemiluminescence was performed for 5-10 minutes and then read at 600 and 700nm for 1 minute using Odyssey Fc Imaging system (LI-COR, Lincoln, NE, USA). Images were analysed using Image

Studio software v5.2.5 (LI-COR, Lincoln, NE, USA). Band intensity was normalised to the GAPDH as the housekeeping protein and loading control.

	Manufacturer and code	Details/notes
Protein gel for electrophoresis	Thermofisher NP0336BOX	NuPAGE™ 4 to 12%, Bis-Tris, 1.5 mm, Mini Protein Gel, 15-well, maximum 25µl loading volume.
Sample loading buffer (4X)	Thermofisher NP0007	NuPAGE™ LDS Sample Buffer (4X). Contains lithium dodecyl sulfate (LDS) at pH 8.5 with Coomassie G250 and phenol red as tracking dyes. Final working concentration 1x.
Protein ladder standard	Thermofisher LC5800	Novex™ Sharp Pre-stained Protein Standard Molecular weights: 260, 160, 110, 80, 60, 50, 40, 30, 20, 15, 10, 3.5 kDa Pre-Stained standard loading buffer consists of 65 mM Tris pH 6.5, 30% glycerol, 2% SDS, and 2.5 mM ETDA.
Running buffer (20X)	Thermofisher NP0001	NuPAGE™ MOPS SDS Running Buffer (20X) 50ml running buffer made up to 1L with deionised water for 1X working solution.
Wash solution	Sigma-Aldrich T9039-10PAK	Contents of pouch dissolved in 1L of deionised water to give 0.05 M Tris buffered saline (NaCl - 0.138 M; KCl - 0.0027 M); TWEEN® 20 - 0.05%, pH 8.0.
Phosphate buffered saline	Sigma-Aldrich59331C-1000ML	Calcium and magnesium free.
Transfer stack	Invitrogen IB301001	Nitrocellulose membrane with 0.2 µm pore size. Transfer 'sandwich' (bottom to top): Anode side with nitrocellulose membrane, gel, wet filter paper, cathode end with copper conducting surface, sponge sandwich placed into iBlot transfer system (Thermofisher) and run for 7 minutes.
Bovine serum albumin		5% BSA used as blocking solution. 3% BSA used to dilute primary and secondary antibodies.
Chemiluminescence reagent	Thermofisher, 32134 Thermofisher, 34094	Sensitive to detect protein concentrations from low picogram to mid-femtogram. Ultra-sensitive to detect protein concentrations from low to mid-femtogram

Table 2-6. Materials and reagents used in Western blotting experiments

Antibody	Type	Manufacturer and code	Details/concentrations
Phospho-MLKL	Primary	Abcam, 187091	Source: Rabbit 1:1000 dilution with 3% BSA
RIPK3	Primary	Thermofisher, 711691	Source: Rabbit 1:1000 dilution with 3% BSA
GAPDH	Housekeeping protein	Cell Signalling, 97166	1:1000 dilution with 3% BSA
Anti-rabbit HRP-linked IgG	Secondary	Thermofisher, G21234	Source: Goat 1:1000 dilution with 3% BSA
Anti-mouse HRP-linked IgG	Secondary	Cell Signalling, 7076S	1:1000 dilution with 3% BSA Source: Horse

Table 2-7. Primary and secondary antibodies used in Western blot experiments

RIPK3; receptor interacting protein kinase 3, GAPDH; glyceraldehyde 3-phosphate dehydrogenase; HRP; horseradish peroxidase, BSA; bovine serum albumin.

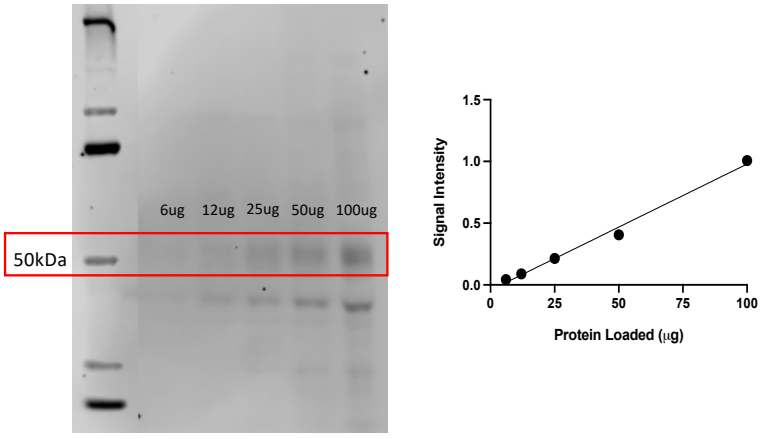


Figure 2-14. Protein loading for target protein detection in skeletal muscle homogenate

Immunoblot of 6ug, 12ug, 25ug, 50ug and 100ug skeletal muscle protein for detection of pMLKL (molecular weight 54kDa) (left). Plot of signal intensity of immunoblot band against protein load demonstrated a linear detection range (right).

2.4.3.1 Western blotting controls

Following identification of positive protein bands for pMLKL at 54kDa, a single patient sample was used as a positive control (after repeatedly identifying the protein of interest). Furthermore, reliability of this positive protein band was reviewed alongside immunohistochemical staining in the same patient. To ensure antibody specificity, controls with no protein load and secondary antibody only were used are shown in Figure 2-15. pMLKL protein band was not seen in either control experiment, thus demonstrating good antibody specificity.

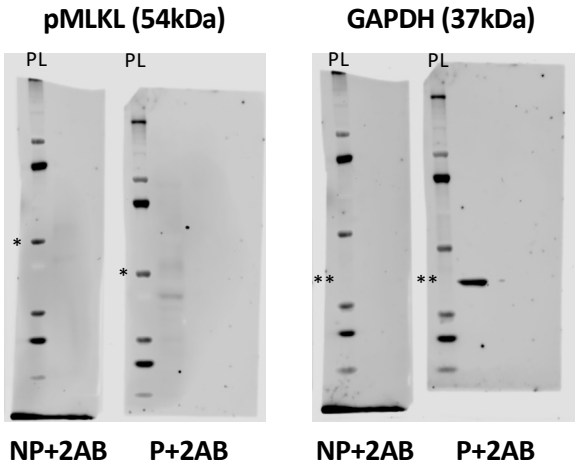


Figure 2-15. Western blotting controls

To determine secondary antibody specificity, protein loading with and without secondary antibody was performed. In NP+2AB experiments, there is absence of the protein band of interest (54kDa) and housekeeping protein (37kDa) as expected. *PL; protein standard ladder, NP; no protein, P; protein, 2AB; secondary antibody.*

2.4.4 Immunohistochemistry of human skeletal muscle

2.4.4.1 Preparing tissue sections of human skeletal muscle

The frozen muscle biopsy samples were sectioned on a Cryostat (Bright Instrument Company Limited, Cambridgeshire, UK) at -20^{o}C with a section thickness of 10 μm. Cut sections were collected on poly-L-lysine slides, dried for at least 1 hour and then stored at -80^{o}C until required. After thawing, sections

were drawn around using a hydrophobic pen before being fixed with 4% paraformaldehyde (PFA) for 10 minutes at room temperature. The PFA was removed, and the sections washed three times with PBS. Sections were then blocked for 1 hour in 5% bovine serum albumin (BSA) (5g BSA in 100ml PBS) before a further wash with PBS. The sections were then incubated with the primary antibodies (Table 2-8) in 1% BSA in a moist chamber at room temperature. After incubation, the sections were washed three times with PBS and once with deionised water. The sections were then incubated for 1 hour with the appropriate secondary antibody (Table 2-8) (made 1:1000 with 1% BSA in a moist chamber at room temperature). Sections were washed a further three times with PBS and once more with deionised water before mounting in mounting medium with containing DAPI.

Antibody	Type	Host	Dilution	Isotype	Source
pMLKL	Primary	Rabbit	1:250	IgG	Abcam, ab1877091
RIPK3	Primary	Rabbit	1:500	IgG	Thermofisher, 711691
Laminin	Primary	Mouse	1:4	IgG2a	DHSB, 2e8
Alexa Fluor 488	Secondary	Goat	1:1000	IgG	Thermofisher, A21121
Alexa Fluor 594	Secondary	Goat	1:1000	IgG	Thermofisher, A11012
DAPI	Nuclear	n/a	1:1000	n/a	Thermofisher, D1306

Table 2-8. Primary and secondary antibodies used in immunohistochemistry

pMLKL; phosphorylated mixed-lineage kinase like, RIPK3; receptor interacting protein kinase 3, DAPI; 4',6-Diamidino-2-Phenylindole, Dihydrochloride, Ig; immunoglobulin.

2.4.4.2 Fluorescence microscopy

Histological sections were fixed (4% PFA for 10 minutes), blocked (1% BSA for 1 hour) then stained with primary antibodies (1% BSA overnight at 4 ^{o}C). Sections were washed three times with PBS then

incubated with appropriate secondary antibodies (1 hour at room temperature). Sections were then cover slipped and imaged using two different imaging systems.

2.4.4.3 Widefield microscopy

Widefield microscopy was used to determine spatial distribution of specific immunostaining. All microscopy was prepared and conducted in fixed and stained coverslips and imaged using an Axiovert upright microscope (Zeiss, Germany) equipped with 10x, 20x and 40x air objectives with a charge-coupled device (CCD) camera. Exposure time and LED power for each fluorophore were keep constant between sections from the same patient and all sections from the same patient were imaged in the same microscopy session.

The microscope was contained within a dark room with no external light. Images were acquired using Axiovision software (version 4.3.2 Carl Zeiss Microimaging, Germany) on a microscope-linked PC. Before capture of images, the light path to the camera was blocked to produce a 'black reference'. This black image is the dark noise level within the camera. This step was performed at the beginning of each microscopy session and the reference image was applied to all the subsequent images. Fluorescence was detected based on the emission wavelengths in blue, green and red spectrum range according to the secondary antibody being studied. Slides were initially viewed to visualise nuclei stained with DAPI and 10-20 images captured per section after calibration of each channel and reduction of background and/or excessive noise-signal. To determine the optimum exposure time and prevent over-saturation of images of each fluorophore, samples were selected based on what was perceived to have the highest expression. For example, DAPI and laminin would be best visualised in earlier samples and pMLKL in later ones.

2.4.4.4 Confocal microscopy

Large images were acquired using NIS Elements software (Nikon Corporation, Japan) on a Nikon Eclipse Ti Inverted spinning disk confocal microscope equipped with a Yokogawa CSU-X1 disk head and an Andor Neo sCMOS camera at x20 magnification with illumination via laser excitation of fluorophores at 405nm, 488nm and 561nm (Nikon Corporation, Japan). Individual fields were combined within NIS elements using 15% stitching overlap to produce larger image areas. After acquisition maximum intensity projections were created using ImageJ. This was performed in Nikon Imaging Centre, King's College London, Guy's Hospital Campus.

2.5 Data handling

Clinical, physiological and imaging data collected from clinical trials were entered on to secure spreadsheets using Microsoft Excel (Microsoft, WA, USA) and stored on a secured hospital network drive. Data was transferred to and analysed in GraphPad Prism 9 (GraphPad, CA, USA) or SPSS v27 (IBM, New York, USA) software statistical software packages as required.

2.6 Statistical analysis

All quantitative data was tested for normality using histogram analysis and Shapiro-Wilk tests using GraphPad Prism v9.0 (GraphPad, CA, USA) before performing statistical analyses. For all analyses, a conventional alpha level of 0.05 will be set for level of statistical significance.

Tabulated data are presented as mean ± standard deviation (SD) or median (interquartile range) (IQR). Student's t-test or Mann-Whitney U tests were used to study differences between two groups after normality testing as above. When comparing data with two or more groups, one way analysis of variance (ANOVA) or Kruskal-Wallace tests were used if the data was normally or non-normally distributed respectively. Correlation between continuous data was assessed using Pearson correlation

coefficient or Spearman correlation coefficient if data was normally or non-normally distributed respectively.

Measurement reliability was assessed using a two-way mixed model of the intra-class correlation coefficient (ICC) for absolute agreement. ICC will be used to determine Inter-observer reliability using two-way random effects for absolute agreement. The following reliability criteria will be used: 0.00-0.49 indicates poor agreement, 0.50-0.74 moderate agreement and 0.75-1.00 indicates excellent agreement.[250] Bland-Altman analysis will be examined to provide a visual representation of the agreement between assessors and to examine whether there was a systematic error present.

In the MUSCLE-ICU study, logistic regression was used to determine independent predictors of low skeletal muscle index, low skeletal muscle density and ICU mortality. Multivariate, logistic regression analysis was performed to examine independent variables and their relationship to outcomes (ICU survival and 90-day survival). These data tables were constructed and analysed in SPSS v27 (IBM, New York, USA). In addition, univariate and multivariate linear regression was performed to examine relationships between independent variables and extent of L3-SkM_{CSA} loss at the time of a second imaging study. Independent variables were chosen a priori after determining their significance to the outcomes: gender, body mass index, COVID19 status, ECMO therapy, skeletal muscle index (SMI) per 10cm^2, skeletal muscle density (SMD) per 10 HU. Multi-variate regression models were then constructed with adjustment for variables that were statistically significant ($p \leq 0.1$). Association with high and low SMI or SMD were also studied (in place of quantitative measurements) using individual patient cut off values based on age, BMI and gender.[168]

Associations between categorical variables were assessed using Chi-squared or Fisher's exact test depending on the number of data points. Additional statistical methods are detailed in the relevant chapters.

Chapter 3: Assessment of skeletal muscle wasting in critical illness using computed tomography imaging

3.1 Background

The number of admissions to ICU in the UK is rising[2] and is expected to continue owing to an ageing population, advances in treatment and utilisation of healthcare services. Despite modernisation and advancement of critical care services, long term restriction in survivors of critical illness has been shown to persist for up to 5 years and represents a significant public health issue. This was described in two important studies by *Herridge et al.,* [10,11] that looked at 109 survivors of critical illness secondary to severe ARDS at 1 and 5 years and the adverse effects on physical function, mental wellbeing and quality of life. A key finding was that at 1 year, survivors reported physical restriction, or more specifically, muscle wasting and weakness as the cause to their limitation – determined by a lower 6 minute walk test distance (6MWT) than predicted (achieving only a mean of 66% predicted distance at 1 year).[11] Muscle weakness was again highlighted as a cause for impairment in a separate study by *Poulsen et al.,* in a non-ARDS cohort at 1 year[12]. Finally, *Herridge et al.,* also found that 49% of survivors returned to work at 1 year[10] (rising to 77% at 5 years[11]) and utilised healthcare services more in the same period with muscle weakness an underlying factor.

Muscle wasting occurs early in critical illness,[15] and muscle mass declines sharply within 7-10 days[14] and is associated with disease severity and multi-organ failure.[14] Muscle weakness has also been shown to be an independent predictor of mortality, associated with prolonged MV and longer hospital length of stay,[16,17] and therefore warrants methods for early identification and intervention. There is a paucity of literature describing the trajectory of skeletal and respiratory muscle wasting in critical illness, particularly in patients with SARF – a group that has an associated mortality of up to 40%.[251]

ICUAW is often diagnosed late[31] and predicting which individuals are most at risk is difficult. This highlights an important need for widely applicable and accessible diagnostic tools that can identify those at risk. CT imaging has been applied in a range of disease states to quantitatively assess skeletal muscle wasting.[165,171,240,252] Muscle mass can be quantified using a single axial slice of abdominal CT imaging at the L3 level.[166] This can then be used to determine the skeletal muscle index (SMI) (cross-sectional area at L3 / height squared) to provide an accurate representation of total body skeletal muscle.[253] Based upon this analysis, there are published clinical thresholds for determining low skeletal muscle mass state by gender alone,[254] or by gender, age and BMI in combination.[168] The L3 level of an abdominal CT provides cross sectional areas of several muscle groups: *erector spinae, quadratus lumborum, psoas, transversus abdominis, internal and external oblique, and rectus abdominis*. Respiratory muscles *(diaphragm, parasternal, intercostals, scalene, sternocleidomastoid, pectoralis)* changes during critical illness have not been described using this technique. Poor muscle *quality* may be a predictor of poor outcome and this has been shown in studies measuring muscle quality using both ultrasound[133] and most recently CT scan where poor muscle quality was found to be an independent predictor of mortality in critically ill patients.[165] Fatty infiltration of the muscle (myosteatosis) has also been reported as a causal factor in declining muscle quality which correlates with a loss of function in survivors of critical illness.[47] Myosteatosis can be measured on CT scan using skeletal muscle density (SMD) and the intermuscular adipose tissue (IMAT).[165] These data suggest that determining the total amount of muscle mass, the trajectory of muscle wasting and the associations with clinical outcomes, may help to guide future assessment and potentially interventions in other clinical populations.

In our tertiary centre, which cares for patients with severe respiratory failure and those undergoing complex cardiothoracic surgery (including heart and lung transplantation) commonly have a baseline CT scan of the chest and abdomen (and sometimes pelvis) as part of routine care. Depending on the clinical course of the patient, a second CT scan is frequently required. Therefore, I sought to utilise

these scans to investigate the trajectory of muscle mass loss in such patients and its association with defined clinical outcomes.

This chapter describes the changes in skeletal muscle mass and quality using CT imaging in patients with severe acute respiratory failure (SARF)/acute respiratory distress syndrome (ARDS), including those with severe COVID19 infection.

3.1.1 The Coronavirus Disease 2019 pandemic

SARS-CoV-2, which causes Coronavirus Disease 2019 (COVID19) has led to a global pandemic in humans. COVID19 has significantly impacted on healthcare utilisation across the world and certainly within the UK and specifically critical care services. The UK has seen a spike in admissions to ICU, with over 10,000 admissions to ICU from 1st March 2020 to 31 May 2020, which translates to approximately 3% of all reported cases. COVID19 is pro-inflammatory, pro-thrombotic and commonly presents as SARF.[106,107] As explained above, severity of illness impacts discharge outcomes of function, psychological state and quality of life, long after leaving the ICU. Thus, patients with SARF and COVID19 disease represent a patient population requiring high levels of mechanical ventilatory support (and often extracorporeal membrane oxygenation (ECMO) support) when admitted to the ICU – and therefore pose a high risk for muscle wasting, weakness and prolonged physical restriction should they survive the acute phase and ICU admission. There is currently no description of the onset, severity and trajectory of muscle wasting in severe COVID19 infection. It is therefore important that the degree of muscle wasting is described as this may predict the number of people with long-term physical restriction and likely to utilise healthcare services for a prolonged period.

3.2 Aims

1. To investigate the quantitative and qualitative CT imaging changes in skeletal muscle during severe critical illness and associations with clinical outcome.
    a. Determine intra- and inter-observer reliability for CT imaging assessment of skeletal muscle.
    b. Describe the incidence of low muscle mass states in critical illness.
    c. Determine the change in muscle quantity and quality in critical illness.
    d. Determine whether changes in muscle quantity and quality during critical illness from severe COVID19 infection differs from the trajectory of non-COVID19 SARF.

3.3 Hypotheses

1. SARF and critical illness is associated with significant muscle wasting during critical illness.
2. Changes in muscle mass and muscle quality changes are associated during critical illness.
3. The extent of muscle wasting and changes in muscle quality does not differ between COVID19 and non-COVID19 SARF.

3.4 Methods

3.4.1 MUSCLE-ICU Study

To investigate these aims, a retrospective, observational study was designed (MUSCLE-ICU, see 2.1.1 for study design and patient selection). In brief, the study utilised clinical and radiological data collected as part of routine care of patients in an ICU at a tertiary centre, specialising in the management of severe respiratory failure. The study was registered with the Health Regulatory Authority (HRA) (IRAS project ID: 285418 and ethical approval was granted via the Research and Ethics Committee (REC) (Fulham, London) (REC reference: 20/HRA/4756). The study was sponsored by Imperial College London (reference: 20IC6279).

3.4.2 Computed tomography image acquisition

A database query of CT scans performed at The Royal Brompton Hospital, London, in the study period was cross-referenced with those patients who satisfied the eligibility criteria (see 2.1 and 2.1.1 CT studies were performed by the department of radiology at The Royal Brompton Hospital in line with local clinical protocols and policy and transferred for viewing using IMPAX software (Agfa-Gevaert, Mortsel, Belgium). CT studies with and without contrast were included. Briefly, linked coronal and sagittal views of eligible CT scans were studied to determine the middle of L3 vertebrae. In some cases, reconstructed images of both coronal and sagittal images were not available and, in these cases, manual localisation in one view was performed. Five-millimetre axial slices were selected to retain image quality and reduce artefact. Following this, single slice images were saved as Digital Imaging and Communications in Medicine (DICOM) files for analysis. If 5mm reconstructions were not available, then the next thickest slice was selected. Each CT slice was assessed for suitability and quality using a soft-tissue window setting and the following criteria: (1) all muscle groups visible in image, (2) no artefacts traversing the tissue groups and (3) ideally, the axial slice should visualise both transverse processes of the third lumbar vertebrae. Images were excluded if the two operators felt that the quantification was likely to be inaccurate at the time of analysis.

Analysis software (ImageJ and slice-O-matic) was used to analyse skeletal muscle density with a Hounsfield unit range of -29 to +150. In the more specialised analysis software, slice-O-matic, four tissue densities (skeletal muscle (SkM) [-29 to +150], intra-muscular adipose tissue (IMAT) [-190 to -30], visceral adipose tissue (VAT) [-150 to -50] and subcutaneous adipose tissue (SAT) [-190 to -30]) were analysed (see 2.1.1.3

3.4.3 Software selection and image analysis

Cross-sectional area of skeletal muscle was initially assessed using ImageJ – a software package with well established, open-access protocols for the analysis of skeletal muscle.[166] ImageJ was limited to

calculation of cross-sectional area only. The outer border of muscle groups was manually delineated to generate the first region of interest (ROI) (Figure 3-1). Tissues with density consistent with muscle tissue within this ROI were then highlighted by setting the viewing threshold to -29 to +150 HU (A1). Next, the inner border of the abdominal muscles was manually delineated and highlighted using the same HU range (A2). Lastly, the third lumbar vertebrae was delineated and an area calculated (A3). SkM_{CSA} was calculated: [(A1-A2-A3)/100]. Each image was analysed twice for intra-observer reliability and between operators (inter reliability). Image analysis using slice-O-matic is detailed in 2.1.1.2

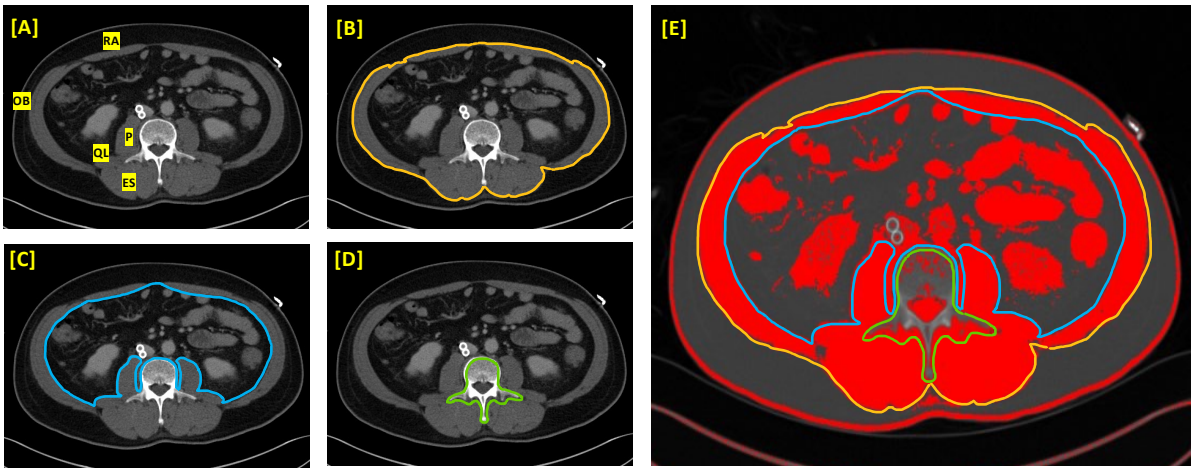


Figure 3-1. Muscle quantification using CT imaging and ImageJ software

Stepwise analysis of skeletal muscle using axial CT images. [A] demonstrates the muscle anatomy in the L3 CT slice: *RA=rectus abdominis, P=psoas, QL=quadratus lumborum, ES=erector spinae, OB=oblique muscles (internal oblique and external oblique).* [B] Outer border of L3 muscles. [C] Inner border of L3 muscles. Structures within the boundaries of (B) and (C) b represent the total skeletal muscle area. The structures bounded by (C) only are abdominal viscera. [D] L3 vertebral body area. [E] Merged images of B-D. The solid red line represents the abdominal perimeter.

3.4.4 CT assessed skeletal muscle wasting – a pilot study

In a small pilot study, I sought to determine the feasibility of quantitative muscle measurements and describe the acuity of wasting in patients with ARDS who presented to hospital, received MV and veno-venous extracorporeal membrane oxygenation (vvECMO) and underwent thoracic and abdominal CT imaging within 24-hours. These strict criteria ensured an initial measurement of muscle

mass was as close to pre-morbid baseline as able. A retrospective query of the hospital database identified 18 patients who satisfied the criteria. Skeletal muscle mass was measured using ImageJ as detailed in 3.4.3 . Clinical thresholds to determine low muscle mass states as per SMI were set as <55.4cm^2/m^2 for males and <38.9cm^2/m^2 for females as per previous clinical studies.[172,240] The results of this study has been published in abstract form (see **Error! Reference source not found.**).[255]

3.5 Statistical analysis

Continuous variables are presented as mean (± standard deviation) or median (interquartile range) after testing for a normal distribution data using Shapiro-Wilks test. Parametric data were compared using Student's t test and non-parametric data using Mann-Whitney U or Wilcoxon signed rank test where applicable. A conventional alpha level of 0.05 will be set for level of significance. Measurement reliability will be assessed using a two-way mixed model of the intra-class correlation coefficient (ICC) for absolute agreement. ICC will be used to determine Inter-observer reliability using two-way random effects for absolute agreement. The following reliability criteria will be used: 0.00-0.49 indicates poor agreement, 0.50-0.74 moderate agreement and 0.75-1.00 indicates excellent agreement.[250] Bland-Altman analysis will be examined to provide a visual representation of the agreement between assessors and to examine whether there was a systematic error present.

A multivariate, logistic regression analysis was performed to examine independent variables and their relationship to outcomes (ICU survival and 90-day survival). In addition, univariate and multivariate linear regression was performed to examine relationships between independent variables and extent of L3-SkM_{CSA} loss at the time of a second imaging study. Independent variables were chosen a priori after determining their significance to the outcomes: gender, body mass index, COVID19 status, ECMO therapy, SMI per 10cm^2, SMD per 10 HU. SMI is a well-regarded measure of total body skeletal muscle mass. Similarly, SMD utilises tissue specific density as a measure of muscle quality. Multi-variate regression models were then constructed with adjustment for variables that were statistically

significant ($p \leq 0.1$). Association with high and low SMI or SMD were also studied (in place of quantitative measurements) using individual patient cut off values based on age, BMI and gender.[168]

3.6 Results

3.6.1 Skeletal muscle wasting pilot study cohort

Eighteen patients (12 (67%) male, median age 47 years (IQR 37-55), body mass index 32.1±10.1) with a diagnosis of severe ARDS, who presented to hospital *and* received MV *and* vvECMO *and* underwent thoracic and abdominal CT imaging within 24-hours were included. ImageJ was used to quantify skeletal muscle cross sectional area on axial CT images.

3.6.1.1 High intra- and inter-observer reliability achieved using ImageJ CT muscle analysis

In the pilot study, 36 pseudonymised images (two per patient) were analysed by two clinicians (SP and HS) ('the raters'). Axial DICOM files were prepared by a third clinician (FL) such that demographics, dates and clinical data were not known to either rater. SP and HS agreed on the analysis protocol in advance. The first and second images were analysed seven days apart to avoid recall bias. Once SP and HS completed the analysis, FL unblinded the image files for further analysis. Bland-Altman plots and correlation plots of scores of each rater and between raters are shown in Figure 3-2. Excellent intra- and inter-rater reliability was obtained for L3-SkM_{CSA} (ICC operator 1 (SP): 0.997 [0.994-0.998], ICC operator 2 (HS) 0.985 [0.972-0.992], inter-rater ICC 0.935 [0.757-0.974]).

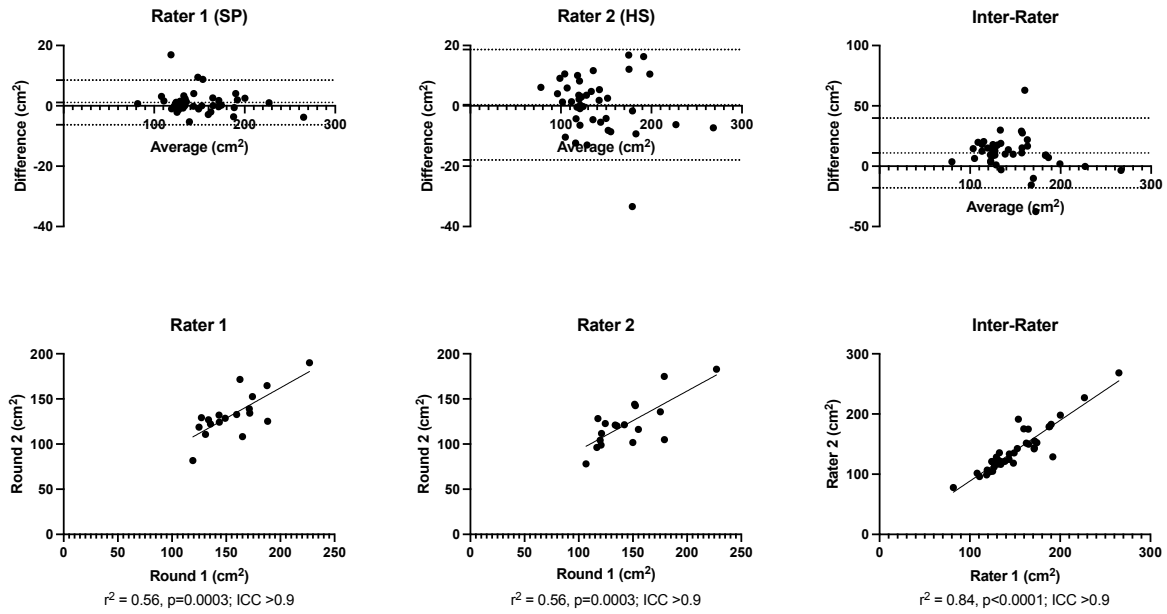


Figure 3-2. Intra and inter-rater correlation and reliability for skeletal muscle cross-sectional area using ImageJ

Skeletal muscle cross-sectional area at L3 level on axial CT images using ImageJ software. (Top Row): Bland-Altman (B-A) plots of each rater and inter-rater data. The difference between measurements is shown on the y-axis and the average on the x-axis. Limits of agreement are shown as dotted horizontal lines on each B-A plot. There was excellent intra- and inter-rater correlation and reliability (ICC operator 1 (SP): 0.997 [0.994-0.998], ICC operator 2 (HS) 0.985 [0.972-0.992], inter-rater ICC 0.935 [0.757-0.974]).

Table 3-1 summarises the radiological and admission data of the cohort. The interval between admission CT imaging and a second imaging study was 8 days (IQR 5-13). There was a significant decline in L3-SkM_{CSA} between the first and second CT scan (12.1% (IQR -20.8 --7.1), p<0.001)) – equating to a daily decline of 1.3% of skeletal muscle mass per day (IQR -2.6--0.5) and suggesting atrophy occurs acutely. All patients with a low muscle mass state (9/18, 50%), and termed 'sarcopenic', as determined by the SMI at admission were male. Males also had a significant decline in SMI of 14.8% (IQR -22.5--11.3), p<0.001). Skeletal muscle atrophy (10% over 7 days, or 1.4%/day[14]) was not significantly different between males and females (male: 58% vs. female: 33%). Patients with low SMI at admission (9/18, 50%) had clinically significant differences in ICU length of stay (LoS) (35

days (IQR 17-44) vs. 19 days (IQR 9-26), p=0.08), duration of mechanical ventilation (35 days (IQR 17-44) vs 21 days (IQR 8-26), p=0.07) and duration of vvECMO (22 days (IQR 8-29) vs. 7 days (6-18), p=0.31) (Table 3-1). These results suggest that severe respiratory failure and the use of vvECMO may lead to more severe skeletal muscle atrophy. The differences in length of MV and vvECMO are clinically significant with the potential for greater incidence of complications and negative ICU sequalae. To investigate this further I studied a larger cohort with SARF/ARDS, including those with severe ARDS secondary to COVID19 disease.

Radiological calculations	***CT Scan 1***	***CT Scan 2***	***p value***
$SkM_{L3\text{-}CSA}$ – cm^2	151.0±28.7	128.0±25.2	<0.001
Skeletal Muscle Index (cm^2/m^2)	Male: 52.4±8.4 Female: 45.3±7.8	Male: 43.2±7.2 Female: 40.8±9.4	<0.001 0.07
Sarcopenia – no. (%)**	Male: 9/12 (75%) Female: 0/6 (0%)	Male: 9/12 (75%) Female: 2/6 (33%)	
Presence of sarcopenia at admission	***Yes***	***No***	***p value***
Mechanical ventilation days – no.	35 (17-44)*	21 (8-26)	0.07
ICU length of stay (days) – no.	35 (17-44)*	19 (9-26)	0.08
vvECMO days – no.	22 (8-29)*	7 (6-18)	0.31

Table 3-1. Admission and CT measurements of skeletal muscle pilot study cohort.

All values given as mean±standard deviation unless otherwise stated. *SMI; Skeletal Muscle index – calculated by dividing the cross-sectional area at L3 in cm squared by height (m) squared. *median (inter-quartile range). **Sarcopenia was classified by a SMI of <38.9 cm^2/m^2 (females) and <55.4 cm^2/m^2 (males).*[172,240]

3.6.2 Investigating inter-software variability in CT imaging muscle analysis

Before analysing the patient cohort in the MUSCLE-ICU study, I sought to compare ImageJ with another software package – sliceOmatic (Tomovision, Canada)) which has dedicated and automated functions to quantify tissue area and density, the latter of which is associated with muscle quality. SliceOmatic has been utilised and validated in a number of clinical studies.[165,166,172,174] Twenty

randomly selected images from eligible patients in the MUSCLE-ICU study were used in a reliability study comparing two raters (SP, rater 1 and NR, rater 2) using ImageJ and sliceOmatic. The primary aim was to determine intra- and inter-observer reliability for each software package with a view to utilise one in the main MUSCLE-ICU study. Analysis protocol was agreed by SP and NR in advance, but image suitability criteria was as described in 3.4.2 . Bland-Altman and correlation plots of skeletal muscle cross-sectional area using ImageJ and sliceOmatic are shown in Figure 3-3 and Figure 3-4 respectively. Bland-Altman and correlation plots of inter-software comparisons are shown in Figure 3-5.

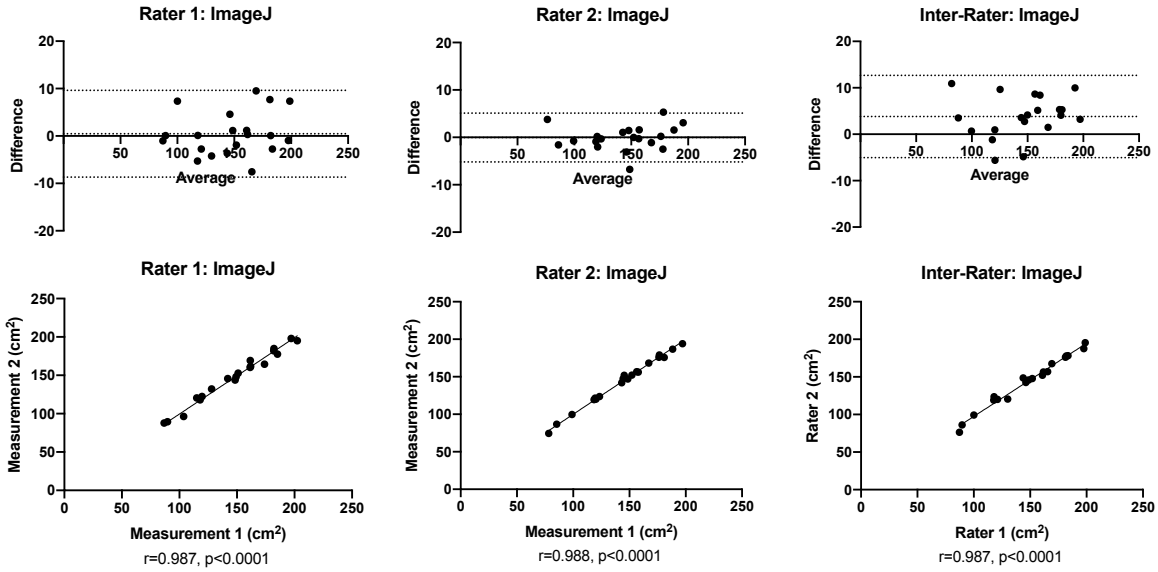


Figure 3-3. Intra and inter-rater correlation and reliability for skeletal muscle cross-sectional area using ImageJ in MUSCLE-ICU patients

Skeletal muscle cross-sectional area at L3 level on axial CT images of patients from the MUSCLE-ICU study, analysed using ImageJ software. (Top Row): Bland-Altman (B-A) plots of each rater and inter-rater data. The difference between measurements is shown on the y-axis and the average on the x-axis. Limits of agreement are shown as dotted horizontal lines on each B-A plot. There was excellent intra- and inter-rater correlation and reliability (>0.9). ICC for both intra- and inter-rater analyses are displayed under the respective graph.

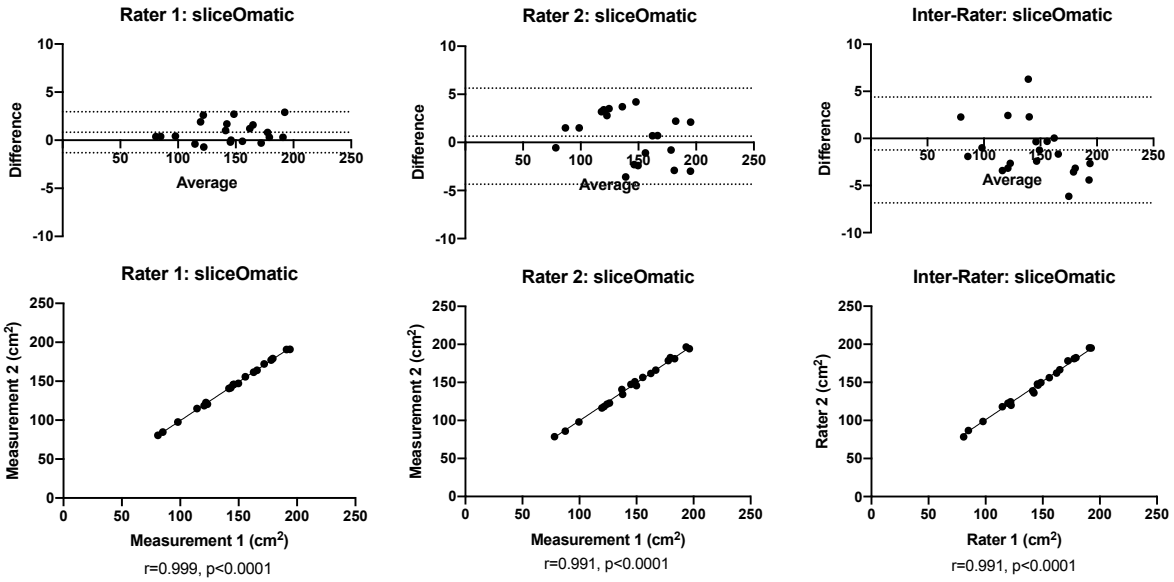


Figure 3-4. Bland-Altman and correlation plots of skeletal muscle cross-sectional area data using sliceOmatic in MUSCLE-ICU patients.

(Top Row): Bland-Altman (B-A) plots of each rater and inter-rater data. The difference between measurements is shown on the y-axis and the average on the x-axis. Limits of agreement are shown as dotted horizontal lines on each B-A plot. There was excellent intra- and inter-rater correlation and reliability (>0.9). ICC for both intra- and inter-rater analyses are listed in Table 3-2.

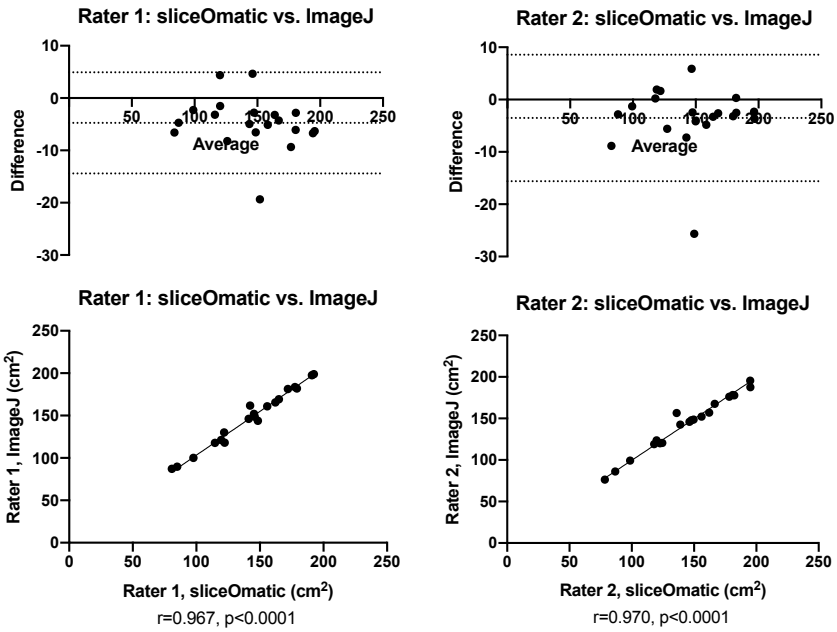


Figure 3-5. Bland-Altman and correlation plots comparing skeletal muscle cross-sectional area data using ImageJ and sliceOmatic.

(Top Row): Bland-Altman (B-A) plots of each rater and inter-rater data. The difference between measurements is shown on the y-axis and the average on the x-axis. Limits of agreement are shown as dotted horizontal lines on each B-A plot. There was excellent intra- and inter-rater correlation and reliability (>0.9). ICC for both intra- and inter-rater analyses are listed in Table 3-2.

	Rater 1 (SP)	Rater 2 (NR)	Inter-Rater
sliceOmatic	1.000 (0.998-1.000)	0.999 (0.996-0.999)	0.998 (0.994-0.999)
ImageJ	0.995 (0.989-0.998)	0.999 (0.996-0.999)	0.992 (0.954-0.998)
sliceOmatic vs. ImageJ	0.990 (0.913-0.997)	0.993 (0.983-0.997)	N/A

Table 3-2. Intra-class correlation coefficients for quantitative analysis using two software packages

Summary of intra-class correlation coefficients from Figures 3-3, 3-4 and 3-5. ICC is expressed as ICC (95% confidence interval).

Excellent agreement was achieved for both raters using each software package (Table 3-2) and is consistent with other comparative studies.[167] Comparing raters, the limits of agreement (LoA) of measurements obtained using ImageJ were wider compared to sliceOmatic (-5.1 to 12.7 vs. -6.8 to 4.4 respectively) and the differences in measurements between the two packages were significantly different ($p<0.001$). In this reliability study, I found that on average, analysis of a single axial image took between 4-9 minutes to fully analyse using our protocol on sliceOmatic and 10-14 minutes on ImageJ. In addition, sliceOmatic also allows additional quantification of other tissue densities (i.e. adipose tissue) with relative ease. Therefore, the consensus agreement between raters was to use sliceOmatic in the MUSCLE-ICU study.

3.6.3 MUSCLE-ICU Study

In the primary study period of January 2018 to February 2021, 580 patients were screened for eligibility (Figure 3-6). From a previous pilot study as part of a BSc project (student NR) in our group, 27 additional patients were added from a search between 2013 and 2018. After exclusions, 346 patients were included in the final analysis (230 male (66%); age 47 years (38-57)), of which 137 patients (40%) had a diagnosis of SARF secondary to COVID19 infection. On admission, SMI was 45.1 cm^2/m^2 (IQR 38.9-52.7) and SMD was 34.4 HU (IQR 28.3-40.3). There were clinically significant elevated levels of CRP on admission (205 mg/L (IQR 121-131)) indicating high levels of inflammation. Eighty-two percent of patients received vvECMO for a median of 16 days (IQR 9-29) and MV for 20 days (13-33).

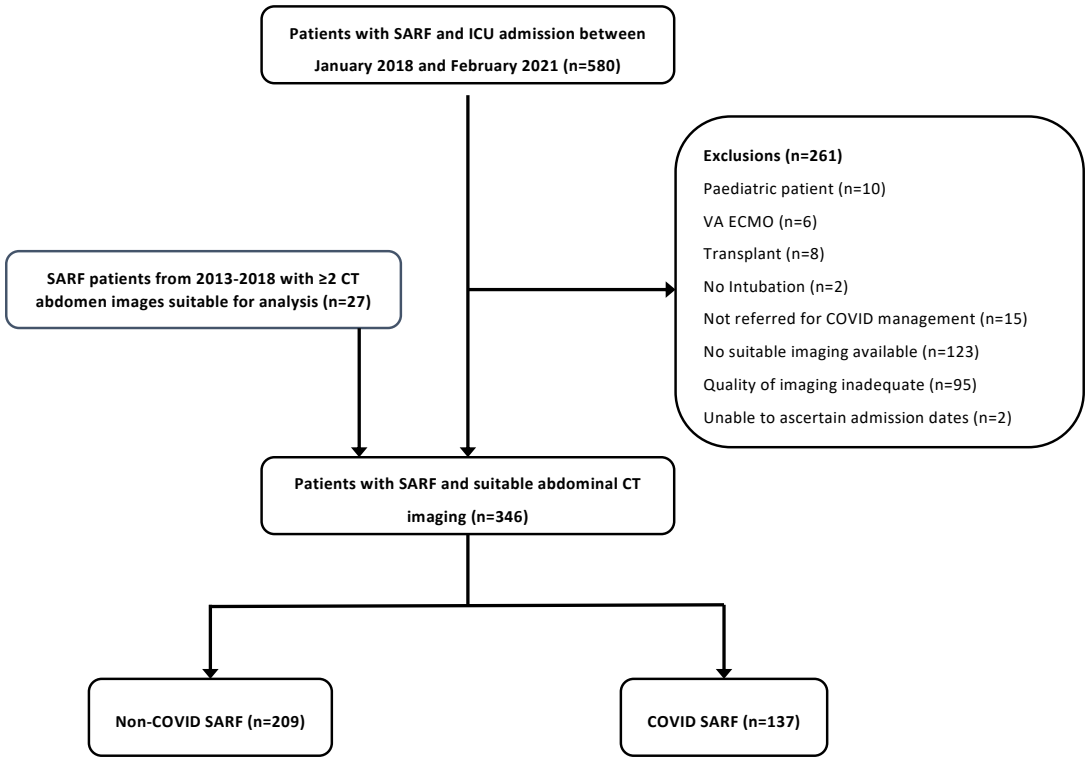


Figure 3-6. Consort diagram for the MUSCLE-ICU study

SARF; severe acute respiratory failure, ICU; intensive care unit, CT; computed tomography, VA ECMO; veno-arterial extracorporeal membrane oxygenation.

3.6.4 Clinical characteristics of critically ill patients with low muscle mass

From the study cohort, 98/345 (28%) patients had a low SMI on their admission CT image when stratified by age, sex and BMI. Similarly, 86/345 (25%) of patients had a low SMD on admission CT when stratified by age, sex and BMI. Clinical and ICU admission characteristics of patients with low and normal SMI/SMD are summarised in Table 3-3. On admission to the ICU, there were significantly more male patients with low SMI than those with a normal SMI (74/98 (76%) vs. 155/247 (45%), p=0.023). Patients from Black, Asian and minority ethnic (BAME) groups were more likely to have a lower SMI on admission to the ICU (BAME: 59/98 (60%) vs. non-BAME: 39/98 (40%), p=0.0003). Patients with lower SMI also had significantly lower SMD on admission (low SMI: 31.4 HU (IQR 24.7-36.7) vs. normal SMI: 35.3 HU (IQR 29.6-40.8), p<0.0001). Intramuscular adipose tissue (IMAT) was higher in patients with low SMI on admission (low SMI: 5.2cm^2 (IQR 2.8-9.0) vs. normal SMI: 3.5cm^2

(IQR 1.5-6.6), p=0.0003). Similarly, patients with low SMD also had higher IMAT on admission (low SMD 8.3cm^2 (IQR 5.6-13.7) vs. normal SMD (3.1cm^2 (IQR 1.4-5.2), p=<0.0001).

Severity of illness, as per APACHE II score, was not significantly different between patients with normal and low SMI (normal SMI: 16 (IQR 13-20) vs. low SMI: 16 (IQR 13-19), p=0.203) corresponding to a mortality of approximately 25%.[73] A greater proportion of patients with normal SMI required vvECMO than those with low SMI (low SMI: 70/98 (71%) vs. 213/247 (86%), p=0.002), however, the duration of vvECMO was significantly longer in those with low SMI (low SMI: 21 days (IQR 11-34) vs. 14 days (IQR 8-27), p=0.004) and patients with low SMI/SMD also had a longer length of stay in the SARF centre (low SMI: 24 days (IQR 15-35) vs. normal SMI: 18 days (IQR 11-31), p=0.007; low SMD: 27 days IQR 13-39) vs. normal SMD: 19 days (IQR 12-31), p=0.035).

Patients were admitted to the ICU within 1 day (IQR 0-4) of hospital admission in both normal and low SMI groups (p=0.144). However, patients with low SMI had a longer period before the first CT imaging study (low SMI: 9 days (IQR 5-18) vs. 4 days (IQR 1-8), p<0.0001). Patients with low SMI had a greater number of mechanical ventilation days compared to those with normal SMI (low SMI: 22 days (IQR 14-35) vs. 18 days (IQR 12-31), p=0.025). Days of neuromuscular blockade, sedation and steroids were not statistically different between groups.

There were similar differences when the clinical cohort was stratified by low and normal SMD (Table 3-3). The differences seen with SMI status and the provision of ECMO, duration of ECMO and SARF centre length of stay were also seen when patients were stratified by SMD status (Table 3-3). Furthermore, mechanical ventilation days was higher in those with low SMD. Statistical difference was not seen in the number of male patients between groups, or in ethnic background. There was a greater proportion of patients with low SMD requiring renal replacement therapy (RRT) during their ICU stay (57/86 (66%) vs. 123/259 (47%), p=0.003). However, the overall number of RRT days was not

statistically different (low SMD: 12 days (IQR 6-23) vs. 11 days (IQR 6-21), p=0.496. This difference was not observed when patients were separated by low/normal SMI.

	Whole Cohort (n=346)	Normal SMI (n=247)	Low SMI (n=98)	p value	Normal SMD (n=259)	Low SMD (n=86)	p value
Age – *years*	47 (38-57)	48 (38-57)	49 (37-57)	0.983	48 (38-56)	49 (38-58)	0.351
Male – *No. (%)*	230 (66)	155 (45)	74 (76)	**0.023**	170 (66)	59 (69)	0.693
BMI – *kg/m²*	27.5 (24.1-31.9)	27.5 (23.9-32.4)	27.3 (24.5-31.9)	0.962	27.5 (24.1-31.6)	27.3 (23.9-33.6)	0.706
APACHE II score	16 (13-19)	16 (13-20)	16 (13-19)	0.203	16 (13-20)	16 (13-18)	0.209
Ethnicity – *No. (%)*							
Caucasian	193 (56)	153 (62)	39 (40)	**0.0003**	139 (54)	53 (61)	0.136
Skeletal Muscle Index – cm²/m²	45.1 (38.9-52.7)	48.7 (42.6-55.0)	37.9 (24.7-36.7)	**<0.0001**	46.3 (40.0-42.0)	41.7 (33.3-47.5)	**<0.0001**
Skeletal Density Index – HU	34.4 (28.3-40.3)	35.3 (29.6-40.8)	31.4 (24.7-36.7)	**<0.0001**	36.8 (32.6-42.0)	25.2 (19.8-27.5)	**<0.0001**
IMAT – cm²	3.8 (1.9-7.0)	3.5 (1.5-6.6)[a]	5.2 (2.8-9.0)	**0.0003**	3.1 (1.4-5.2)	8.3 (5.6-13.7)	**<0.0001**
CRP – *mg/L*	205.0 (121.0 – 311.2)	205.0 (117.0-309.5)	209.3 (19.3-49.3)	0.683	205.0 (121.5-304.8)	214.7 (112.2-341.9)	0.339
WCC – *x10⁹/L*	11.7 (8.5-16.5)	11.8 (8.4-17.0)	11.4 (8.5-15.9)	0.524	11.6 (8.8-16.6)	12.2 (7.7-16.6)	0.989
Lactate – *mmol/L*	1.28 (1.01-1.95)	1.4 (1.0-2.1)	1.2 (1.0-1.7)	**0.030**	1.3 (1.0-1.9)	1.5 (1.0-2.1)	0.483
ECMO – *No. (%)*	284 (82)	213 (86)	70 (71)	**0.002**	212 (81)	71 (83)	>0.999
ECMO days	16 (9-29)	14 (8-27)	21 (11-34)	**0.004**	15 (9-27)	20 (10-33)	**0.090**
SARF centre length of stay – *days*	20 (12-34)	18 (11-31)	24 (15-35)	**0.007**	19 (12-31)	27 (13-39)	**0.035**
Admission to intubation – *days*	1 (0-4)	1 (0-4)	1 (0-4)	0.144	1 (0-4)	1 (0-3)	0.814
Hospital admission to CT1 – *days*	5 (2-10)	4 (1-8)	9 (5-18)	**<0.0001**	5 (2-9)	7 (3-15)	**0.001**
Intubation to CT1 – *days*	2 (1-6)	2 (1-4)	6 (2-14)	**<0.0001**	2 (1-6)	5 (1-10)	0.0001
Intubation to CT2 – *days*	12 (6-19)	11 (5-16)	17 (11-31)	**<0.0001**	12 (6-17)	12 (7-24)	**0.404**
Intubation to CT3 – *days*	22 (14-33)	22 (14-30)	29 (15-34)	0.478	31 (14-30)	24 (13-33)	0.652
Mechanical ventilation days	20 (13-33)	18 (12-31)	22 (14-35)	**0.025**	18 (12-30)	28 (14-39)	**0.007**
Neuromuscular blockade days	6 (3-11)	5 (3-11)	7 (3-12)	0.198	5 (3-11)	6 (3-11)	0.741
Sedation days	18 (12-30)	17 (11-28	20 (12-33)	0.058	17 (11-28)	24 (12-33)	**0.032**
Steroid days	11 (6-21)	10 (6-18)	15 (6-24)	0.052	11 (6-19)	11 (6-23)	0532
Renal replacement – *No. (%)*	181 (52)	129 (52)	51 (52)	>0.999	123 (47)	57 (66)	**0.003**
Renal replacement days	11 (5-22)	11 (6-21)	11 (5-24)	0.836	11 (6-21)	12 (6-23)	0.496
Renal replacement within 48hr – *No. (%)*	103 (30)	80 (32)	23 (23)	0.118	73 (28)	30 (35)	0.277
Cumulative fluid balance in first 7d – *millilitres*	0.45 (-3.40-5.53)	35.5 (-81.0-186.9)	55.6 (-65.9-170.9)	0.737	38.3 (-69.1-175.0)	43.9 (-91.4-181.4)	0.997

Table 3-3. Patient cohort data in the MUSCLE-ICU study

BMI; body mass index, SMI; skeletal muscle index, SMD; skeletal muscle density, APACHE II; acute physiology and chronic health evaluation score, IMAT; intramuscular adipose tissue, CRP; C-reactive protein, WCC; white cell count, ECMO; extracorporeal membrane oxygenation, SARF; severe acute respiratory failure, CT1; first CT image etc.

3.6.5 Baseline skeletal muscle bulk and quality are only weakly correlated

Admission SMI had a weak positive correlation with SMD (r=0.26 (95% CI 0.15-0.35), p<0.0001) (Figure 3-7). There was a negative correlation between SMI and age (r=-0.12 (95% CI -0.22- -0.01), p=0.033) and between SMD and age (r=-0.38 (95% CI -0.47- -0.29), p<0.0001). Body mass index had a positive correlation with SMI (r=-0.44 (95% CI 0.35-0.52), p<0.0001) but a weak negative correlation with SMD (r=-0.25 (95% CI -0.35- -0.15), p<0.0001). Admission SMI was not correlated with admission IMAT (r=-0.05 (95% CI -0.17-0.05), p=0.287) but had a strong negative correlation with SMD (r=-0.71 (95% CI -0.76- -0.65), p<0.0001) (Figure 3-8).

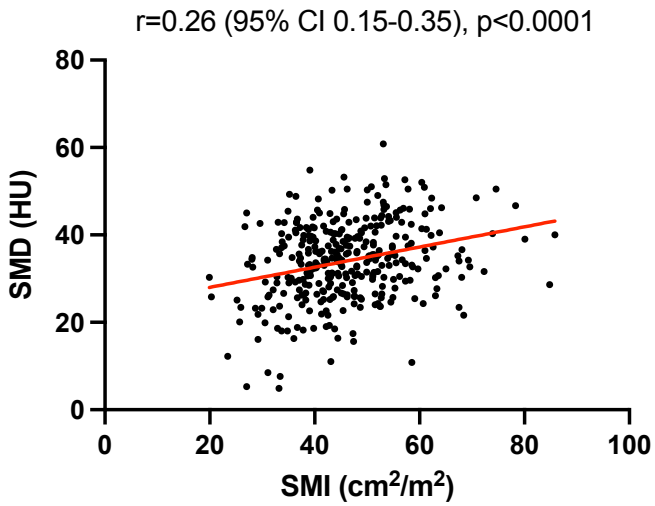


Figure 3-7. Correlation between admission skeletal muscle index and density

Admission skeletal muscle index and skeletal muscle density were positively correlated (r=0.26 (95% CI 0.15-0.35), p<0.0001. *SMI; skeletal muscle index, SMD; skeletal muscle density, HU; Hounsfield unit.* Correlation analysed using non-parametric Spearman's test.

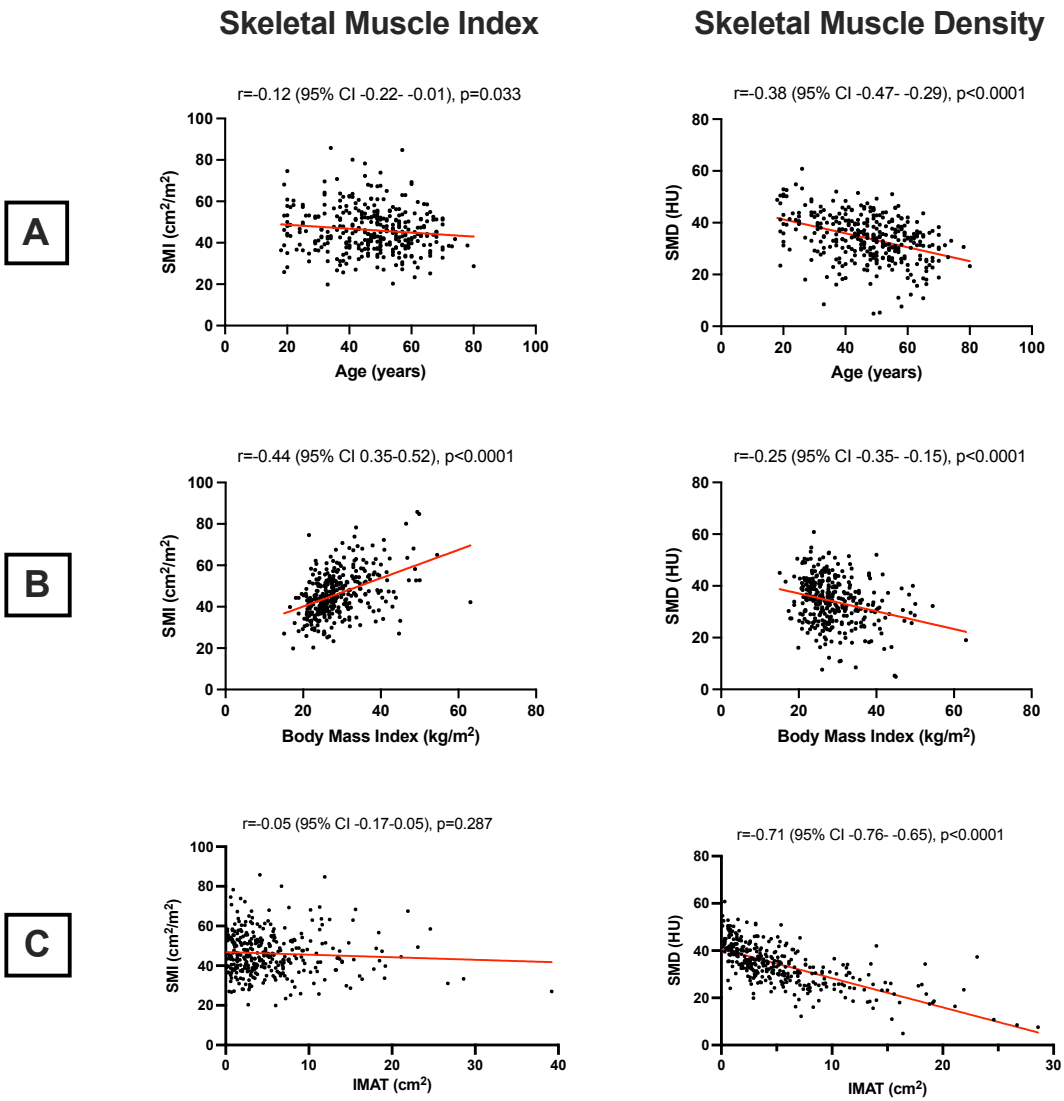


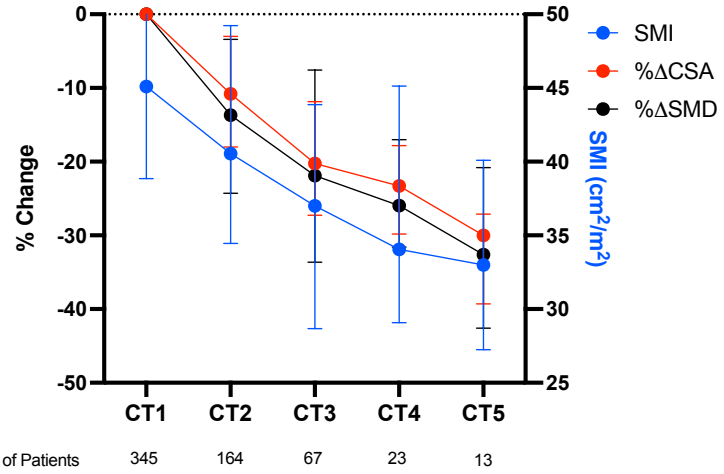
Figure 3-8. Correlation between patient demographics and skeletal muscle index and density

SMI; skeletal muscle index, SMD; skeletal muscle density, HU; Hounsfield unit. Correlation analyses performed using non-parametric Spearman's test.

3.6.6 Muscle bulk and quality decline continuously in severe ARDS

Longitudinal assessment of muscle wasting was determined by analysing additional CT imaging studies during the ICU admission. Of the 346 patients enrolled in the study, 164 (47%) patients underwent at least one more CT study with adequate axial L3 appearances. Of these, 67 patients (19%) had a third CT study, 23 patients (6%) had a fourth study and 13 patients (3%) a fifth study (Figure 3-9). At CT2, there was a change in L3-SkM_{CSA} of -10.8% (IQR -18--3.0) and -20.3% (IQR -27.3--11.9) by CT3. Similarly,

at CT2, muscle density declined by -13.7% (IQR -23.4--3.4) and -21.9 (IQR -33.6--7.6) by CT3. This suggests that loss of muscle mass is accompanied by a reduction in muscle quality.



	CT1 (n=345)	CT2 (n=164)	CT3 (n=67)	CT4 (n=23)	CT5 (n=13)
ΔL3-SkM$_{CSA}$ – %	-	-10.8 (-18.0--3.0)*	-20.3 (-27.3--11.9)*	-23.3 (-29.8--17.8)*	-30.0 (-39.3--27.1)*
ΔSMD – %	-	-13.7 (-24.3--3.4)*	-21.9 (-33.6--7.6)*	-26.0 (-31.6--17.0)*	-32.6 (-42.6--20.8)*
SMI – cm²/m²	45.1 (38.9-52.7)	40.6 (34.5-49.2)*	37.0 (28.7-43.9)*	34.1 (29.1-45.1)§	33 (27.3-40.1)§
SMD – HU	34.4 (28.3-40.3)	30.3 (23.0-35.6)*	28.5 (19.6-33.2)*	28.2 (17.0-33.9)#	29.1 (19.1-31.3)#
Time to CT – days	2 (1-6)	12 (6-19)	22 (14-33)	24 (12-43)	31 (16-48)

Figure 3-9. Longitudinal changes in skeletal muscle during critical illness

Top: graph showing longitudinal change in SMI, SMD and CSA in parallel. Below: table showing quantitative changes in various muscle data from the data shown in the graph. *ΔL3-SkM$_{CSA}$=change in axial L3 skeletal muscle cross sectional area, ΔSMD=change in L3 axial skeletal muscle density, SMI=skeletal muscle index, SMD=skeletal muscle density.* Time to CT=days from intubation. #p<0.01 §=p<0.001 *p<0.0001 when compared to baseline (CT1). All data in graph shown as median with error bars indicating interquartile range.

3.6.6.1 Low muscle states are common in patients with severe ARDS

After initial stratification into low SMI and low SMD groups using published data collected from healthy volunteers,[168] longitudinal assessment of low muscle states was performed for patients with multiple CT imaging studies. Currently literature suggests that cross sectional area, SMI or muscle density can be used to characterise low muscle states. A greater proportion of patients were classified as 'low muscle mass' state when using skeletal muscle cross-sectional area criteria (vs. SMI and SMD

criteria) at the time of CT1, CT2 and CT3 (Figure 3-10). Similarly, a greater proportion of patients were classified as 'low muscle state' when using SMI and compared to those classified by SMD criteria. The proportion of patients with low muscle state on the first CT image was between 24.9-41.4% depending on the quantitative method utilised (L3-SkM_{CSA}: 41.4%, SMI: 28.4%, SMD 24.9%). The proportion of patients with a low muscle mass state increased on sequential CT imaging regardless of method applied. By CT3 (20 days after intubation (IQR 13-29)), low muscle state was between 59-81% of patients depending on the criteria applied (L3-SkM_{CSA}: 80.6%, SMI: 66.7%, SMD 59.7%).

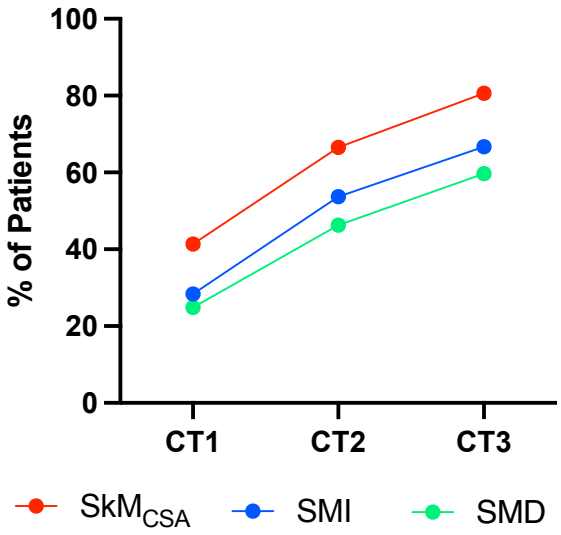


Figure 3-10. Change in incidence of low muscle state during critical illness

Low muscle mass states in patients with severe respiratory failure. Individual patients were stratified into low-muscle mass states using published cut-offs based on age, sex and BMI. Patients are stratified by skeletal muscle cross-sectional area at L3 ($SkML3_{CSA}$) (red line), skeletal muscle index (SMI) (blue line) or skeletal muscle density (SMD) (green line). CT1=first CT image, CT2=second CT image, CT3=third CT image.

3.6.7 Skeletal muscle density and pre-ICU length of stay are associated with ICU mortality

Linear and logistic regression was performed to investigate association between SMI and SMD on ICU survival. Furthermore, factors affecting loss of muscle mass at CT2 was also investigated. Independent variables (gender, body mass index, COVID19 status, ECMO therapy, skeletal muscle index (SMI) per $10cm^2$, skeletal muscle density (SMD) per 10 HU) were chosen a priori after determining their

significance to the outcomes. The univariate analysis is summarised in (Table 3-4). SMI (per 10 cm^2) (OR 0.787 (0.616-1.005), p=0.055) , SMD (per 10 HU) (OR 0.640 (0.482-0.851), p=0.002), APACHE II score (OR 1.059 (1.006-1.114), p=0.029) and pre-ICU length of stay (OR 1.068 (1.019-1.120), p=0.007) were all significantly associated with ICU mortality in univariate regression analysis and included in the main model. When adjusted for SMI (per 10 cm^2), APACHE II and pre-ICU length of stay, SMD (per 10 HU) remained significantly associated with ICU mortality (OR 0.666 (0.488-0.909), p=0.010). Similarly, when adjusted for SMI (per 10 cm^2), SMD (per 10 HU) and APACHE II, pre-ICU length of stay remained significantly associated with ICU mortality (OR 1.064 (1.014-1.117), p=0.011). Therefore, a decrease in muscle density of 10 HU, increases the ICU mortality by a factor of 1.5. (95% CI 1.10-2.05). Similarly, an additional day in hospital before ICU admission in these patients increased the ICU mortality by a factor of 1.06 (95% CI 1.01-1.12).

Variable	Univariate Odds Ratio (95% CI)	P value	Multivariate Odds Ratio (95% CI)	P value
ICU survival				
SMI – per 10 cm²	0.787 (0.616-1.005)	**0.055**	0.915 (0.704-1.189)	0.506
SMD – per 10 HU	0.640 (0.482-0.851)	**0.002**	0.666 (0.488-0.909)	**0.010**
IMAT – per 10 cm²	1.362 (0.863-2.151)	0.185		
Admission APACHE II score	1.059 (1.006-1.114)	**0.029**	1.053 (0.998-1.111)	0.057
BMI – cm/m²	1.019 (0.983-1.056)	0.315		
Pre-ICU length of stay – days	1.068 (1.019-1.120)	**0.007**	1.064 (1.014-1.117)	**0.011**
Male	1.015 (0.589-1.748)	0.958		
COVID19 positive	1.022 (0.604-1.729)	0.936		
vvECMO	0.859 (0.431-1.713)	0.667		
Admission CRP (mg/L)	1.000 (0.998-1.002)	0.745		
Low SMI status	0.828 (0.472-1.450)	0.509		
Low SMD status	0.655 (0.371-1.157)	0.145		

Table 3-4. Univariate/multivariate logistic regression model of factors associated with ICU survival

Skeletal muscle density and pre-ICU length of stay were significantly associated with ICU survival in multivariate logistic regression. Multivariate analysis adjusted for significant variables (p<0.1) from univariate analysis. *ICU; intensive care unit, SMI; skeletal muscle index, SMD; skeletal muscle density, HU; Hounsfield units, IMAT; intramuscular adipose tissue, APACHE II; acute physiology and chronic health evaluation, BMI; body mass index, COVID19; coronavirus disease 2019, vvECMO; veno-venous extracorporeal membrane oxygenation, CRP; C-reactive protein.*

3.6.8 Factors predicting longitudinal change in skeletal muscle mass

Univariate and multivariate regression models were constructed to assess the factors that affected changes in L3-SkM_{CSA} and L3-SkM_{SMD} at CT2 (12 days (IQR 6-19)). Independent variables were chosen *a priori* based on clinical significance to the dependent variable as previously described.

From univariate analysis, APACHE II score, COVID19 status and vvECMO use were all significantly associated with the degree of loss of L3-SkM_{CSA} at CT2 (Table 3-5). In the multivariate model, a positive COVID19 status and associated ARDS diagnosis was associated with a 4.0% reduction in L3-SkM_{CSA} at CT2 (95% CI -7.5--0.4, p=0.029) and institution of vvECMO support was associated with a loss of L3-SkM_{CSA} at CT2 of -6.3% (95% CI -11.9--0.8, p=0.025). Admission SMI (per 10 cm^2/m^2) and SMD (per 10 HU) were not found to be significantly associated with the change in L3-SkM_{CSA} at CT2 in the univariate analysis. In the multivariate model, APACHE II score, COVID19 status and vvECMO significantly predicted the percentage loss of L3-SkM_{CSA} at the time of CT2 but with low association ($F(3,159) = 3.315$, p=0.022, adjusted R^2=0.04), however only COVID19 status and vvECMO support was statistically significant in the prediction ($p<0.05$).

From univariate analysis, admission CRP levels and requirement of vvECMO were significantly associated with change in L3-SkM_{SMD} at CT2 (Table 3-5). In the multivariate model, the requirement for vvECMO support was associated with a loss in SMD of -12.9% (95% CI -21.3--4.4, p=0.003). Admission CRP levels had borderline significance (unstandardised B 0.02 (0.00-0.04), p=0.052) with loss of L3-SkM_{SMD} at CT2. Again, admission SMI (per 10 cm^2/m^2) and SMD (per 10 HU) were not found to be significantly associated with the change in SMD at CT2 in the univariate analysis.

Variable	Univariate Unstandardised B (95% CI)	P value	Multivariate Unstandardised B (95% CI)	P value
Change in L3-SkM$_{CSA}$ at CT2				
SMI – per 10 cm²	-0.74 (-3.14-1.66)	0.545		
SMD – per 10 HU	0.73 (-1.44-2.90)	0.505		
Admission APACHE II score	2.27 (-11.99-16.53)	**0.105**	-0.31 (-0.69-0.06)	0.101
BMI – cm/m²	-0.31 (-0.38-0.39)	0.977		
Pre-ICU length of stay – days	-0.07 (-0.41-0.27)	0.676		
Male	-0.64 (-4.90-3.61)	0.766		
COVID19 positive	-3.78 (-7.69-0.13)	**0.058**	-3.97 (-7.54--0.41)	**0.029**
Admission CRP (mg/L)	-0.01 (-0.02-0.00)	0.150		
vvECMO	-6.30 (-12.01-0.58)	**0.031**	-6.32 (-11.85--0.78)	**0.025**
Change in SMD at CT2				
SMI – per 10 cm²	0.29 (-2.15-2.72)	0.815		
SMD – per 10 HU	-0.84 (-3.77-2.08)	0.570		
Admission APACHE II score	-0.28 (-0.89-0.33)	0.364		
BMI – cm/m²	-0.11 (-0.53-0.30)	0.590		
Pre-ICU length of stay – days	-0.29 (-0.81-0.23)	0.280		
Male	-1.93 (-7.60-3.74)	0.503		
COVID19 positive	-0.05 (-5.57-5.66)	0.987		
Admission CRP (mg/L)	0.02 (0.00-0.04)	**0.085**	0.02 (0.00-0.04)	**0.052**
vvECMO	-12.29 (-20.74--3.83)	**0.005**	-12.85 (-21.27--4.43)	**0.003**

Table 3-5. Univariate/multivariate linear regression model of factors associated with skeletal muscle change at follow-up CT imaging

Change in L3-SkM$_{CSA}$ at CT2 was significantly associated with admission APACHE II score, COVID19 status and vvECMO support in univariate analysis. Multivariate analysis adjusted for significant variables ($p<0.1$) from univariate analysis. In multivariate regression analysis, COVID19 status and vvECMO support were significantly associated with loss of L3-SkM$_{CSA}$ at CT2. Change in SMD at CT2 was significantly associated with admission CRP levels and vvECMO support in both univariate and multivariate analysis. *ICU; intensive care unit, SMI; skeletal muscle index, SMD; skeletal muscle density, HU; Hounsfield units, IMAT; intramuscular adipose tissue, APACHE II; acute physiology and chronic health evaluation, BMI; body mass index, COVID19; coronavirus disease 2019, vvECMO; veno-venous extracorporeal membrane oxygenation, CRP; C-reactive protein.*

3.6.9 Clinical characteristics in COVID19 ARDS

Of the 346 patients, 137 (40%) had a diagnosis of COVID19 ARDS. There were more males with COVID19 ARDS than those with non-COVID19 ARDS (104 (76%) vs. 126 (60%) respectively, p=0.003) and patients with COVID19 ARDS were older (49±13 years vs. 45±14, p=0.018). The BMI in those with COVID19 ARDS was higher 27.8kg/m^2 (IQR 25.2-33.4) vs. 26.8kg/m^2 (IQR 23.4-31.2), p=0.016). In the COVID19 ARDS group, there were more patients from an Asian/Asian-British (64 (47%) vs. 33 (16%), p<0.0001) and Black/Black-British (17 (12%) vs. 11 (5%), p=0.017) ethnic background than in the non-COVID19 group. There was a higher proportion of patients from a White/White-British background with non-COVID19 ARDS (154 (74%) vs. 39 (28%), p<0.0001). Severity of illness, as indicated by the APACHE II score, was not statistically different between the groups (COVID19 ARDS: 15 (IQR 13-19) vs. non-COVID19 ARDS: 17 (IQR 13-20), p=0.137). Patients with COVID19 ARDS had a higher incidence of cardiovascular (62/137, 45% vs. 55/209, 26%; p=0.001) and endocrinological (predominantly diabetes mellitus) (37/137, 27% vs. 37/209, 18%; p=0.039) co-morbidity compared to those with non-COVID19 ARDS. However, those with non-COVID19 ARDS had higher incidence of respiratory (59/209, 28% vs. 25/137, 18%; p=0.034) and psychiatric (40/209, 19% vs. 7/137, 5%; p<0.001) co-morbidity.

284/346 (82%) patients with ARDS received vvECMO support. More patients with non-COVID19 ARDS received vvECMO than those with COVID19 ARDS (non-COVID19 ARDS: 191/209, 91% vs. COVID19 ARDS: 93/137, 68%; p<0.0001). However, the length of vvECMO support in patients with COVID19 ARDS was greater (COVID19 ARDS: 23 days vs. non-COVID19 ARDS: 13 days; p<0.0001). Patients spent a median of 1 day (IQR 0-4 days) in hospital before undergoing intubation and mechanical ventilation. Those with COVID19 ARDS had a greater number of days before receiving mechanical ventilation (COVID19 ARDS: 2 days (IQR 0-6) vs. non-COVID19 ARDS 1 day (IQR 0-3); p<0.0001). The numbers of patients who received sedation, steroid, neuromuscular blockade and mechanical ventilation days were all significantly higher in patients with COVID19 ARDS (Table 3-6).

	Whole Cohort (n=346)	COVID19 (n=137)	Non-COVID19 (n=209)	P value
Age – *years*	47 ± 13	49 ± 11	45 ± 14	**0.018**
Male – *No. (%)*	230 (66)	104 (76)	126 (60)	**0.003**
BMI – *kg/m²*	27.5 (24.1-31.9)	27.8 (25.2-33.4)	26.8 (23.4-31.2)	**0.016**
Ethnicity – *No. (%)*				
Caucasian	193 (56)	39 (28)	154 (74)	**<0.0001**
Asian	97 (28)	64 (47)	33 (16)	**<0.0001**
Black	28 (8)	17 (12)	11 (5)	**0.017**
Other	16 (5)	6 (4)	10 (5)	
Not specified	12 (3)	11 (8)	1 (0)	
Admission SMI – cm²/m²	45.1 (38.9-52.7)	44.5 (39.1-51.8)	45.2 (38.8-53.1)	ns
Low SMI – No. (%)	98 (28)	49 (36)	49 (23)	**0.014**
Low SMD – No. (%)	86 (25)	23 (17)	63 (30)	**0.007**
Co-morbidities – *No. (%)*				
Cardiovascular	119 (34)	62 (45)	57 (27)	**0.001**
Respiratory	84 (24)	25 (18)	59 (28)	**0.034**
Neurological	7 (2)	3 (2)	4 (2)	0.859
Psychiatric	47 (14)	7 (5)	40 (19)	**<0.001**
Endocrine	74 (21)	37 (27)	37 (18)	**0.039**
Renal	2 (0)	1 (1)	1 (0)	0.763
Gastroenterology	8 (2)	4 (1)	4 (2)	0.543
Rheumatology	13 (4)	3 (2)	10 (5)	0.215
Cancer	8 (2)	2 (1)	6 (3)	0.393
Chronic viral infection	7 (2)	1 (1)	6 (3)	0.167
APACHE II score	16 (13-19)	15 (13-19)	17 (13-20)	0.137
SOFA score				
PaO2/FiO2 ratio – *kPa*	28.7 (19.9-41.2)	25.1 (17.6-34.5)	32.0 (22.3-45.7)	0.653
CRP – *mg/L*	205.0 (121.0 – 311.2)	205.0 (131.0-303.9)	206 (116.3-321.6)	0.832
WCC – *x10⁹/L*	11.7 (8.5-16.5)	10.8 (8.1-14.0)	12.4 (8.9-17.7)	**0.008**
Lactate – *mmol/L*	1.28 (1.01-1.95)	1.22 (1.00-1.59)	1.39 (1.01-2.50)	**0.011**
ECMO – *No. (%)*	284 (82)	93 (68)	191 (91)	**<0.0001**
ECMO days	16 (9-29)	23 (13-42)	13 (8-23)	**<0.0001**
SARF centre length of stay – *days*	20 (12-34)	28 (16-41)	17 (11-28)	**<0.0001**
Admission to intubation – *days*	1 (0-4)	2 (0-6)	1 (0-3)	**<0.0001**
Hospital admission to CT1 – *days*	5 (2-10)	9 (5-16)	3 (1-7)	**<0.0001**
Intubation to CT1 – *days*	2 (1-6)	5 (2-11)	1 (0-4)	**<0.0001**
Intubation to CT2 – *days*	12 (6-19)	15 (12-25)	10 (4-16)	**<0.0001**
Intubation to CT3 – *days*	22 (14-33)	28 (21-39)	17 (7-29)	**0.004**
Intubation to CT4– *days*	24 (12-43)	43 (24-52)	12 (8-20)	0.534
Intubation to CT5 – *days*	31 (16-48)	54 (32-55)	22 (14-30)	**0.004**
Ventilator days	20 (13-33)	27 (15-40)	17 (12-27)	**<0.0001**
Neuromuscular blockade days	6 (3-11)	9 (4-14)	4 (3-8)	**<0.0001**
Sedation days	18 (12-30)	24 (14-35)	16 (11-25)	**<0.0001**
Steroid days	11 (6-21)	14 (7-30)	10 (5-16)	**0.001**
Renal replacement – *No. (%)*	181 (52)	60 (43)	121 (58)	**0.010**
Renal replacement days	11 (5-22)	13 (5-26)	11 (6-18)	0.348
RRT within 48hr – *No. (%)*	103 (30)	28 (20)	75 (36)	**0.002**
Cumulative fluid balance – *litres*	0.45 (-3.40-5.53)	1.80 (-2.90-8.70)	-0.40 (-4.25-4.10)	**0.0004**

Table 3-6. Patient characteristics and ICU admission detail in MUSCLE-ICU study.

COVID19; Coronavirus disease 19, BMI; body mass index, SMI; skeletal muscle index, SMD; skeletal muscle density, APACHE II; acute physiology and chronic health evaluation score, IMAT; intramuscular adipose tissue, CRP; C-reactive protein, WCC; white cell count, ECMO; extracorporeal membrane oxygenation, SARF; severe acute respiratory failure, RRT; renal replacement therapy, CT1; first CT image etc.

3.6.9.1 COVID19 ARDS patients had a longer time to first CT study

Following intubation, those with COVID19 ARDS had a greater number of days before the first CT image was acquired (COVID19 ARDS 5 days (IQR 2-11) vs. non-COVID19 ARDS: 1 day (IQR 0-4), p<0.0001). Similarly, those with COVID19 ARDS had a greater number of days before the second and third CT images were acquired ([CT2] COVID19 ARDS: 15 days (IQR 12-25) vs. non-COVID19 ARDS: 10 days (IQR 4-16), p<0.0001 and [CT3] COVID19 ARDS: 28 days (IQR 21-39) vs. non-COVID19 ARDS: 17 days (IQR 7-29), p<0.004 respectively). The hospital length of stay before obtaining the first CT image was higher in those with COVID19 ARDS (COVID19 ARDS: 9 days (IQR 5-16) vs. non-COVID19 ARDS: 3 days (IQR 1-7), p<0.0001). These data reflect processes of care with respect to our tertiary centre and demonstrate slower progression of COVID19 SARF compared to non-COVID19 SARF.

3.6.10 Skeletal muscle bulk, but not quality was lower in COVID19 ARDS patients

Skeletal muscle cross-sectional area, index, density and intramuscular adipose tissue on the first CT imaging study for COVID19 and non-COVID19 patients is summarised in Table 3-7 and illustrated in Figure 3-11. No significant differences for L3-SkM_{CSA}, SMI, SMD or IMAT were seen on the first imaging study of ICU admission between COVID19 and non-COVID19 patients. However, when individual level cut off values were applied for SMI, there was a greater proportion of patients with COVID19 ARDS with a low SMI on admission (COVID19 ARDS: 49/136 (36%) vs. non-COVID19 ARDS: 49/209 (23%), p=0.014). However, the proportion of patients with a low SMD state was higher in non-COVID19 patients on admission (non-COVID19 ARDS 63/209 (30%) vs. COVID19 ARDS: 23/137 (17%), p=0.007).

	Whole Cohort (n=346)	COVID19 (n=137)	Non-COVID19 (n=209)	p value
L3-SkM$_{CSA}$ (cm^2)	133.1 (108.7-158.4)	133.5 (113.0-158.4)	133.1 (104.4-158.5)	ns
SMI (cm^2/m^2)	45.1 (38.9-52.7)	44.5 (39.1-51.8)	45.2 (38.8-53.1)	ns
SMD (HU)	34.4 (28.3-40.3)	35.4 (30.2-40.3)	33.3 (27.1-40.1)	ns
IMAT (cm^2)	3.8 (1.9-7.0)	4.0 (2.1-7.1)	3.7 (1.8-7.0)	ns

Table 3-7. Quantitative analysis of skeletal muscle in COVID19 and non-COVID19 patients on admission to the ICU

Skeletal muscle values compared using Mann-Whitney test for unpaired, non-parametric data. *L3-SkM$_{CSA}$; skeletal muscle cross-sectional area, SMI; skeletal muscle index, SMD; skeletal muscle density, HU; Hounsfield units, IMAT; intra-muscular adipose tissue, COVID19; Coronavirus disease 2019.* Data expressed as median (inter-quartile range).

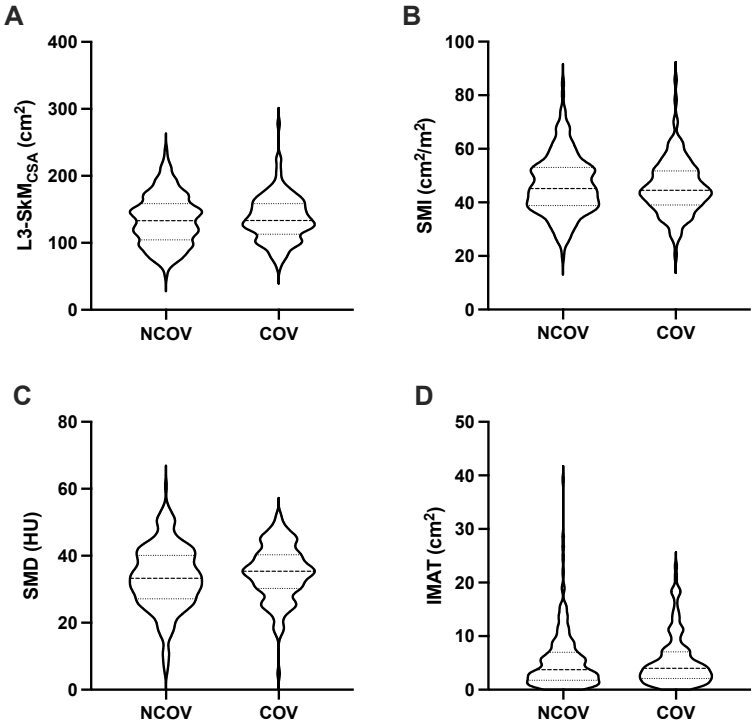


Figure 3-11. L3 level muscle data in patients with COVID19 and non-COVID19 ARDS on admission to the ICU

Comparison of quantitative skeletal muscle measurements on ICU admission in COVID19 (COV) and non-COVID19 (NCOV) patients. (A) cross-sectional area (CSA) calculated at the L3 vertebral level (L3-SkM$_{CSA}$). (B) Skeletal muscle index (SMI), (C) muscle density of L3-SkM$_{CSA}$ in Hounsfield units (HU) and (D) intra-muscular adipose tissue (IMAT). The central dashed line in each plot represents the median and the upper and lower dotted lines the upper and lower quartiles respectively. Difference between groups analysed using Mann-Whitney test for unpaired, non-parametric data.

3.6.11 Acute skeletal muscle wasting is higher in patients with COVID19

Loss of L3-SkM$_{CSA}$ at CT2 was significantly greater in COVID19 ARDS patients compared to non-COVID19 ARDS patients (COVID19 ARDS: -12.7% (IQR -20.3--8.0) vs. non-COVID19 ARDS: -9.2 (IQR -16.8--1.6), p=0.03) (Figure 3-12). However, time to CT2 from intubation was significant higher in COVID19 ARDS patients (COVID19 ARDS: 15 days (IQR 12-25) vs. non-COVID19 ARDS: 10 days (IQR 4-16), p<0.0001). At CT3, the loss of L3-SkM$_{CSA}$ was not significantly different to that seen in non-COVID19 ARDS (COVID19 ARDS: 23.2% (IQR -26.7--17.0) vs. non- COVID19 ARDS: -16.6% (IQR -28.0--6.1), p=0.07). At CT2, the change in SMD in COVID19 ARDS patients was comparable to that seen in L3-SkM$_{CSA}$ (-12.5% (IQR -23.8--4.8) suggesting similar loss of muscle bulk and quality. Conversely, in non-COVID19 ARDS patients there was a greater loss in SMD compared to the loss in L3-SkM$_{CSA}$ (SMD: -14.6% (-26.0--1.3) vs. L3-SkM$_{CSA}$: -9.2% (IQR -16.8--1.6) (Figure 3-12).

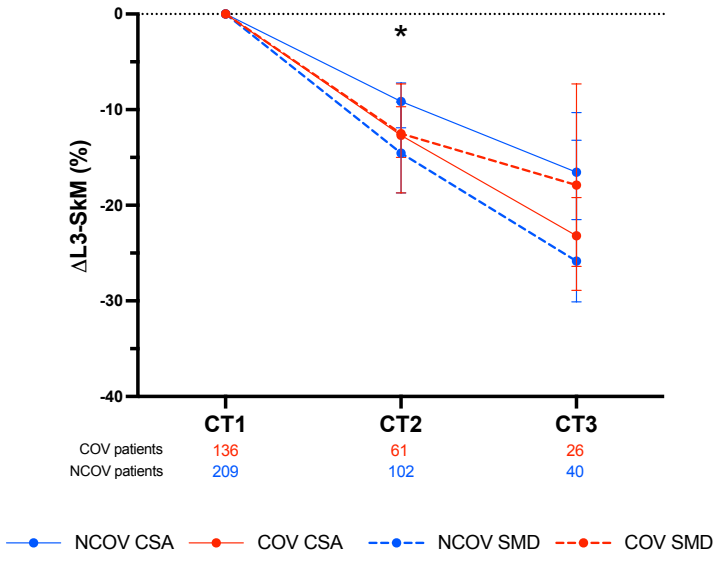


Figure 3-12. Skeletal muscle cross-sectional area and density change in COVID19 and non-COVID19 patients

ΔL3-SkM; change in skeletal muscle measurement, SMI; skeletal muscle index, SMD; skeletal muscle density, COV; COVID19 patients, NCOV; non-COVID19 patients. CT1; first CT image, CT2; second CT image, CT3; third CT image. All data shown as median with error bars indicating 95% confidence interval. *p<0.05 for ΔL3-SkM$_{CSA}$ of COV compared to NCOV patients.

The rate of decline in L3-SkM_{CSA} between CT1 and CT2 (median 12 days (IQR 6-19) from intubation) in all patients was 0.7% per day (IQR -1.4--0.3). The rate of decline in L3-SkM_{CSA} COVID19 ARDS patients was 0.7% per day (IQR -1.3--0.4) compared to 0.8% per day (IQR -1.6--0.2) in non-COVID19 ARDS patients (p=0.478). By CT3, the rate of decline increased to 0.9% per day in COVID19 ARDS patients compared to 1.0% per day in non-COVID19 ARDS patients (p=0.253).

3.6.11.1 ICU mortality is similar in COVID19 and non-COVID19 patients

Overall, 74/346 (21.4%) patients died whilst admitted to the ICU. The proportion of patients that died whilst admitted on the ICU was similar between non-COVID19 and COVID19 groups (NCOV: 21.5% vs. COV 21.2%) and there was no association between COVID19 status and ICU mortality. A log rank test found no difference in the survival distribution between COVID19 and non-COVID19 patients during the ICU admission and up to 60 days (p=0.461) (Figure 3-13).

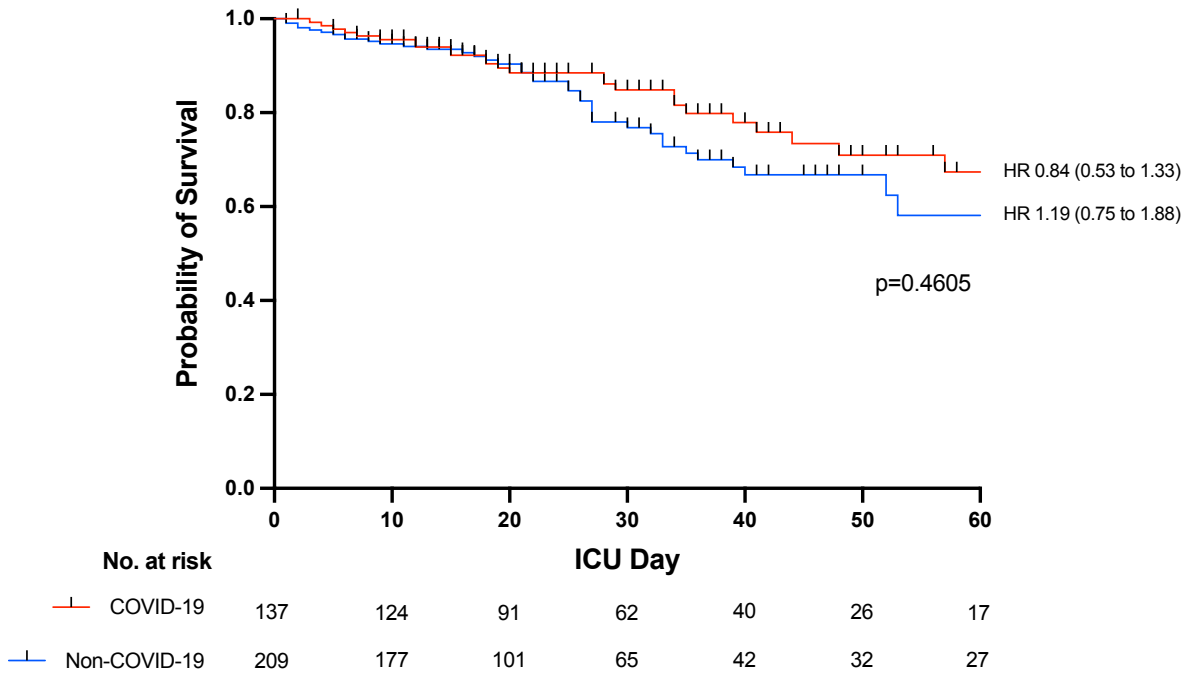


Figure 3-13. Kaplan-Meier plot for ICU survival at 60 days in COVID19 and non-COVID19 patients

Survival differences analysed by log-rank (Mantel-Cox) method, p=0.461.

3.6.12 Inflammation in COVID19 associated muscle wasting

To ascertain whether there was an association between generalised inflammation and muscle wasting, daily CRP levels were compared between patients with COVID19 ARDS and non-COVID19 ARDS patients. Peak CRP levels were seen on admission and not significantly different between COVID19 ARDS and non-COVID19 groups. Following ICU admission, there was a decline up to day 3-4 of ICU admission. There was a sustained rise in CRP in COVID19 ARDS patients between days 14-20 whilst levels in non-COVID19 patients' levels continued to decline, however the differences were not statistically significant. Overall, from ICU admission (day 0) through to day 28, there was no significant difference in CRP levels between patients with and without COVID19 ARDS (Figure 3-14).

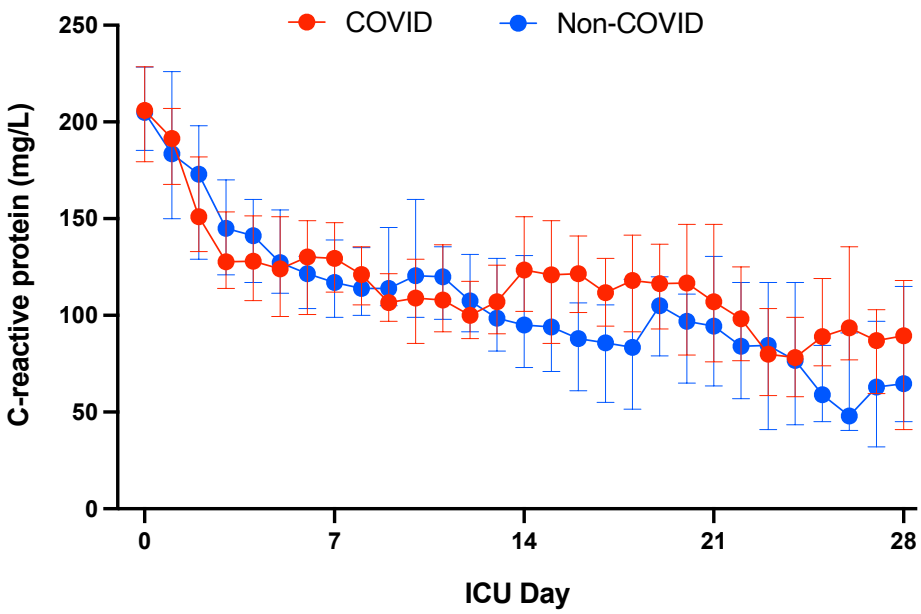


Figure 3-14. Daily C-reactive protein trend in COVID19 and non-COVID19 ARDS.

Data plotted as median with error bars of interquartile range. *COVID; patients with COVID19 ARDS, Non-COVID; patients with non-COVID19 ARDS.* Longitudinal differences between CRP levels and day of ICU admission were analysed using Sidak's multiple comparisons test for non-parametric data, with individual variances computed for each comparison, $p>0.05$ from admission through to day 28.

3.7 Discussion

In a cohort of 346 critically ill patients with severe respiratory failure and acute respiratory distress syndrome, I demonstrate an incidence of low muscle mass state (as given by admission SMI) of 28% and low muscle quality (as given by admission SMD) of 25%. This is lower than previously reported in critical care studies using similar methodology.[165,171,172]

Longitudinal assessment in those with a second CT image demonstrated a significant loss in L3-SkM_{CSA} of 10.8% (IQR -18.0--3.0), a loss in SMD of -13.7% (IQR -24.3--3.4) with an image interval of 12 days (IQR 6-19). These findings were comparable to those from Bear *et al.,* who showed that in 54 patients receiving vvECMO, L3-SkM_{CSA} declined by 17.7% (IQR -23.9--8.2) and SMD by 10.6% (IQR -23.6-13.4) at the time of the second CT image (9 days (IQR 7-18)).[174] These data also align with that shown in ultrasonography studies of peripheral muscle in non-COVID19 patients[14,47] but early data from rectus femoris ultrasound studies (using cross-sectional area) in COVID19 patients have reported a loss of between 19-30% by day 10 of the ICU admission.

I show that lower SMD (per 10 HU) was associated with a higher ICU mortality when corrected for APACHE II score and length of hospital stay prior to ICU admission highlighting its potential importance as a predictive measure. In contrast, low SMI (per 10cm^2) was not associated with an increased ICU mortality in our cohort and in contrast to other studies on vvECMO patients.[252] Thus, muscle quality rather than bulk may be more predictive with respect to ICU related outcome measures. I report a unique critical care cohort of ARDS patients (of any aetiology) with an associated in-hospital mortality of up to 60% in its most severe forms.[251] The majority of these patients required extracorporeal membrane oxygenation and have comparable rates of in-hospital mortality.[256] Currently there is a degree of equipoise as to whether there is higher morbidity and mortality in survivors of COVID19 ARDS,[109,257] including those requiring ECMO.[258,259] Similar retrospective imaging studies have found associations between L3-SkM_{CSA} and SMI and ICU mortality.[171,172] However, it is important to highlight

that these studies enrolled patients that were significantly older (79 years (IQR 72-85)[172]; 52 years (±19)[171] and none of the patients required ECMO support. However, patients in these studies did have similar admission APACHE II scores and similar predicted ICU mortality. Interestingly, I found a greater proportion of patients with normal SMI on admission required vvECMO than those with low SMI. This may reflect the patient selection in the provision of extra-corporeal support. Whilst the median age was not significantly different between low SMI and normal SMI patients, patients selected for ECMO are likely to have fewer co-morbidities and chronic health issues as well as less likely to have multi-organ failure (as it is a relative contra-indication to vvECMO in most centres) and therefore greater muscle bulk at baseline and lower degree of atrophy.[14]

At our tertiary referral centre, I often admitted patients up to 7 days after their referring centre ICU admission in line with the diagnosis of ARDS and avoiding excessive periods of mechanical ventilation. This of course would mean that by the time I assessed an admission (or subsequent) CT in our centre, critical illness is likely to be established, and it is possible that significant acute muscle wasting may have occurred, thus giving a low SMI (and maybe SMD) on recruitment to the study. This was also evident in the greater number of days from intubation to CT1 in those patients requiring vvECMO and in those with COVID19. This was negated when an admission CT was performed at the referring centre. In our cohort 260/346 (75%) had their first CT imaging study performed either before ICU admission (and intubation) or within 10 days of hospital presentation. Similarly, as a tertiary centre, patients who no longer require specialist support would often be repatriated to their referring hospital. This would mean that data sets of the entire ICU stay (referring centre and tertiary centre) would be incomplete. As a compromise, I used vvECMO survival as an end-point criterion.

I evaluated the longitudinal changes in muscle area and density in COVID19 ARDS patients and show that loss of muscle mass followed loss of muscle density (and hence quality) (Figure 3-9). However, the retrospective nature of the study meant that associations with physical function and outcomes

were not possible to ascertain. I did not have access to complete, post-ICU follow-up data detailing functional measures in those that survived to discharge. However, gross restrictions to non-essential healthcare systems meant that establishing routine post-critical illness follow up was not possible. Established scoring systems assessing physical function in the ICU, such as the CPAx score[39], may be useful to study longitudinally especially in those who are deeply sedated in early ARDS management.

The study utilised imaging studies conducted as part of routine ICU care. Therefore, I could not control for the initial CT timing nor any interval imaging and thus could not comment precisely when acute changes in muscle mass and density had occurred. However, the median time to CT2 of 12 days (IQR 6-19) represents an acceptable interval to measure acute and most severe wasting and reflects the process of care at our tertiary centre. Given the severity of illness and lability of some patients, further imaging was often reserved for when stability had been achieved. However, given that all imaging was performed in the ICU whilst receiving mechanical ventilation, our data describes the effects of critical illness on muscle mass and is not confounded by follow-up imaging following ICU and/or hospital discharge.

I rigorously evaluated two software applications to establish and apply robust methodology to utilise in the formal clinical study. Analysis protocols were clear and reproducible between multiple users. Currently, there are no standardised radiological methods of assessing and quantifying muscle mass or quality and as such protocols and consensus of muscle groups are the subject of debate. I demonstrated high levels of intra- and inter-operator reliability (>0.9) to evaluate body composition in critically ill patients and utilised a single assessor in the main clinical study following reliability studies and analysed study images in batches of no more than 30 images in a single session to prevent errors, analysis fatigue and mis-identifying structures. I studied multiple muscle groups at the L3 level rather than single muscles such as the erector spinae as in previous studies. Previous studies have also utilised cut off values for low and normal SMI and SMD in different patient populations (oncology,[169]

elderly[172]) and may not reflect those of a critically ill cohort. However, studies in the critically ill have also adopted gender based cut off values which may not accurately reflect the patient population.[171] Therefore, in our study, I stratified patients into low and normal SMI and SMD state by gender, age and BMI which are significant factors in the determination of muscle mass.

The study relied on the availability of high-quality imaging studies. I excluded 40% of eligible patients (234/580) due to lack of imaging, poor image quality and analytical limitations discovered after recruitment. Thus, there is a possibility that the true degree of low muscle mass state is under or overstated. In those that I included, I did not assess CT acquisition protocols and pragmatically assumed consistency in process by the specialist radiology departments. I made attempts to control image inclusion by using thick 5mm slice axial images to preserve image quality throughout. Similarly, I did not adjust or control for contrast studies as there is limited data to suggest this affects quantification of muscle on CT imaging.[260]

When used as a continuous variable, changes in SMD (per 10 HU) was associated with higher ICU mortality. It is currently unclear what drives the changes in muscle quality, but this is likely to be multi-factorial in the context of critical illness. Previous qualitative studies suggest that intramuscular fat accumulation and underlying myofibre necrosis[14,133] may have active roles. The latter has been consistently reported in histological studies of skeletal muscle in critical illness.[133,199,200] Evaluation of CRP, a general marker of inflammation, identified very high levels in early critical illness and sustained levels through to day 21 of admission. CRP historically was used as a marker of infection, rather than generalised inflammation, however, studies have shown that variations in daily CRP levels as little as >4mg/dL can predict underlying infection, and hence inflammation (AUC 0.86 95% CI 0.75-0.93, sensitivity 92% and specificity 71%.)[261] In contrast, other studies in critical care show that rising levels >48-hours after critical care admission are associated with higher ICU mortality.[262] This warrants further review of inflammatory phenotypes during critical illness associated muscle wasting as

elevated CRP levels are associated with pro-inflammatory cytokine release which are a risk factor for muscle catabolism.[187,263]

Whilst this study was retrospective in nature, it represents one of the largest with regards to body composition assessment in critically ill patients, including first descriptions of patients with COVID19 ARDS. This chapter shows that low muscle mass state is common on admission to the ICU and reflects that seen in similar studies of severe respiratory failure patients.[174] I show that the incidence of low muscle mass states increase throughout the admission and represent a significant risk factor for ICU mortality. Whilst single axial slice CT imaging analysis provides indices of whole-body skeletal muscle, it is difficult to determine whether small respiratory muscles such as the diaphragm and intercostal muscles follow similar rates of decline. CT imaging, whilst common and widely utilised confers significant risk and logistical issues and thus makes prospective assessment difficult.

In the next chapter, I will use these findings to prospectively assess a variety of muscle groups and evaluate whether the rate of change in skeletal and respiratory muscle is similar to that seen using CT imaging. I will introduce ultrasound in this regard and determine whether dynamic and functional measurements can be reliably performed in a critically ill cohort. The impact of inflammation on muscle wasting will also be explored Chapter 4.

Chapter 4: Longitudinal evaluation of skeletal and respiratory muscle wasting in critical illness using ultrasound

4.1 Background

In chapter 3 I show that CT imaging represents a reliable method of quantifying skeletal muscle in critical illness and the longitudinal changes in muscle bulk and quality during admission. However, repeated CT assessment carries risks of radiation exposure as well as the logistical concerns of moving critically ill patients to the imaging department, thus making controlled, repeated prospective studies difficult. Alternative imaging techniques such as ultrasound are non-invasive, cheap and widely available. It can be used to assess both respiratory[129–131] and peripheral skeletal muscle in critical illness.[126,132,133] Peripheral skeletal muscle ultrasound, has long been used as a method to assess function in respiratory disease[126] but its use in critical illness has gained much interest[14,47,133,137,140] as it is associated with severity of disease,[14] prolonged MV and ICU length of stay.[172] Due to variability in methodology reporting, there are no recognised standards of musculoskeletal ultrasound techniques and this can make comparisons between studies and generalisability difficult.

There is a need to identify ways of diagnosing muscle wasting and weakness early as the impact of critical illness can persist long after the patient leaves the ICU.[10,11] Respiratory muscle testing in critical illness has largely consisted of invasive procedures,[264] and there are a number of associated quantitative indices that can indicate underlying respiratory muscle weakness in critical illness.[265,266] However, these techniques are often limited to research settings, specialist centres and require specific equipment and expert interpretation. Ultrasonography is a widely adopted imaging modality in the ICU. As the principal respiratory muscle, the diaphragm and its dysfunction in MV has been the focus of much research.[114,152,267] However, there is a paucity of literature describing extra-diaphragmatic respiratory muscles and ultrasound can provide real-time, dynamic assessment and

data regarding dimension, area and function of such muscles – all of which are not possible with current accepted gold standards. The parasternal muscles (PSM) offer an easily accessible muscle group with defined ultrasonographic anatomy.[131] Clinical studies have largely studied the changes in a single muscle group – such as rectus femoris. To our knowledge, no prospective clinical trials have evaluated peripheral skeletal and respiratory muscle concurrently using ultrasound. Furthermore, longitudinal description of inflammatory phenotypes in the context of muscle wasting are also poorly described. With respect to the practical assessment, there are no standardised guidelines for skeletal and respiratory muscle ultrasonography in the context of ICUAW. This highlights the importance of publication of methods, reliability data and technical restrictions to be clearly stated.

Lastly, the COVID19 worldwide pandemic has led to a surge in intensive care provision and as such raising the number of patients at risk of ICU-acquired weakness (ICUAW) and muscle wasting as a high proportion of patients require mechanical ventilation. At the time of writing, longitudinal descriptions of muscle wasting in different muscle groups are yet to be described in patients with severe COVID19 infection.

4.2 Aims

1. Establish a reliable ultrasound protocol to assess respiratory and peripheral skeletal muscle in critically ill patients receiving mechanical ventilation.
2. Describe the changes in respiratory and peripheral skeletal muscle mass in critically ill patients.
3. Describe associations between muscle wasting and underlying inflammatory cytokines.
4. Describe the differences in severity of muscle wasting in COVID19 patients.

4.3 Hypotheses

1. Measurement of peripheral and respiratory muscle quantity using ultrasound is a reproducible and reliable technique in critically ill patients.
2. Severity of peripheral skeletal muscle and respiratory muscle wasting is not significantly different in critically ill patients.
3. Inflammatory phenotypes of patients with acute muscle wasting can differentiate high and low wasting states in patients with COVID19.

4.4 Methods

Full detail of the ultrasound imaging protocol is given in 2.2.2

4.4.1 Study cohorts

WAVE-RMU is a prospective feasibility study with a primary aim to establish reliability and reproducibility of skeletal and respiratory muscle ultrasound. All imaging and data for WAVE-RMU was collected at The Royal Brompton Hospital, London, UK. Age, gender, weight, height and diagnosis (for critical care patients) was collected. In addition, time from ICU admission was also recorded. The feasibility study included two cohorts – healthy volunteers and mechanically ventilated patients on the ICU. Selection of patients in each cohort were not randomised and selected on availability to participate. The main clinical cohort consisted of patients recruited to the WAVE and DeVENT studies as detailed in 2.1

4.4.2 Quantitative measurements of skeletal and respiratory muscle

Rectus femoris cross-sectional area (RF_{CSA}), parasternal muscle cross-sectional area (PSM_{CSA}), parasternal muscle end-expiratory thickness (PSM_{EXP}), parasternal muscle end-inspiratory thickness (PSM_{INSP}), diaphragm end-expiratory thickness (DIA_{EXP}), diaphragm end-inspiratory thickness (DIA_{INSP}),

diaphragm excursion (DIA_{EXC}) and diaphragm thickening fraction (DIA_{TF}) were measured as detailed in 2.2.2

4.4.3 Reproducibility study protocol

In the feasibility study, the ultrasound protocol was applied to patients in each cohort as outlined above on two separate occasions, 15 minutes apart, for each operator. Operators acquired images independently. If the clinical status of the patient was likely to imminently change (i.e. repositioning of patient, administration of neuromuscular blockade/additional sedation, endotracheal suction etc), then images were collected less than 15 minutes apart to avoid significant variation in study conditions.

All healthy participants were at least 18-years old and able to provide informed, written consent for themselves. Critical care patients were also >18-years old and were actively receiving mechanical ventilation, however, ICU patients within 48 hours of extubation were also considered. Consent for ICU patients was sought from a nominated consultee when the patient could not provide consent themselves. Both healthy volunteers and critically ill patients were excluded if they have a clear indication that the specific ultrasound technique cannot be performed. For example, limb amputations, restricting dressings, surgical wound sites, site infection. Similarly, for intercostal/diaphragm studies; chest wall deformities (including open chest), chest wall wounds, site infection, chest drains obscuring anatomical landmarks. Those receiving ECMO were not considered in the reliability study.

In this study, myself (SP – operator 1 (Op1)) and two other clinicians (SS – operator 2 (Op2)) and RH – operator 3 (Op3)) were enlisted as operators in the reliability study only. SP was formally trained in thoracic ultrasound and led and developed the respiratory and peripheral muscle ultrasound technique. SS and RH were experienced with ultrasound in critical care but with no prior experience

with respiratory muscle assessment. SS and RH were provided with a study manual and received training by SP to demonstrate operational ability of the ultrasound equipment and application of the protocol at the bedside before being allowed to participate in the studies. SP taught SS and RH all aspects of the technique and protocol including image acquisition, storage and transfer.

The reliability study using healthy volunteers was performed by SP and RH. The reliability study using critical care patients was performed by SP and SS. Details of image acquisition, transfer and analysis are detailed in 2.2.2

4.4.4 Statistical analysis

The statistical model and calculation of sample size for the reliability study was via a two-way mixed model of the intra-class correlation coefficient (ICC) for absolute agreement. ICC was used to determine intra- and inter-observer reliability using two-way random effects for absolute agreement. An ICC of <0.49 (poor agreement) 0.50-0.74 (moderate agreement) and >0.75 (excellent agreement) was used. ICC calculated using a two-way mixed effects model where people effects are random and measure effects are fixed. Literature concerning sample size for reliability studies suggests that to compare two operators, where two measurements per anatomical site are taken, a minimum of 12 participants are required, anticipating coefficients between 0.6 and 0.9 and using a significance level of 0.05 and power of 80%.[250] Similarly, a minimum of 19 participants are required, anticipating coefficients between 0.7 and 0.9 and using a significance level of 0.05 and power of 80%[250]. Therefore, to ensure that I demonstrated excellent agreement before application within the clinical trial setting, I targeted an ICC of >0.9 and envisage this to be achieved within 20 patients. Bland-Altman analysis was used to examine and provide a visual representation of the agreement between assessors and to examine any systematic errors that may be present. Data was assessed for normality using the Shapiro-Wilk test. Mann-Whitney tests were used to assess differences between non-parametric continuous data. Categorical variables were analysed using Chi-squared test or Fisher's exact test

when the sample size was less than 10. ANOVA or Kruskal-Wallis test was used for multiple comparisons between groups depending on whether data was normally distributed. Statistical analyses were performed using SPSS 27 (IBM, New York, USA) and GraphPad Prism v9.0 (GraphPad, CA, USA).

4.5 Results

4.5.1 Reliability and reproducibility study

Twelve healthy volunteers and 12 ICU patients were recruited to the reliability study. In the ICU patient cohort, 14 patients were initially included but two were excluded after consent (one patient was too agitated during the study and one patient had inadequate views of both hemi-diaphragms). The patient demographics are summarised in Table 4-1. At the time of analysis, DIA_{EXC} images for one patient in the ICU cohort had not transferred correctly from the ultrasound machine and were no longer retrievable. DIA_{EXC} analysis therefore had a total of 11 ICU patients. The Bland-Altman plots for diaphragm, parasternal muscle and rectus femoris muscle measurements for healthy volunteers and ICU patients are shown in Figure 4-1, Figure 4-2 and Figure 4-3 respectively. Further admission detail and mechanical ventilation parameters for the ICU cohort are summarised in Table 4-2.

	Healthy Volunteers (n=12)	**ICU Patients (n=12)**
Age (years)	30.0 ± 9.3	60.0 ± 21.3
Male – no. (%)	6 (50)	11 (92)
Body Mass Index (kg/m^2)	22.8 ± 2.7	26.6 ± 2.8
APACHE II	N/A	27.0 (19-29)
MV Days	N/A	8 (3-20)
Days in mandatory mode	N/A	5 (3-11)
Sedation days	N/A	7 (3-20)

Table 4-1. Basic baseline demographics of ICU patients in the ultrasound reliability study

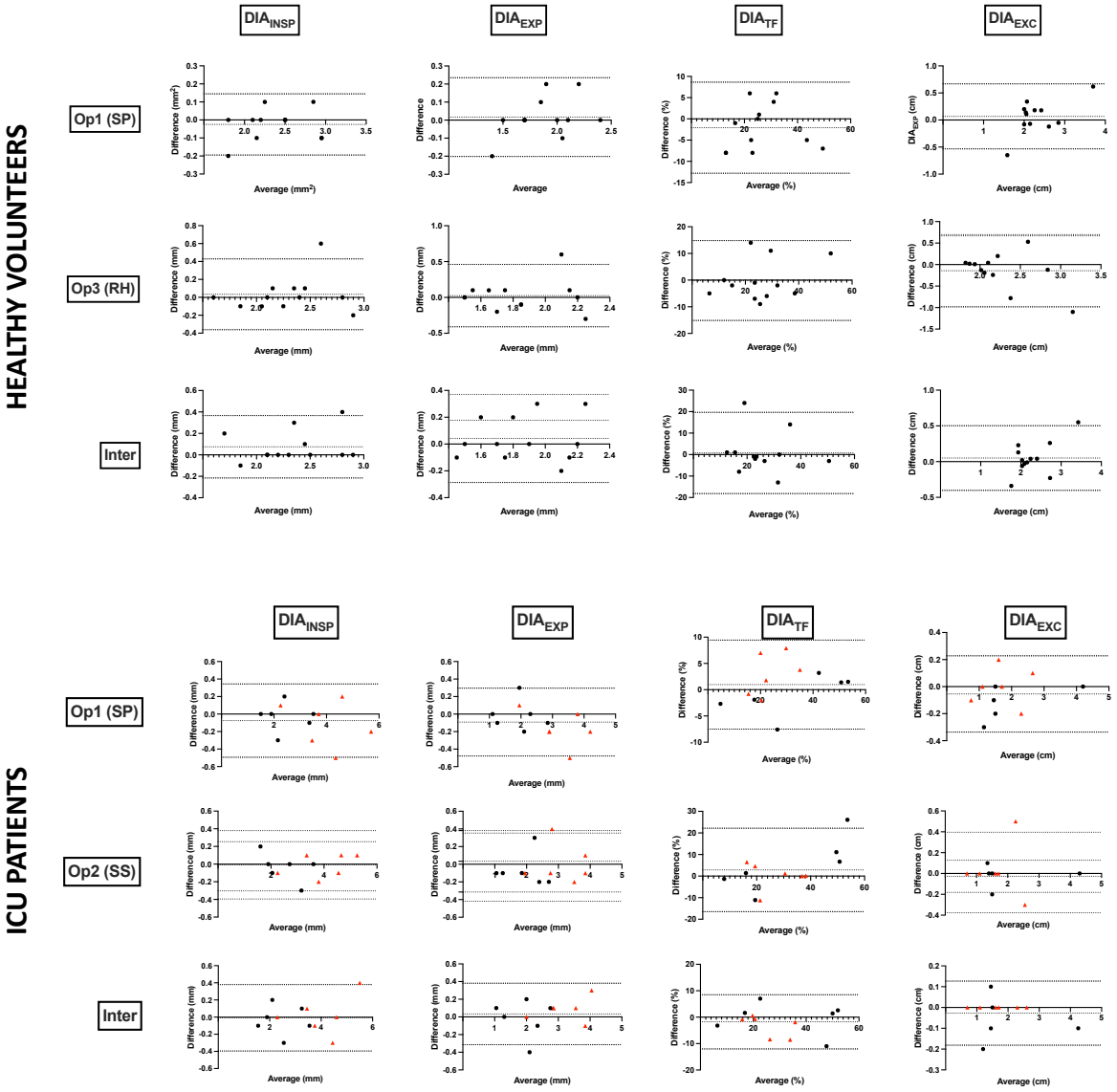


Figure 4-1. Bland-Altman plots for diaphragm measurements for healthy volunteers and ICU patients in ultrasound reliability study

For all plots, average measurement of operator(s) is on the x-axis, and absolute difference of measurements on the y-axis. The upper and lower dotted lines represent the 95% upper and lower limits of agreement respectively. The middle-dotted line is the bias which represents the mean of the differences between operators. Red triangles indicate measurements that were made without surface marking. *Op1; operator 1, Op2; operator 2, Inter; inter-observer, DIA_{EXP}; diaphragm end-expiratory thickness diaphragm, DIA_{INSP}; diaphragm end-inspiratory thickness, DIA_{EXC}; diaphragm excursion; DIA_{EXC}.*

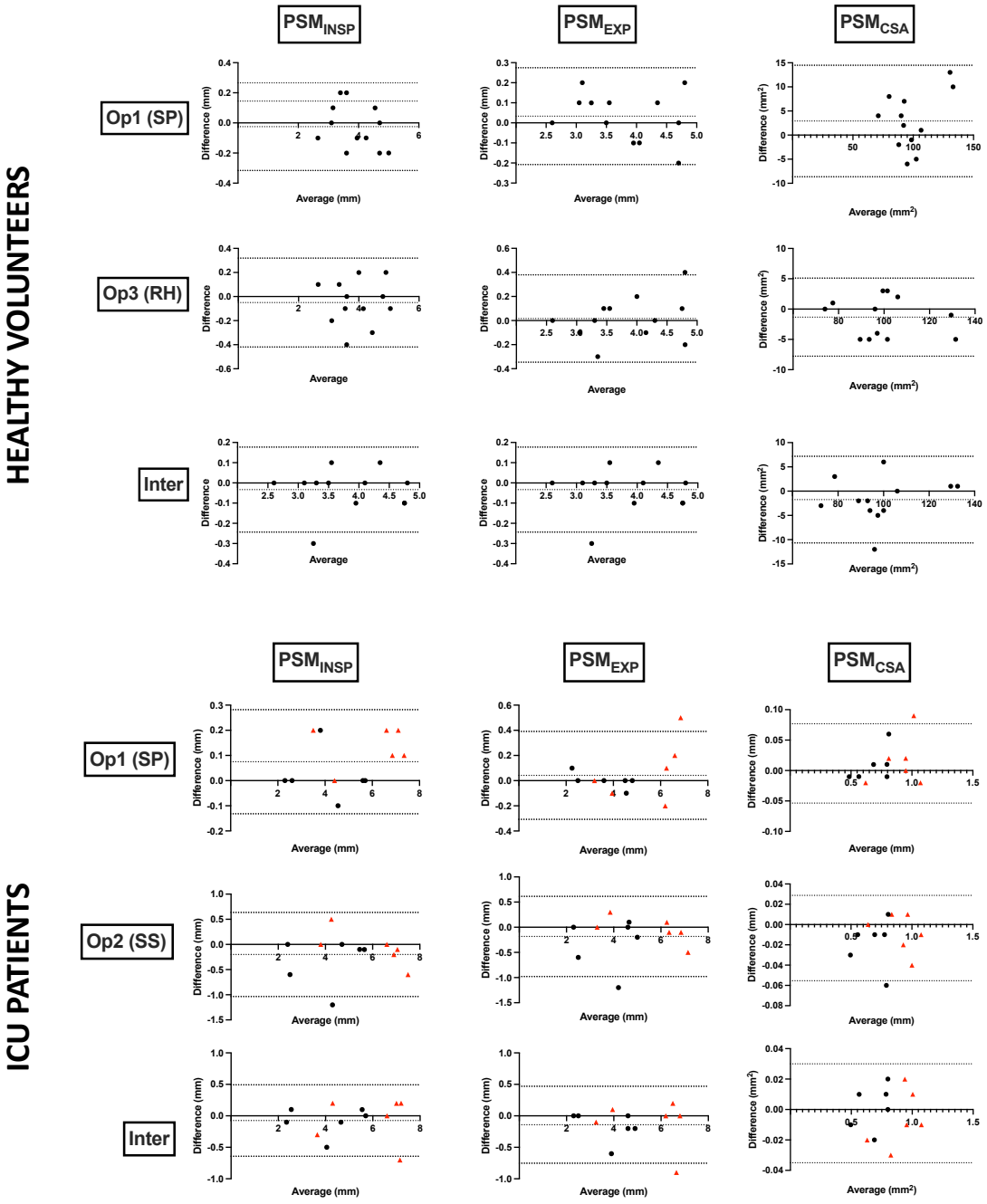


Figure 4-2. Bland-Altman plots for parasternal muscle measurements for healthy volunteers and ICU patients in ultrasound reliability study

For all plots, average measurement of operator(s) is on the x-axis, and absolute difference of measurements on the y-axis. The upper and lower dotted lines represent the 95% upper and lower limits of agreement respectively. The middle-dotted line is the bias which represents the mean of the differences between operators. Red triangles indicate measurements that were made without surface marking. *Op1; operator 1, Op2; operator 2, Inter; inter-observer, PSM_{INSP}; parasternal end-inspiratory thickness, PSM_{EXP}; parasternal end-expiratory thickness, PSM_{CSA}; parasternal cross-sectional area.*

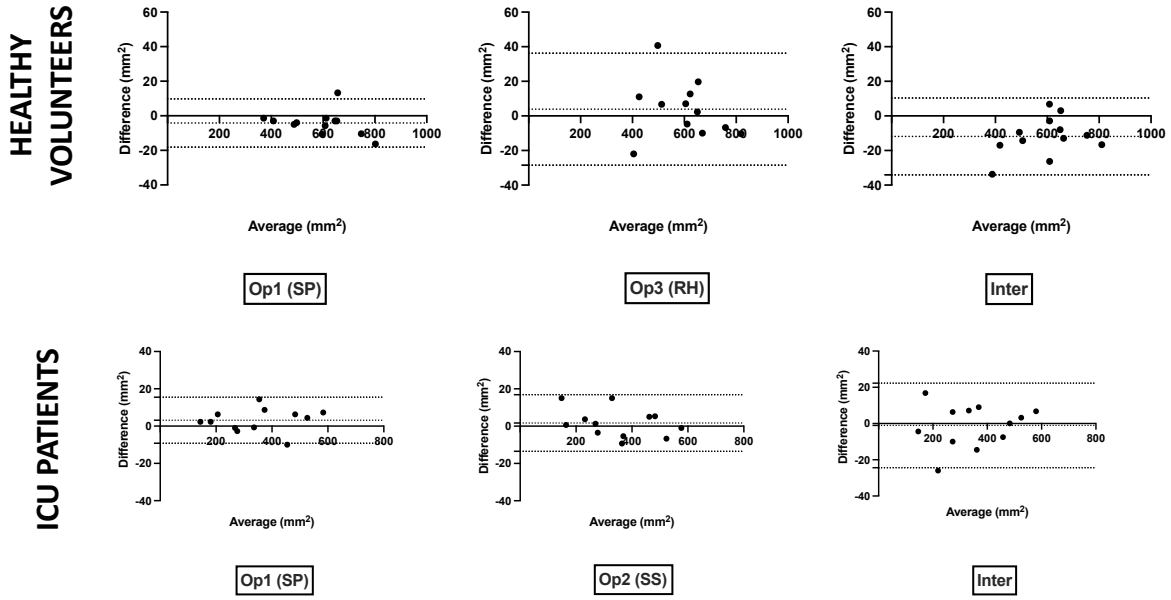


Figure 4-3. Bland-Altman plots for rectus femoris muscle measurements for healthy volunteers and ICU patients in ultrasound reliability study

For all plots, average measurement of operator(s) is on the x-axis, and absolute difference of measurements on the y-axis. The upper and lower dotted lines represent the 95% upper and lower limits of agreement respectively. The middle-dotted line is the bias which represents the mean of the differences between operators. *Op1; operator 1, Op2; operator 2, Op3; operator 3, Inter; inter-observer.*

Age – years	**68 (43 – 74)**
Male – no. (%)	11 (92%)
BMI – kg/m²	26.6 (24.9 – 27.9)
Co-morbidities	
Chronic respiratory disease	1 (8%)
Hypertension	5 (42%)
Diabetes mellitus	5 (42%)
Valvular heart disease	2 (16%)
Ischaemic heart disease	2 (16%)
Alcohol excess	2 (16%)
Arrhythmia disorder	4 (32%)
None	2 (16%)
APACHE II	27 (20 – 29)
Transferred in from another HDU/ICU – no. (%)	9 (75%)
Mechanical Ventilation	
Indication for intubation	
Respiratory failure – no. (%)	5 (42%)
Cardiac failure – no. (%)	2 (16%)
Elective surgery – no. (%)	5 (42%)
Receiving MV at the time of study – no. (%)	8 (67%)
Support mode, pressure-controlled	5 (62%)
Mandatory mode, pressure-controlled	3 (38%)
Mechanical ventilation days at time of scan – no. (%)	7.5 (3 – 19.8)
Days spent in mandatory mode ventilation	4.5 (3.25 – 9.5)
Support mode ventilation at time of scan – no. (%)	5 (42%)
Days of sedation	7 (3.5 – 19.8)
FiO2 – %	31 (28 – 45)
PEEP (cmH_2O)	8 (5 – 10)
Pressure Support (cmH_2O)	10 (2.5 – 11)
Tidal volume (ml)	469 (442 – 554)
Tidal volume 6-7ml/kg? (n=9)	4 (44%)
pH (pre-scan)	7.46 (7.44 – 7.47)
P_aO_2 (kPa) (pre-scan)	13.5 (11.1 – 16.2)
$PaCO_2$ (kPa) (pre-scan)	5.42 (4.86 – 5.73)

Table 4-2. Clinical details for ICU patients included in reliability study

Twelve patients were recruited into the reliability study. *BMI; body mass index, APACHE II; acute physiology and chronic health evaluation score, MV; mechanical ventilation, FiO2; fraction of inspired oxygen, PEEP; positive end-expiratory pressure, P_aO_2; partial pressure of arterial oxygen, P_aCO_2; partial pressure of arterial carbon dioxide.*

4.5.1.1 Intra- and inter-observer agreement

Intra-observer agreement was calculated for all three operators (SP, RH and SS). Inter-observer agreement was calculated between SP and RH (healthy volunteers) and SP and SS (ICU patients) only. Individual patient values and coefficient of variation (CoV) are summarised in Table 4-3 and all raw measurement data in Appendix **9**-**2**. An ICC of >0.9 was achieved for all but two quantitative measurements (DIA_{EXC} and DIA_{EXP} for operator 2 in the healthy cohort) (Table 4-3). An ICC of >0.9 was achieved within 12 patients for other measurements and are comparable to published data with similar cohorts.[121,143,268]

HV	Op1	Op1 ICC	CoV	Op3	Op2 ICC	CoV	Op1-Op3 ICC	CoV
DIA_{INSP} (cm)	0.24 (0.21-0.26)	0.988 (0.961-0.997)	1.8	0.23 (0.20-0.25)	0.932 (0.767-0.980)	3.1	0.955 (0.837-0.987)	3.8
DIA_{EXP} (cm)	0.19 (0.17-0.21)	0.966 (0.883-0.990)	2.7	0.18 (0.17-0.20)	0.848 (0.464-0.957)	5.8	0.908 (0.692-0.973)	5.6
DIA_{TF} (%)	24 (19-32)	0.937 (0.790-0.982)	13.4	24 (16-32)	0.908 (0.673-0.974)	17.0	0.803 (0.289-0.944)	20.5
DIA_{EXC} (cm)	2.11 (1.97-2.59)	0.923 (0.742-0.978)	7.0	2.13 (2.00-2.49)	0.721 (0.088-0.918)	8.9	0.941 (0.802-0.983)	9.1
PSM_{INSP} (cm)	0.38 (0.33-0.44)	0.991 (0.969-0.997)	2.1	0.38 (0.34-0.44)	0.985 (0.949-0.996)	2.5	0.990 (0.965-0.997)	2.4
PSM_{EXP} (cm)	0.38 (0.33-0.43)	0.993 (0.977-0.998)	1.7	0.38 (0.33-0.43)	0.985 (0.949-0.996)	2.3	0.995 (0.982-0.998)	2.1
PSM_{CSA} (cm^2)	0.94 (0.86-1.10)	0.970 (0.891-0.991)	3.8	0.99 (0.89-1.10)	0.990 (0.966-0.997)	2.0	0.982 (0.940-0.995)	3.5
RF_{CSA} (mm^2)	610 (498-668)	0.999 (0.996-1.000)	0.8	617 (515-677)	0.996 (0.986-0.999)	1.5	0.996 (0.949-0.999)	2.0
ICU	**Op1**	**Op1 ICC**	**CoV**	**Op2**	**Op2 ICC**	**CoV**	**Op1-Op2 ICC**	**CoV**
DIA_{INSP} (cm)	0.34 (0.20-0.41)	0.992 (0.975-0.998)	3.9	0.33 (0.20-0.46)	0.997 (0.988-0.999)	2.5	0.994 (0.979-0.998)	3.6
DIA_{EXP} (cm)	0.26 (0.19-0.36)	0.988 (0.959-0.997)	4.2	0.26 (0.19-0.35)	0.989 (0.963-0.997)	4.3	0.992 (0.972-0.998)	5.3
DIA_{TF} (%)	24 (17-42)	0.981 (0.936-0.994)	8.7	26 (16-49)	0.899 (0.663-0.970)	16	0.969 (0.898-0.991)	13.3
DIA_{EXC} (cm)	1.50 (1.10-2.60)	0.995 (0.982-0.999)	3.7	1.50 (1.10-2.60)	0.992 (0.969-0.998)	4.1	0.998 (0.994-1.000)	4.5
PSM_{INSP} (cm)	0.51 (0.35-0.68)	0.999 (0.993-1.000)	1.3	0.51 (0.38-0.69)	0.983 (0.938-0.995)	4.1	0.993 (0.977-0.998)	4.4
PSM_{EXP} (cm)	0.46 (0.32-0.62)	0.997 (0.990-0.999)	1.9	0.47 (0.33-0.64)	0.983 (0.939-0.995)	4.1	0.989 (0.962-0.997)	4.7
PSM_{CSA} (cm^2)	0.81 (0.62-0.95)	0.991 (0.971-0.997)	2.0	0.80 (0.64-0.96)	0.995 (0.79-0.999)	1.6	0.998 (0.993-0.999)	2.3
RF_{CSA} (mm^2)	345 (242-425)	0.999 (0.998-1.000)	1.1	346 (232-483)	0.999 (0.997-1.000)	1.2	0.998 (0.994-1.000)	2.1

Table 4-3. Intra- and inter-observer agreement in respiratory and peripheral skeletal muscle ultrasound in healthy volunteers and ICU patients

Op1; operator 1, Op2; operator 2, Op3; operator 3, Op1-Op2; inter operator reliability coefficient between operator 1 and operator 2, Op1-Op3; inter operator reliability coefficient between operator 1 and operator 3, ICC; intra-class correlation coefficient, CoV; coefficient of variation; HV; healthy volunteer, ICU; ICU patients, PSM_{CSA}; parasternal muscle cross-sectional area, PSM_{EXP}; parasternal muscle end-expiratory thickness, PSM_{INSP}; parasternal muscle end-inspiratory thickness, DIA_{EXP}; diaphragm end-expiratory thickness, DIA_{INSP}; diaphragm end-inspiratory thickness, DIA_{EXC}; diaphragm excursion. Measurement values for each observer given as median (IQR) and ICC values given as ICC (95% confidence interval).

4.5.2 Protocol amendments for main clinical study

For the first six patients in the ICU patient reliability cohort, I initially adopted an anatomical approach without surface anatomy marking (excluding RF_{CSA}). Previous studies have found that marking the site prior to scan improves reproducibility and reliability, particularly for less experienced ultrasonographers.[152] No significant difference was found within or between operator measurements. Operators agreed that surface markings should be made for the main clinical study to reduce inter-operator variability if the same operator cannot perform a study.

4.5.3 Clinical study cohort

Forty-four patients (31 (70%) male; mean age 51 $\pm$ 16 years) were recruited to the prospective clinical studies (16 (36%) WAVE-INFLAME; 28 (64%) DeVENT). Patients recruited to DeVENT all had an admission diagnosis of acute respiratory distress syndrome (ARDS) and therefore are referred to as the 'ARDS' cohort from here on. Conversely, patients in WAVE are referred to as the 'non-ARDS' cohort. The study cohort demographics and admission characteristics are summarised in
Table 4-4.

The mean age of non-ARDS patients was significantly greater than patients with ARDS (62$\pm$17 years vs. 45$\pm$12 years respectively, p<0.001). BMI of non-ARDS patients was significantly lower compared to those with ARDS (non-ARDS: 25.4 kg/m^2 (IQR 22.4-29.1) vs. ARDS: 30.6 kg/m^2 (IQR 23.8-37.4), p=0.011). There was no significant difference in the proportion of male patients in each study (non-ARDS: 10 (62%) vs. ARDS: 21 (75%), p=0.380). Of the three ethnicity groups identified (Caucasian, Asian and Black), there were more Caucasians in the non-ARDS group (non-ARDS: 14 (88%) vs. ARDS: 14 (50%), p=0.013). There were more patients with Asian ethnicity in the ARDS group (non-ARDS: 0 (0%) vs. 9 (32%), p=0.011). The number of Black and African patients in each study was not significantly different (non-ARDS: 2 (12%) vs. ARDS: 5 (18%), p=0.640). There was a greater proportion of patients in the non-ARDS group with cardiovascular comorbidity compared to those with ARDS (non-ARDS: 14

(88%) vs. ARDS: 14 (50%), p=0.013). No other significant differences were seen with respiratory, renal, diabetes, malignancy history.

Non-ARDS patients had a significantly higher admission sequential organ failure assessment (SOFA) score than those with ARDS (non-ARDS: 12 (IQR 9-13) vs. ARDS: 8 (IQR 6-9), p=0.006). Patients with ARDS had a clinically significantly higher number of sedation and mechanical ventilation days (Table 4-4). The median ICU length of stay was 9 days more than those without ARDS (ARD: 21 (IQR 9-41) vs. non-ARDS: 12 (IQR 9-19), p=0.059). C-reactive protein was higher on admission in those with ARDS (ARDS: 162.5mg/L (IQR 92.0-218.9) vs. non-ARDS: 47.2mg/L (IQR 20.9-142), p<0.001). The time to intubation and time to acquiring the first ultrasound image from intubation was significantly higher in those with ARDS (ARDS: 5 days (IQR 3-9) vs. non-ARDS: 1 day (IQR 0-4); p=0.004, and ARDS: 3 days (IQR 2-5) vs. non-ARDS: 2 days (IQR 1-2); p<0.001 respectively).

	All patients (n=44)	Non-ARDS (n=16)	ARDS (n=28)	p value
Age – years	51 ± 16	62 ± 17	45 ± 12	**<0.001**
Male – no. (%)	31 (70)	10 (62)	21 (75)	0.380
Body mass index – kg/m²	29.0 (23.4-32.4)	25.4 (22.4-29.1)	30.6 (23.8-37.4)	**0.011**
Ethnicity				
Caucasian – no. (%)	28 (64)	14 (88)	14 (50)	**0.013**
Asian – no. (%)	9 (20)	0 (0)	9 (32)	**0.011**
Black – no. (%)	7 (16)	2 (12)	5 (18)	0.640
Co-morbidities				
Cardiac	21 (48)	12 (75)	9 (32)	**0.011**
Respiratory	10 (23)	4 (25)	6 (21)	>0.999
Renal	2 (4)	1 (6)	1 (3)	>0.999
Diabetes mellitus	6 (13)	2 (12)	4 (14)	>0.999
Malignancy	3 (7)	1 (6)	2 (7)	>0.999
Other	20 (45)	7 (43)	13 (46)	>0.999
None	5 (11)	1 (6)	4 (14)	0.638
APACHE II score	15 (12-19)	16 (11-23)	15 (13-17)	0.632
SOFA score	9 (7-12)	12 (9-13)	8 (6-9)	**0.006**
SARF centre LoS – days	18 (9-26)	12 (9-19)	21 (9-41)	0.059
MV days	15 (10-26)	12 (9-16)	22 (10-41)	**0.007**
Sedation days	13 (9-25)	9 (6-12)	21 (9-41)	**<0.001**
Neuromuscular blockade days	3 (2-10)	2 (1-4)	4 (2-12)	0.091
RRT within 48-hr of admission – no (%)	10 (36)	4 (25)	6 (21)	>0.999
Cumulative fluid balance – Litres	1.0 (-4.9-3.8)	2.1 (-5.1-3.8)	-0.3 (-4.8-4.3)	0.928
White cell count – x10⁹/L	12.8 (10.0-22.8)	11.3 (10.3-13.7)	15.1 (9.7-26.9)	0.105
C-reactive protein – mg/L	136.5 (34.8-192.8)	47.2 (20.9-142)	162.5 (92.0-218.9)	**<0.001**
Time to intubation – days	3 (1-7)	1 (0-4)	5 (3-9)	**0.004**
Hospital admission to 1st image – days	6 (3-11)	3 (1-6)	9 (6-13)	**<0.001**
Intubation to 1st image – days	2 (2-3)	2 (1-2)	3 (2-5)	**<0.001**

Table 4-4. Patient demographics and clinical characteristics of patients recruited to prospective clinical studies

Parametric data displayed as mean ± standard deviation. Non-parametric data displayed as median (interquartile range). p<0.05 classified as statistically significant. *ARDS; acute respiratory distress syndrome, APACHE II; acute physiology and chronic health evaluation, SOFA; sequential organ failure assessment, LoS; length of stay, MV; mechanical ventilation, SARF; severe respiratory failure.*

4.5.4 Number of suitable imaging studies

Quantitative measurements at baseline, day 3, day 7 and day 14 was available for 22 patients for RF_{CSA} and DIA_{EXP} and for 21 patients for PSM_{EXP} and PSM_{CSA}. Quantitative measurements at baseline, day 3 and day 7 was available for 34 patients for RF_{CSA}, 35 patients for DIA_{EXP} and 33 patients for PSM_{EXP} and PSM_{CSA}.

4.5.4.1 Peripheral skeletal muscle wasting occurred acutely and continuously

Of the 44 patients recruited, four patients could not undergo rectus femoris ultrasound. One patient died within 48 hours of recruitment and only had baseline imaging, three other patients were not able to be imaged on the day of recruitment and the first images were collected on day 3.

At day 3, there was a cross-sectional area loss of 6.3% (IQR -9.5--3.9, p<0.0001) when compared to baseline. This loss increased to 16% (IQR -19.0--9.0, p<0.0001) at day 7 and 23% (-30.0--17.7, p<0.0001) at day 14 (Figure 4-4). Only 11 patients were admitted to day 21 at which the loss increased further to 28% (IQR -38--18, p<0.0001). An example of longitudinal RF_{CSA} imaging on ultrasound is shown in Figure 4-5. One patient had significantly greater baseline muscle mass compared to the rest of the cohort. When excluding this patient from analyses, significant changes between baseline and subsequent time points remained.

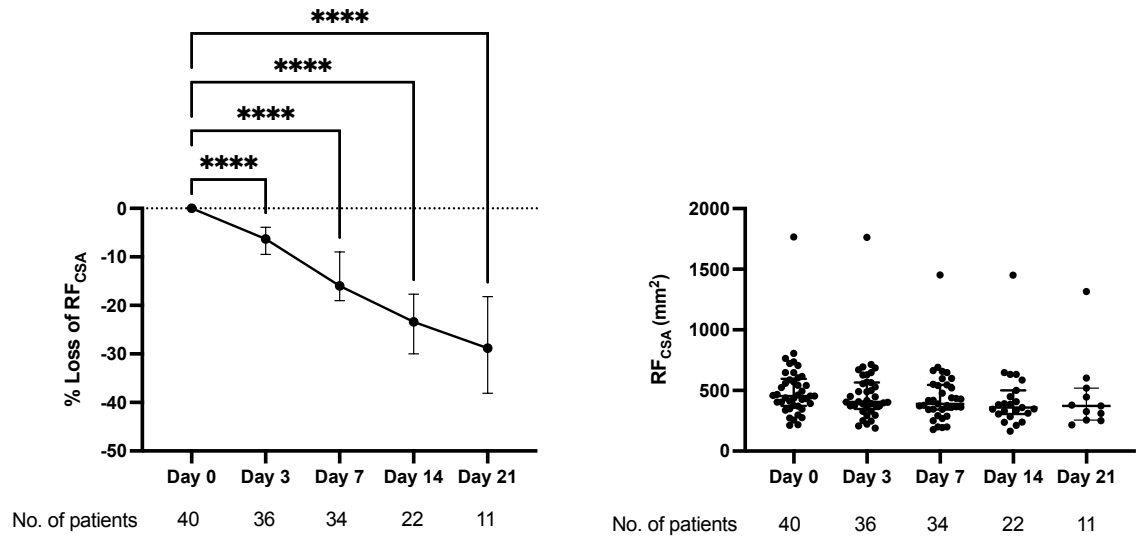


Figure 4-4. Change in rectus femoris cross-sectional area during critical illness

Longitudinal change in rectus femoris cross-sectional area (RF_{CSA}). At day 3, there was a cross-sectional area loss of 6.3% (IQR -9.5--3.9, p<0.0001) when compared to baseline. This loss increased to 16% (IQR -19.0--9.0, p<0.0001) at day 7 and 23% (-30.0--17.7, p<0.0001) at day 14. Data in left panel shown as median change with inter-quartile range error bars. Individual values for RF_{CSA} shown in right panel. ****p<0.0001. Difference between day 0 and subsequent time-points analysed using Kruskal-Wallis test for multiple comparisons.

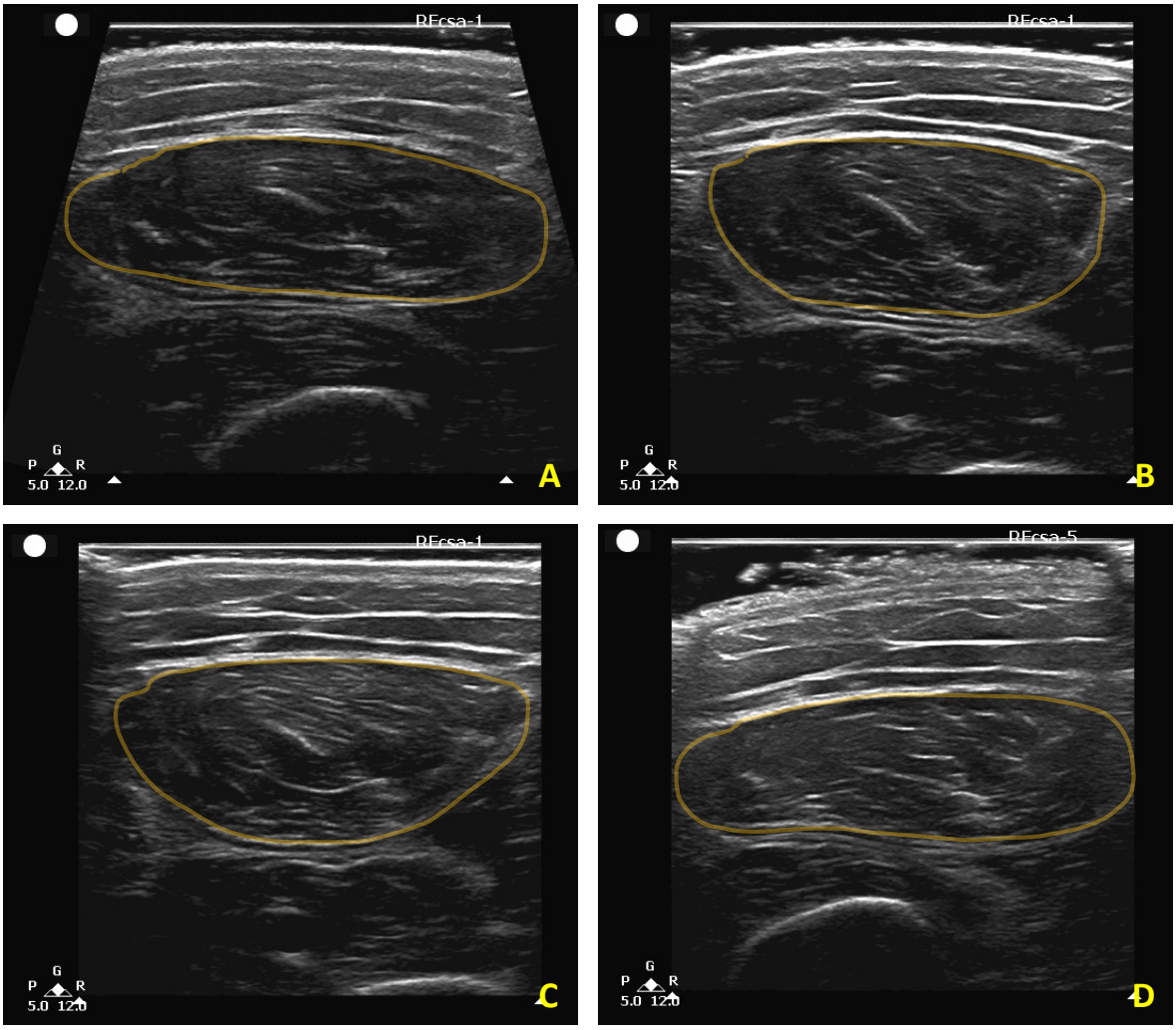


Figure 4-5. Longitudinal changes in rectus femoris cross-sectional area during critical illness

Rectus femoris ultrasound images of a patient at day 0 [A], day 3 [B], day 7 [C] and day 14 [D] with cross-sectional area (illustrated by yellow outline) of 805.5mm^2, 714.0mm^2, 690.5mm^2 and 647.5mm^2 respectively. The percentage loss of muscle mass from day 0 to day 14 was 19.6%.

4.5.4.2 Parasternal muscle cross-sectional area and end-inspiratory thickness

Of the 44 patients recruited, three patients could not undergo parasternal muscle ultrasound. Two patients had an open splinted chest on the day of recruitment, and one was too agitated to participate. Longitudinal data (up to and including day 14) was available for 21 patients for PSM_{EXP} and PSM_{CSA}. Changes in PSM_{EXP} and PSM_{CSA} are summarised in Table 4-5 and shown in Figure 4-6 and Figure 4-7. There was a significant loss of PSM_{EXP} and PSM_{CSA} from baseline at day 3, day 7 and day 14 (Figure 4-7).

At all study points, there was a greater loss of PSM_{CSA} compared to PSM_{EXP}. The percentage loss in these two quantitative measures was significantly different at day 3 and day 14 only (Table 4-5).

At day 3, 5 patients (4 non-ARDS, 1 ARDS) had an increase in PSM_{EXP} (median 4.5% (IQR 2.7-13.9) and 5 patients (3 non-ARDS, 2 ARDS) had no change. By day 7, there were only 2 patients (1 non-ARDS, 1 ARDS) who had an increase in PSM_{EXP} (median 6.6% (IQR 21-11.1) and 4 (3 non-ARDS, 1 ARDS) who had no change. However, at day 3, PSM_{CSA} remained unchanged in only 1 non-ARDS patient and increased in one patient. Similarly, at day 7, PSM_{CSA} increased in one patient, but all others demonstrated a loss.

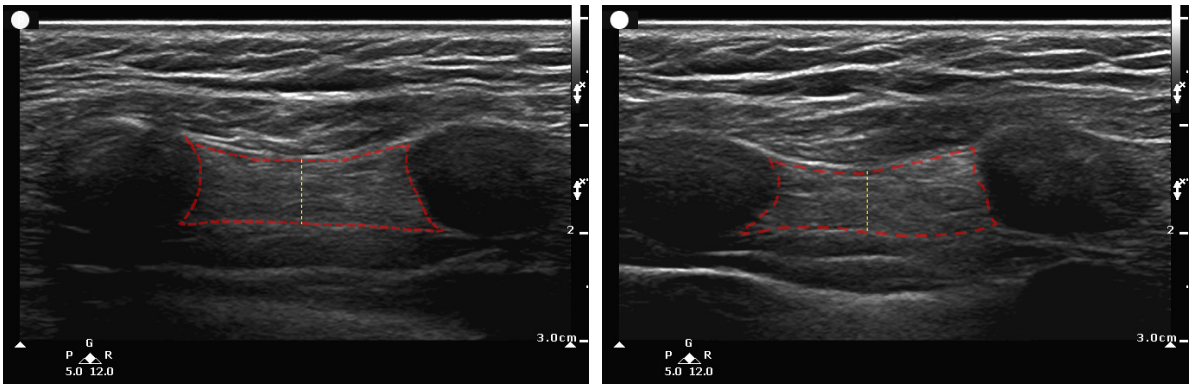


Figure 4-6. Parasternal muscle ultrasound changes in critical illness

Parasternal muscle cross-sectional area (PSM_{CSA}) (dashed red outline) and parasternal muscle end-expiratory thickness (PSM_{EXP}) (vertical yellow line) quantified using B-mode ultrasound. In this example, the left image was taken on admission to the ICU (day 0) and the right image on day 3. PSM_{CSA} and PSM_{EXP} declined by 5.0% (1.44cm^2 to 1.33cm^2) and 6.5% (6.2mm to 5.8mm) respectively.

Study day	% change in PSM_{EXP}	% change in PSM_{CSA}	p value
Day 3	-5.0 (-6.2--0.0)	-7.3 (-12.4--3.6)	0.003
Day 7	-9.8 (-13.7--2.2)	-12.2 (-17.8--7.2)	0.104
Day 14	-10.4 (-15.6--4.1)	-16.4 (-22.3--9.5)	0.015
Day 21	-11.8 (-23.5--4.7)	-20.3 (-28.0--17.9)	0.085

Table 4-5. Changes in parasternal muscle during critical illness

Comparison of changes in parasternal muscle bulk during critical illness. Generally, greater loss was observed for PSM_{CSA} than PSM_{EXP}, however, significant differences only seen at day 3 and 7. Difference between groups analysed using Mann-Whitney test. Data shown as median (IQR). *PSM_{EXP}; parasternal muscle end-expiratory thickness, PSM_{CSA}; parasternal muscle cross-sectional area.*

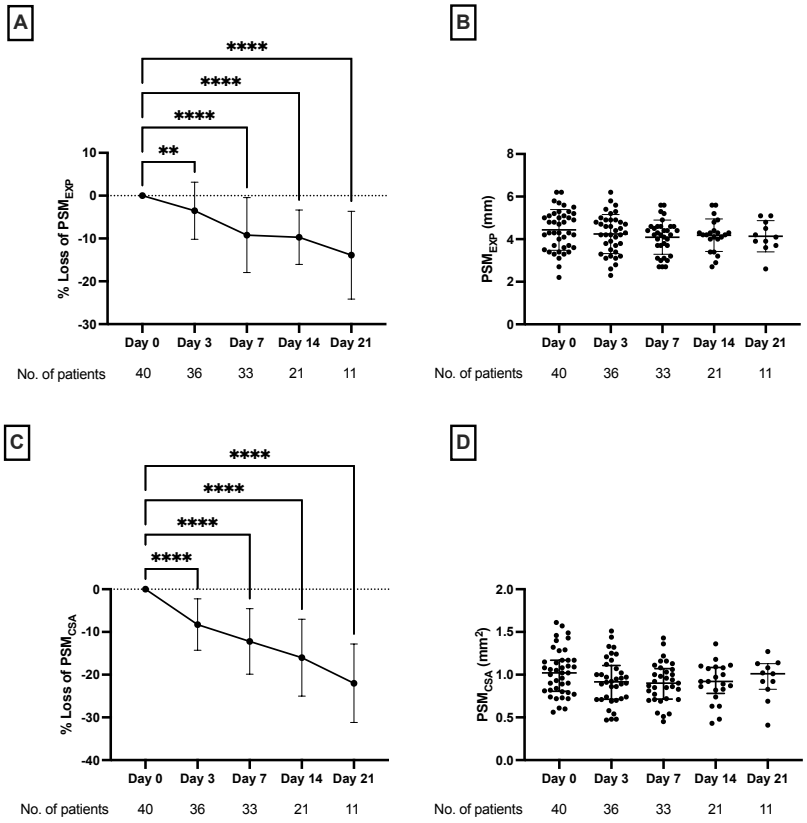


Figure 4-7. Change in parasternal muscle during critical illness

Data presented as median values with inter-quartile range error bars. (B) and (D) also show actual values for PSM_{EXP} and PSM_{CSA} respectively. **p<0.01, ****p<0.0001. Difference between day 0 and subsequent time-points analysed using Kruskal-Wallis test for multiple comparisons.

4.5.4.3 Diaphragm end-expiratory thickness

Of the 44 patients recruited, one patient could not undergo diaphragm ultrasound as they were too agitated. An example of DIA_{EXP} measurement is shown in Figure 4-8. Longitudinal data up to and including day 7 and day 14 was available for 34 and 21 patients respectively. Eleven patients had consecutive imaging to day 21. By day 3 there was a loss of 4.1% (IQR -13.3--3.7). This increased to -9.1% (IQR -14.8--0.0) by day 7 and -11.6% (IQR -23.5--3.8) by day 14. When compared to baseline measurements, changes were significant at each timepoint (Figure 4-9).

At day 3, 10 patients (5 non-ARDS, 5 ARDS) had an increase in DIA_{EXP} (5.1% (IQR 4.1-12.8) and 6 patients (2 non-ARDS, 4 ARDS) had no change. By day 7, there were 7 patients (3 non-ARDS, 4 ARDS) who had an increase in DIA_{EXP} (4.5% (IQR 3.8-11.1) and 3 ARDS patients who had no change.

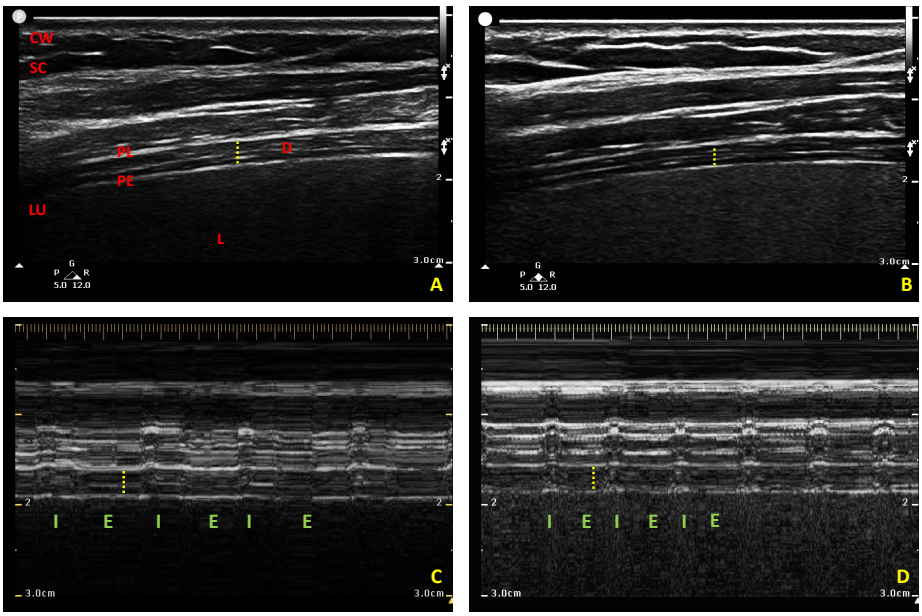


Figure 4-8. Diaphragm thickness assessment using ultrasound

Diaphragm thickness ultrasound images of a patient at day 0 [A] and day 7 [B] using B-mode ultrasound. Images [C] and [D] are the M-mode images used to quantify thickness for [A] and [B] respectively. In this example the end-expiratory thickness on day 0 is 2.5mm, and at day 7 it is unchanged and measures 2.5mm (from a mean of three consecutive breaths). Dotted vertical line illustrates the end-expiratory thickness point. *I = inspiration, E = expiration, CW = chest wall, SC = subcutaneous fat, PL = pleura, PE = peritoneum, D = diaphragm, LU = lung, L = liver*.

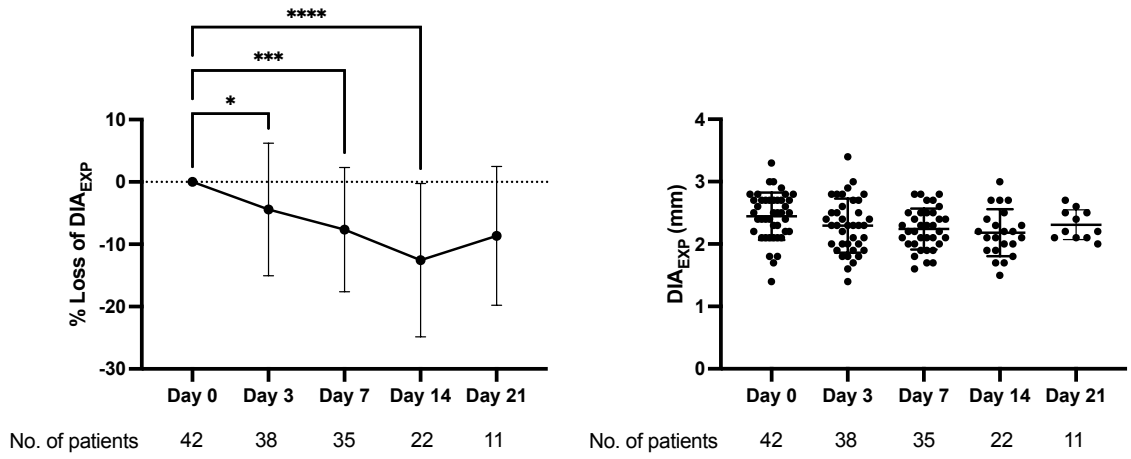


Figure 4-9. Change in diaphragm thickness during critical illness

Data presented as median values with inter-quartile range error bars. In the right panel, measurements are plotted as the average of three consecutive measurements. *p<0.05, ***p<0.001, ****p<0.0001. Difference between day 0 and subsequent time-points analysed using Kruskal-Wallis test for multiple comparisons. *DIA_{EXP}; diaphragm end-expiratory thickness.*

4.5.5 Peripheral versus respiratory muscle wasting

Longitudinal changes in each muscle group for each patient beteen day 0 and day 7 are shown in Figure 4-10. The change in muscle groups was compared at different study time points (Figure 4-11). At day 3, there were no significant differences in percentage change of muscle mass/thickness between muscle groups. However, at day 3, PSM_{CSA} change was significantly different to PSM_{EXP} (PSM_{CSA}: -7.3% (IQR -12.6--3.6) vs. PSM_{EXP}: -5.0% (IQR -6.2--2.2), p=0.040).

At day 7, RF_{CSA} change was significantly different to the change seen in DIA_{EXP} (RF_{CSA}: -16.0% (-19.0--9.0) vs. DIA_{EXP}: -9.1% (-14.8-0.0, p= 0.006) and PSM_{EXP} (RF_{CSA}: -16.0% (-19.0--9.0) vs. PSM_{EXP}: -9.8% (IQR -13.7--2.2, p= 0.011) but not when compared to PSM_{CSA}. At day 14, RF_{CSA} change was significantly different to the change seen in DIA_{EXP} (RF_{CSA}: -23.4% (IQR -30.0--17.7) vs. DIA_{EXP}: -11.6% (IQR -23.5--3.8), p=0.007) and PSM_{EXP} (RF_{CSA}: -23.4% (IQR -30.0--17.7) vs. $PSM_{EXP:}$ -10.4% (IQR -15.6—4.1),

p<0.0001) but not to the change in PSM_{CSA} (RF_{CSA}: -23.4% (IQR -30.0--17.7) vs. PSM_{CSA}: -16.4% (IQR -22.3--9.5), p=0.105).

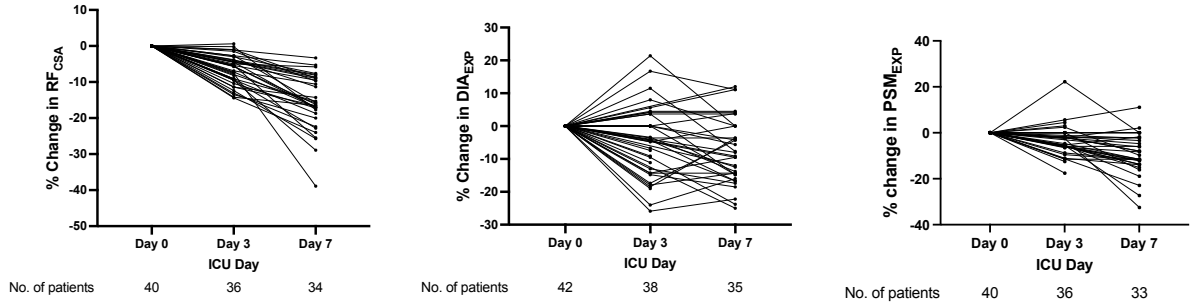


Figure 4-10. Longitudinal patient changes in respiratory and peripheral skeletal muscle

Longitudinal individual patient changes in diaphragm, parasternal and rectus femoris muscle during critical illness. *RF_{CSA}; rectus femoris cross-sectional area, DIA_{EXP}; diaphragm end-expiratory thickness, PSM_{EXP}; parasternal muscle end-expiratory thickness,*

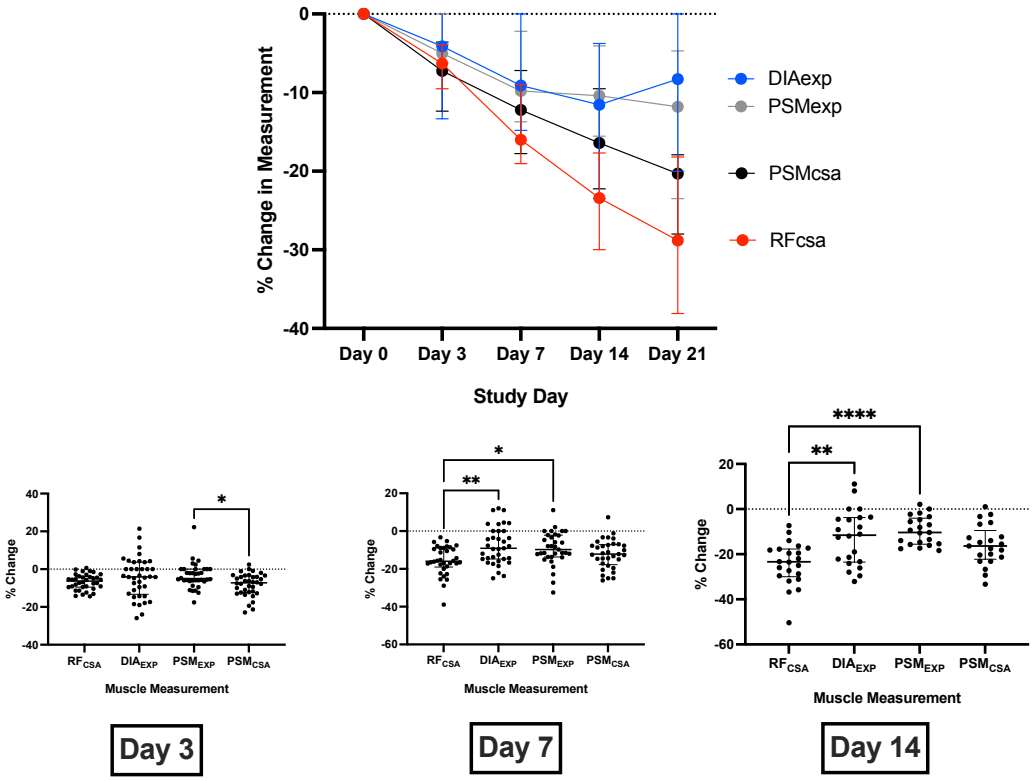


Figure 4-11. Comparison of changes in peripheral and respiratory muscle during critical illness

Top panel compares the median change in muscle groups during the ICU admission up to day 21. Data is plotted as median values with IQR error bars. The bottom panel of graphs illustrate the actual values and differences between muscle groups. *RF_{CSA}; rectus femoris cross-sectional area, DIA_{EXP}; diaphragm end-expiratory thickness, PSM_{EXP}; parasternal muscle end-expiratory thickness, PSM_{CSA}; parasternal muscle cross-sectional area*. *p<0.05, **p<0.01, ****p<0.0001. Difference between muscle groups analysed using Kruskal-Wallis test for multiple comparisons.

4.5.6 Diaphragm and parasternal muscle changes

PSM_{EXP} was positively correlated with DIA_{EXP} across all timepoints (r=0.400 (95% CI 0.078-0.647), p=0.014). Similarly, there was a positive correlation between PSM_{TF} and DIA_{TF} (r=0.589 (95% CI 0.281-0.788), p<0.001) suggesting active contraction of the diaphragm and PSM at the time of study (Figure 4-12).

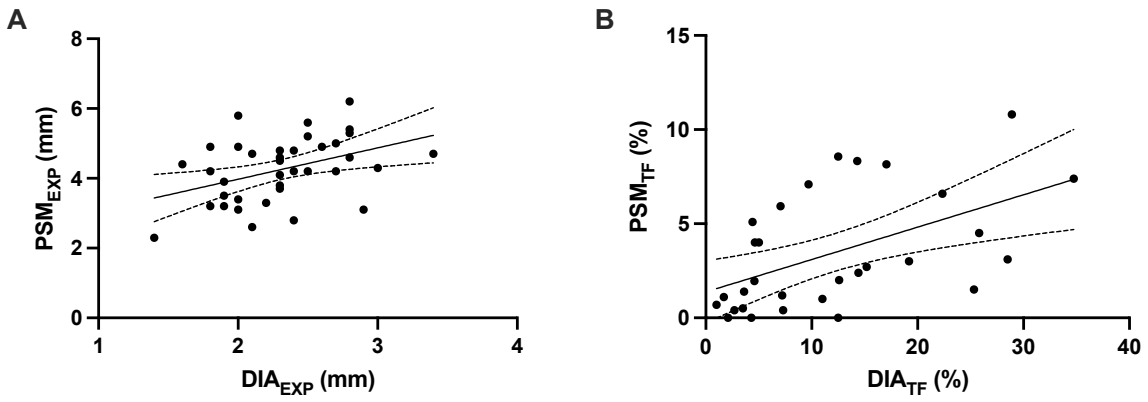


Figure 4-12. Comparison of respiratory muscle thickness and contraction

(A) Correlation plot of parasternal muscle end-expiratory thickness (PSM_{EXP}) and diaphragm end-expiratory thickness (DIA_{EXP}) showing positive correlation (r=0.400 (95% CI 0.078-0.647), p=0.014). (B) Correlation plot of parasternal muscle thickening fraction (PSM_{TF}) and diaphragm thickening fraction (DIA_{TF}) showing positive correlation (r=0.589 (95% CI 0.281-0.788), p<0.001). Dashed curved lines represent 95% confidence intervals. Correlation analysed using Spearman's test.

4.5.7 Defining high and low muscle wasting groups

In line with previous longitudinal critical care studies of rectus femoris muscle, a 10% loss in cross-sectional area at day 7 (or >1.4% loss/day) was used to represent significant muscle wasting.[14,126] 34/44 (77%) patients had RF_{CSA} measured at day 7. Of the 10 patients (22%) that did not, 6 had RF_{CSA} measurements taken at day 3 and therefore daily change in muscle mass was calculated for a total of 40 patients. Four patients (9%) did not have longitudinal data to analyse. For those with only baseline and day 3 measurements, these patients were also classified as 'high wasters' if the loss exceeded 1.4%/day. Overall, for RF_{CSA}, 28/40 patients (70%) had a daily percentage loss of ≥1.4%/day and classed as 'high wasters'. The daily percentage loss of RF_{CSA} was significantly greater for the high wasters (-2.5% per day (IQR -3.2--2.2) vs. -1.1%/day (IQR -1.3--0.8), p<0.0001).

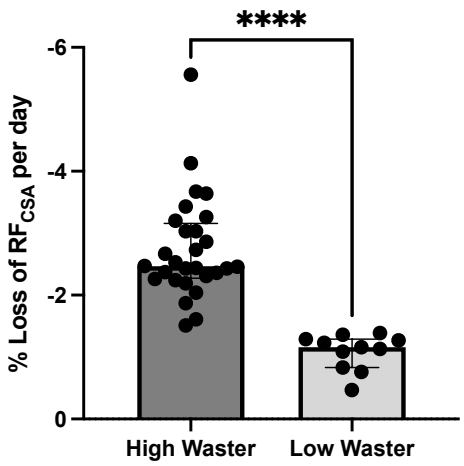


Figure 4-13. High- and low-waster groups by daily loss of rectus femoris cross-sectional area

Patients with a rate of muscle wasting >1.4% per day at the time of a second imaging study were classed as 'High Waster' patients. Those with a rate of wasting <1.4% were classed as 'Low Waster' patients. ****p<0.0001. Difference between groups analysed using Mann-Whitney test.

4.5.7.1 Associations with rate of muscle wasting

Given that 70% of patients had median daily muscle wasting rate of >1.4%, clinical associations for this group were investigated. Clinical characteristics of low and high wasters is summarised in Table 4-6. Gender was not associated with low- or high-waster status (male low-waster: 6 (50%) vs. male high-waster: 22 (79%), p=0.130). Severity of illness, as per admission APACHE II score, was not significantly different between groups (low-waster: 14 points (IQR 10-15) vs. high-waster: 15 points (IQR 13-19), p=0.062). BMI was not statistically different (low-waster: 26.2 kg/m^2 (IQR 22.8-33.5) vs. high-waster: 29.1 kg/m^2 (IQR 24.3-33.1), p=0.475). Patients in the low-waster group had a fewer number of days of mandatory mode mechanical ventilation (low-waster: 4.8 days (IQR 3.5-6.2) vs. high-waster: 6.8 days (IQR 5.3-7.0), p=0.018) and neuromuscular blockade (low-waster: 1.5 days (IQR 0.0-2.8) vs. high-waster: 3.0 days (IQR 1.0-6.8), p=0.047) in the first 7 days of admission (Figure 4-14). Patients in the high-waster group had a longer ICU length of stay compared to the low waster group (low-waster: 12 days (IQR 7-20) vs. high-waster: 22 days (IQR 11-39) p=0.074) and whilst clinically relevant, the difference was not statistically significant.

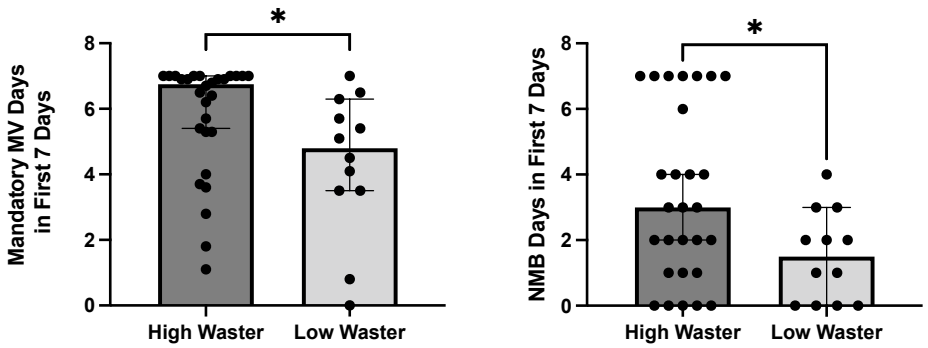


Figure 4-14. High- and low-waster groups and clinical risk factors

High muscle waster group patients had a greater number of mandatory mechanical ventilation days in the first 7 days and received a greater number of days of neuromuscular blockade. *MVB; mechanical ventilation, NMB; neuromuscular blockade.* *p<0.05. Difference between groups analysed using Mann-Whitney test.

	Low Waster (n=12)	High Waster (n=28)	p value
Age – years	50 (35-64)	51 (30-64)	0.710
Male – no. (%)	6 (50)	22 (79)	0.130
Body mass index – kg/m²	25.8 (22.4-34.0)	29.1 (24.2-33.1)	0.406
APACHE II score	14 (10-15)	15 (13-19)	0.062
SOFA score	6 (5-8)	7 (4-10)	0.388
Mandatory MV days in 7 days	4.8 (3.5-6.2)	6.8 (5.3-7.0)	**0.018**
Neuromuscular blockade days in 7 days	1.5 (0.0-2.8)	3.0 (1.0-6.8)	**0.047**
C-reactive protein – mg/L	80.7 (30.4-191.8)	147.5 (56.6-196.1)	0.668
Hospital admission to 1st image – days	3 (1-11)	6 (4-11)	0.154
Intubation to 1st image – days	2 (1-3)	2 (2-3)	0.079
SARF centre LoS – days	12 (7-20)	22 (11-39)	0.074

Table 4-6. Clinical characteristics of high- and low-wasting rate patients

Low waster = <1.4% per day loss in rectus femoris cross-sectional area at the time of a second imaging study, high waster = >1.4% per day loss in rectus femoris cross-sectional area at the time of a second imaging study. *APACHE II score; acute physiology and chronic health evaluation score, SOFA; sequential organ failure assessment score, MV; mechanical ventilation, SARF; severe acute respiratory failure, LoS; length of stay.*

4.5.8 Clinical associations and risk factors for muscle wasting

4.5.8.1 Differences in muscle wasting patterns by admission diagnosis

Patients with ARDS did not have significantly different patterns of muscle wasting when compared to those without ARDS (Figure 4-15). Whilst the loss of RF_{CSA} and DIA_{EXP} was greater in COVID19 patients at days 3 and 7, there was no statistical difference. In addition, there was no significant difference seen at day 3, day 7 or day 14 for RF_{CSA}, DIA_{EXP}, or PSM_{CSA}. At day 3, patients with ARDS had a significantly greater loss of PSM_{EXP} when compared to those without ARDS (ARDS: -5.8% (-7.7--2.1) vs. non-ARDS: 0.0% (-5.4-4.5), p=0.008). However, no differences were seen at day 7 or day 14 (Appendix **9**-**3**).

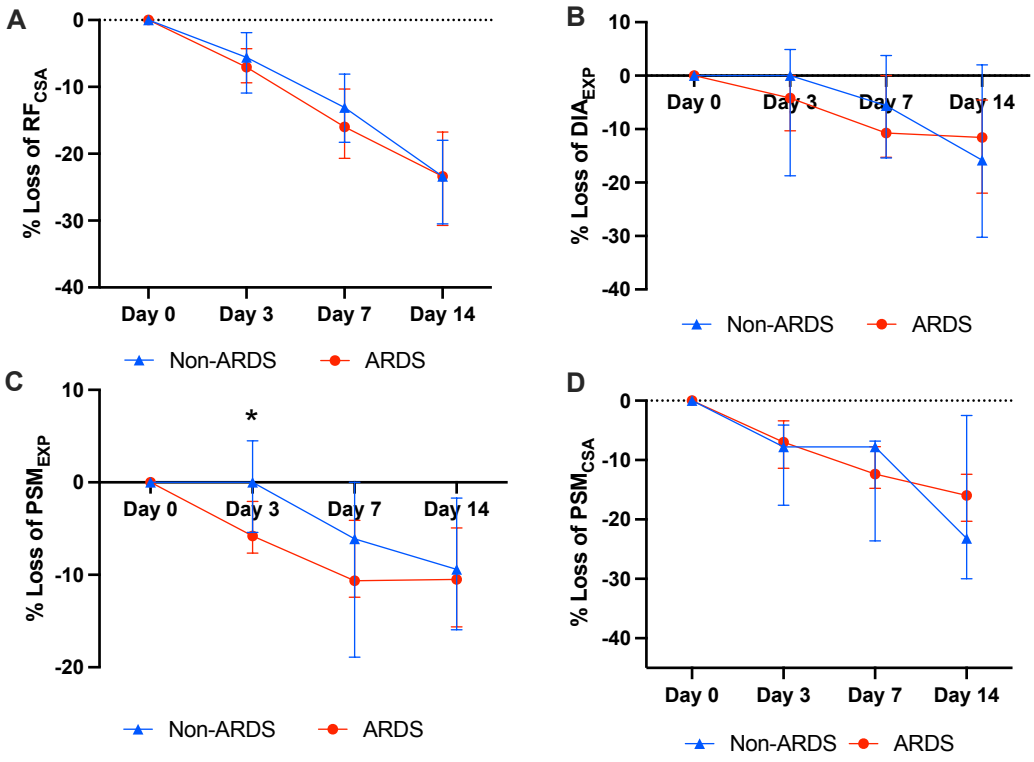


Figure 4-15. Comparison of muscle mass changes by ARDS diagnosis status

Changes in rectus femoris cross-sectional area (RF_{CSA}) (A), diaphragm end-expiratory thickness (DIA_{EXP}) (B), parasternal muscle end-expiratory thickness (PSM_{EXP}) (C) and parasternal muscle cross-sectional area (PSM_{CSA}) (D) between non-ARDS and ARDS related critical illness. *p<0.05. Differences from day 0 and subsequent time points analysed using Kruskal-Wallis multiple comparisons test.

4.5.8.2 Muscle wasting in COVID19 ARDS

19/44 (43%) patients had a diagnosis severe COVID19 ARDS. There were no significant differences in the trajectory of muscle wasting between non-ARDS, non-COVID19 ARDS and COVID19 ARDS patients (Figure 4-16). 12/15 (80%) COVID19 patients with longitudinal ultrasound data (at least baseline and a second imaging study) were found to have a daily loss of RF_{CSA} of ≥1.4%/day ('high waster') compared to 16/25 (64%) in the non-COVID cohort. Overall, patients with COVID19 disease and high-waster status represented 43% of the high-wasting cohort. However, COVID19 disease was not significantly associated with a greater rate of muscle wasting (relative risk 1.7 (95% CI 0.7-5.1), p=0.4774).

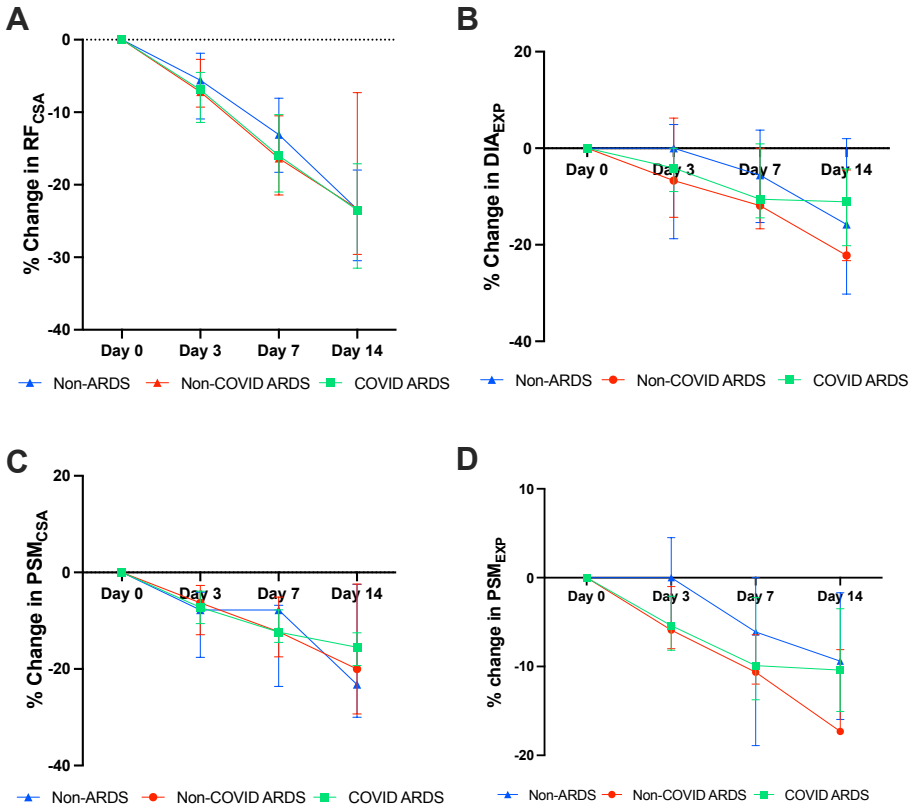


Figure 4-16. Comparison of muscle changes in COVID19 and non-COVID19 critical illness

Changes in rectus femoris cross-sectional area (RF_{CSA}) (A), diaphragm end-expiratory thickness (DIA_{EXP}) (B), parasternal muscle end-expiratory thickness (PSM_{EXP}) (C) and parasternal muscle cross-sectional area (PSM_{CSA}) (D) between non-ARDS and non-COVID19 ARDS and COVI19-ARDS related critical illness. Differences from day 0 and subsequent time points analysed using Kruskal-Wallis multiple comparisons test.

4.5.9 Echogenicity and muscle mass

Rectus femoris and parasternal muscle quality was assessed using ultrasound echogenicity (EG) measurement. EG values at baseline and subsequent study points are shown in Table 4-7.

	Day 0	Day 3	Day 7	Day 14	Day 21
RF_{EG} – pixels	51 (42-61)	53 (43-71)	55 (42-64)	61 (45-62)	58 (55-72)
Percentage change[a]	0	12 (-8-21)	7 (0-28)	17 (2-40)	20 (4-28)
PSM_{EG}[*] - pixels	79 (69-97)	86 (70-101)	86 (75-103)	83 (66-95)	83 (70-102)
Percentage change[a]	0	0 (-3-8)	10 (-2-17)	7 (-1-19)	6 (-3-16)

Table 4-7. Longitudinal changes in echogenicity in rectus femoris and parasternal muscles

[*]using square method, [a]percentage from baseline. RF_{EG}: day 0 (n=31), day 3 (n=24), day 7 (n=22), day 14 (n=17), day 21 (n=7). PSM_{EG}: day 0 (n=37), day 3 (n=34), day 7 (n=26), day 14 (n=19), day 21 (n=9).

Percentage change in echogenicity from baseline was assessed for rectus femoris (ΔRF_{EG}) and parasternal muscle (ΔPSM_{EG}). Echogenicity analysis was possible on 23 patients at day 7 and for 18 patients at day 14. Patients (or study points) were excluded due to differences in gain and/or depth settings from the baseline images of that patient. Anatomical variation in patients meant that controlling for depth and gain between patients was difficult and unreliable.

The ΔRF_{EG} was significantly higher at day 7 and 14 when compared to baseline (day 7: ΔRF_{EG}: 6.6% (IQR 0.3-28.1), p=0.020; day 14: ΔRF_{EG}: 16.9% (IQR 2.3-40.3), p<0.001). (Figure 4-17). In comparison, ΔPSM_{EG} was only significantly different at day 7 when compared to baseline but not at any other time point (day 7: ΔPSM_{EG}: 10.3% (IQR -1.8-17.3) (Figure 4-17). At day 14 and 21, PSM_{EG} trended towards baseline. There was no significant difference in $\%\Delta RF_{EG}$ or $\%\Delta PSM_{EG}$ and low- and high-waster groups at day 7 (Figure 4-18).

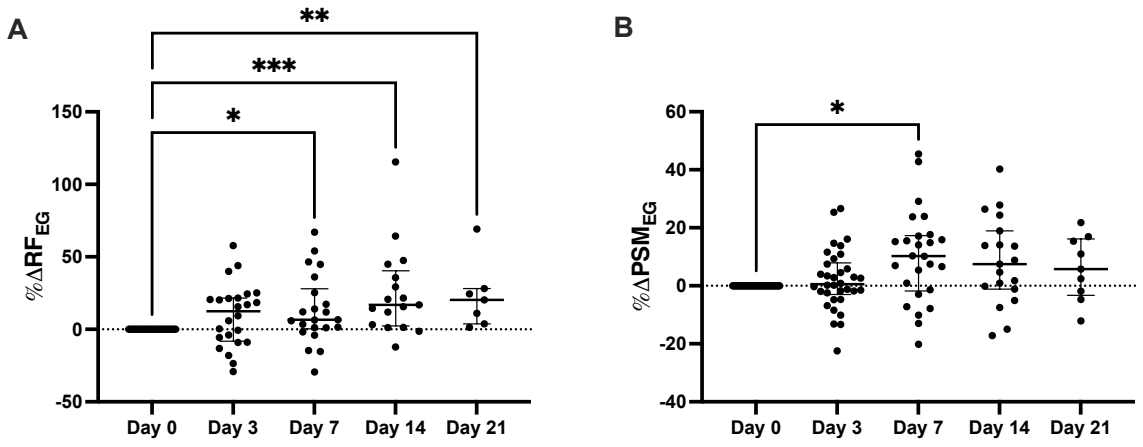


Figure 4-17. Change in muscle echogenicity during critical illness

Longitudinal changes in muscle of echogenicity of rectus femoris (A) and parasternal muscle (B). Changes from baseline were assessed using Kruskal-Wallis multiple comparison tests. *p<0.05, **p<0.01, ***p<0.0001. *%ΔRF_{EG}; change in rectus femoris echogenicity, %ΔPSM_{EG}; change in parasternal muscle echogenicity.*

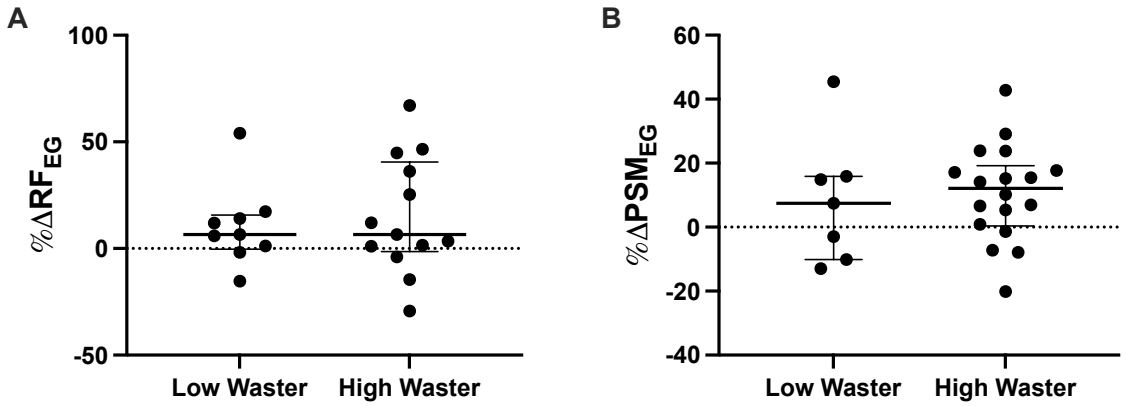


Figure 4-18. Comparison of echogenicity changes and wasting status in rectus femoris and parasternal muscle

When stratified by daily rate of muscle wasting, no significant differences were seen in percentage change of echogenicity in rectus femoris muscle (A) or parasternal muscle (B). Analysis performed with Mann-Whitney test on unpaired, non-parametric data. *%ΔRF_{EG}; change in rectus femoris echogenicity, %ΔPSM_{EG}; change in parasternal muscle echogenicity.*

There was a weak negative association between ΔRF_{CSA} and ΔRF_{EG} (e.g. a greater loss of RF_{CSA} correlated with a higher RF_{EG}), and between change in ΔPSM_{EXP} and ΔPSM_{EG} but neither were

statistically significant. There was a weak positive correlation between ΔPSM_{CSA} and ΔPSM_{EG}, but this was also not statistically significant (Figure 4-19). Together, these data suggest that the changes in muscle size/bulk do not result in significant changes in muscle quality when using non-invasive ultrasonography.

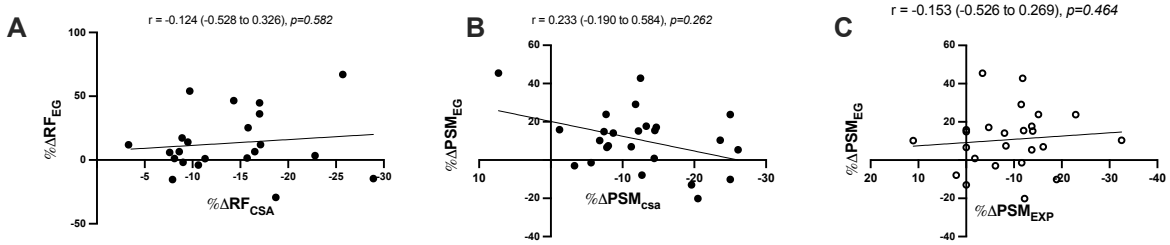


Figure 4-19. Relationship between change in muscle mass and echogenicity

Change in rectus femoris cross-sectional area ($\%\Delta RF_{CSA}$, A), parasternal muscle cross-sectional area ($\%\Delta PSM_{CSA}$, B) and parasternal muscle end-expiratory thickness ($\%\Delta PSM_{EXP}$, C) were not significantly associated with percentage change in echogenicity. Correlation analysis using Spearman's test. *$\%\Delta RF_{EG}$; change in rectus femoris echogenicity, $\%\Delta PSM_{EG}$; change in parasternal muscle echogenicity.*

4.5.10 Inflammation in acute muscle wasting

Serum CRP levels were used as an initial biomarker of inflammation on admission. The baseline CRP of the clinical cohort was 137mg/L (IQR 35-193). CRP levels remained >100mg/L in the first two weeks of ICU admission indicating persistence of high levels of inflammation. Baseline CRP levels were not significantly different between low and high waster groups (high waster: 147.5mg/L (IQR 56.6-196.1) vs. low waster: 80.7mg/L (IQR 30.4-191.8), p=0.668) (Figure 4-20). Similarly, assessment of CRP levels longitudinally in the first 21 days of ICU stay between 'high-wasters' and 'low wasters' showed higher CRP levels between days 3-7 and between days 13-17 but only significantly higher at day 14 in 'low wasters' compared to 'high wasters' (low waster: 290.0mg/L (126.5-324.5) vs. high waster: 105.3mg/L (56.5-159.6), p=0.041) (Figure 4-21).

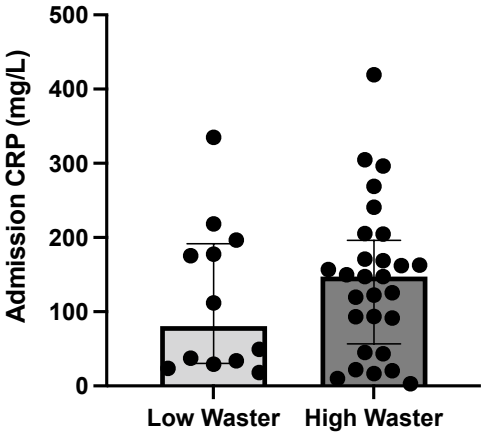


Figure 4-20. C-reactive protein levels in patients with high and low daily rate of muscle wasting

CRP levels at baseline in low- and high-waster groups (high waster: 147.5mg/L (IQR 56.6-196.1) vs. low waster: 80.7mg/L (IQR 30.4-191.8), p=0.668). Difference between groups analysed using Mann Whitney test.

Patients with ARDS had a significantly higher CRP at baseline compared to those without ARDS (162.5mg/L (IQR 92.0-218.9) vs. 47.2mg/L (IQR 20.9-142.0), p=0.008). When subcategorising ARDS into non-COVID19 and COVID19 ARDS aetiologies, there was no significant difference in baseline CRP (non-COVID19 ARDS; 157.0mg/L (IQR 75.9-282.8) vs. COVID19 ARDS; 163.0mg/L (IQR 91.5-205.5), p=0.736). However, when comparing COVID19 ARDS to non-ARDS diagnoses, patients with COVID19 ARDS had a lower CRP at baseline and at day 3 only (Figure 4-22) (day 0, COVID19 ARDS: 163 mg/L (IQR 92-206) vs. non-ARDS: 47mg/L (IQR 21-142), p=0.028, day 3, COVID19 ARDS: 84mg/L (IQR 28-127) vs. non-ARDS: 166mg/L (IQR 95-298).

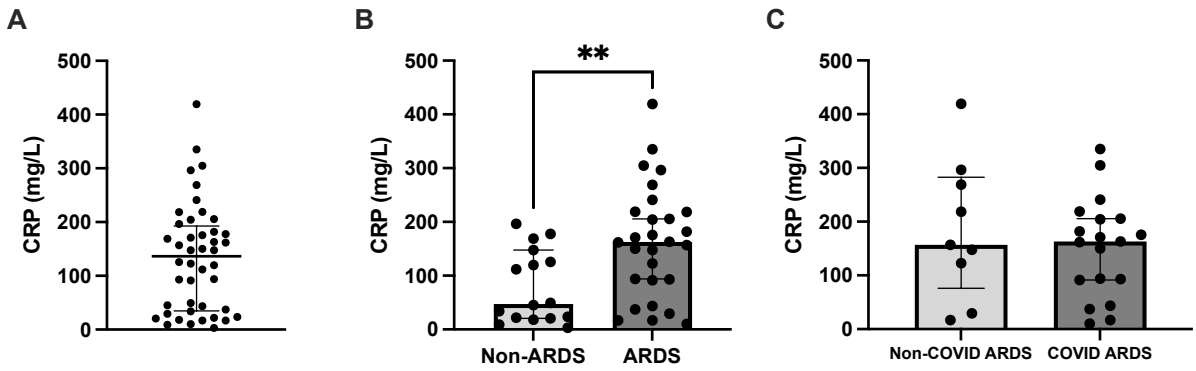


Figure 4-21. Baseline CRP levels by admission diagnosis

Median baseline CRP was 137mg/L (IQR 35-193) (A). When stratified by non-ARDS or ARDS diagnosis, there was a significant difference in baseline CRP (B). No significant difference in baseline CRP levels was seen between non-COVID19 ARDS and COVID19 ARDS (C). **p<0.01. Difference between groups analysed using Mann Whitney test.

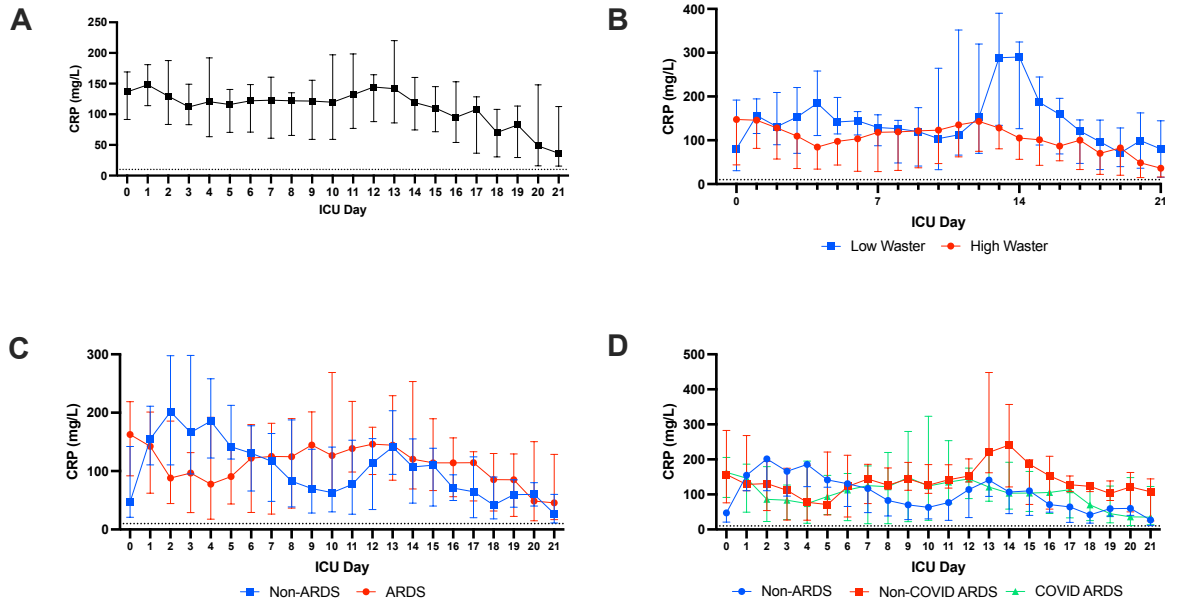


Figure 4-22. Longitudinal trends in CRP levels during ICU admission.

Longitudinal changes in CRP levels using ICU admission. Across all patients, median CRP was >100mg/L for the first 14 days (A). When stratified by daily rate of muscle wasting, CRP levels in high wasters were not significantly different from admission to day 21 (B). Patients with ARDS had a significantly higher baseline CRP level (ARDS: 162.5mg/L (IQR 92.0-218.9) vs. non-ARDS: 47.2mg/L (IQR 20.9-142.0), p=0.008) (C). Non-ARDS patients had higher baseline (day 0) and day 3 levels of CRP when compared to COVID19 ARDS patients (p=0.032 and p=0.047 respectively) (D). Dotted horizontal line = upper normal value of 10mg/L. Longitudinal differences in CRP and between groups were analysed using Sidak's multiple comparisons test.

In addition, day 7 changes in RF_{CSA}, PSM_{CSA}, PSM_{EXP} and DIA_{EXP} were not significantly associated with mean CRP levels over the same period (Figure 4-23).

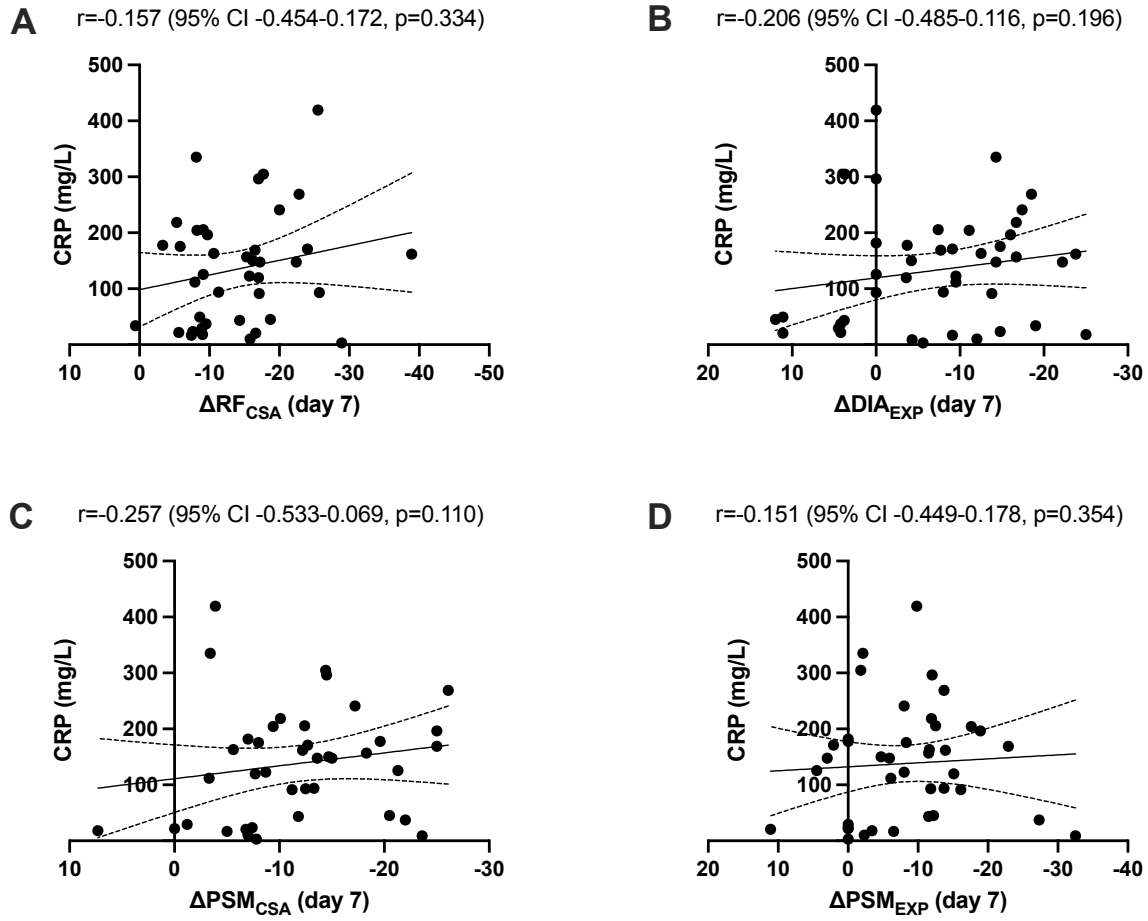


Figure 4-23. Association between CRP levels over the first 7 days and change in respiratory and peripheral skeletal muscle bulk

Seven-day average C-reactive protein levels were plotted against change in rectus femoris cross-sectional area (A), diaphragm end-expiratory thickness (B), parasternal muscle cross-sectional area (C) and parasternal end-expiratory thickness (D). Lines of best fit are plotted on each graph with dotted lines representing the 95% confidence interval. No significant association was seen in all muscle groups. Correlation analyses performed using non-parametric Spearman's correlation test.

4.5.11 Predicting muscle wasting status

A binomial logistic regression was performed to determine the effects of independent variables on the wasting rate ('high-waster vs. 'low-waster'). Linearity of the continuous variables with respect to the logit of the dependent variable was assessed via the Box-Tidwell procedure. Independent variables were deemed statistically significant and included in the final model when $p<0.1$. Based on this assessment, all continuous independent variables were found to be linearly related to the logit of the dependent variable. Outliers were identified by standardized residuals with a value of >2.5 standard deviations. These were inspected individually and included in the subsequent analysis as necessary.

The number of mandatory mechanical ventilation days, steroid days and neuromuscular blockade days (in the first 3 days of admission), admission CRP level, COVID19 status, provision of ECMO, APACHEII score, admission SOFA score, body mass index, gender, and pre-ICU length of stay were chosen as independent variables based on *a priori* assessment of risk factors. Of the 11 independent variables only 4 were statistically significant (Table 4-8). The number of neuromuscular blockade days in the first 3 days was significantly associated with wasting status (OR 3.5 (95% CI 1.1-11.5), p=0.039). An increase in APACHE II score on admission was associated with a higher odds of wasting status (APACHE II OR 2.4 (95% CI 1.1-5.4), p=0.036). Conversely, reduction in admission SOFA score was associated with reduced odds of high muscle wasting (SOFA OR 0.48 (95% CI 0.25-0.93), p=0.029). Increasing BMI was associated with lower wasting status (OR 0.76 (95% CI 0.58-0.99), p=0.041). The logistic regression model was statistically significant, $\chi^2(11) = 24.442$, p =0.011. The model explained 64.8% (Nagelkerke R2) of the variance in wasting status and correctly classified 70% of cases. Sensitivity was 92.9%, specificity was 66.7%, positive predictive value was 86.7% and negative predictive value was 80%. The area under the ROC curve (AUC) was 0.949 (95% CI 0.877 to 1.000), which suggests an excellent level of discrimination. Of note, receiving ECMO therapy was associated with a 15.7 times higher odds of higher wasting status but was not statistically significant.

Variable	B	S.E.	Odds Ratio (95% CI)	p-value
Male	1.35	1.22	3.84 (0.35-42.0)	0.270
Pre-ICU LoS	-0.38	0.24	0.68 (0.43-1.08)	0.105
BMI	-0.28	0.13	0.76 (0.58-0.99)	**0.041**
SOFA	-0.74	0.34	0.48 (0.25-0.93)	**0.029**
APACHE II	0.87	0.42	2.39 (1.06-5.4)	**0.036**
MV days	0.37	0.38	1.44 (0.69-3.02)	0.329
Steroid days	-0.20	0.34	0.82 (0.42-1.58)	0.549
NMB days	1.25	0.61	3.50 (1.07-11.5)	**0.039**
CRP	0.00	0.01	1.00 (0.99-1.01)	0.986
COVID19 status	-1.77	2.21	0.17 (0.00-12.92)	0.422
ECMO	2.75	2.78	15.67 (0.07-3656.23)	0.323
Constant	-1.69	3.69	.185	0.647

Table 4-8. Binomial logistic regression of muscle wasting status

Odds ratio of independent variables in predicting muscle wasting status. *ICU; intensive care unit, BMI; body mass index, SOFA; sequential organ failure assessment, APACHE II; acute physiology and chronic health evaluation, MV; mechanical ventilation, NMB; neuromuscular blockade, CRP; c-reactive protein, COVID19; coronavirus disease 2019, ECMO; extracorporeal membrane oxygenation.*

4.5.11.1 Pro-inflammatory cytokine profiles in acute muscle wasting

Concentration of CRP was a poor predictor of subsequent extent of muscle atrophy in this cohort. However, high levels of underlying inflammation were present throughout ICU admission. Therefore, I sought to measure levels of serum pro-inflammatory cytokines and inflammatory mediators alongside changes in muscle mass to determine whether inflammatory phenotypes exist with respect to muscle wasting state and admission aetiology.

A total of 43 patients had baseline serum available for analysis. Baseline levels of pro-inflammatory cytokines (TNFR1, IL-6, IL-8, IL-10) and systemic markers of necrosis (RIPK3 and CCK18) were compared to the degree of peripheral muscle wasting (change in rectus femoris cross-sectional area at day 7, ΔRF_{CSA}). The data presented earlier in this chapter demonstrated that significant atrophy had occurred at day 7 and hence served as an appropriate time point. There was no significant correlation between ΔRF_{CSA} and baseline IL-6, IL-8, TNFR1, RIPK3 or CCK18 (Figure 4-24). There was borderline statistical

significance between ΔRF_{CSA} and baseline IL-8 (p=0.051). Extent of ΔRF_{CSA} was weakly negatively correlated with baseline IL-10 levels (r=-0.382 (95% CI -0.651-0.028), p=0.031).

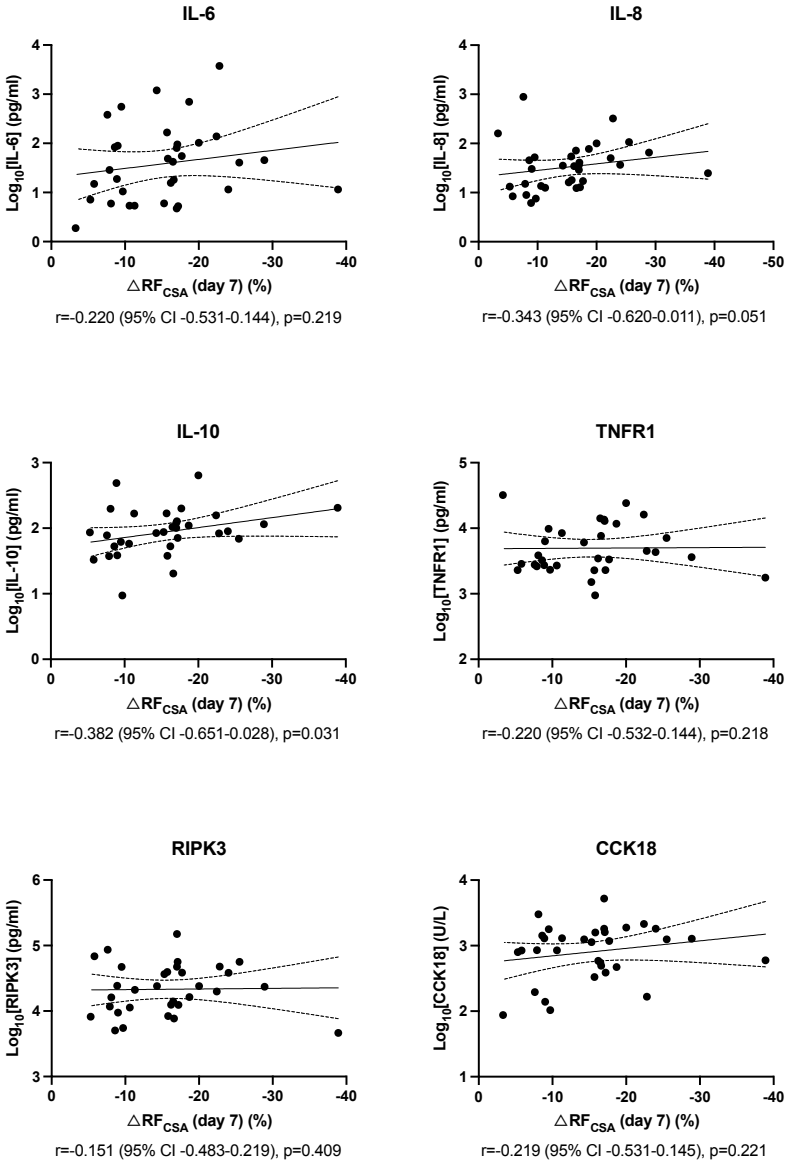


Figure 4-24. Correlation between baseline pro-inflammatory mediators and extent of rectus femoris muscle atrophy

Correlation plots of percentage change in RF_{CSA} at day 7 and baseline concentrations of pro-inflammatory cytokines IL-6, IL-8, IL-10 and TNFR-1 and systemic markers of necrosis, RIPK3 and CCK-18. There was a significant positive correlation between baseline levels of IL-10 and loss of RF_{CSA} (p=0.031) and borderline significance with IL-8 (p=0.051). *IL-6; Interleukin-6, IL-8; interleukin-8, IL-10; interleukin 10, TNFR1; tumour necrosis factor receptor 1, RIPK3; receptor interacting protein kinase 3, CCK18; cleaved cytokeratin 18, ΔRF_{CSA}; change in rectus femoris cross-sectional area.* Correlation analyses performed using non-parametric Spearman's correlation test.

Given that significant respiratory muscle atrophy occurs within 72 hours,[15] the same baseline levels of pro-inflammatory cytokines were compared to the change in PSM_{CSA} at day 3 (Figure 4-25). There were no significant correlations between baseline IL-6, IL-8, IL-10, TNFR1, RIPK3 and CCK18 and the change in PSM_{CSA} at day 3. Similarly, Change in DIA_{EXP} at day 3 was not significantly correlated with baseline levels of IL-6, IL-8, IL-10, TNFR1, RIPK3 and CCK18 (Figure 4-26).

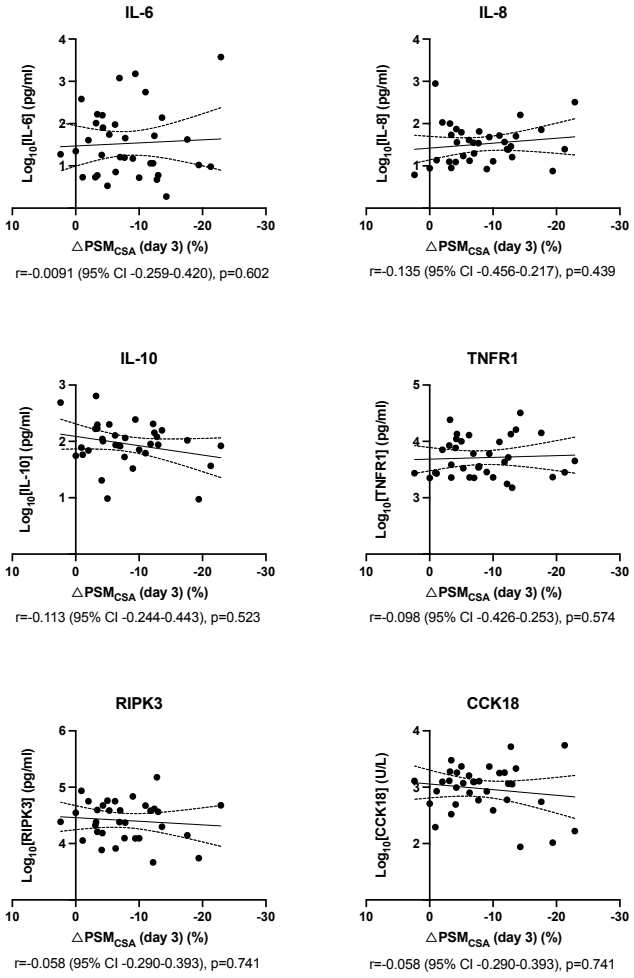


Figure 4-25. Correlation between baseline pro-inflammatory mediators and extent of parasternal muscle atrophy at day 3

Correlation plots of percentage change in PSM_{CSA} at day 7 and baseline concentrations of pro-inflammatory cytokines IL-6, IL-8, IL-10 and TNFR-1 and systemic markers of necrosis, RIPK3 and CCK-18. No significant associations were found. *IL-6; Interleukin-6, IL-8; interleukin-8, IL-10; interleukin 10, TNFR1; tumour necrosis factor receptor 1, RIPK3; receptor interacting protein kinase 3, CCK18; cleaved cytokeratin 18, ΔPSM_{CSA}; change in parasternal muscle cross-sectional area.* Correlation analyses performed using non-parametric Spearman's correlation test.

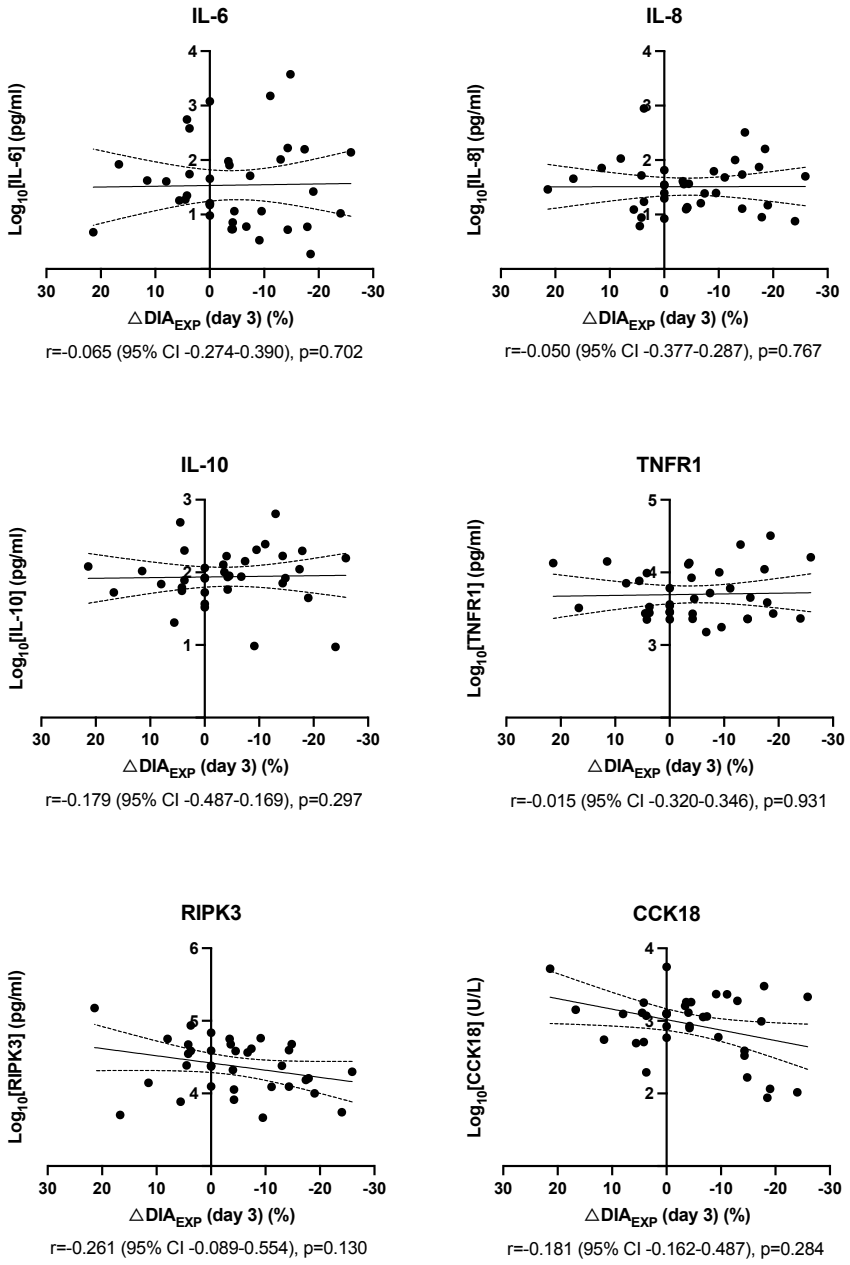


Figure 4-26. Correlation between baseline pro-inflammatory mediators and extent of diaphragm muscle atrophy at day 3

Correlation plots of percentage change in DIA_{EXP} at day 3 and baseline concentrations of pro-inflammatory cytokines IL-6, IL-8, IL-10 and TNFR-1 and systemic markers of necrosis, RIPK3 and CCK-18. No significant associations were found. *IL-6; Interleukin-6, IL-8; interleukin-8, IL-10; interleukin 10, TNFR1; tumour necrosis factor receptor 1, RIPK3; receptor interacting protein kinase 3, CCK18; cleaved cytokeratin 18, ΔDIA_{EXP}; change in diaphragm end-expiratory thickness.* Correlation analyses performed using non-parametric Spearman's correlation test.

Longitudinally, there were few significant differences between concentrations at baseline, day 3, day 7 and day 14 (

Appendix 9-5). Baseline IL-6 levels were only statistically different when compared to day 14 (baseline: 28.8pg/ml (IQR 9.6-102.4) vs. day 14: 13.5pg.ml (IQR 7.1-18.5), p=0.046). TRAIL was significantly elevated at day 3, day 7 and day 14 when compared to baseline (baseline: 38.7pg/ml (IQR 19.8-96.3), day 3: 73.7pg/ml (IQR 45.9-107.4), day 7: 70.9pg/ml (IQR 53.0-105.3), day 14: 69.3pg/ml (IQR 49.1-109.8); $p<0.05$). Given there were few differences observed in the cohort, sub-group comparisons were then studied.

When the cohort was stratified by high or low wasting groups, there were no statistical differences in baseline, day 3, day 7 or day 14 concentrations of TNFR1, TNF-α, RIPK3, CCK18, IL-6, IL-8, IL-10, IL-18, IFN-γ, MCP-1 and TRAIL (Figure 4-27, Appendix 9-4). When categorised by admission diagnosis, patients with ARDS had significantly higher baseline levels of IL-10, IFN-γ, TNF-α, CCK-18 and TRAIL. Levels of RIPK3 and MCP-1 were also higher at baseline but not statistically significant (Figure 4-28, Appendix **9-5**). In addition, levels of TNF-α, RIPK3 and TRAIL were higher at all study points in ARDS patients.

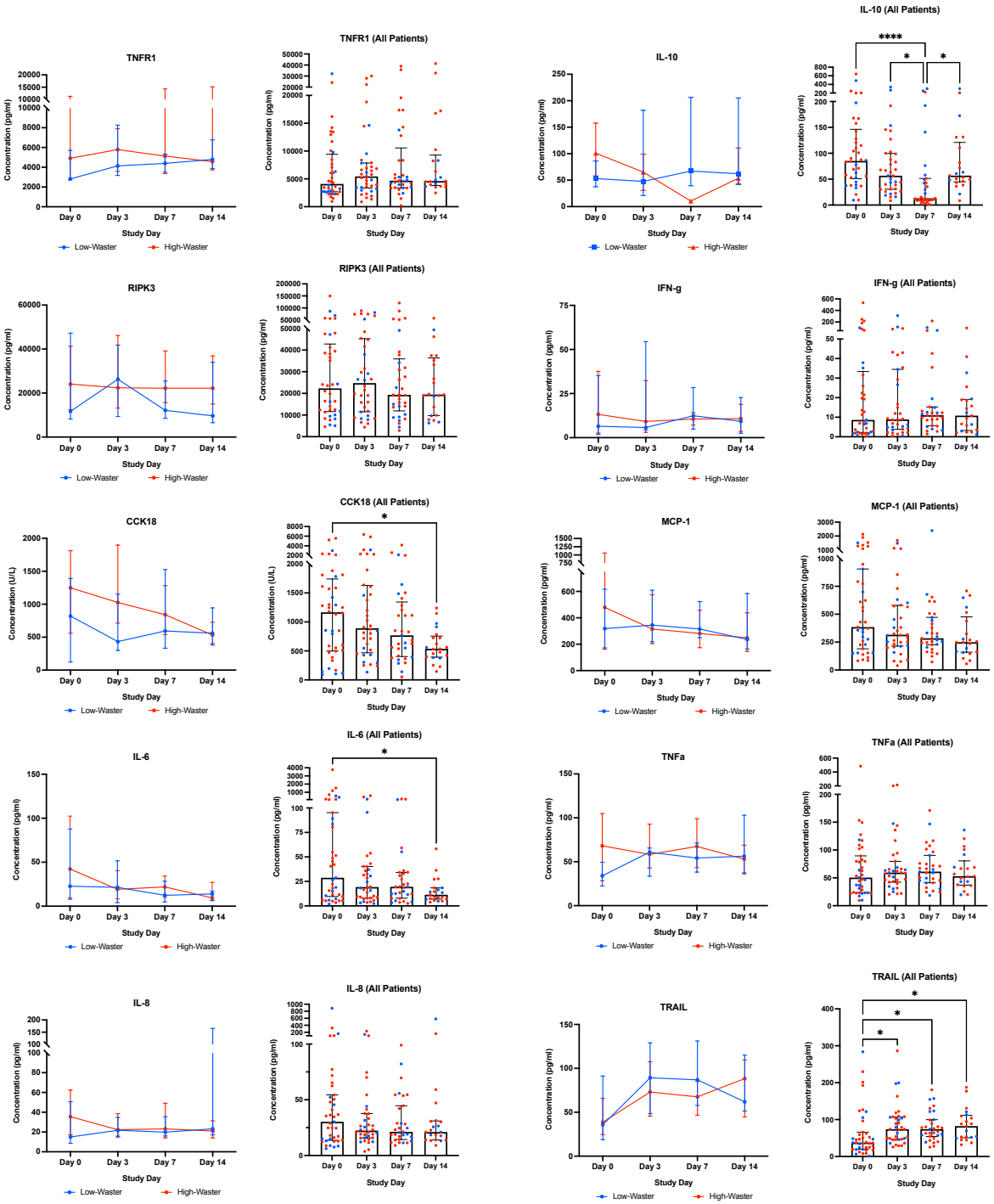


Figure 4-27. Pro-inflammatory cytokine profiles for high and low muscle wasting status

Between group comparisons at each study point compared using Sidak's test for multiple comparisons. Differences between levels of analyte and study day for all patients analysed using Kruskal-Wallis test for multiple comparisons. *p<0.05. **p<0.01, ***p<0.001, ****p<0.0001. Data shown as median and inter-quartile range error bars.

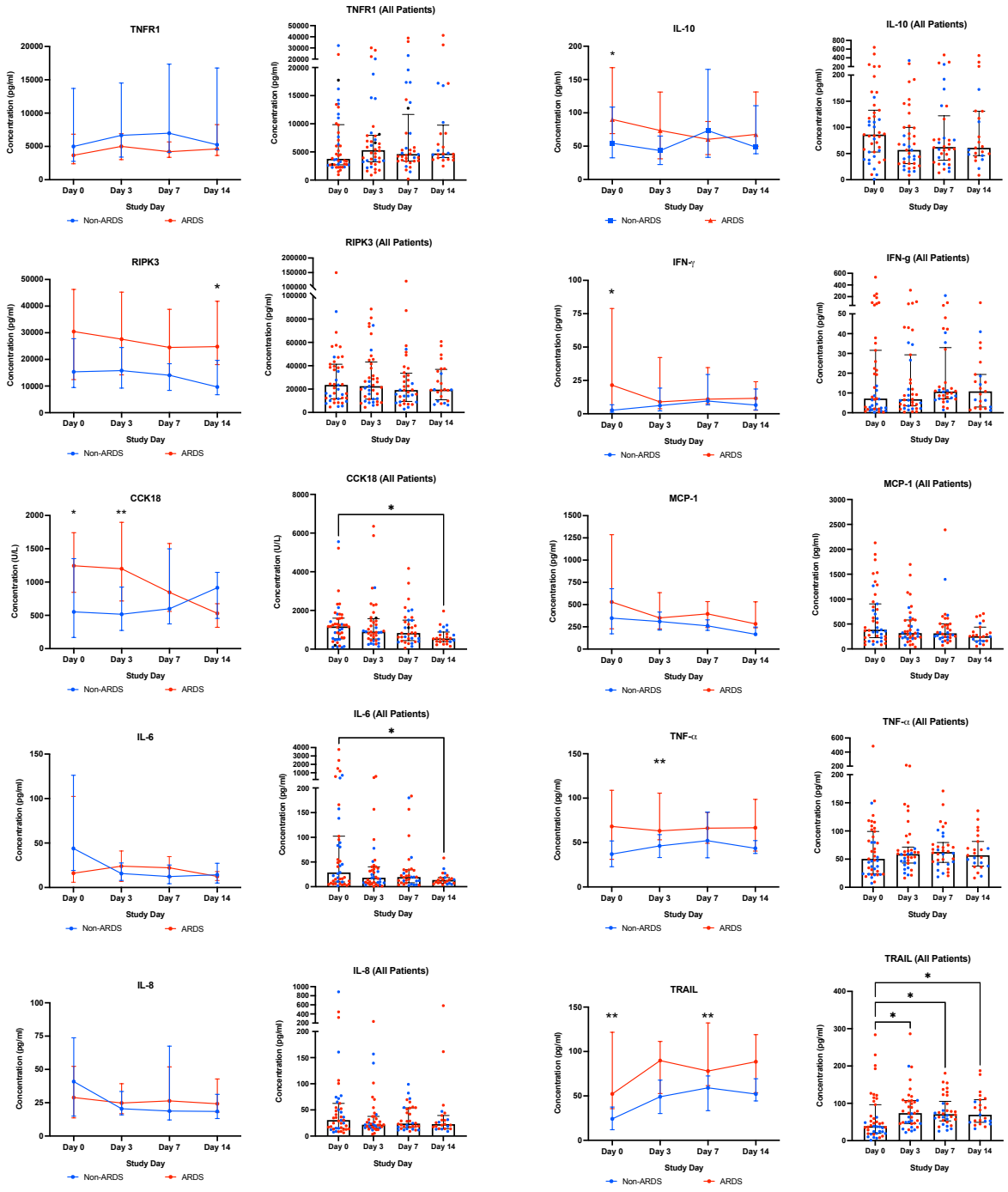


Figure 4-28. Pro-inflammatory cytokine profiles in ARDS and non-ARDS critical illness

Between group comparisons at each study point compared using Sidak's test for multiple comparisons. Differences between levels of analyte and study day for all patients analysed using Kruskal-Wallis test for multiple comparisons. *p<0.05. **p<0.01, ***p<0.001, ****p<0.0001. Data shown as median and inter-quartile range error bars.

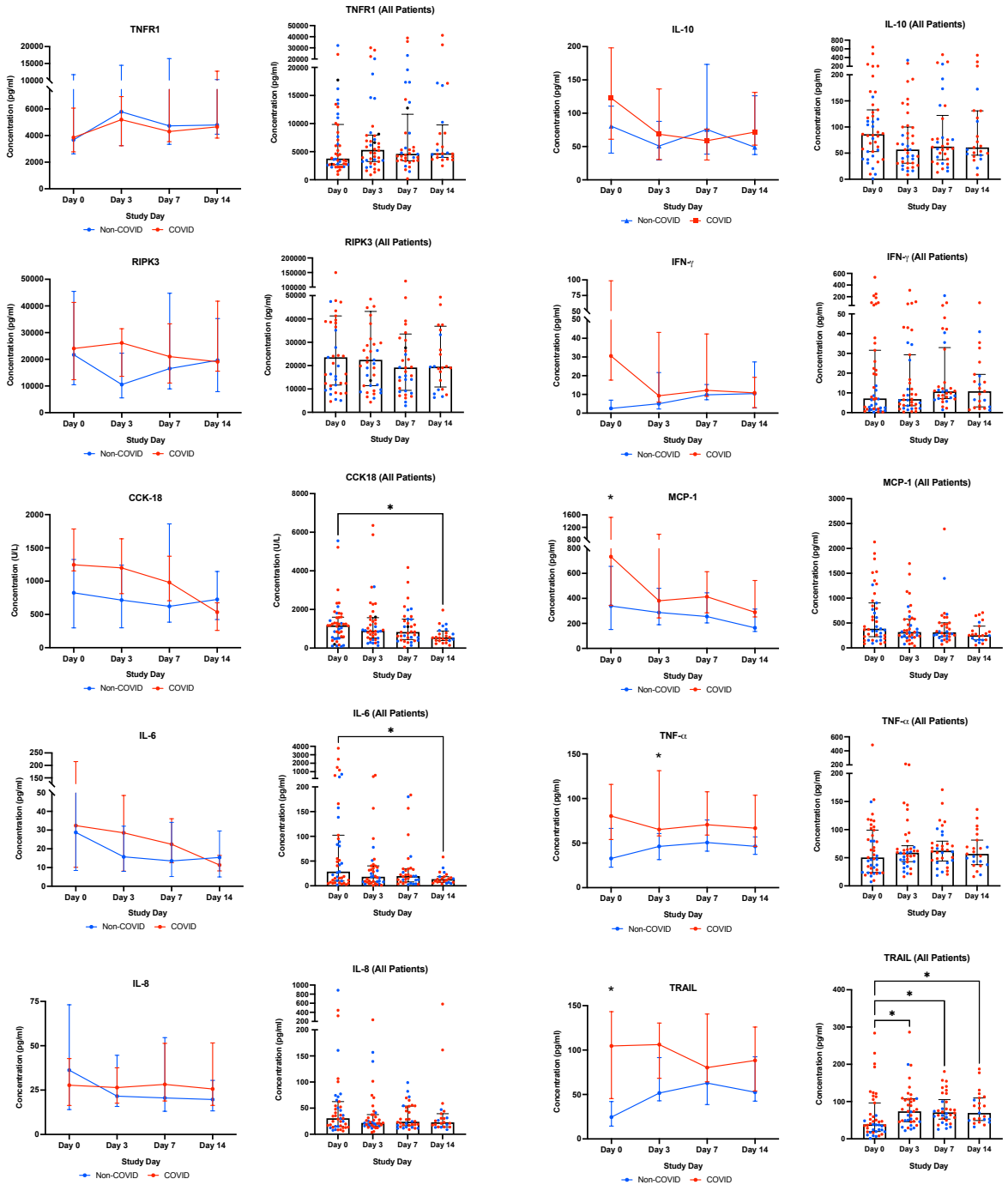


Figure 4-29. Pro-inflammatory cytokine profiles by in COVID19 and non-COVID19 critical illness

Between group comparisons at each study point compared using Sidak's test for multiple comparisons. Differences between levels of analyte and study day for all patients analysed using Kruskal-Wallis test for multiple comparisons. *p<0.05. **p<0.01, ***p<0.001, ****p<0.0001. Data shown as median and inter-quartile range error bars.

4.5.11.2 Programmed necrosis signals in critical illness associated muscle wasting

TNFR1, RIPK3 and CCK18 whilst not significantly different, when compared to low-waster patients, were consistently higher in patients with >1.4%/day loss of muscle in early critical illness. Furthermore, in COVID19 related ARDS, levels of RIPK3 and CCK18 not statistically different when compared to non-COVID19 patients.

4.6 Discussion

In this observational cohort study of critically ill patients receiving mechanical ventilation, I provide a comprehensive longitudinal description of peripheral and skeletal muscle changes in early critical illness and up to 21 days using non-invasive ultrasonography. These data show that peripheral and respiratory muscle wasting occurs acutely (within 3 days) and is progressive in all muscle groups in the first 14 days of critical illness. Furthermore, I demonstrate that the magnitude of muscle wasting is similar in peripheral and respiratory muscle, as well as in patients with COVID19 ARDS and non-COVID19 ARDS. Whilst I found a high inflammatory burden in this cohort, there was no obvious inflammatory phenotype or predictors of muscle wasting.

Using low- and high-waster status, 70% of our cohort were characterised as the latter. In turn, clinical factors such as neuromuscular blockade use, and use of mandatory ventilation in the first 7 days were associated with this group of patients. Our RF_{CSA} data demonstrated a higher degree of wasting at day 7 when compared to notable prospective clinical trials of acute muscle wasting (16% vs 10%),[14] and comparable degree of loss in COVID19 patients from smaller studies (23% in our cohort vs. 30%[269]). There remains a lack of prospective studies detailing the changes in PSM during critical illness. I show that PSM_{CSA} and PSM_{EXP} both decline in the first 14 days of critical illness and the former to a greater extent. This difference may be due to greater chance of misrecognising muscle borders during analysis, but the low coefficient of variance and high intra-operator reliability provides reassurances for this. I found that peripheral muscle changes were greater at day 7 and 14 when compared to DIA_{EXP}

and PSM_{EXP}. This observation may be due to a greater degree of inactivity of limb muscles in early critical illness compared to respiratory muscles which are continuously active. Secondly, the larger rectus femoris muscle may be more prone to intramuscular oedema thus affecting image quality and subsequent EG values.

I present data to show that echogenicity of RF and PSM significantly increased at day 7 of ICU admission. Furthermore, over the same period, RF_{CSA} and PSM_{EXP}/PSM_{CSA} respectively, had declined suggesting that muscle atrophy is related to loss of muscle quality also, however this was not statistically significant in linear regression analyses. I found that that muscle quality of peripheral muscle and small extra-diaphragmatic respiratory muscle decline at similar rates. I did not corroborate, nor is it practical, to corroborate these findings in a mechanically ventilated patient with histological analysis. However, ultrasound cannot differentiate whether the loss of quality was due to IMAT increase (which is possible using CT), pro-inflammatory infiltrates or significant fluid accumulation. Ultrasound setup was difficult to control for as anatomical variation amongst patients meant depth and gain needed to be adjusted to optimise image appearances – thus making inter-patient comparisons unreliable. Changes in EG in early critical illness may reflect underlying myonecrosis,[133] and again, this could not be confirmed with histological specimens. However, the findings of higher systemic concentrations of RIPK3 and CCK18 in high-waster patients highlights an interesting area to explore as to whether programmed necrosis pathways are activated. More recent studies have suggested that higher EG is associated with greater ICU mortality,[270] however the differing gain and depth settings between patients meant that pooled echogenicity data was not possible in our data set.

In chapter 3, I showed that there was a significant L3-SkM_{CSA} loss of 10.8% (IQR -19--3.0) at a second CT study (median interval: 12 days (IQR 6-19)). Further, there was a concurrent -13.7% (IQR -24.3--3.4) reduction in muscle quality as per change in SMD. Whilst change in CT derived SMD and EG could

not be directly compared to our ultrasound data (due to lack of CT studies in study patients), the comparable rates of change in two different techniques provide a degree of reassurance of quantitative changes in peripheral and axial muscle.

I explored general and small molecule pro-inflammatory mediators. Initially, baseline CRP levels suggested a high degree of underlying inflammation that persisted (>72hr after admission) in early critical illness which has been associated with ICU mortality and risk of infection with levels as low at 10mg/L.[261,262] I then studied small molecule pro-inflammatory cytokines which have been implicated in skeletal muscle wasting in range of diseases[66,183,184] as well during mechanical ventilation (MV)[185]. Tumour necrosis factor alpha (TNF-α), interleukin (IL) 1 beta (IL-1β) and IL-6 are commonly associated,[66,186,187] either through stimulation of downstream mediators of proteolysis or through further activation of cytokines. The imbalance between protein synthesis and breakdown leads to muscle atrophy. TNF-α, with respect to skeletal muscle, triggers a catabolic pathway after binding to its type 1 TNF receptor (TNFR1), causing downstream stimulation of nuclear factor kappa-light-chain-enhancer of activated B cells (NF-κB) – a transcription factor that is pivotal in cell differentiation, apoptosis and in the coordination of inflammatory responses. Subsequent activation of the inhibitor of NF-κB kinase (IKK) complex which causes phosphorylation of the otherwise quiescent inhibitor (in non-stimulated cells), IkB. This leads to NF-κB activation and subsequent upregulation of proteins specific to striated muscle and associated with skeletal muscle atrophy – MURF1 and MAFBX (atrogin).[191,192] This downstream signalling stimulates the ubiquitin-proteasome pathway[193] (UPP) leading to breakdown of the dominant muscle proteins – actin and myosin.[194] These proteins have been shown to be present in diaphragm muscle of patients receiving longer periods (compared to those receiving 3 hours or less) of MV.[15] Furthermore, TNF-α in particular triggers cell death cascades independent of proteolytic pathways and may present novel mechanisms for the pathophysiology underlying muscle necrosis in critically ill patients – a common finding in histopathological studies of muscle in critical illness.[14,199,200] In this regard, our data showed that markers of systemic necrosis,

RIPK3 and CCK18, were higher in patients categorised at high-wasters, in those with ARDS and in those with COVID19. Thus, patients who have a higher degree of muscle wasting during critical illness may also have a greater degree of circulating markers of necrosis. What I did not elicit is the source of necrosis and whether this necrotic focus originated in the muscle or in the lungs during early ARDS. I did not acquire muscle tissue to quantify intra-muscular concentrations of pro-inflammatory cytokines. However, data from a large prospective study of acute muscle wasting showed that intramuscular pro-inflammatory cytokines differed from systemic levels of the same mediator.[14,34]

A comprehensive ultrasound protocol was constructed using data and methodology from the current literature. I show that reproducibility and reliability within, and between operators, as well as at each anatomical site was high (ICC>0.9). In the clinical studies, a single operator was used to reduce variation at each study time point. For example, the operator would be aware of anatomical restrictions, clinical stability and challenges presented (such as ECMO cannula, gross fluid retention). Longitudinal intra-operator reliability inter-operator reliability was maintained at an ICC of >0.9. This is in keeping with similar musculoskeletal ultrasound studies.[140] Operators in the reliability and main study performed repeat studies at least 15 minutes apart to reduce variation that may have occurred over a longer period of time (movement of the patient, deterioration etc).

In our cohort, patients with ARDS had a longer period in hospital before intubation and institution of MV compared to non-ARDS patients (ARDS: 5 days (IQR 3-9) vs. 1 day (IQR 0-4), p=0.004). As such, there is a possibility that acute muscle wasting may have occurred prior to the acquisition of the first ultrasound imaging study as ARDS patients had a longer hospital length of stay before the first imaging study (ARDS: 9 days (IQR 6-13) vs. non-ARDS: 3 days (IQR 1-6), p<0.001). This may also mean that the true acuity of muscle mass loss was missed in the ARDS cohort. Nevertheless, I found significant levels of atrophy following study recruitment, but the true baseline prior to critical illness could not be determined. The nature of our tertiary referral centre often means that patients are cared for initially

with remote advice and if there is a lack of improvement then retrieval and admission is often required. This interval of time varies and can be between up to 7 days after MV is started. In logistic regression analysis, pre-ICU length of stay was not found to be significantly associated with high wasting status, however, the true rate of loss may have been missed for the reasons mentioned above. The disruption in critical care networks and saturation of critical care services in the UK due to the COVID19 pandemic is one cause for this disparity.

Whilst the respiratory mechanics of the intercostal and parasternal muscles are well described,[48,60,149] at the time of the clinical studies and data acquisition parasternal muscle ultrasound had a paucity of literature available relating to their ultrasonographic appearances,[131] and only a few studies specific to critical illness.[150,154,271] I chose to study a single PSM at the 3rd intercostal space. De Troyer *et al.,* found that the fractional change in muscle length of the PSM per unit volume increase of the relaxed chest wall changed with maximum airway pressure.[60] This is known as the PSM mechanical advantage. More specifically during passive inflation there was PSM shortening in all intercostal spaces, but the absolute decline reduced from the second to the fifth ICS. Thus, detecting changes in thickening fraction may have been lost if I chose to study PSM in the 4th, 5th, 6th ICS. With regards to laterality, studies in chronic lung disease have shown no significant differences between PSM thickness of the left and right 2nd and 3rd intercostal spaces,[243] therefore, I saw no advantage of summating multiple levels of PSM and adopted the pragmatic approach to study a single PSM level on one side.

There are currently no accepted criteria on what is classified as healthy PSM cross-sectional area or end-expiratory thickness and similarly what constitutes significant PSM wasting when using ultrasound. In our healthy cohort, PSM_{EXP} was 3.82mm ± 0.72, and was higher in other feasibility studies studying PSM at the same level using similar methodlogy.[150] Clearly further reliability studies and publication of ranges for sex, age and other determinants of muscle such as body mass index are required, but also the need for longitudinal studies to study change rather than static baseline

measurements. For example, whilst detecting loss of muscle bulk identifies individuals at risk of ICUAW, the loss of PSM bulk would only be significant if there is an impact in respiratory loading as the primary function is in the support of inspiration.[59] Therefore, incorporating functional assessment of the PSM using ultrasound may identify individuals with high degree of respiratory muscle loading during mechanical ventilation. Furthermore, diaphragm and parasternal muscles have been found to increase, decrease or remain close to baseline in clinical studies, thus making significant changes difficult to compare across studies. Studies have reported 6-10% loss in diaphragm thickness per day[272,273] or up to a 26% loss by day 3 of MV and interestingly changes within the first 72hrs do no correspond to the overall length of MV.[273] Whilst respiratory muscles are small in comparison to peripheral muscle, ultrasound allows detection of longitudinal changes as small as 0.2mm.[152] Muscles of the quadricep are often rendered immobile in early critical illness with little active movement possible. In contrast, the diaphragm, whilst frequently paralysed following deep sedation and neuromuscular blockade there can be underlying activity.[152] Similarly, PSM are often recruited when the respiratory pump is overloaded and PSM is recruited to aid inspiration with or without diaphragm acitivity.[48,123,156] The rectus femoris however will be subject to little loading or active movements and this may explain why a greater degree of wasting is seen in comparison to PSM_{EXP}/PSM_{CSA} and DIA_{EXP}. It is important to note that PSM_{CSA} in this study is that of only the right 3rd ICS. It is unlikely that loss of area or thickness occurs in only isolated PSM, and the degree of wasting is like to be similar in other PSM, but this was not measured in this study. Furthermore, I did not measure the differences in wasting extent at different PSM levels.

In some patients, study images at each time point was not possible. Early ICU discharges/repatriation, acute illness and obscuration of anatomical site (i.e. with ECMO cannula, chest drains, open chest, sternotomy dressings) were the most common reasons for missing study points.

Patients were recruited from two separate clinical studies. The impact of the COVID19 pandemic meant that the WAVE study was suspended owing to prioritisation of clinical services within the National Health Service. This impacted study time points, post-ICU follow-up and access to patients in general. The DeVENT study introduced a separate cohort of patients with that were often admitted later in their illness for tertiary centre assessment. There were multiple issues with acquiring functional data in study patients. In the ARDS cohort, patients were often repatriated soon after vvECMO was successfully stopped, this meant ICU discharge data could not be acquired. Similarly, the invitation to follow-up after discharge had either been declined or not possible due to the COVID19 pandemic and local hospital restrictions. In addition, strict infection control procedures meant that usual rehabilitation teams and process were reduced. Therefore, I could not draw accurate associations between degree of muscle wasting and functional and physical restriction at hospital discharge or longer-term.

In summary, I show that peripheral and skeletal muscle wasting patterns are similar in critical illness. Furthermore, I show that a significant proportion of patients have a high daily rate of wasting which may be due higher concentrations of systemic inflammatory and necrotic mediators. I also show for the first time that COVID19 ARDS patients have similar wasting patterns to those with non-COVID19 ARDS. Finally, I show that small respiratory muscles, illustrated by the PSM, may have reduced muscle quality at day 7 which is associated with a reduction in muscle bulk. The next chapter will focus on PSM changes and introduce the concept of strain measurement as a tool for muscle loading during mechanical ventilation.

Chapter 5: Non-invasive assessment of parasternal muscle in critical illness

5.1 Background

Chapter 3 and 4 showed that using CT imaging and ultrasound, peripheral skeletal and respiratory muscle wasting occurred acutely and continuously during MV and critical illness. Prolonged MV is associated with adverse ICU outcomes,[14,15,25,58] particularly ICUAW where muscle wasting and weakness is commonly implicated. To compound this, the COVID19 pandemic raised the need and strained the provision for MV and by May 2020, and at the peak of the 'first-wave' (April 2020), approximately 5,100 (63%) patients required MV due to COVID19 pneumonia alone. These data illustrate that whilst the incidence of MV has risen due to severe COVID19 disease, detrimental sequelae of prolonged MV will almost inevitably follow. There is a clear need to develop rapid and reproducible methods of assessing respiratory muscle function during mechanical ventilation to help optimise strategy, support weaning and prevention of long-term morbidity.

As the principal respiratory muscle, the diaphragm and its dysfunction in MV (ventilator induced diaphragm dysfunction (VIDD)) has been the focus of much research.[114,152,267] Rapid onset of diaphragmatic weakness and alterations in contractile proteins have been reported to occur early.[15] Specialist invasive diagnostics to study diaphragmatic function during mechanical ventilation and critical illness is well described.[139,265,274] Non-invasive imaging of the diaphragm, mainly using ultrasonography, has also gained much interest.[33,57,58] However, there is a paucity of data describing longitudinal changes in extra-diaphragmatic respiratory muscles. The parasternal muscles (PSM) offer an easily accessible extra-diaphragmatic muscle group with defined ultrasonographic anatomy and play a crucial role in supporting inspiration,[131] particularly when there is diaphragm dysfunction. The respiratory muscles require a delicate balance when delivering mechanical ventilation such that to prevent excessive muscle loading, but also excessive support (leading to muscle atrophy) and

ventilator induced dysfunction. These changes likely to increased neural respiratory drive. Measuring neural respiratory central output at the brain stem level is not easily done, as such surrogate measures using superficial muscle groups such as PSM are relatively well established in specialist centres.[275,276] In non-critically ill patients, neural respiratory drive index (expressed as the product of PSM electromyography (EMG) activity normalised to peak activity and respiratory rate) offers some potential in predicting patients that will recover or deteriorate from acute exacerbations of chronic disease.[276] However, specialist diagnostics such as surface EMG of the PSM can be employed to study function of PSM as a surrogate and indirect measure of neural respiratory drive.[275–277] Therefore, these are often not translatable to the bedside in everyday clinical practice and thus are not integrated into clinical management.

In addition to assessment of muscle bulk, assessment of muscle strain (ε) can provide insights into respiratory muscle loading.[122,151,155] Strain is the fractional deformation experienced by a structure when a force (or a stress) is applied, i.e. the relative movement of muscle fibres during contraction. The fundamental relationship between stress and strain in musculoskeletal physiology is dictated by the limits of stretch and elasticity of the muscle in question (Hooke's law: strain of a material is proportional to the applied stress within the elastic limit of the material). Low levels of muscle stress imply adequate muscle load (and therefore less strain) but conversely, high levels of stress lead to high strain and load imbalance on the myofibre. If the degree of stress exceeds a threshold, then there is a risk of contractile failure and dysfunction. Mathematically, stress (σ) = force/area. Therefore, when contractile force is kept constant, muscles with low cross-sectional area will experience greater levels of stress compared to larger ones. Muscle strain measurements have already been widely employed in the myocardium using echocardiography[157] but only in a small number of conceptual studies of the diaphragm,[158–160] and none involving PSM. EMG measures the sum of active motor units at the point of the electrode position and is not a direct measure of muscle strain.[161] In the context of mechanical

ventilation, it is unclear how the institution of invasive ventilation affects parasternal muscle bulk and function.

Ultrasonography is cheap and widely available and therefore offers a ubiquitous method of studying small respiratory muscle activity and changes during critical illness, particularly during variable levels of MV. The changes in muscle morphology and a subsequent increased strain and velocity of contraction can indicated reduced compliance of the respiratory muscle pump.

This chapter describes the prospective assessment of PSM in critically ill patients, including descriptions of muscle bulk and activity. In addition, I develop and apply statistical modelling methods to better understand longitudinal changes to: (1) describe the changes and trajectory of parasternal muscle bulk and strain during critical illness, and (2) the relationship with peripheral muscle and diaphragm wasting and discover putative clinical drivers of these changes.

5.2 Chapter contributions

Dr Ryan Haines (RWH) helped to develop modelling structure to harness information from longitudinal data for this chapter using knowledge and physiological phenotypes from SP. Several linear mixed effects models to include patient level effects (random intercepts and slopes) were developed to allow more general description of changes over time of several muscle groups. RWH cleaned data from SP, built models, and provided data visualisation using R software (v4.1.3, www.r-project.org). With respect to parasternal strain measurement, Professor Sam Orde (Clinical Associate Professor, University of Sydney, Australia), helped construct the analysis methodology. Furthermore, Professor Orde analysed all pseudonymised B-mode video files that I supplied. Professor Orde acted as a blinded rater in the reliability study along with Dr Emma Bowcock (ICU specialist/echocardiography fellow, Intensive Care Unit, Nepean Hospital, Sydney, Australia).

5.3 Aims

1. ***Describe the longitudinal changes in PSM in critical illness using ultrasonography.***
2. ***Describe PSM changes relative to peripheral skeletal muscle and diaphragm wasting.***
3. ***Develop methodology for ultrasonographic strain analysis of PSM and describe its evolution during critical illness and mechanical ventilation.***

5.4 Hypotheses

1. Changes in parasternal muscle quantity and quality in critical illness are comparable to peripheral skeletal muscle and diaphragm during critical illness.
2. Parasternal muscle strain increases with increased loss of parasternal muscle.

5.5 Methods

5.5.1 Additional study cohort data

RWH provided clinical and ultrasound data from a separate clinical study (clincaltrials.gov ref. NCT03736005) at a tertiary academic ICU of a major trauma centre in London, United Kingdom between January 2019 to August 2020. This study was approved by the joint research and management office at Queen Mary University of London and sponsored the study protocol and ethical approval was granted by the Wales research ethics committee (Wales REC6, ref:18/WA/0304) and informed consent was obtained from patients or their decision makers prior to enrolment. Clinical information and quantitative musculoskeletal ultrasound data of rectus femoris and parasternal muscle was provided by RWH. Patients from this study (study A) were combined with the patient cohorts from the WAVE (study B) and DeVENT studies (study C).

In all three studies, patients ≥18 years admitted to ICU, anticipated to be mechanically ventilated for ≥24 hours and considered likely to survive to ICU discharge by the treating physician were enrolled. Study A consisted of general ICU patients and included major trauma. Patients with major trauma were defined as a new injury severity score of ≥15. In study A, patients with traumatic brain injury (abbreviated injury scale head injury score ≥5), spinal cord injury with paralysis, lower limb amputation, end stage kidney disease or disseminated cancer, lack of independence with activities of daily living or non-ambulatory status prior to admission were excluded.

5.5.2 Clinical data

Demographic data, co-morbidities and admission diagnosis were collected at baseline. SOFA score was calculated daily for the first 7 days of the study. Ventilator strategy/mode, use of neuromuscular blockade, depth of sedation (as per the Richmond agitation and sedation scale (RASS)), vasopressor days in the first 3-7 days of admission and requirement for vvECMO were also recorded. Data was collected on patients providing they were still admitted on the ICU.

5.5.3 Ultrasonography of parasternal, diaphragm and rectus femoris muscle

PSM and rectus femoris (RF) measurements were collected as part of secondary outcomes in all three studies (A, B and C) and PSM, RF and diaphragm (DIA) in study B and C. PSM cross-sectional area (PSM_{CSA}), PSM end-expiratory thickness (PSM_{EXP}), rectus femoris cross-sectional area (RF_{CSA}) and diaphragm end-expiratory thickness (DIA_{EXP}) measurement methods are all detailed in 2.2.2 .

All imaging was acquired during normal tidal breathing only. Healthy volunteers and patients were positioned on an examination couch (or bed) at 30 degrees and allowed 1 minute to ensure a stable respiratory cycle. The ultrasound probe was then placed in position and 3 further respiratory cycles were observed before recording. Fifteen to twenty second B-mode video files were recorded for

analysis. During acquisition of images in mechanically ventilated patients, ventilator graphics were studied to ensure all recorded breaths were either all mandatory or all assisted in nature.

Before application in the clinical study, intra- and inter-observer reliability was assessed for all anatomical sites in a feasibility study which has already been detailed in 4.5.1 . A CoV of less than 7.5% and an ICC of >0.9 was achieved for all muscle groups. All imaging analysis was performed offline by an operator blinded to patient and clinical information. Images were collected at ICU admission, day 3, day 7 and day 14 with additional studies when deemed suitable.

5.5.4 Parasternal function measurements

Parasternal muscle strain (PSM_{ε}) and PSM thickening fraction (PSM_{TF}) were used as functional measures of PSM activity. Detailed methodology is given in 2.2.2.3

5.5.5 Rectus femoris and diaphragm ultrasound

RF_{CSA} and DIA_{EXP} (and subsequent thickening fraction, DIA_{TF}) have been detailed in 2.2.2

5.5.6 Statistical analysis

Continuous data is expressed as mean (±standard deviation) or median (interquartile range (IQR)) after testing for normality. Changes between study time points or groups were evaluated using 1-way ANOVA or Kruskal-Wallis test respectively. The number of measurements of each group are reported where appropriate. There was no missing data for adjusted covariates in models.

A linear mixed effects model was used to evaluate change in parasternal muscle thickness over time and identify determinants of change in thickness (primary model). This modelling strategy allows incorporation of repeated muscle measurements on all patients. Several secondary linear mixed effects models were used. First, to explore the time-varying association of parasternal muscle

thickness with RF_{CSA}. Second, to explore effects of parasternal muscle contractile activity (strain and thickening fraction) over time. Third, we replicated modelling by Goligher *et al.,*[114] to examine changes in diaphragm thickness and contractile activity to then allow examination of the effects on parasternal muscle measurements. In an exploratory analysis, we harnessed the cohort of vvECMO patients to explore effects of vvECMO and lung rest on respiratory and skeletal muscle measurements.

Subsequent models were extensions of the primary linear mixed effects model of PSM thickness over time. In studies with available parasternal muscle thickening fraction and strain measurements we repeated the primary model of parasternal muscle thickness to examine the effect of contractile activity over time using interaction terms. The coefficients for these interaction terms represent the magnitude by which the exposures modified the variation in parasternal muscle thickness over time.

5.6 Results

5.6.1 Study cohort

A total of 76 patients were enrolled across the three studies (32 in study A, 16 in study B, 28 in study C) (Figure 5-1). Baseline PSM and/or repeat PSM studies were not possible in 9 patients (due to multiple rib fractures and/or presence of surgical emphysema). Therefore, 67 patients had a baseline and at least one more PSM study during the ICU admission and were included in the study. Of these, 66 had a paired PSM_{EXP} and RF_{CSA} measured at baseline and second time point. Suitable video files from Study B and C were available for PSM_{TF} and PSM_{ε} analyses in 41/44 (93%) patients. Similarly, baseline PSM_{EXP} and DIA_{EXP} and a second study was available in 40/44 (91%). Patients were enrolled in the studies for a median of 7 days (IQR 5–11). PSM measurements were obtained on a total of 265 patient-days during ICU admission (4 measurements per subject (IQR 3–5). Demographics, clinical characteristics, and baseline muscle group measurements of the patient cohort are shown in Table 5-1.

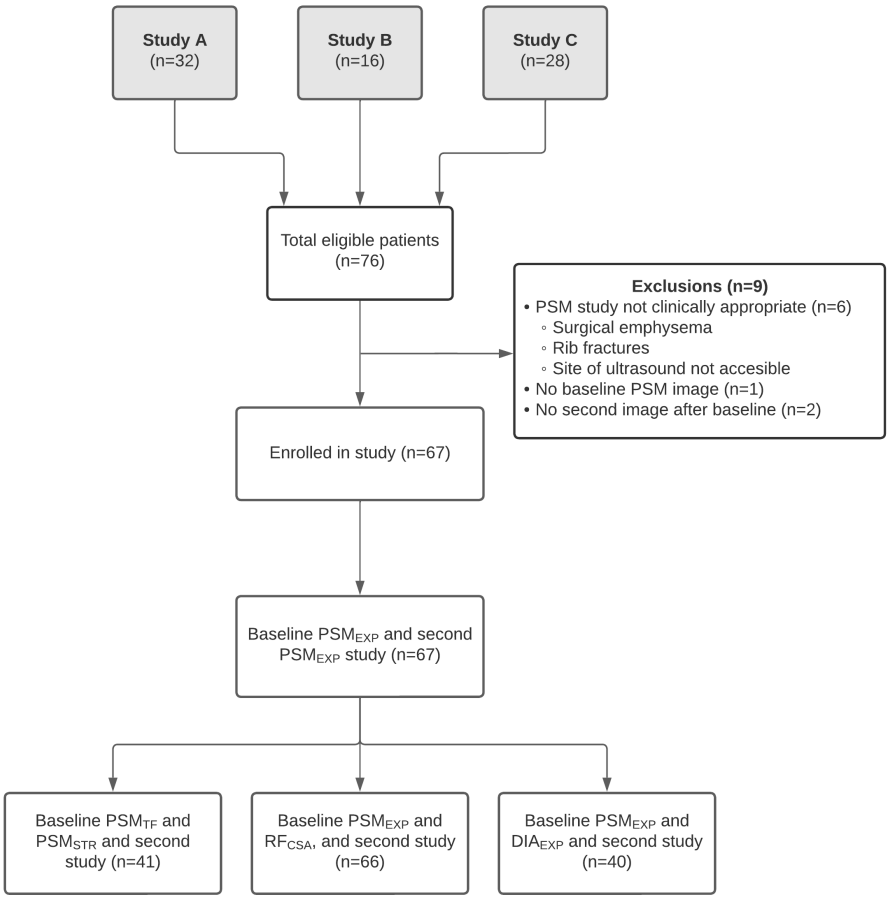


Figure 5-1. Consort diagram of parasternal muscle study

Sixty-seven patients recruited from 3 studies with at least two parasternal muscle (PSM) imaging studies. Forty-one patients were studied for strain (PSM_E) (from study B and C only). *PSM_{EXP}; parasternal muscle end-expiratory thickness, PSM_{TF}; parasternal muscle thickening fraction, PSM_E; parasternal muscle strain, RF_{CSA}; rectus femoris cross-sectional area, DIA_{EXP}; diaphragm end-expiratory thickness.*

	All patients (n=67)
Age – years	49.7 ± 15.9
Male – no. (%)	48 (69)
BMI – kg/m²	26.8 (23.4-31.2)
Ethnicity – no. (%)	
Caucasian	44 (66)
Asian	13 (19)
Black	10 (15)
Admission APACHE II score – points	14 (11-18)
Admission SOFA score – points	7 (6-10)
Admission diagnosis – no. (%)	
COVID-ARDS – no. (%)	19 (27)
Other ARDS	6 (9)
Cardiac	19 (27)
Respiratory	4 (6)
Trauma	17 (24)
Gastroenterology/Liver	4 (6)
Neurological	1 (1)
Pre-ICU length of stay – days	1 (0-5)
Average RASS in first 7 days	-2.7 (-4.0--2.0)
Vasopressor days in first 3 days	3 (2-3)
Steroid days in first 7 days	1.5 (0.0-6.0)
Renal replacement requirement in first 48h – no. (%)	16 (22)
Ventilation management	
Mandatory mechanical ventilation in first 7d – days	
Veno-venous ECMO – no. (%)	27 (40)
Mechanical ventilation days	13 (9-24)
Neuromuscular blockade infusion in the first 3d. n (%)	22 (33)
Baseline muscle ultrasound measurements	
RF_{CSA} (cm^2)	4.4(3.8-5.6)
PSM_{EXP} (mm)	4.3 (3.6-5.1)
PSM_{TF} (%)	1.1 (0.5-2.5)
PSM_{STR} (mm)	-1.4 (-2.6--0.6)
DIA_{EXP} (mm)	2.5 (2.2-2.7)

Table 5-1. Cohort data of parasternal muscle study

Clinical data from patients pooled from studies A, B and C. *BMI; body mass index, APACHE; acute physiology and chronic health evaluation score, SOFA; sequential organ failure assessment, COVID; coronavirus-19 disease. ARDS; acute respiratory distress syndrome, ICU; intensive care unit, RASS; Richmond agitation and sedation scale, ECMO; extracorporeal membrane oxygenation, RF_{CSA}; rectus femoris cross-sectional area, PSM_{EXP}; parasternal muscle end-expiratory thickness, PSM_{TF}; parasternal muscle thickening fraction, PSM_{STR}; parasternal muscle strain, DIA_{EXP}; diaphragm end-expiratory thickness. Vasopressor day = patient received a continuous infusion of any vasopressor for at least 3-hours in a 24-hour period, steroid days = number of days on which any parenteral or enteral corticosteroid (dexamethasone, prednisolone, hydrocortisone) was given in a 24-hour period.*

5.6.2 Baseline parasternal muscle mass measurement

Changes in PSM mass, given by PSM_{EXP} and PSM_{CSA}, for studies B and C has been described in Chapter 4. Pertinent data will be replicated and referred to where necessary. After combining patient cohorts

from studies A, B and C, baseline PSM_{EXP} and PSM_{CSA} was 4.3mm (IQR 3.6-5.1) and 1.1cm^2 (IQR 0.8-1.2) respectively. Baseline PSM_{EXP} was positively correlated with baseline PSM_{CSA} (r=0.628 (95% CI 0.451-0.757), p<0.0001) (Figure 5-2). There was no significant difference between the percentage change of PSM_{EXP} and PSM_{CSA} at any study time point (Figure 5-3).

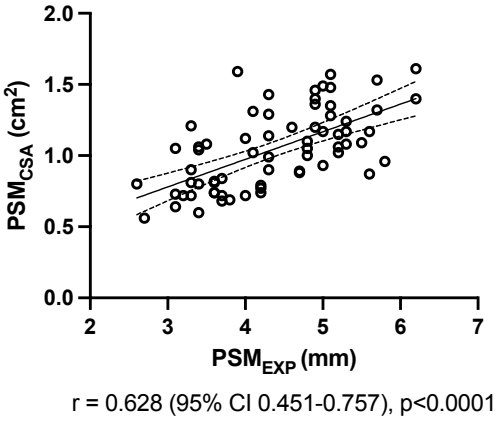


Figure 5-2. Baseline parasternal muscle measurements

Correlation between baseline PSM end-expiratory thickness (PSM_{EXP}) and cross-sectional area measurements of PSM (PSM_{CSA}). Dashed line represents 95% confidence interval. There was a positive correlation between the baseline measures of PSM bulk (using Spearman's correlation, p<0.0001).

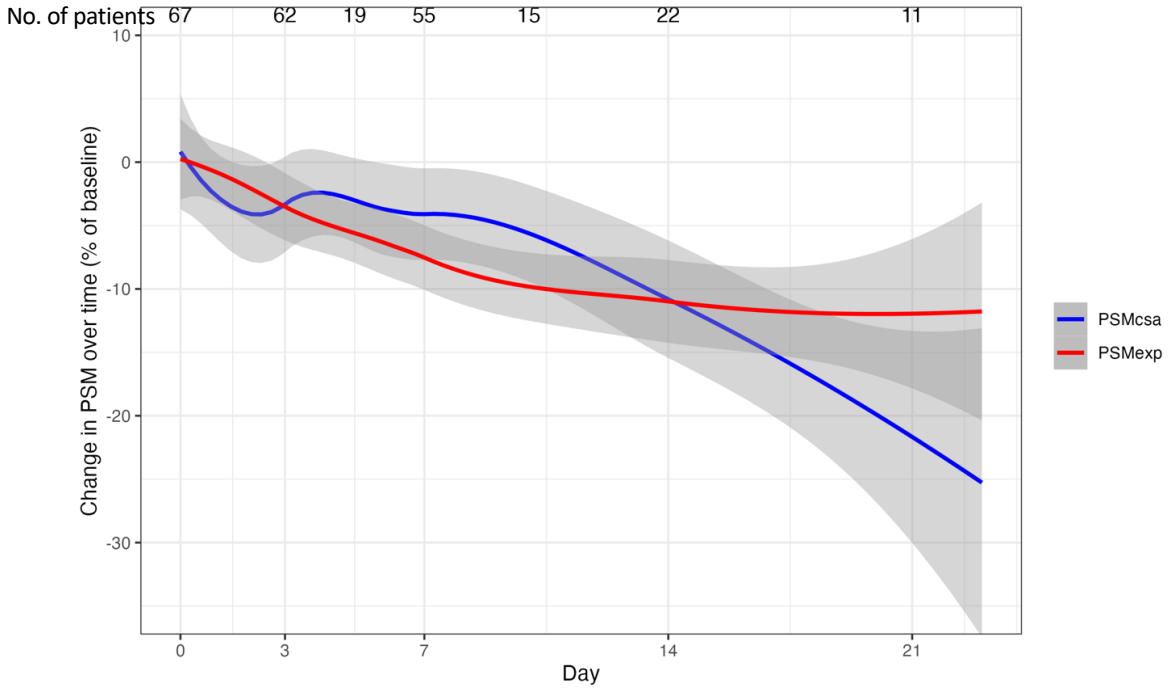


Figure 5-3. Longitudinal changes in parasternal muscle during critical illness.

Pooled patients from study A, B and C. Changes in parasternal muscle using thickness or cross-sectional area were similar up to day 14 and not statistically different at baseline (day 0), day 3, day 7 or day 14. After day 14 there is a more marked decline in cross-sectional area. LOESS curve with 95% confidence intervals shown in grey. *PSM_{EXP}; parasternal muscle end-expiratory thickness, PSM_{CSA}; parasternal muscle cross-sectional area.*

5.6.2.1 Longitudinal variation in PSM thickness and cross-sectional area measurement

Reliability data showed high ICC (>0.9), and low CoV (2.1% and 3.5% for PSM_{EXP} and PSM_{CSA} respectively in healthy volunteers (n=12) (see 4.5.1). Similarly, a low CoV of 4.7% and 2.3% was achieved for PSM_{EXP} and PSM_{CSA} respectively in an ICU population at a single time point (Appendix **9**-**2**). After combining patients in study A, B and C, longitudinal comparison of CoV in PSM_{EXP} and PSM_{CSA} showed significantly lower CoV for PSM_{EXP} at baseline, day 3 and day 7 (Figure 5-4). Therefore, from here on, I report PSM_{EXP} data and in the primary model.

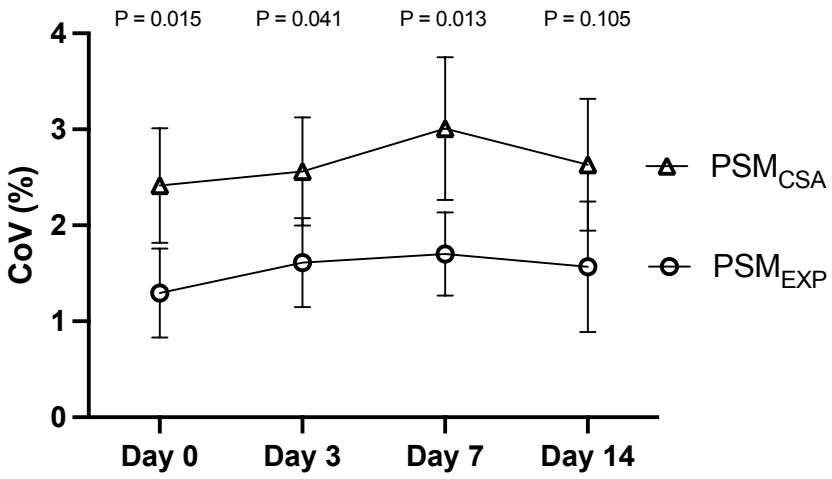


Figure 5-4. Longitudinal change in coefficient of variation of parasternal muscle measurements

Coefficient of variance (CoV) for parasternal muscle cross-sectional area (PSM_{CSA}) was significantly higher at baseline, day 3 and day 7 compared to parasternal muscle end-expiratory thickness (PSM_{EXP}) measurements. Data points displayed as median with error bars representing 95% confidence intervals. Comparison between PSM measurements and time points performed using Sidak's multiple comparisons test. P value significant if <0.05.

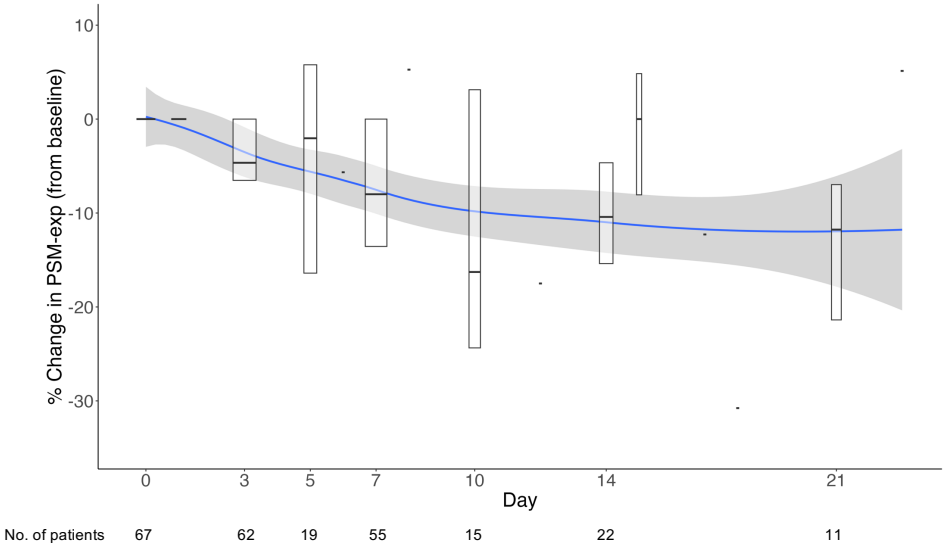


Figure 5-5. Longitudinal changes in parasternal muscle thickness in critical illness

Longitudinal changes in parasternal muscle end-expiratory thickness (PSM-exp). Data bars shown as median and interquartile range. LOESS curve plotted in blue with 95% confidence intervals in grey.

There was a 0.9% (95% CI 0.6-1.3) decrease per day in PSM_{EXP} at the time of the second study (3.5 ±1.5 days) (Figure 5-5, Appendix **9**-**10**). Furthermore, at this time point PSM_{EXP} decreased by more than 10% in 37 patients (55.2%) and decline in PSM_{EXP} was more pronounced in patients who received greater than five days of mandatory mode MV from admission (Figure 5-6).

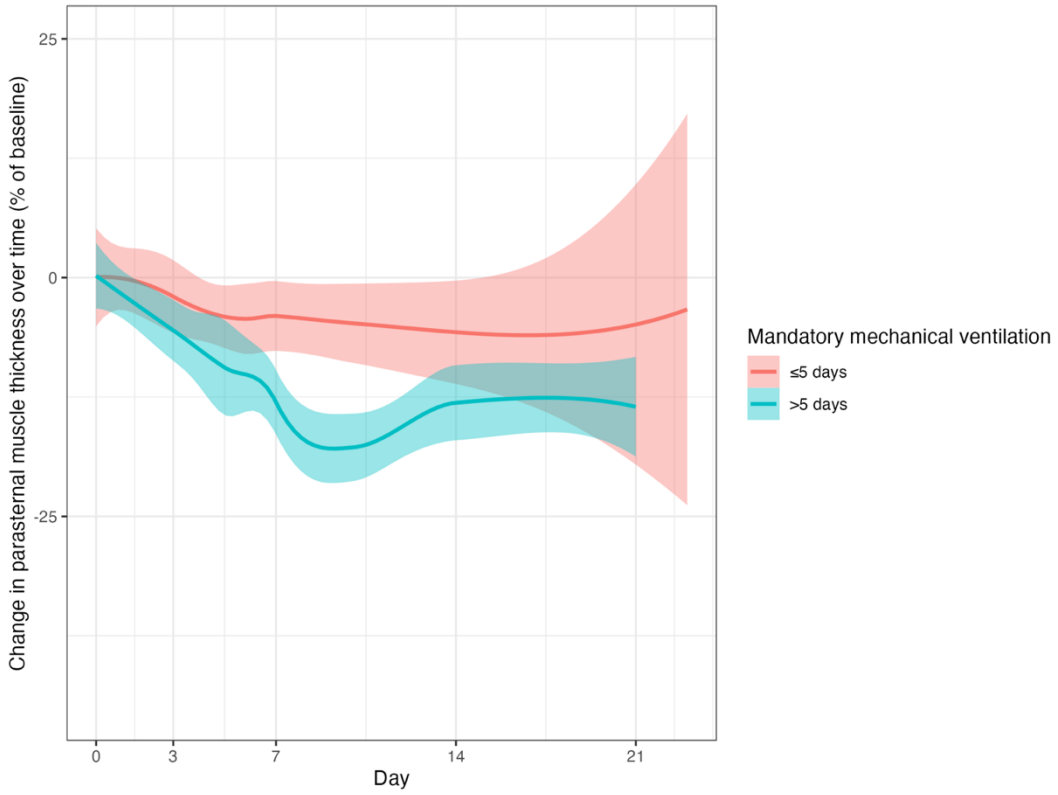


Figure 5-6. Effect of early mandatory ventilation on parasternal muscle

Patients receiving more than 5 days of mandatory mode mechanical ventilation had more pronounced loss of PSM thickness by day 7-10. LOESS curve plotted in respective colours with 95% confidence shaded.

5.6.3 Parasternal muscle activity studies

A total of 56 patients were included for parasternal muscle strain analysis (44 clinical trial patients, 12 healthy volunteers) from which there were 163 B-mode ultrasound studies available for analysis. Of these, 142 studies (87%) were reviewed and suitable for analysis for both PSM_{ε} and PSM_{TF}. Of the studies that were excluded, PSM_{TF} could not be accurately determined from the respiratory cycle. Of

the 44 clinical trial patients, 41/44 (93%) had baseline PSM studies, 37/44 (84%) had baseline and day 3, 34/44 (77%) had baseline, day 3 and day 7 and 22/41 (53%) had a further study at day 14. B-mode video files were not available from study A and therefore PSM_{TF} or PSM_{ε} calculations could not be performed.

5.6.4 Parasternal muscle strain measurement reliability

Bland-Altman plots for parasternal muscle measurements for healthy volunteers and ICU patients in the ultrasound reliability studies is shown in Chapter 4. Briefly, inter-observer ICC of PSM_{EXP}, PSM_{INSP} and PSM_{CSA} in healthy volunteers was 0.995, 0.990 and 0.982 respectively, and PSM_{EXP}, PSM_{INSP} and PSM_{CSA} in ICU patients was 0.989, 0.993 and 0.998. Given that PSM_{ε} measurements were performed on a separate and dedicated workstation with two new operators using separate software, intra- and inter-observer reliability was determined. Twelve randomly selected image files from the eligible study cohort were selected and all data allocated pseudonymised labels (Appendix **9**-**26**). The intra-observer reliability for PSM_{ε} for SO (rater 1) was 0.983 (95% CI 0.945-0.995) and for EA (rater 2) was 0.992 (95% CI 0.972-0.998). The inter-observer reliability was 0.972 (95% CI 0.906-0.992). The Bland-Altman plots are shown in Figure 5-7.

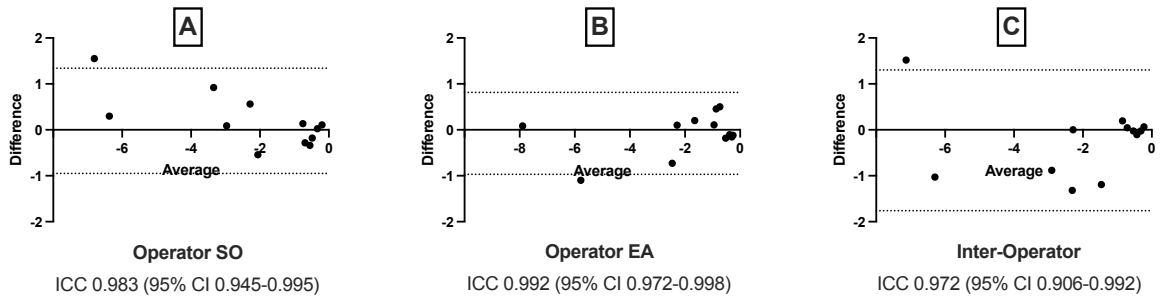


Figure 5-7. Bland-Altman plots of parasternal muscle strain measurements.

Bland-Altman plots of parasternal muscle strain measurement with two independent operators (SO and EA). The intra-operator reliability for SO, EA and the inter-operator reliability are shown in (A), (B) and (C) respectively. Average parasternal muscle strain is plotted along the x-axis, measurement difference along the y-axis and the upper and lower dotted lines represents the upper and lower limits of agreement. *ICC; intra-class correlation coefficient.*

5.6.5 Parasternal muscle strain in critical illness

Table 5-2 summarises the characteristics of the patients included in strain analysis.

	All (n=41)	Non-ARDS (n=14)	ARDS (n=27)	P value
Age	52±16	65±17	46±12	**<0.001**
Male	30 (73)	10 (71)	20 (74)	Ns
APACHE II	16 (12-20)	18 (12-24)	15 (13-19)	0.553
SOFA	9 (7-12)	12 (8-13)	8 (7-10)	**0.021**
Ventilation Mode				
Mandatory	38 (93)	12 (86)	26 (96)	0.265
Spontaneous	3 (7)	2 (14)	1 (4)	0.265
Neuromuscular blockade	13 (32)	2 (14)	11 (41)	0.156
Hospital length of stay before ICU admission – days	4 (1-8)	1 (0-4)	6 (3-10)	**0.016**
Time from intubation to first image – days	2 (1-2)	2 (1-2)	3 (2-5)	**<0.001**
CRP – mg/L	147.5 (29.3-181.7)	78.5 (19.9-152.9)	163.0 (92.6-229.8)	**0.014**
Baseline PSMε	-1.44 (-2.65--0.66)	-2.59 (-4.05--1.48)	-0.76 (-1.72--0.56)	**<0.001**
Baseline PSM_{TF} – %	1.3 (0.51-3.7)	3.2 (1.9-9.0)	0.85 (0.3-1.6)	**0.001**

Table 5-2. Clinical characteristics of patients included in parasternal muscle activity study

These patients were recruited from study B and C and had stored video files for parasternal muscle activity analysis. *ARDS; acute respiratory distress syndrome, APACHE II; acute physiology and chronic health evaluation score, SOFA; sequential organ failure assessment score, ICU; intensive care unit, CRP; C-reactive protein, PSM_{ε}; parasternal muscle strain, PSM_{TF}; parasternal muscle thickening fraction.*

5.6.6 Parasternal muscle characteristics by admission aetiology

Patients with a primary ICU admission diagnosis of ARDS were younger (46±12 years vs. 65±17 years, p=0.0001). There was no difference in the number of male patients in each group (71% non-ARDS vs. 74% ARDS, p>0.05). Non-ARDS patients had higher APACHE II scores (18 (IQR 12-24) vs. 15 (IQR 13-19), p=0.553) and SOFA scores (12 (IQR 8-13) vs. 8 (IQR 7-10), P=0.021). More patients in the ARDS group were on mandatory modes of ventilation and neuromuscular blockade at baseline but neither were significantly different to the non-ARDS group. Patients with ARDS had a longer hospital length of stay before ICU admission (6 days (IQR 3-10) vs. 1 day (IQR 0-4), p=0.016) and longer period between intubation and the first imaging study (3 days (IQR 2-5) vs. 2 days (IQR 1-2), p=0.0006). Baseline CRP levels were also higher in those with ARDS (163.0 mg/L vs. 78.5 mg/L, p=0.014). Baseline

PSM_{ε} was significantly greater in those with ARDS (non-ARDS: -0.76mm (IQR -1.72--0.56) vs. ARDS: -2.59mm (IQR -4.05--1.48), p=0.0004) as was PSM_{TF} (0.85% (IQR 0.3-1.6) vs. 3.2% (IQR 1.9-9.0), p=0.001). Of note, 26/27 ARDS patients received vvECMO compared to none of the non-ARDs patients.

5.6.7 Parasternal muscle strain changes during ICU admission

At baseline, PSM_{ε} was -1.42 (IQR -2.59--0.62) and PSM_{TF} was 1.1% (IQR 0.5-2.5) with 35/38 (92%) patients receiving mandatory mode MV with or without NMB. There was no significant difference in PSM_{ε} at day 3 compared to baseline (baseline: -1.42mm (IQR -2.59--0.62) vs. day 3: -1.84mm (IQR -2.79--1.18), p=0.078). However, at day 7, PSM_{ε} was significantly higher compared to baseline (baseline: -1.42mm (IQR -2.59--0.62) vs. day 7: 2.56mm (IQR -4.88--1.15), p=0.034). Whilst PSM_{ε} at day 14 was higher than baseline, the difference was not statistically significant (baseline: -1.42mm (IQR -2.59--0.62) vs. day 14: 3.08mm (IQR -4.40--0.94), p=0.078) (Figure 5-8).

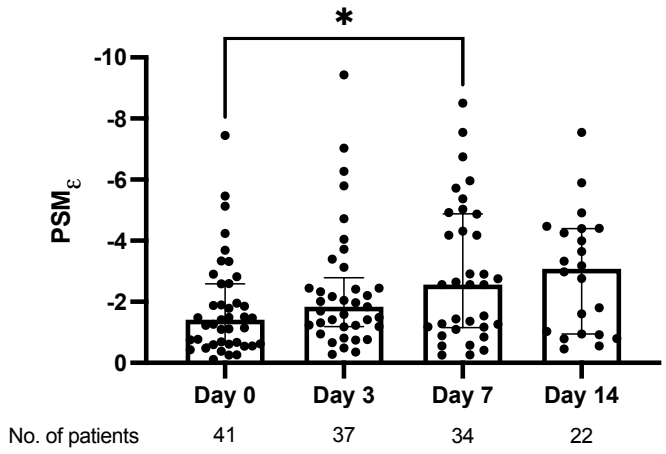


Figure 5-8. Change in parasternal muscle strain during critical illness.

Parasternal muscle strain (PSM_{ε}) in ICU patients during ICU admission. Data points plotted as the median and error bars represent interquartile range. Difference between day 0 and subsequent time points analysed using Kruskal-Wallis test for multiple comparisons. *p<0.05.

5.6.8 Change in parasternal muscle activity during different ventilation modes

There were 159 recorded PSM_{ε} measurements across all patients and time points (36 during MV and receiving neuromuscular blockade (NMB), 68 during mandatory mode MV (MAND), 30 during spontaneous mode MV (SPONT), 13 during self-ventilating after extubation (SV) and 12 healthy, non-ventilated volunteers (HV)). Three patients in HV group were omitted as the PSM_{STR} values appeared to be outliers compared to the remaining cohort.

PSM_{ε} in SV patients was higher than HV patients but not statistically different (SV: -4.40 (IQR -6.32--2.65) vs. HV: -1.88 (IQR -3.44--1.16), p=0.657). Furthermore, there was no difference in PSM_{ε} between SV patients and SPONT patients (SV: -4.40 (IQR -6.32--2.65) vs. SPONT: -3.71 (IQR -5.45--2.58), p=0.999). PSM_{ε} was significantly lower in MAND patients and in those who are receiving neuromuscular blockade when compared to SV and SPONT patients (Figure 5-9). PSM_{ε} was lowest in the NMB group when compared to all other groups during the ICU admission (Figure 5-9). There was no significant difference between PSM_{ε} in the HV and NMB groups (HV: -1.88mm (IQR -3.44--1.16) vs. NMB: -0.95mm (IQR -1.43--0.56), p=0.233). During ICU admission, PSM_{ε} was greatest in SPONT patients at all study time points but only significantly different to NMB patients (Figure 5-10). After baseline measurement, PSM_{ε}, was higher in MAND patients than NMB patients at all study time points but not statistically different (Figure 5-10). At day 7, PSM_{ε} in patients on spontaneous modes of MV was greater compared to MAND and NMB (MAND: -1.49 (IQR -2.91--1.09) vs. SPONT: -4.25 (IQR -5.78--2.56), p=0.012) (NMB: -0.85 (IQR -0.26--1.44) vs. SPONT: -4.25 (IQR -5.78--2.56), p<0.001) (Figure 5-10).

PSM_{TF} values had identical significant differences between ventilation mode groups. There was one additional significant difference between HV and SV where HV patients had significantly lower PSM_{TF} (HV: 2.0% (IQR 0.7-4.2) vs. SV: 7.9% (IQR 4.0-22.9), p=0.031) (Figure 5-9).

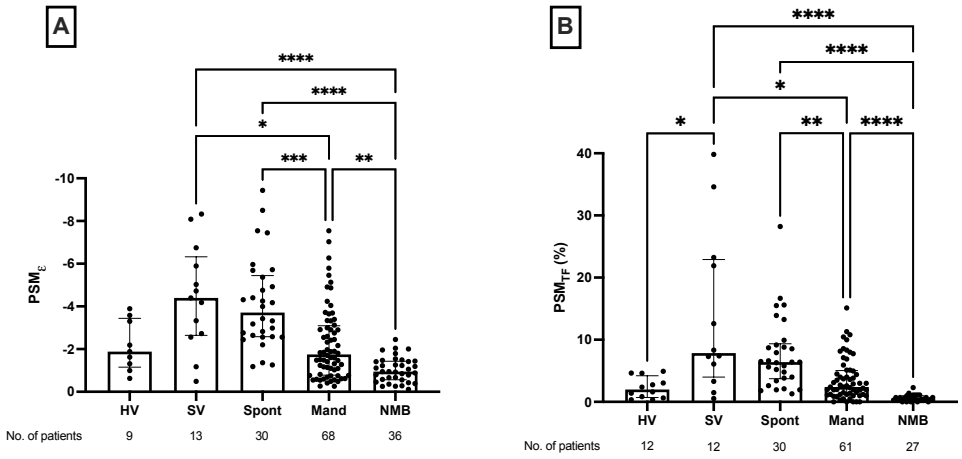


Figure 5-9. Parasternal muscle activity during mechanical ventilation

Parasternal muscle strain (A) and parasternal muscle thickening fraction (B) during different mechanical ventilatory modes. *HV = healthy volunteer, SV = self-ventilating without airway support post-extubation, Spont = spontaneous mode of mechanical ventilation such as continuous positive airway pressure with pressure support (CPAP/PS), Mand = mandatory mode of mechanical ventilation such as BIPAP (bi-level positive airway pressure), NMB = neuromuscular blockade and mandatory mode of ventilation.* * p<0.05, ** p<0.01, *** p<0.001, **** p<0.0001). Data bars represent median and error bars represent interquartile range. Difference between groups analysed using Kruskal-Wallis test for multiple comparisons.

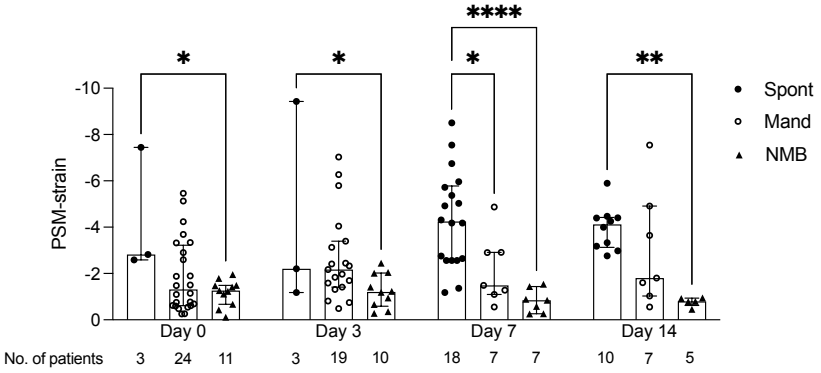


Figure 5-10. Longitudinal change in parasternal muscle strain during mechanical ventilation

PSM strain was significantly lower in mandatory modes at day 7. *Parasternal muscle strain; PSM_{ε}, HV = healthy volunteer, SV = self-ventilating without airway support post-extubation, Spont = spontaneous mode of mechanical ventilation such as continuous positive airway pressure with or without pressure support (CPAP/PS), Mand = mandatory mode of mechanical ventilation such as BIPAP (bi-level positive airway pressure) and all mandatory breaths, NMB = neuromuscular blockade and mandatory mode of ventilation.* * p<0.05, ** p<0.01, **** p<0.0001). Data bars represent median and error bars represent interquartile range. Difference between groups analysed using Tukey's test for multiple comparisons.

5.6.9 Changes in parasternal muscle activity and parasternal muscle atrophy

Lower PSM_{EXP} correlated with increased PSM_{ε} (r=0.321, 95% CI 0.158-0.493, p<0.001; Figure 5-11(A)) where an increase in PSM_{ε} paralleled a loss of PSM_{EXP} (Figure 5-11(B)), i.e. loss of mass increased strain by increasing susceptibility to muscle stress (stress (σ) = force / area). PSM_{TF} and PSM_{ε} were correlated (r=-0.510 (95% CI -0.647-0.344), p<0.001) suggesting that contraction and degree of loading are related rather than passive effects of insufflation (Figure 5-11(C)). In keeping with this, mandatory ventilation modes (with or without NMB) were found to have lower PSM_{TF} and PSM_{ε} (Figure 5-11(D)).

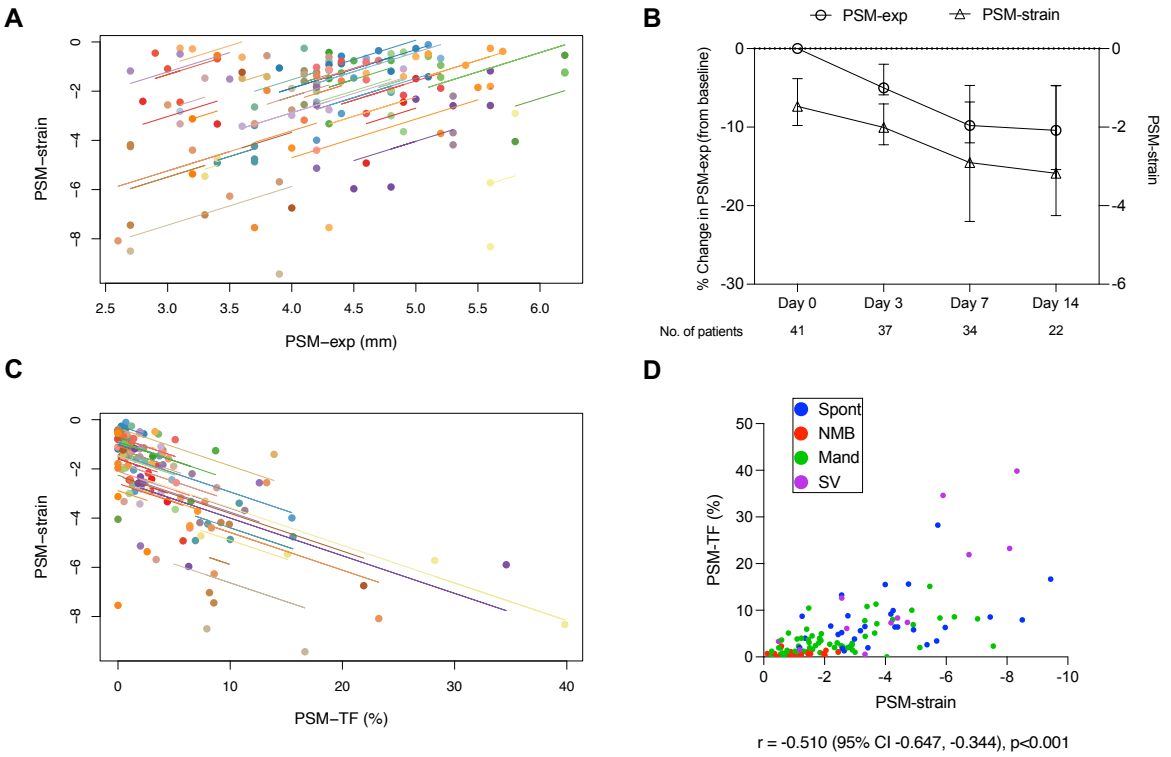


Figure 5-11. Parasternal muscle activity in critical illness

(A) repeated correlation plot of parasternal muscle end-expiratory thickness (PSM-exp) and parasternal muscle strain (PSM-strain). (B) change in PSM-exp and PSM-strain throughout ICU admission. (C) repeated correlation plot of PSM-strain and parasternal muscle thickening fraction (PSM_{TF}). (D) correlation between PSM-strain and PSM_{TF} categorised by ventilation mode demonstrating that most patients with Mand or NMB MV modes have lower PSM-strain and PSM_{TF}. *SPONT = spontaneous mechanical ventilation mode; NMB = mandatory mechanical ventilation mode with neuromuscular blockade; MAND = mandatory mechanical ventilation without neuromuscular blockade; SV = spontaneously ventilating without mechanical support.*

5.6.10 Parasternal muscle strain and ventilation

Analysis of all study points found that PSM_{ε} was positively correlated with tidal volume (r=-0.612 (95% CI -0.716 to -0.493), p<0.0001) (Figure 5-12). This effect appeared to plateau at higher degrees of strain. This suggests that PSM contractile activity is contributing to inspiratory volumes at the time of the study. To determine whether this observation was not simply due to effects of passive insufflation, associations with delivered inspiratory pressure were sought. A higher daily average peak inspiratory pressure (PIP) was associated with lower PSM_{ε} (r=0.393 (95% CI =0.230 to 0.534), p<0.0001). Thus, at lower levels of MV support, parasternal contractile activity was higher in these patients and possibly suggested a degree of underloading of the respiratory muscle pump, recruitment of extra-diaphragmatic muscles and higher tidal volumes at the time of imaging.

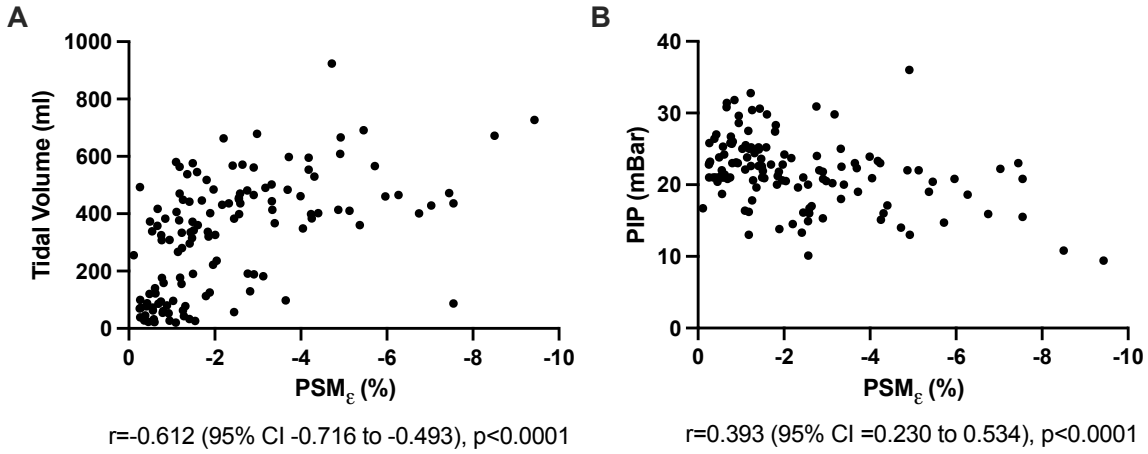


Figure 5-12. Parasternal muscle strain and observed effects on tidal volume

Parasternal muscle strain (PSM_{ε}) was positively correlated with measured tidal volume (A). PSM_{ε} was also positively correlated with measured peak inspiratory pressure (PIP) (B) suggesting that at lower levels of support, there is excessive respiratory loading leading to increased muscle strain. Correlation analysis performed using Spearman's test.

5.6.10.1 Determinants of change in parasternal muscle thickness

Age, illness severity (average SOFA in the first 7 days), levels of sedation (average RASS in the first seven days) and use of neuromuscular blockade infusion in the first three days did not affect PSM_{EXP} over the time course of ICU admission (Appendix **9**-**10**). Male patients had a greater PSM_{EXP} at baseline

and throughout the study (p=0.001) (Appendix **9**-**10**). After adjustment for common causes (age, sex, average SOFA, NMB days, and RASS), PSM_{EXP} and rate of change of PSM_{EXP} were not altered by time-varying PSM_{TF}, (adjusted p for interaction 0.953, Appendix **9**-**11**) – i.e. greater activity does not lead to greater atrophy. Similarly, PSM_{EXP} and rate of change of PSM_{EXP} were not altered by time-varying PSM_{ε}, (adjusted p for interaction 0.666, Appendix **9**-**12**) – i.e. greater strain did not lead to greater muscle atrophy.

5.6.11 Changes in parasternal muscle mass compared to other muscle groups

5.6.11.1 Changes in parasternal and rectus femoris muscle

RF_{CSA} decreased by 2.6% (95% CI 2.2-3.0) per day and was related to change in PSM_{EXP} at the same time point (Figure 5-13 (A)). A 10% loss in RF_{CSA} at time (t) meant a 1.6% (95% CI 0.4 – 2.8%) decrease in PSM_{EXP} (Appendix **9**-**13**). There was a positive correlation between PSM_{EXP} and RF_{CSA} (r=0.32 (95% CI 0.20-0.50), p<0.001) (Figure 5-13 (B)). Longitudinal loss of RF_{CSA} did not affect the rate of decrease of PSM_{EXP} (p=0.214) (Appendix **9**-**13**).

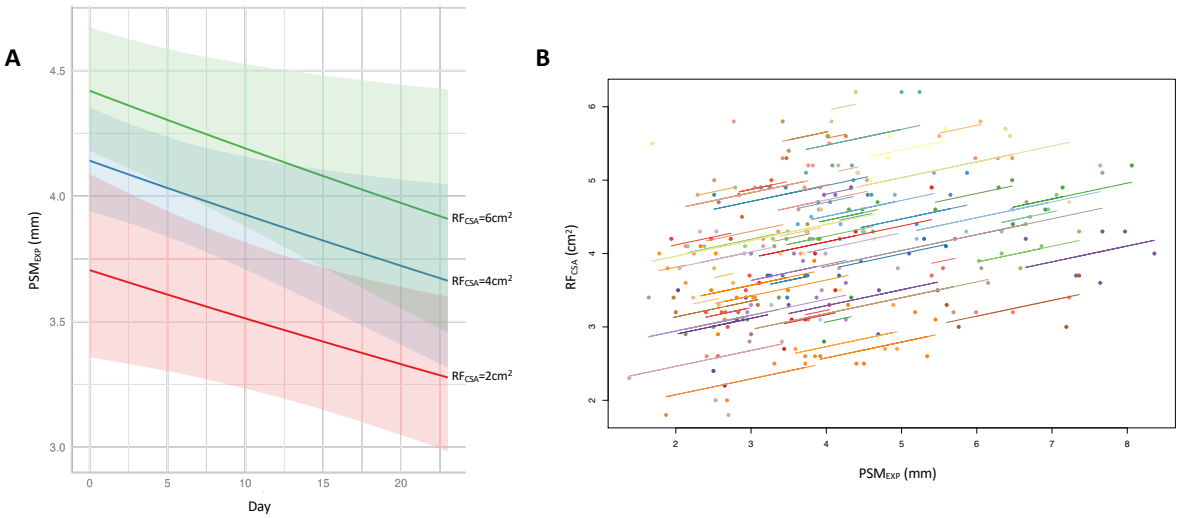


Figure 5-13. Changes in parasternal muscle thickness and rectus femoris cross-sectional area

(A) effects plot examining relationship of time-varying rectus femoris cross sectional area (RF_{CSA}) with PSM end-expiratory thickness (PSM_{EXP}) over time. Three coloured lines represent three different rectus femoris area values chosen as an illustrative range of the marginal effects. (B) Repeated correlation measure of PSM_{EXP} and RF_{CSA} demonstrating a positive correlation (r=0.32 (95% CI 0.20-0.50), p<0.001)).

5.6.11.2 Changes in parasternal and diaphragm muscle

Baseline DIA_{EXP} was 2.5mm (IQR 2.2-2.7) (Figure 4-9, Figure 5-14). There was a 1.0% (95% CI 0.6-1.4) daily decrease in DIA_{EXP} which correlated with a loss of PSM_{EXP} (r=0.37, 95% CI 0.19-0.56, p<0.001) (Figure 5-14, C). PSM_{EXP} decreased at a greater rate in patients with a thicker time varying DIA_{EXP} measurement (p=0.014) (Figure 5-14, C and Appendix **9**-**14**). Diaphragm thickening fraction (DIA_{TF}) increased by 0.8% (95% CI 0.3 – 1.3%) per day, from low baseline levels[152] (median 9% (IQR 4–18) (Figure 5-14, D, Appendix **9**-**15**). At day 7, DIA_{TF} was 13.6% (IQR 4.6 – 22.5%). with 18/35 patients receiving supported modes of MV.

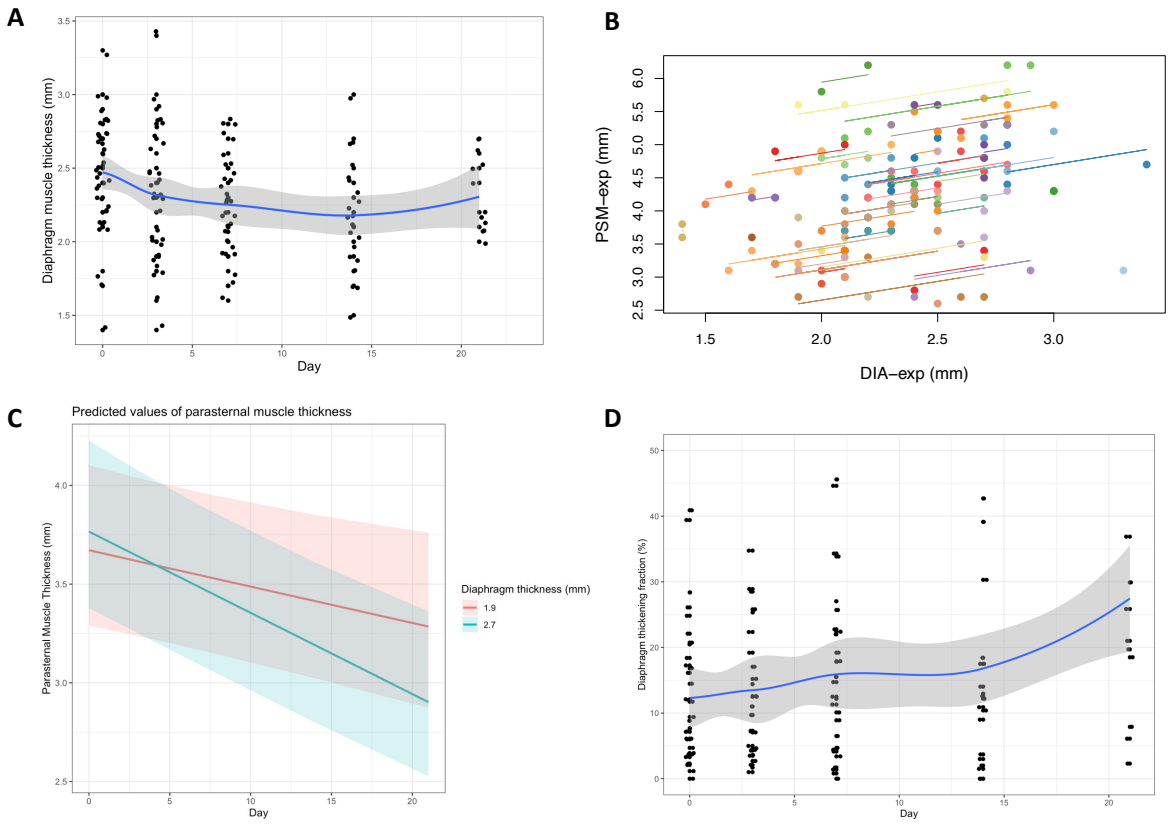


Figure 5-14. Parallel changes in parasternal muscle and diaphragm

(A) Longitudinal change in diaphragm end-expiratory thickness (DIA-exp). (B) repeated correlation plot of PSM_{EXP} and DIA_{EXP} demonstrating positive correlation throughout ICU admission. (C) Patients with thicker DIA_{EXP} had a greater rate of loss in PSM_{EXP} throughout ICU admission. DIA-exp values in this plot were chosen as an illustrative range of the marginal effects. (D) Changes in diaphragm thickening fraction during critical illness. LOESS curve is shown in blue, and 95% confidence intervals shaded grey.

Before examining the effect of diaphragm contractile activity on PSM thickness, we repeated the model of Goligher *et al* to attempt to replicate and establish the relationship between diaphragm thickness and diaphragm contractile activity in our study cohort.[114] In our cohort, the rate and direction of change in DIA_{EXP} over time was influenced by DIA_{TF} (p=0.005, adjusted for age, sex, average SOFA, NMB use, and RASS days) (Appendix **9**-**16**). In contrast, PSM_{EXP} was not affected over time by DIA_{TF} (p=0.305, Appendix **9**-**17**). However, there was a positive correlation between PSM_{TF} and DIA_{TF} (r=0.343 (95% CI 0.237, 0.554), p=0.001) and PSM_{ε} and DIA_{TF} (r=-0.503, 95% CI -0.648, -0.258),

p<0.0001) (Figure 5-15) suggesting activity of both muscle groups. DIA_{EXP} was preserved at higher degrees of parasternal strain (p=0.054) and parasternal thickening fraction (p=0.091) (Appendix **9**-**18**) which may suggest abnormal loading on the extra-diaphragmatic muscles.

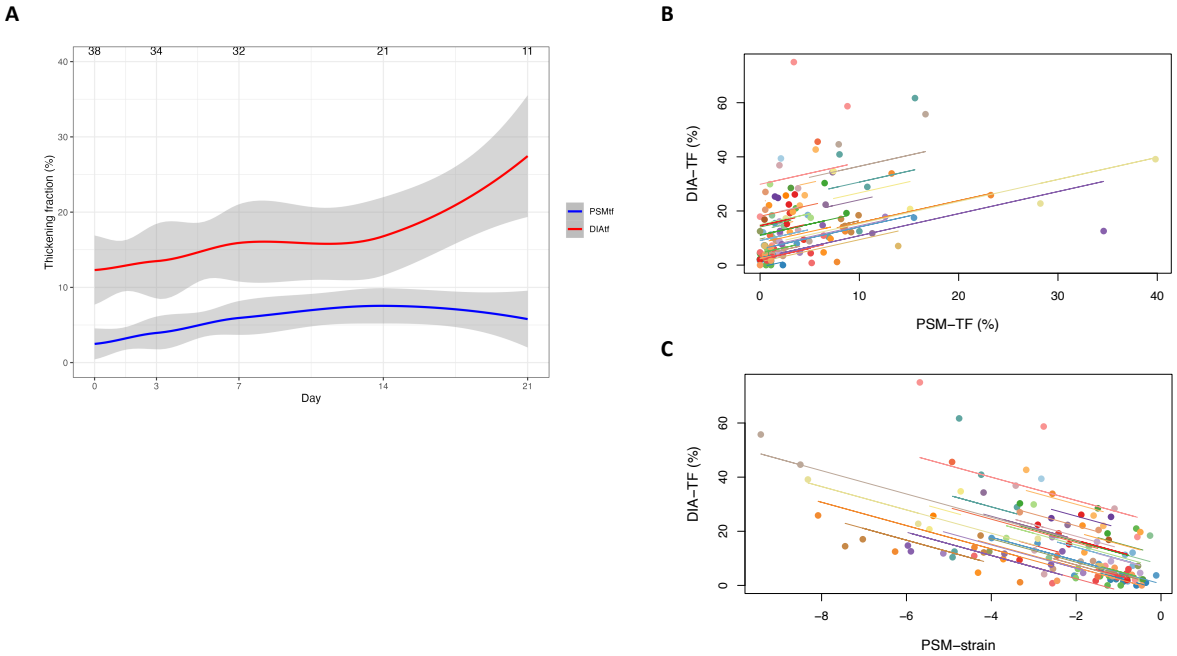


Figure 5-15. Changes in parasternal muscle and diaphragm activity

Longitudinal change in parasternal muscle thickening fraction (PSM-TF) and diaphragm thickening fraction (DIA-TF) during critical illness (A). The number of patients at each time point are given along the top of the graph. There is a paralleled change up to day 14 before an increase in DIA-TF and plateau of PSM-TF. Repeated correlation plot between PSM-TF and DIA-TF (B) and parasternal muscle strain (PSM-strain) and DIA-TF (C) showing that both PSM measures were positively correlated with diaphragm activity.

5.6.12 Impact of ventilation on parasternal muscle contractile activity

Over the study period, PSM_{TF} tended to increase. Patients with higher average tidal volumes had a higher PSM_{TF} over ICU admission (p=0.036). Neuromuscular blockade use and increased PEEP did not reduce PSM_{TF} (p=0.07). Similarly, neuromuscular blockade use in the first 3 days, PEEP and tidal volume did not lower PSM_{ε} (Appendix **9**-**19**).

5.6.12.1 Ultra-protective ventilation and effect on parasternal and other muscle groups

Twenty-seven patients (65%) received vvECMO support. In these patients, unadjusted models suggested a similar daily decrease in PSM_{EXP} when compared to those not receiving vvECMO (p=0.478, Figure 5-16, A). However, PSM_{TF} increased at a greater rate over time in non-vvECMO patients (p=0.003, Figure 5-16, B, Appendix **9**-**20**). PSM_{ε} increased at a similar rate in both groups (p=0.714, Figure 5-16, C) suggesting abnormal respiratory muscle loading in both groups. In further unadjusted models, patients receiving vvECMO had a slower rate of decrease in RF_{CSA} (p=0.013, Figure 5-16, D). However, DIA_{EXP} decreased at similar rates in vvECMO and non-vvECMO patients (p=0.883, Figure 5-16, D).

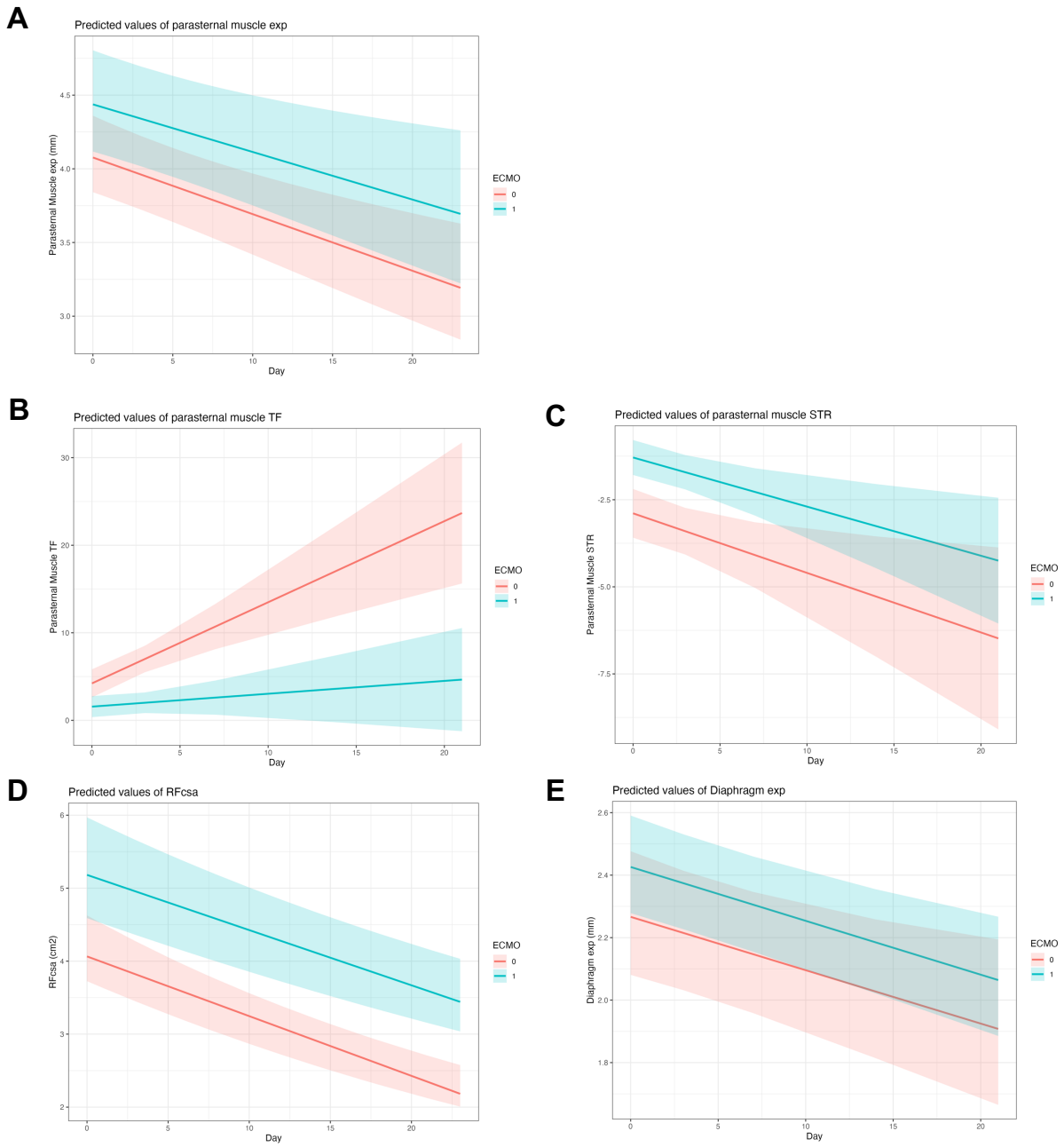


Figure 5-16. Longitudinal changes in parasternal, diaphragm and rectus femoris muscle during extracorporeal support

Effects plot examining relationship between provision of extracorporeal membrane oxygenation and ultra-protective mechanical ventilation on multiple muscle groups: parasternal end-expiratory thickness (A), parasternal muscle thickening fraction (B), parasternal muscle strain (C), rectus femoris cross-sectional area (D) and diaphragm end-expiratory thickness (E).

5.7 Discussion

These data describe the longitudinal change in respiratory and peripheral skeletal muscle mass in critically ill patients using a combination of B-mode and speckle-tracking ultrasonography. Data from chapter 4 showed that parasternal muscle atrophy occurs early and acutely, and I now show that the trajectory is similar to changes seen in rectus femoris and diaphragm muscle. Furthermore, loss of parasternal muscle mass is associated with an increase in muscle strain, indicative of increased respiratory muscle loading and possible increased neural respiratory drive. This is the first such description to link mass, strain and load using a non-invasive technique in critically ill patients.

A 1% daily loss in PSM mass was observed in more than 50% of patients losing more than 10% from baseline. There is little data to describe significant thresholds of PSM loss in critical illness and there is also a paucity of data describing normal baseline values for PSM measurements. However, regardless of the expected variation amongst healthy and clinical cohorts, our data show that loss of mass results in increased strain. Defining significant thresholds of PSM mass loss are therefore unlikely to be required to define a significant loss and it is the resultant effect on muscle loading that is likely to be the significant measurable endpoint. The clinical and physiological implications of a combination of reduced PSM mass and increased strain is yet to be determined in a critical care cohort. In patients with chronic obstructive pulmonary disease, PSM electromyogram monitoring of neural respiratory drive can monitor change in acute exacerbations, predict deteriorations and safe discharge.[275,276,278] Monitoring PSM mass and strain is likely therefore to be useful in monitoring acute respiratory failure, but needs to be assessed prospectively during the delivery of mechanical ventilation.

ICU patients in our study had baseline PSM_{EXP} that was greater than that reported in clinical studies of healthy volunteers (our cohort: 4.3mm (IQR 3.6-5.1) vs. 2.8 (2.2-3.4)[156]) and this may simply reflect natural variation across gender and age and selection of specific patient cohorts. This is supported by data in our reliability study of a healthy population (n=12, 50% male, aged 27 years (IQR 23-35)). In

this healthy cohort, I found that PSM_{EXP} (3.8mm (IQR 3.2-4.6)) and PSM_{CSA} (0.94 mm^2 (IQR 0.89-1.05)) were both less than measurements in our clinical cohort (4.3mm (IQR 3.6-5.1) and 1.05 (IQR 0.80-1.24) respectively).

Critical illness induced muscle wasting is often the product of multiple factors and there is an assumption all muscle groups undergo atrophy at similar rates because of exposure to common risk factors. From our data, parasternal and rectus femoris muscle wasting were correlated and whilst both muscle groups are exposed to systemic risk factors such as organ dysfunction, inflammation and acidosis, there are significant variations in load/unloading risk factors. Immobility of the large muscle groups of the lower limbs crucial to locomotion and physical function would affect peripheral skeletal muscle but not respiratory muscles. Conversely, choice of ventilation mode and use of neuromuscular blockade would affect respiratory muscles but less so peripheral skeletal muscle.[279–281] MV induced inflammation specifically may represent a crucial driver of inflammatory respiratory muscle wasting through sensitisation of the diaphragm to excessive loads from MV.[282] The increase in potential determinants of parasternal muscle mass, and the unknown relationship between these factors may explain the lack of associative relationship seen with determinants of peripheral skeletal muscle wasting. In line with this, loss of parasternal muscle mass was also associated with loss of diaphragm mass, and I found that a greater DIA_{EXP} at baseline and throughout the admission led to a greater decline in PSM_{EXP}. It has been postulated that evolving diaphragm hypertrophy is the result of intramuscular adipose tissue[15] leading to a reduction in muscle quality, reduction in function and increased loading of respiratory accessory muscles.

Clinical studies of the diaphragm have in fact showed that bulk can increase or decrease during early MV.[15,58,113,116] In our study of the extra—diaphragmatic PSM muscle, I observe predominantly a loss throughout critical illness. Potential disruption of muscle homeostasis was not the focus of this study, but extrapolating data from diaphragm studies in critical illness would suggest structural injury from

upregulation of catabolic proteins (as well as downregulation of anabolic pathways), myofibre atrophy and resultant reduction in force generating capacity as hypothesised findings.[15,116] Similarly, muscle atrophy, reduced protein synthesis and histological evidence of necrosis are commonly seen in critically ill patients.[14,199] Of course, the true underlying pathophysiology in accessory muscles longitudinally may be best assessed with histology but this is of course challenging to achieve in the high-risk, mechanically ventilated patient during critical illness and supports the need to develop non-invasive methods to assess muscle quality. In this regard, findings of increased muscular echogenicity using ultrasound as a measure of reduced muscle quality has been previously been shown to be related to prolonged MV,[133,283] and conversely, lower echogenicity is associated with reduced duration of MV and lower mortality.[270] Our data demonstrate loss of muscle quality occurs alongside atrophy in PSM muscles, in a similar fashion to rectus femoris[133] (see 4.5.9) where increased echogenicity is associated with underlying myonecrosis and may suggest a necromyopathy affecting all skeletal muscles may be a significant pathophysiological process.

Critical illness and MV with excessive respiratory muscle loading (and therefore increased strain) can lead to ventilator induced muscle dysfunction[125,284] and increase neural respiratory drive. Measuring central (brain stem) neural output is through surrogate measures and PSM_{EMG} is considered to be the gold standard diagnostic tool but its use and interpretation is largely confined to specialist and research centres.[275,276] Given these difficulties, PSM activity measurement via ultrasound offers an excellent non-invasive modality and conveys numerous benefits. I used PSM_{TF} and PSM_{ε} as measures of PSM activity rather than as markers of pressure-generating ability.[114] Our data shows that PSM atrophy was associated with increased PSM_{TF}, PSM_{ε} and DIA_{TF}, which does not necessarily lead to reduced function and strength, but to increased loading of respiratory muscle, an imbalance which may predispose patients to respiratory muscle fatigue and thereafter failure. PSM_{ε} and PSM_{TF} are measured in planes perpendicular to each other. A strong correlation between the two suggests the

changes in muscle morphology is due to intrinsic muscle activity and respiratory effort rather than passive change during lung insufflation.

An interesting finding was that the degree of PSM activity on admission and throughout ICU admission did not impact the degree of muscle atrophy. Increase in PSM_{TF} over time may reflect the higher likelihood of spontaneous and/or supported modes of ventilation and less frequent use of neuromuscular blockade and mandatory modes of ventilation. Alternatively, the increase in thickening fraction, and indeed strain values, may serve as early indicators of respiratory load imbalance as ventilator strategies are titrated. Thus, the delicate balance of lung rest and excessive load appears to be influenced by additional factors leading to change in the parasternal muscle structure – findings which were similar in diaphragm studies.[114,285] Studies have shown that during low (and possibly sub-optimal) levels of ventilatory support, PSM_{TF} is higher in patients with underlying diaphragm dysfunction[156] and help to identify those that may fail a trial of extubation. Furthermore, a PSM_{TF} >8% has been suggested as a quantitative cut-off for predicting extubation failure in the context of VIDD.[122] This may in part be due to PSM contractility serving as measures of respiratory muscle loading rather than measures of inspiratory effort as their primary function is as supporting structures to during inspiration rather than primary muscles of ventilation. I demonstrate that greater number of days of mandatory mode ventilation led to a greater decrease in parasternal muscle thickness, and increases seen in PSM_{TF} and PSM_{ε}. This suggests that excessive loading occurs on atrophied muscle which agrees with the mathematical relationship between stress, force and area. Interestingly, severity of illness, degree of sedation and administration of neuromuscular blockade did not impact the change in PSM over time but did reduce PSM contractility measurements which are somewhat predicted clinically. Further research is required to assess the effect of changes in ventilatory support and PSM functional measures and whether these impact weaning failure and length of mechanical ventilation.

I observed relationships between MV and neuromuscular blockade with parasternal muscle strain. Strain measurements were able to distinguish the various unloading abilities of ventilation strategies. Tidal volumes delivered were associated with higher parasternal thickening fractions, and the lack of relationship between neuromuscular blockade and PEEP use may be the result of insufficient numbers. Interestingly receiving vvECMO did not result in a different strain pattern from mechanical ventilation, suggesting that underlying mechanical ventilation loading may be similar.

Forty percent of our cohort received vvECMO and 'ultra-protective' lung rest for severe ARDS. vvECMO allows small (and sometimes negligible) tidal volumes to be delivered during MV while maintaining adequate gas exchange through the extra-corporeal circuit. I showed that patients receiving vvECMO and an ultra-protective MV strategy had greater parasternal muscle bulk and diaphragm thickness throughout admission, but this did not impact rate of loss of thickness in either muscle. Previous large clinical trials investigating the use of vvECMO in the management of ARDS included patients with a mean age of 51.9 ± 14.2 years.[286] In our study, the mean age for ECMO patients was 45.2±12.0 years (versus 52.6±17.5 years in the non-ECMO cohort) and thus physiological variation and patient selection for ECMO may offer a simple explanation for this.[287] The provision of vvECMO seemed to result in lower parasternal thickening fraction when compared to those without vvECMO, likely owing to the ultra-protective ventilation strategy and administration of neuromuscular blockade. However, PSM strain was not significantly different between the groups, suggesting similar muscle loading.

Conversely, it is not known whether the commencement of vvECMO leads to more severe disuse atrophy in extra-diaphragmatic muscles than providing lung protection without vvECMO. Parasternal muscles respond to respiratory load[59] and there is early evidence to suggest that parasternal muscle activity increases with sub-optimal levels of support during mechanical ventilation.[156] More intricate ventilatory mechanics were not the focus of this study, and it is not clear whether higher PSM contractility leads to significantly higher tidal volumes and more effective gas exchange. At our centre,

in early phases of vvECMO management, MV strategy is kept constant in the delivery of ultra-protective lung management (PEEP 10cmH_2O, mandatory respiratory rate 10 per minute, peak inspiratory pressure 20cmH_2O). Similarly, any additional metabolic cost and energy expended during periods of higher PSM_{ε} was not investigated but clearly represents an exciting area of future research. It is also worth considering pro-inflammatory effects from exposure to an extracorporeal circuit, which is a concept well described in cardio-pulmonary bypass.[288] With respect to RF_{CSA}, whilst there was an overall decline, the rate of decline in patients receiving vvECMO was less than those not receiving vvECMO. Without careful patient matching and control for ventilatory factors, this finding may be purely coincidental.

The observation of increased strain from loss of muscle mass suggests that the inspiratory muscles may have a greater role to play in weaning and extubation, and that it is possible to non-invasively monitor mass, strain and load at the bedside using easily available tools. Further these muscles are likely to be recruited to aid ventilation in the setting of moderate-severe exercise, which is the level of perceived exercise for bed to chair mobilisation in ICU survivors because of muscle weakness.[289] Respiratory muscle weakness may be a contributing factor to the inability of critical illness survivors to perform exercise rehabilitation.[290]

Our findings have several limitations. Observational studies are at risk of selection bias. The estimates of changes in muscle groups in patients admitted to critical care cannot be certain from these data due to risk of confounding from selection bias in a convenience sample of patients across two sites. However, longitudinal modelling that robustly incorporated patient specific trajectories, varying baseline differences, and repeated measurements of muscle groups over time give confidence that these observations are true.

Parasternal muscle ultrasound is an evolving tool in the assessment of ICUAW and weaning failure in the critically ill.[33,125,284] I ensured that ultrasound protocols were robust and subjected to intra- and inter-observer reliability testing. I did not evaluate the effects of muscle atrophy or activity on ICU outcomes such as time to extubation, success of a spontaneous breathing trial or ICU mortality, as our sample size would have been inadequate. Whilst there is growing evidence that diaphragm weakness is associated with higher ICU mortality,[265,291] this is unclear in extra-diaphragmatic muscle. Similarly, I did not assess patients following ICU discharge or within longer term follow-up following hospital discharge.

The purpose of this study was not to compare changes in bulk or function with current gold-standard methods of respiratory muscle activity in critical illness such as parasternal electromyography. However, such techniques may help to verify findings as increase activity of extra-diaphragmatic muscles suggests inadequate support and also may confirm whether the measured increase in PSM contractility is truly from active contraction rather than passive effects from ventilator insufflation.[292] Furthermore, whilst I evaluated quantitative measures in healthy and critical illness cohorts, this was only performed during tidal breathing and not during coached or maximal inspiratory breaths. Thus, the true range of PSM_{TF} and PSM_{ε} in this population are not reported. However, volitional tests during mechanical ventilation are often not possible and our study offers a more pragmatic description.

The parasternal muscle is small yet vital in adjunctive support of the respiratory muscle pump during spontaneous and supported breathing during mechanical ventilation. Studies of PSM_{CSA} in chronic respiratory disease has shown that increased PSM atrophy leads to reduced lung function (as per predicted FEV_1) and increased physical restriction (as per reduced percentage of predicted 6 minute walk test).[243,293] The long-term effects of small respiratory muscle atrophy in critical care survivors is currently unknown. Common complaints in those that survive are of muscle weakness and wasting, and these persist for up 5 years.[11] Recent data in survivors of COVID19 requiring hospital admission

have reported similar symptoms but the functional impact in the context of respiratory muscle wasting remains unclear.[109] Future research should focus on the use of dynamic measures of respiratory muscle strain and understanding their use in predicting weaning success and failure, and engagement with physical rehabilitation. Parasternal electromyography signals have direct relationships to respiratory muscle load,[294] and may help to verify findings of increase activity of extra-diaphragmatic muscles as a measure of inadequate support.

In summary, I describe the longitudinal muscle atrophy and loss of muscle quality in parasternal muscle during early critical illness. PSM atrophy is associated with atrophy of the diaphragm and rectus femoris muscles. I have introduced non-invasive methods of assessing PSM function through parasternal strain quantification and demonstrate its evolution through critical illness. PSM strain increased despite marked muscle atrophy and increased echogenicity. These initial changes in strain quantification require further investigation to determine whether they can be applied as a measure of respiratory load and/or be used in weaning from mechanical ventilation.

In the next chapter I will explore the incidence of myonecrosis in critical illness associated muscle wasting and the differences in intra-muscular and systemic cytokines to determine whether there is evidence of programmed necrosis.

Chapter 6: Programmed necrosis in critical illness associated muscle wasting

6.1 Background

Our data has shown that peripheral skeletal muscle wasting greater than 10% from baseline occurs within seven days of critical illness. Furthermore, using two imaging modalities, the observed atrophy is paralleled by significant decline in muscle density (loss in SMD and increase in EG), and thus quality. The MUSCLE-UK study showed increased echogenicity of the rectus femoris muscle by day seven of critical illness was associated with histological features of myonecrosis.[3,6] Despite the significant prevalence of this finding in prospective clinical studies, the underlying pathophysiology remains poorly understood.

Intramuscular inflammation and altered protein homeostasis contribute to a reduction in muscle mass.[295] Necrosis, is a form of pro-inflammatory cell death,[202,216] and is frequently observed in skeletal muscle of critically ill patients.[14,199] However, the interplay between myonecrosis and muscle inflammation remains uncertain. Myonecrosis leads to a loss of muscle quality[133] and has been described in up to 40% of critically ill patients.[3,6] Necroptosis is one form of programmed necrosis implicated in critical illness[204,232,234] and is archetypally activated by ligation of TNFR1 by TNF-α.[216,217] Following on, a crucial step in necroptosis is the formation of a RIPK1 and RIPK3 complex[218–221] and subsequent RIPK3-mediated phosphorylation of MLKL[222,223] Subsequent oligomerisation of pMLKL in the cell membrane leads to formation of pores, inducing sodium influx, cellular oncosis and eventually cellular lysis.[202,224,225,227] Lysis of the cell causes systemic exposure to a number of DAMPs[216,226–228] which leads to 'necro-inflammation' through release of these intracellular contents and may translate clinically as end-organ dysfunction.[202] Tissues with increased expression of RIPK3 and MLKL may favour necroptosis as this may suggest upstream receptor binding and formation of the necrosome.[296] To date, necroptosis in peripheral skeletal muscle has only been described in dystrophin-deficient human skeletal muscle where RIPK3 and pMLKL were significantly upregulated.[8] Given the high incidence of

ICUAW and persistence of physical disability in ICU survivors, investigation of underlying mechanisms are warranted. Myonecrosis represents an interesting focus of unravelling the underlying drivers of severe muscle wasting as those with necrotic features have an association with higher degrees of organ failure which is related to higher mortality and morbidity.[14,199] I therefore sought to evaluate whether there is evidence of necroptosis activation in skeletal muscle of critically ill patients and whether any circulating markers of necrosis can differentiate these histological subtypes.

The UK-MUSCLE study (clinicaltrials.gov: NCT01106300; ethics reference: 05/q0505/30) represents the largest study of prospectively collected human skeletal muscle in critical illness and described acute skeletal muscle wasting in critically ill patients using musculoskeletal ultrasound and muscle histology, coupled to markers of anabolic and catabolic signalling and protein turnover.[14] In this study an association between histological myonecrosis and increased ultrasound echogenicity was described. Therefore, I sought to study available specimens from this study for markers of inflammation and necroptosis. More specifically, identification of RIPK3 and pMLKL may suggest upregulation and programmed necrosis pathway activation.[222,297,298]

6.2 Aims

1. ***Determine whether downstream necroptotic machinery, RIPK3 and pMLKL, are present in skeletal muscle of critically ill patients.***
2. ***Determine whether systemic markers of inflammation and necrosis differentiate patients with and without myonecrosis during critical illness.***

6.3 Hypotheses

1. ***The presence of RIPK3 and pMLKL in necrotic skeletal muscle suggests activation of necroptosis during critical illness associated muscle wasting.***

6.4 Methods

6.4.1 Sample acquisition

Clinical samples (human serum and skeletal muscle tissue) were kindly donated by Dr Zudin Puthucheary (Clinical Senior Lecturer, William Harvey Research Institute, Queen Mary University of London) and the UK-MUSCLE study consortium (Appendix **9**-**1**). In the original study, at enrolment, written assent was obtained from the next of kin with retrospective patient consent obtained when full mental capacity was regained. Serum was received pre-aliquoted and stored at -80^{o}C until required. Frozen muscle histology sections were prepared and analysed as described in2.4.2.1 2.4 2.4.4.2 and stored at -80^{o}C until needed. Pre-prepared histology sections were also available and are specifically referred to below. Serum and muscle tissue were collected on day 1 of ICU admission (referred here on as T1) and again on day 7 or 10 (referred here on as T2). Pieces of skeletal muscle tissue (weighing 20-30 mg) were snap frozen at the time of biopsy and stored at -80^{o}C until required.

In addition, snap frozen pieces of skeletal muscle tissue from healthy volunteers were kindly provided by Professor Steve Harridge (Centre for Human & Applied Physiological Sciences, Faculty of Life Sciences & Medicine, King's College London) as part of the research and ethics committee approved study 12/LO/0457 and subsequent experiments were conducted at Centre for Human & Applied Physiological Sciences, Faculty of Life Sciences & Medicine, King's College London.

6.4.2 Defining myonecrosis

In the original study, the presence of necrosis in skeletal muscle was determined via histological assessment by an expert histopathologist in the UK-MUSCLE consortium (Professor Rahul Phadke, senior lecturer and honorary consultant histopathologist at the National Hospital for Neurology and Neurosurgery, Queens Square, London). Haemotoxylin and eosin (H&E) stained sections of skeletal muscle were studied for necrotic features. Myonecrosis was confirmed by the loss of cytoplasmic

eosinophilia and basophilic nuclear staining, lytic changes and infiltration by macrophages. In addition, more severe and acute necrosis was accompanied by fascial oedema and influx of neutrophils and macrophages. Regenerating fibres were identified on H&E stained sections as fibres with increased cytoplasmic basophilia and large vesicular nuclei with prominent nucleoli. Muscle samples with sharply circumscribed groups of necrotic and/or regenerating fibres were excluded from that analysis, as iatrogenic necrosis could not be excluded. Patients were then separated into necrotic (NEC) and non-necrotic (NONEC) groups by Professor Phadke. In the original study, 20/38 (53%) patients had necrotic features on histology at T2.

6.4.3 Systemic markers of inflammation and necrosis

Systemic and intra-muscular concentrations of inflammatory mediators in the sub-cohort of the UK-MUSCLE study were provided by the UK-MUSCLE consortium. Intramuscular data has previously been reported[34,295] and replication of any of these data is clearly referenced. Concentrations of systemic inflammatory mediators were provided with permission from Dr Zudin Puthucheary and have not previously been reported. Original serum assays were performed using a Luminex platform (Millipore xMAP©, Billerica, MA, USA) and analysed on a Luminex platform machine (FLEXMAP 3D®, Merck, Darmstadt, Germany). Systemic concentrations of IL-1β, IL-6, IL-8, IL-10, IFN-γ, TNF-α, TNFR1 and VEGF were analysed. Systemic concentrations of RIPK3 and CCK18 as markers of necrosis were determined using standalone ELISA as detailed in 2.3.1 .

6.4.4 Quantitative and qualitative measurement of necroptosis machinery

Expression of pMLKL in skeletal muscle tissue was used as the main terminal effector protein to indicate activation of programmed necrosis. Quantification of pMLKL was performed Using Western blotting and qualitative analysis by immunohistochemistry. RIPK3, another crucial protein in the formation of the necrosome was assessed alongside pMLKL using immunohistochemistry.

6.4.4.1 pMLKL protein quantification

Protein extraction and quantification is detailed in 2.4.2.1 . Protein loading and antibody concentration was determine using serial dilution of samples and is shown in Figure 2-14. Protein for Western blotting samples were run in pairs for each patient (i.e. T1 and T2). Six separate Western blot gels were required and expression of pMLKL was given as a relative density after normalising to GAPDH expression (see 2.4.3). Following this, relative expression of pMLKL at T1 and T2 was recorded. In addition, the T2:T1 signal intensity ratio was also calculated to determine fold change from each patient's individual baseline (T1).

6.4.4.2 pMLKL confirmation with immunohistochemistry

Detailed methods of immunohistochemical staining of skeletal muscle is given in 2.4.4 and 2.4.4.2 Optimal concentration of pMLKL antibody (Abcam, ab1877091) for immunohistochemistry was determined by serial dilution of sections with 1:100, 1:250, and 1:500 pMLKL (data not shown). Clear immunostaining after adjusting for background signal was obtained using 1:250 dilution and this dilution was maintained for the remaining sections. Dr Thomas Francis (TF) (Centre for Human & Applied Physiological Sciences, Faculty of Life Sciences & Medicine, King's College London) helped perform the staining and image acquisition in line with departmental protocols. A minimum of 10 digital images per patient per time point were acquired and reviewed by SP and TF independently offline. Both SP and TF recorded images as 'definite staining', 'possible staining' and 'no staining' for pMLKL. Those with 'possible' staining were repeated or fresh sections were performed depending on sample availability.

6.5 Statistical analyses

Quantitative data was assessed for normality using Shapiro-Wilk's test. Parametric variables are reported as mean (± standard deviation) and differences between two groups were analysed using Student's t test. Non-parametric variables are reported as median (interquartile range) and analysed

using Mann-Whitney test or Wilcoxon signed rank test as appropriate. To compare differences between multiple groups, ANOVA or Kruskal-Wallis tests were used for comparisons between groups as appropriate. Statistical significance was indicated by a p value of <0.05.

6.6 Results

6.6.1 Clinical cohort

Data from 38 patients in the MUSCLE-UK study was made available for further analyses relating to inflammation and cell death with permission (Appendix **9**-**1**). Clinical data included demographics, ICU admission (APACHE II and SOFA scores, biochemical data etc), percentage loss of RF_{CSA} and presence of necrosis on histological specimens. The cohort is summarised in Table 6-1. There were no significant differences in age or sex between NEC and NONEC patients. Severity of disease was similar, as given by the admission APACHE II and SOFA scores – with a predicted mortality of 40% or 50% respectively in this cohort.[73] Admission CRP levels were higher in NEC patients but was not statistically significant (122mg/L (IQR 33-250) vs. 75mg/L (IQR 17-166), p=0.357). The extent of muscle loss (using rectus femoris cross-sectional area ultrasound) was significant at T2 when compared to baseline (16.2% $\pm$ 12.4) but there was no difference between groups (NEC: 16.4% $\pm$ 13.7 vs. NONEC: 16.1% $\pm$ 11.3, p=0.960).

Whole muscle tissue and serum sample availability was determined from the MUSCLE-UK sample database. I found that 14 patients with pre-determined histological necrosis had serum samples. Of these, 10 patients also had muscle biopsy tissue at T1 and T2. Similarly, 6 patients without evidence of myonecrosis had available muscle tissue and serum at T1 and T2. Therefore, in the present study, 16 patients (10 NEC, 6 NONEC) had serum and skeletal muscle tissue samples at T1 and T2. An additional 12 patients (4 NEC, 8 NONEC) were identified with paired serum samples but had no muscle

tissue. Therefore 28 patients were included in serum analyses (NEC=14, NONEC=14). The sub-cohort (NEC=14, NONEC=14) is summarised in Table 6-2.

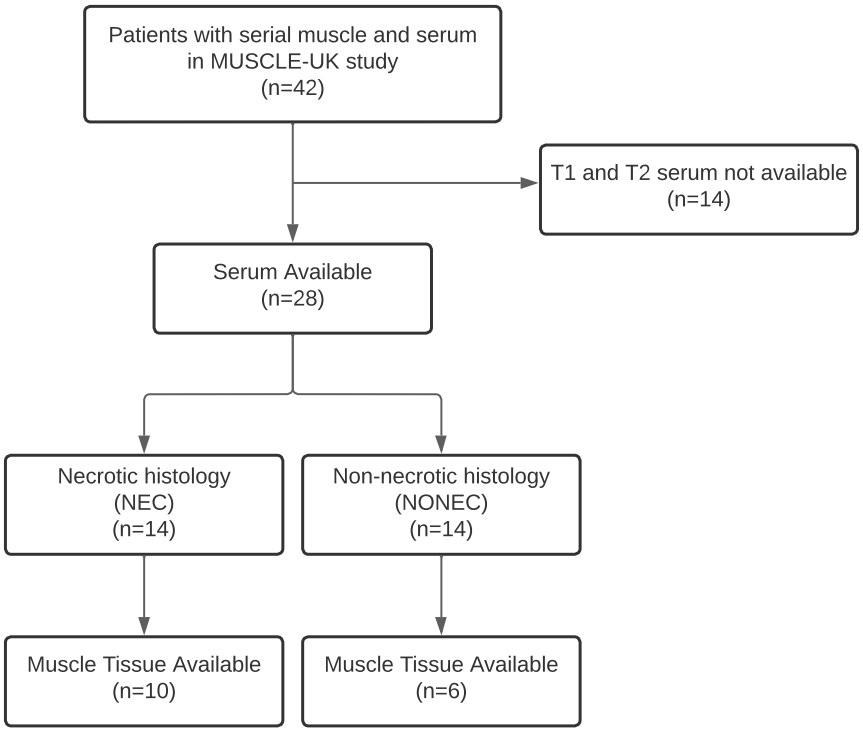


Figure 6-1. Consort diagram for inclusion of patients from MUSCLE-UK study

In the current study, 28 patients (NONEC=14, NEC=14) patients were included in the serum analyses and of these, 16 (NONEC=6, NEC=10) had muscle tissue from the same study point. *T1=day 1 of ICU admission, T2=day 7-10 of ICU admission. NEC=underlying necrotic histology, NONEC=no features of necrosis on histology*.

	All (n=38)	NEC (n=20)	NONEC (n=18)	P value
Age – years	52 (33-65)	49 (33-63)	54 (35-67)	0.723
Male – No. (%)	27 (71%)	10 (50)	12 (67)	0.299
APACHE II score – points	21 (19-27)	22 (17-29)	22 (20-27)	0.999
Admission SOFA score – points	10 (8-12)	11 (7-11)	11 (9-12)	0.332
CRP – mg/L	101.6 (19.3-195.2)	121.8 (32.5-250.0)	75.0 (16.7-165.9)	0.357
WCC – x10^9/L	10.3 (7.9-18.7)	12.4 (8.4-22.3)	9.4 (6.7-15.0)	0.113
Lactate – mmol/L	1.5 (1.0-2.6)	1.5 (1.0-2.5)	1.4 (0.9-2.8)	0.834
PaO2/FiO2 – kPa	31.9 (22.3-44.0)	32.5 (24.4-45.6)	30.0 (20.0-43.8)	0.346
% loss of RF_{CSA} at day 10*	16.2 ± 12.4	16.4 ± 13.7	16.1 ± 11.3	0.960

Table 6-1. Clinical characteristics of MUSCLE-UK study patients

Clinical data of MUSCLE-UK study patients before stratification for the current study. In the former, there were 38 patients. *APACHEII; acute physiology and chronic health evaluation, SOFA; sequential organ failure assessment, CRP; C-reactive protein, WCC; white cell count, PaO2/FiO2; ratio of partial pressure of arterial oxygen to the fraction of inspired oxygen, RFCSA; rectus femoris cross-sectional area, NEC; underlying necrotic histology, NONEC; no features of necrosis on histology.* Data displayed as median (inter-quartile range) unless otherwise specified. *mean ± standard deviation.

	All (n=28)	NEC (n=14)	NONEC (n=14)	P value
Age – years	50 (33-71)	43 (32-64)	59 (37-78)	0.306
Male – No. (%)	27 (71%)	10 (71%)	12 (86%)	0.357
APACHE II score – points	22 (10-29)	23 (19-32)	22 (20-27)	0.658
Admission SOFA score – points	11 (9-12)	11 (10-11)	11 (9-12)	0.738
CRP – mg/L	107.2 (25.2-186.8)	95.1 (10.2-180.3)	120.2 (35.5-213.3)	0.701
WCC – x10^9/L	12.1 (8.2-17.9)	12.7 (9.2-25.2)	10.0 (7.3-15.0)	0.137
Lactate – mmol/L	1.5 (0.9-2.6)	1.7 (1.0-2.6)	1.5 (0.9-2.8)	0.955
PaO2/FiO2 – kPa	31.9 (23.1-43.0)	32.5 (24.6-42.7)	30.0 (21.7-43.8)	0.454
Hospital LoS pre-ICU	1.0 (1.0-3.0)	1.0 (1.0-1.5)	2 (1-3.3)	0.620
% loss of RF_{CSA} at day 10*	17.5 ± 13.3	17.3 ± 14.9	17.7 ± 12.2	0.937

Table 6-2. Clinical characteristics of MUSCLE-UK patients with serum and muscle tissue

Clinical data of patients with available serum samples for the current study. Of these patients, 10 NEC patients and 6 NONEC patients had available skeletal muscle samples in addition. *APACHEII; acute physiology and chronic health evaluation, SOFA; sequential organ failure assessment, CRP; C-reactive protein, WCC; white cell count, PaO2/FiO2; ratio of partial pressure of arterial oxygen to the fraction of inspired oxygen, LoS; length of stay, RF_{CSA}; rectus femoris cross-sectional area, NEC; underlying necrotic histology, NONEC; no features of necrosis on histology*. Data displayed as median (inter-quartile range) unless otherwise specified. *mean ± standard deviation.

In the present study, there were no differences in patient demographics or admission characteristics (Table 6-2). Of note, hospital length of stay before ICU admission was similar between groups (NEC: 1 day (IQR 1-3) vs. NONEC: 2 days (IQR 1-3), p=0.620). Admission CRP levels were lower in the NEC group but not statistically significant (95mg/L (IQR 10-180) vs. 120mg/L (IQR 36-213), p=0.701).

6.6.2 Prevalence of pMLKL in skeletal muscle during critical illness

I first studied tissue sections of all 20 previously determined necrotic patients in the MUSCLE-UK study to determine the prevalence of pMLKL in the sample cohort. Sections were cut at the time of the original study analysis and stored at -80^{o}C and were fixed in the current study after thawing. After antibody optimisation, I found 8/20 patients (40%) had clear evidence of interstitial pMLKL staining at T2 agreed by two raters independently – suggesting activation of programmed necrosis (Figure 6-2). Of the remaining 12 patients, 6/20 (30%) did not have visible interstitial pMLKL or had poor quality sections (due to cryodamage or cutting artifact), and 6/20 (30%) required further discussion between raters. Of these, only 2 had additional tissue sections for confirmatory analysis. Therefore, a total of 10 necrotic patients were studied for protein and IHC. Similarly, 6 NONEC patients with fixed tissue sections were also stained for pMLKL and all six sections did not show evidence of interstitial pMLKL – suggesting that the cell membrane was intact (Figure 6-3). One of the NEC patients with interstitial staining for pMLKL was selected as a positive control and for titration of antibody concentrations and protein loading in the Western blot experiments.

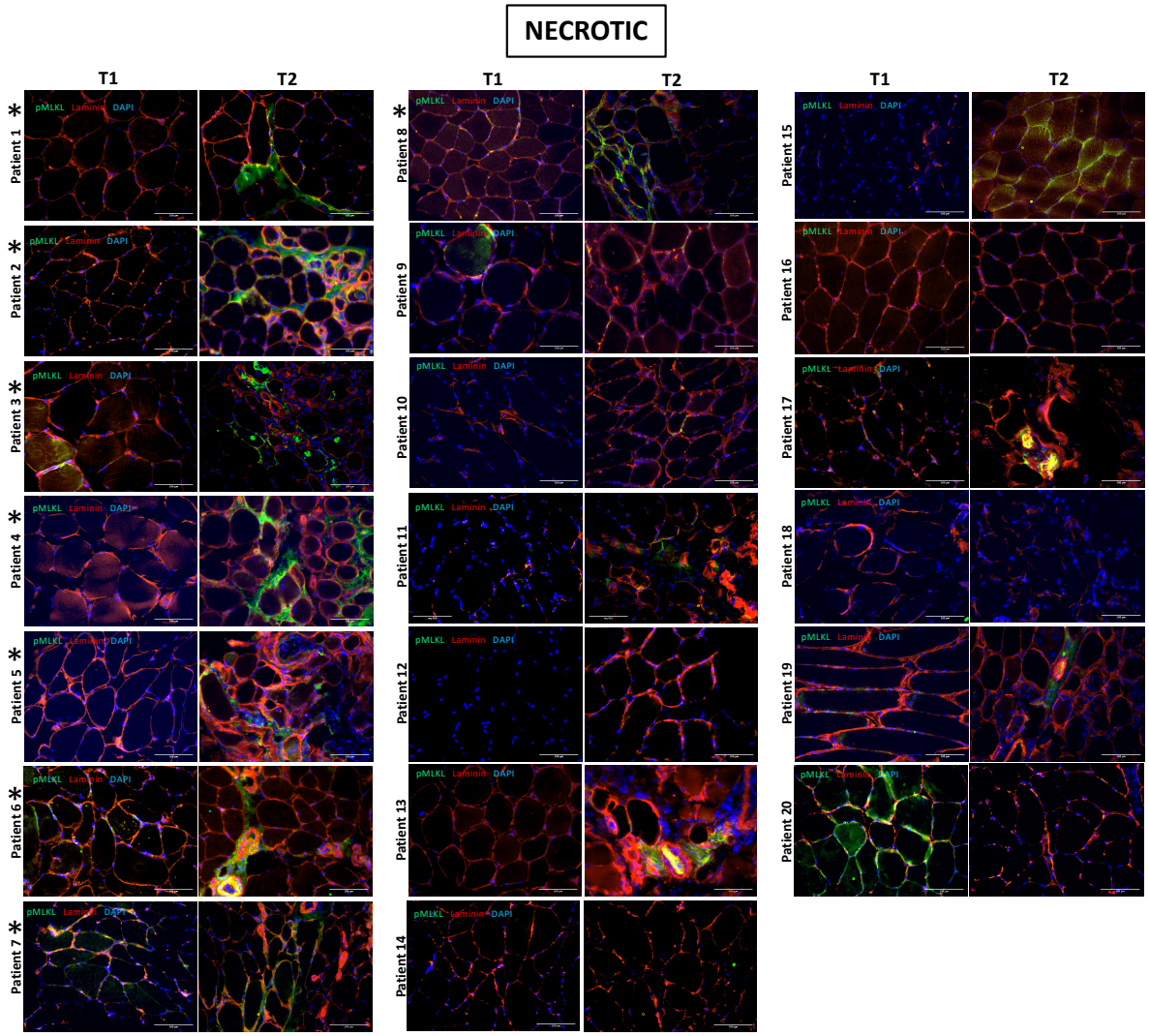


Figure 6-2. Prevalence of pMLKL in necrotic skeletal muscle during critical illness

Twenty patients from MUSCLE-UK study with skeletal muscle biopsies showing histological features of necrosis. Patients 1-8 have positive interstitial immunostaining for pMLKL at T2. Patients 9-20 did not show evidence of positive pMLKL immunostaining at T1 or T2. *T1 = day 1 of ICU admission, T2 = day 7-10 of ICU admission.* *=classified as positive pMLKL immunostaining.

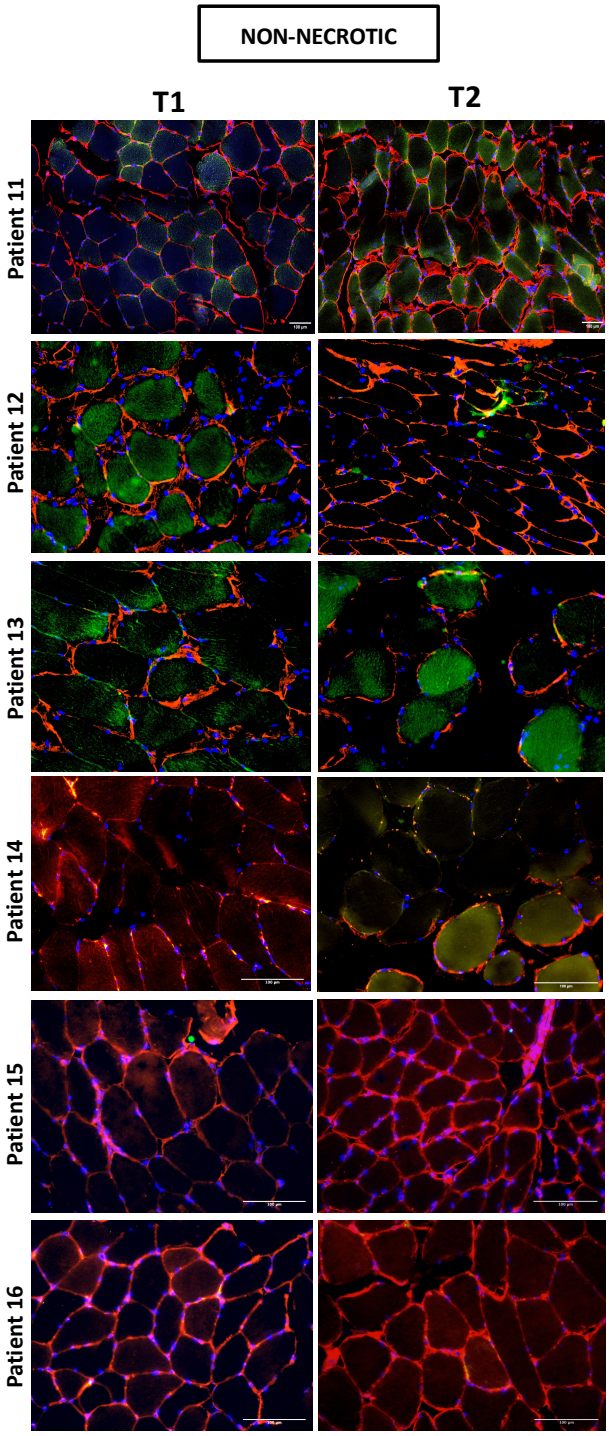


Figure 6-3. Prevalence of pMLKL in non-necrotic skeletal muscle during critical illness

Immunohistochemistry of skeletal muscle from 6 non-necrotic patients at T1 and T2. Widefield microscopy performed with single field of view and 20x magnification. There was no evidence of interstitial pMLKL in all 6 patients at T1 or T2. In two patients (Patient 13 and 14) there was cytoplasmic immunostaining for pMLKL. All scale bars represent 100μm. *T1 = day 1 of ICU admission, T2 = day 7-10 of ICU admission.*

6.6.3 Protein expression of pMLKL is upregulated in necrotic tissue

Western blotting for pMLKL for 16 patients (10 NEC, 6 NONEC) and 4 healthy volunteers was performed (Figure 6-4 and Figure 6-5). Overall, there was no difference in T1 expression (signal intensity) of pMLKL between NEC , NONEC and healthy volunteers (NEC: 0.14 (IQR 0.02-0.345); NONEC: 0.218 (IQR 0.06-0.420); HV: 0.256 (0.03-0.506), HV vs. NONEC; p=0.996, HV vs. NEC; p=0.999) At T2, pMLKL expression was higher in NEC patients compared to NONEC and HV but not statistically different (NEC: 0.481 (IQR 0.192-3.00); NONEC: 0.118 (IQR 0.05-0.430); HV: 0.256 (0.03-0.506), HV vs. NONEC; p=0.997, HV vs. NEC; p=0.160, NONEC vs. NEC; p=0.069).

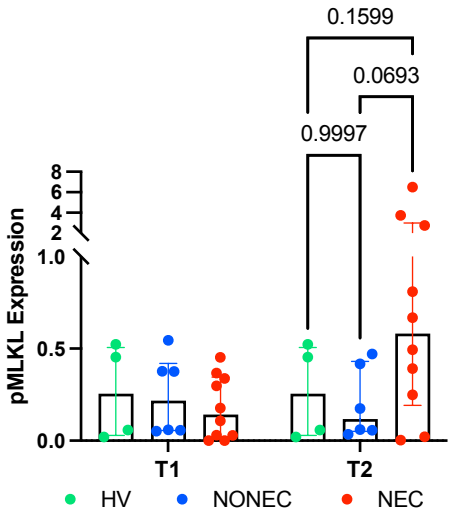


Figure 6-4. Expression of pMLKL in skeletal muscle of critically patients and healthy volunteers

Comparison of pMLKL expression in critically patients and healthy volunteers at baseline and for critically ill patients at day 7-10 of admission. *HV = healthy volunteer, NONEC = non-necrotic muscle, NEC = necrotic muscle. T1 = day 1 of ICU admission, T2 = day 7-10 of ICU admission.* Comparisons performed using Sidak's test for multiple comparisons.

In the NEC group, across all immunoblot experiments, there was a trend towards greater pMLKL expression at T2 (Figure 6-5). Two of the three sample pairs demonstrated between 7-37 fold increase in pMLKL expression at T2. The third pair, whilst pMLKL expression was evident, T2 expression (as

given by signal intensity) was lower than T1. This was later attributed to sample loading error and this patient was excluded from the subsequent analysis and repeated in subsequent experiments.

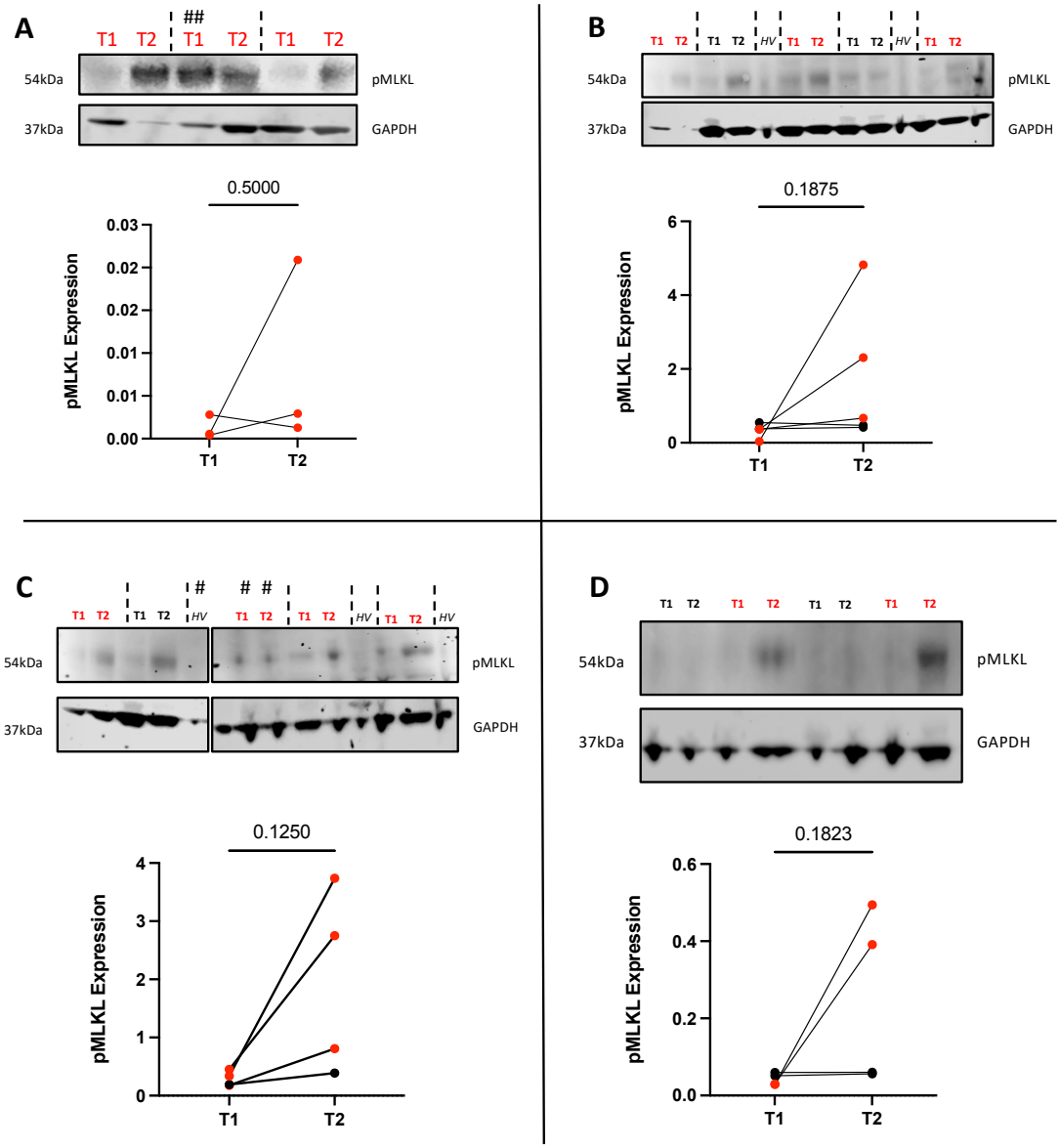


Figure 6-5. Western blotting of non-necrotic and necrotic human skeletal muscle

Four representative Western blots with corresponding quantitative analysis in the figure directly below each cropped blot. Red text and dots indicate samples from NEC patents, black dots represent NONEC patients. *HV=healthy volunteer.* (A) 3 NEC patients at day 1 (T1) and day 7 or 10 (T2). (B) 3 NEC, 3 NONEC patients. (C) 5 patients (4 NEC and 1 NONEC). (D) 2 NEC and 2 NONEC. Difference between T1 and T2 analysed using Mann-Whitney test. *Protein expression = signal intensity normalised to GAPDH. #Western blot data not included in analysis due to unreliable sample loading. ##T1 of a patient may be overly expressed due to sample loading error and was not included in subsequent analyses.*

Figure 6-6 summarises the change in pMLKL expression by necrotic state. There was a significant increase in pMLKL expression at T2 in NEC patients (T1: 0.142 IQR (0.022-0.345) vs. T2: 0.581 (0.192-2.999), p=0.041), but not in NONEC patients (T1: 0.218 (IQR 0.056-0.419) vs. T2: 0.118 (IQR 0.051-0.430), p=0.998). Using 2-way ANOVA to assess change between groups and time-points, NEC patients had significantly higher pMLKL expression at T2 (p=0.041).

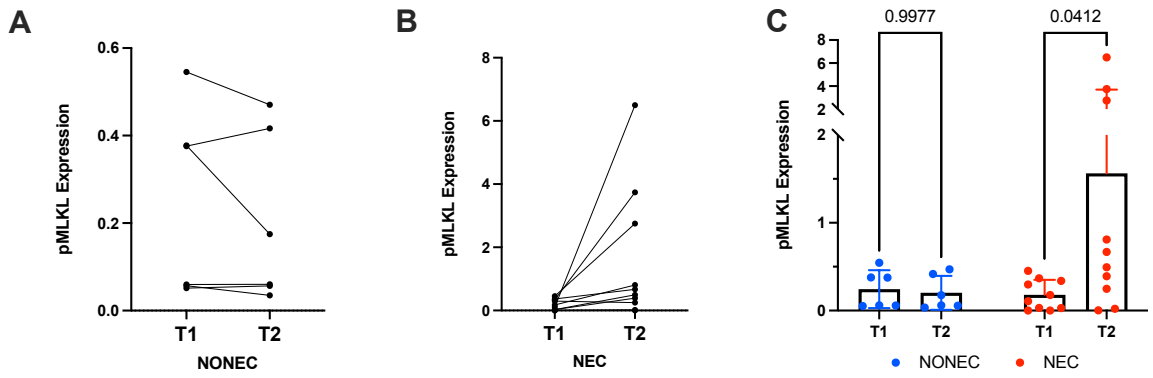


Figure 6-6. pMLKL changes between T1 and T2 in NEC and NONEC groups

(A) and (B) represent pairwise comparisons of patients in NONEC and NEC patients respectively. (C) comparison of NONEC and NEC groups. There is a significant increase in pMLKL expression in NEC patients but not in NONEC patients between T1 and T2 (p=0.041). Difference between T1 and T2 in (A) and (B) analysed using Mann-Whitney test. Differences between groups in (C) analysed using Sidak's multiple comparisons test.

Pooled signal intensity ratios demonstrated a significantly higher T2:T1 ratio of pMLKL protein expression in the NEC group compared to NONEC (NEC: 9.1 (3.9-22.3) vs. NONEC: 0.9 (0.6-1.1), p=0.003). The ratio of T2:T1 signal intensity was calculated by dividing the normalised signal intensity at T2 by the normalised signal intensity at T1 (Figure 6-7).

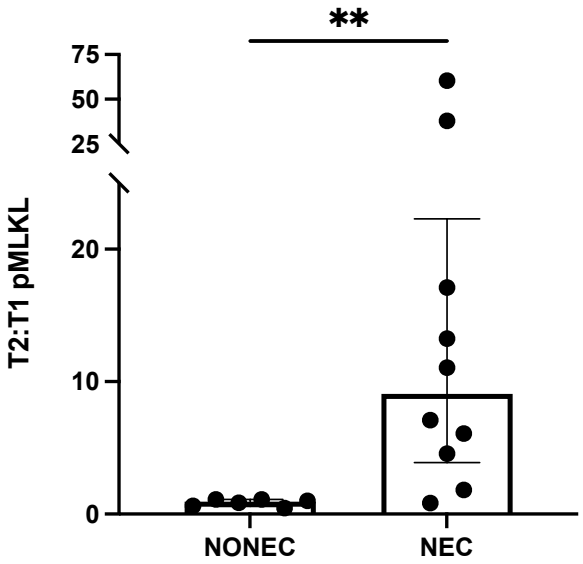


Figure 6-7. pMLKL expression compared to admission in non-necrotic and necrotic patients

Relative pMLKL expression at T2 was significantly higher in patients with underlying necrosis (NEC) when compared to T1 expression (T2:T1). Group comparisons performed using Mann-Whitney test. **p<0.01. *NEC; underlying necrotic histology, NONEC; no features of necrosis on histology*.

One NONEC patient consistently demonstrated positive signal intensity for pMLKL at T2 in three separate Western blot experiments (Figure 6-8). However, the mean fold change from T1 to T2 was 2.2 ± 1.2 (p=0.121) (n=3). This was further evaluated below using immunohistochemistry.

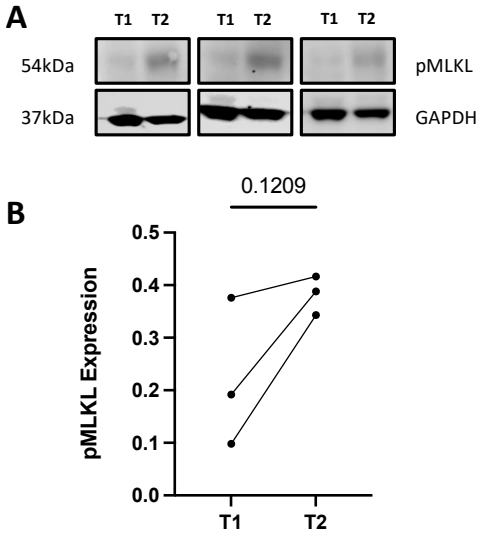


Figure 6-8. pMLKL expression in non-necrotic human skeletal muscle using Western blotting

Increased pMLKL expression at T2 in a patient without histological evidence of necrosis using H&E staining. Replicates are from three separate biopsy specimens and were immunoblotted separately (A) alongside other patient sample pairs. (B) corresponding quantitative analysis of immunoblots in (A). The T2:T1 expression ratio was 2.2 ± 1.2 (p=0.121) (n=3). Difference between T1 and T2 analysed using Mann-Whitney test.

6.6.4 Programmed necrosis immunohistochemistry of healthy skeletal muscle

Skeletal muscle of the four healthy volunteers in Western blotting experiments were further evaluated using immunohistochemistry to determine whether pMLKL is present in health and in the absence of critical illness. In all four healthy volunteers, sarcolemma integrity was well defined and maintained with no evidence of sarcoplasmic or interstitial immunostaining for pMLKL (Figure 6-9, Appendix **9**-**23**). These findings are consistent with the absence of pMLKL protein expression seen using Western blotting.

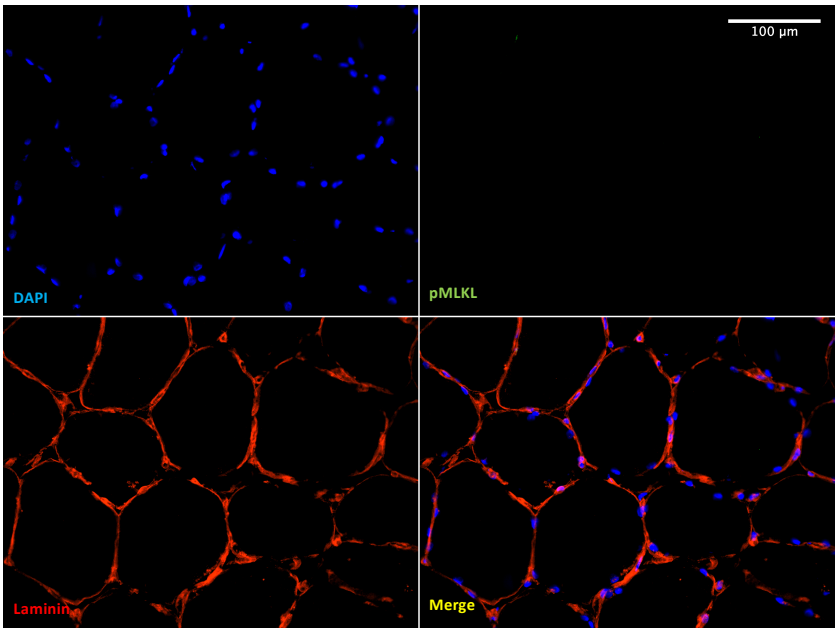


Figure 6-9. Immunohistochemistry of pMLKL expression in healthy human skeletal muscle

Immunohistochemistry of healthy human skeletal muscle from a healthy volunteer. Single field of view using widefield microscope taken at 20x magnification. The section demonstrates an absence of pMLKL staining, and preserved myofibre morphology including myofibre diameter and intact cell membrane (sarcolemma). The merged image is shown in the bottom right. 20x magnification.

6.6.4.1 Absence of pMLKL in non-necrotic skeletal muscle during critical illness

I then studied whether pMLKL was present in the NONEC cohort using immunohistochemistry. Six muscle biopsy samples were processed and stained for immunostaining as described in 2.4.4 . In all 6 patients, there was an absence of interstitial pMLKL at T1 and T2 (Figure 6-10) suggesting an absence of myofibre lysis and preserved sarcolemma integrity.

To ensure that the region of interest did not exclude more focal areas of pMLKL, I used wide-field and spinning disc microscopy to confirm the absence of pMLKL in the entire section (Figure 6-11). In the spinning disc images, pMLKL remained absent. In one NONEC patient, Western blot experiments demonstrated positive bands at day 7 for pMLKL (Figure 6-8). T1 fluorescence microscopy imaging of this patient demonstrated no pMLKL. However, at T2, there was possible evidence of pMLKL within

the sarcoplasm. This may suggest the possibility of late-onset necroptosis activation. Despite evidence of morphological myofibrillar disruption in terms of circular fibres and disruption to the connective tissue, there was no evidence of sarcolemma rupture, interstitial pMLKL staining or infiltration of nuclei into the muscle tissue.

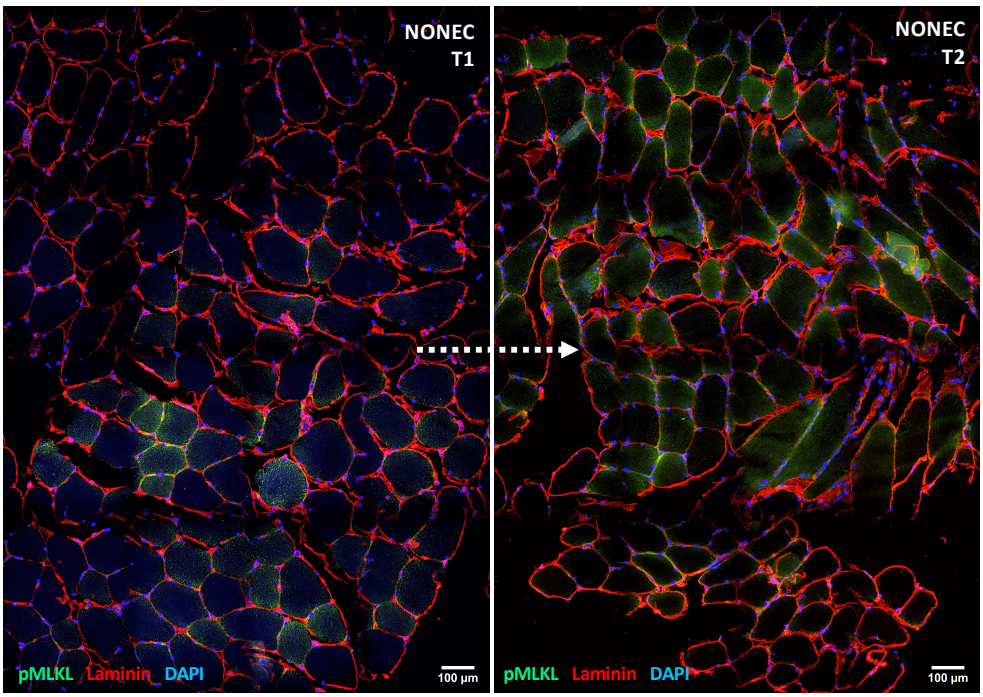


Figure 6-10. Immunohistochemistry of non-necrotic skeletal muscle

Immunohistochemistry of non-necrotic skeletal muscle during critical illness. Stitched image of multiple fields of view using spinning disc confocal microscopy at 40x magnification. At T1, there is well defined sarcolemma with absence of cytoplasmic and interstitial staining. At T2, whilst there is distortion of the sarcolemma, there is no evidence of interstitial pMLKL and therefore no evidence to suggest necrolysis has taken place.

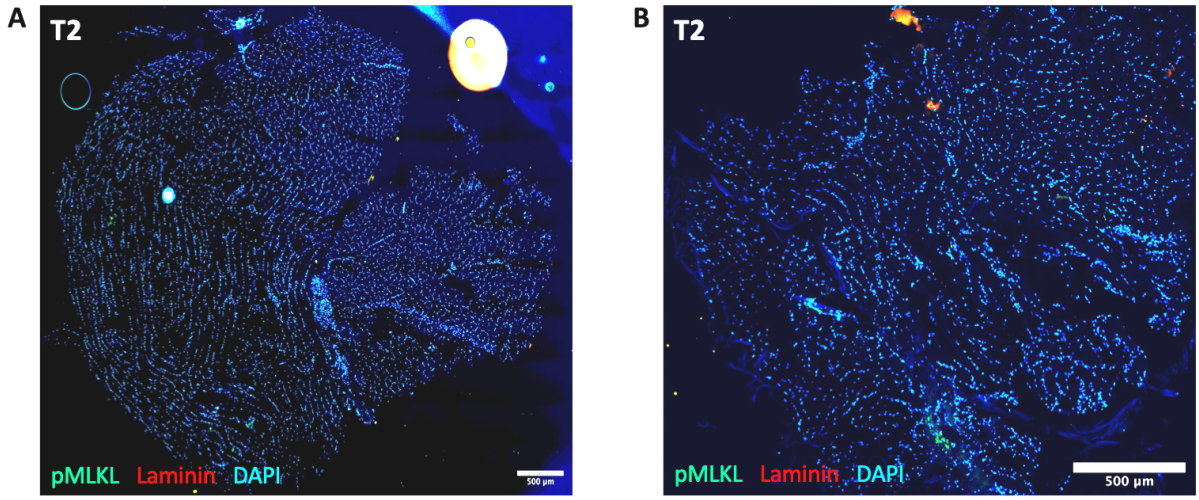


Figure 6-11. Spinning disc microscopy of non-necrotic skeletal muscle at day 7

Stitched image of multiple fields of view on a widefield microscope taken at 20x magnification. (A) and (B) represent wide field spinning disc microscopy of skeletal muscle at T2 in two different patients with non-necrotic muscle. The entire section of muscle has been included in each example. There is no clear evidence of pMLKL staining either focally or irregularly distributed throughout the section.

6.6.5 Upregulation of pMLKL in necrotic skeletal muscle during critical illness

To corroborate the significant increase in pMLKL expression at T2 from Western blot experiments, histological sections of corresponding skeletal muscle were studied using fluorescence microscopy. In all 10 NEC patients there was no evidence of interstitial pMLKL at T1 to suggest necrolysis had taken place at ICU admission (Figure 6-3). However, at T2, in the NEC group, interstitial pMLKL was evident in 8/10 patients, suggesting necrolysis has taken place (Figure 6-12, Figure 6-13).

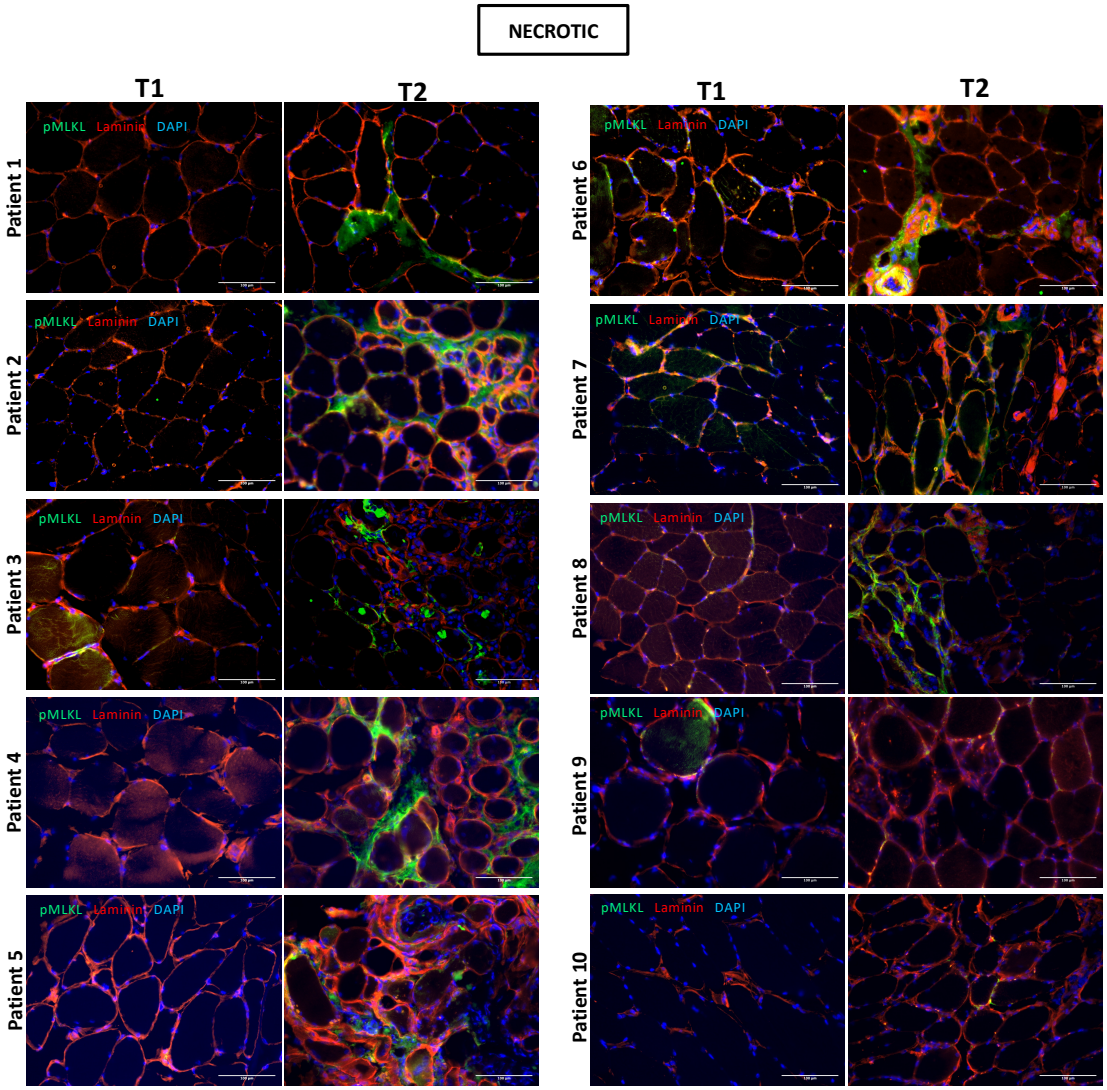


Figure 6-12. pMLKL expression in necrotic human skeletal muscle during critical illness

Immunohistochemistry of 10 NEC patients at T1 and T2. There is marked interstitial pMLKL at T2 in 8/10 patients. There is no evidence of pMLKL in two patients (Patient 9 and 10) despite morphological distortion at T2. All images are single field of view taken on a widefield microscope at 20x magnification. Scale bars represent 100μm.

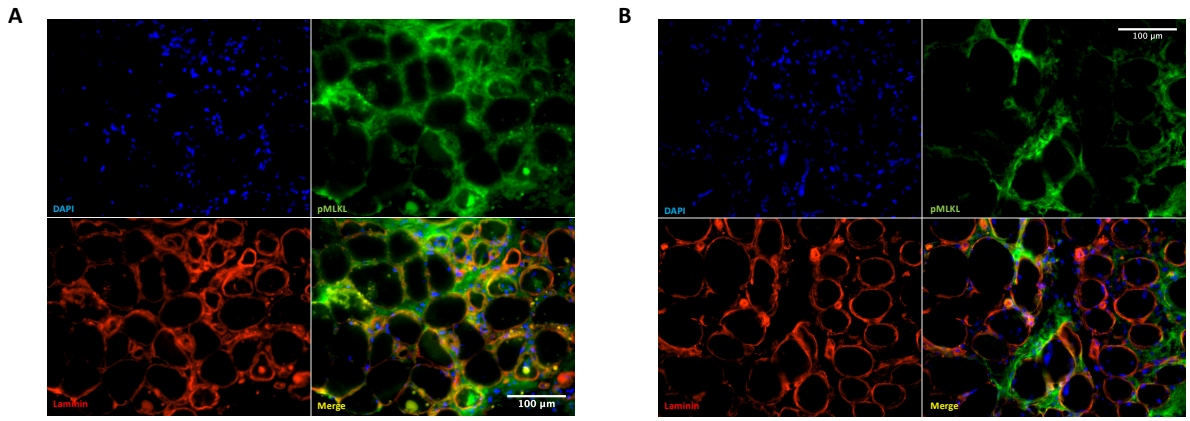


Figure 6-13. Presence of pMLKL in human skeletal muscle during critical illness

Immunohistochemistry of human skeletal muscle at T2 in two different patients, A and B. Strongly positive interstitial pMLKL immunostaining was seen with fluorescent microscopy with a multifocal distribution both patients. Microscopy performed using widefield with 20x magnification.

6.6.5.1 Distribution of pMLKL in necrotic muscle

In the NEC patients, it was noted that from the panel of captured images (minimum 10 regions of interest per sample) that interstitial pMLKL staining was multi-focal and non-homogenous (Figure 6-14). Therefore, I used wide-field and spinning disc confocal microscopy to further study the distribution of pMLKL within the section. pMLKL was confirmed in wide-field microscopy to adopt a multi-focal distribution throughout the section (Figure 6-16, Figure 6-17).

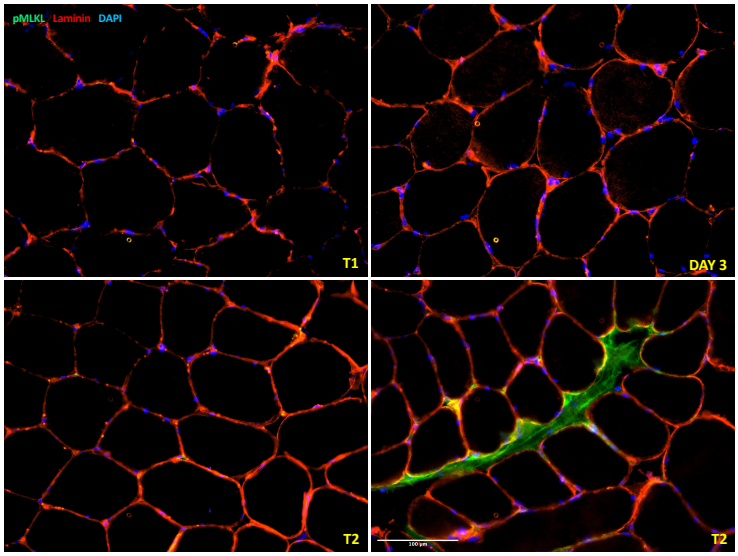


Figure 6-14. Distribution of pMLKL within necrotic skeletal muscle

Skeletal muscle immunohistochemistry of human skeletal muscle during critical illness in a single patient. Each image is a single field of view taken on a wide field microscope at 20x magnification. Each image displayed as merged images of DAPI, laminin and pMLKL. There is an absence of pMLKL staining at T1 and day 3 (across all 10 captured images). At T2, there is patchy, focal areas of pMLKL staining that was detected in some regions of interest (bottom right) but not in others (bottom left). Scale bars represent 100μm.

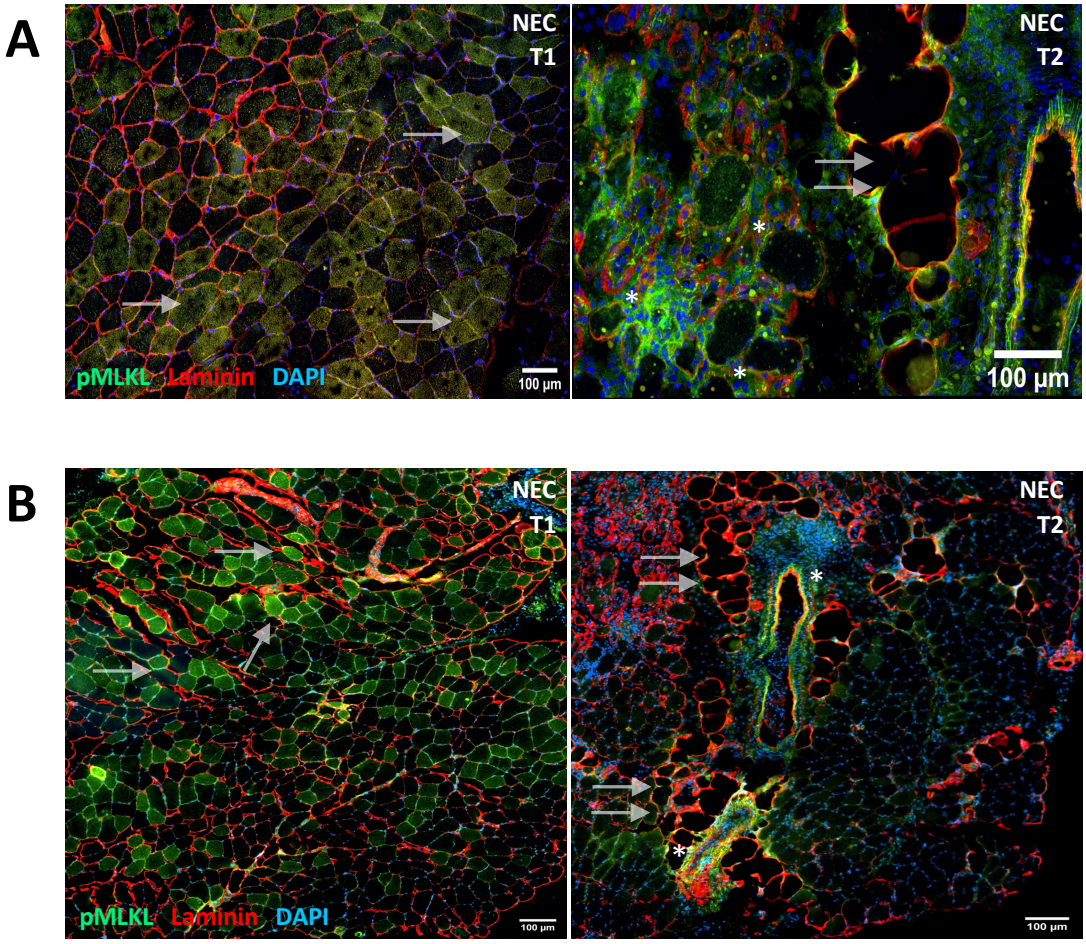


Figure 6-15. Multi-focal pMLKL in necrotic skeletal muscle

pMLKL distribution in necrotic skeletal muscle during critical illness. (A) widefield microscopy of a NEC patient and stained for pMLKL. There is patchy sarcoplasmic pMLKL staining with some localisation seen at the cell membrane (single solid arrow). At T2, there is evidence of interstitial staining indicating cell lysis (indicated by *) and morphological distortion (double arrow). (B) confocal microscopy of a second NEC patient showing the localisation of pMLKL in the sarcoplasm and sarcolemma at T1 (single arrow) and later in the interstitium at T2 (indicated by *). Each image is a stitched image of multiple fields of view taken on a wide field microscope at 20x magnification.

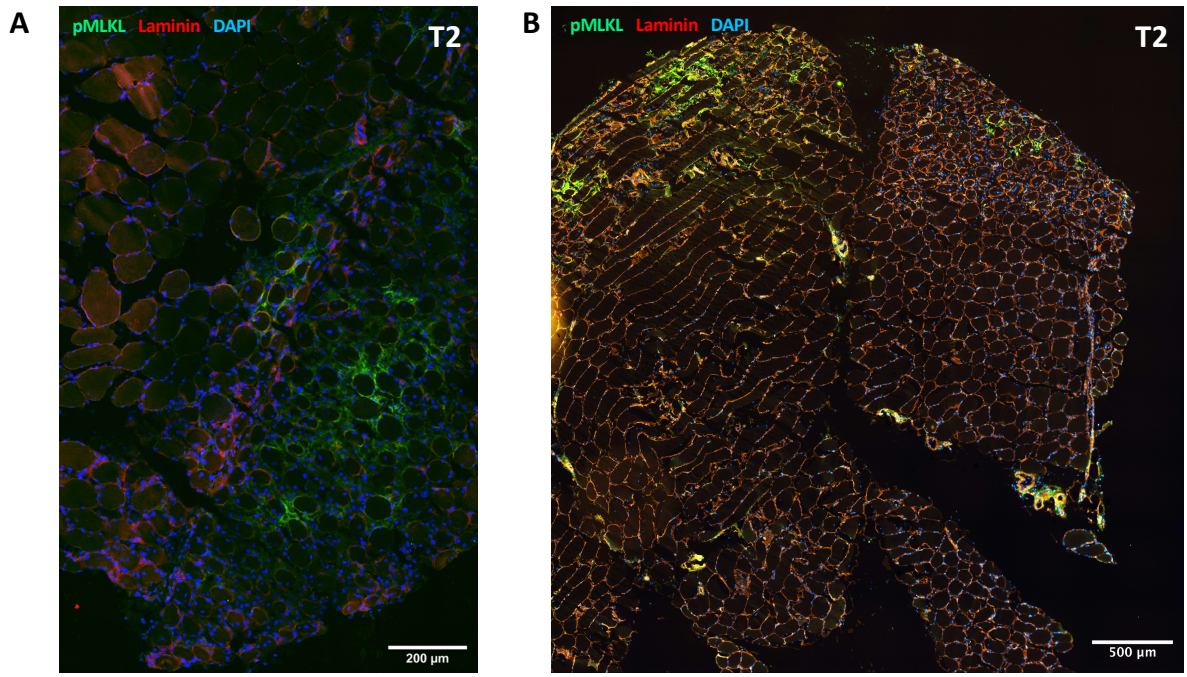


Figure 6-16. Distribution of pMLKL in necrotic skeletal muscle.

Immunohistochemistry of human skeletal muscle in two different NEC patients taken at T2. Interstitial pMLKL staining is patchy and multi-focal. Stitched images of multiple fields of view taken on a spinning disc confocal microscope at 40x magnification. Scale bars shown in bottom right of each image.

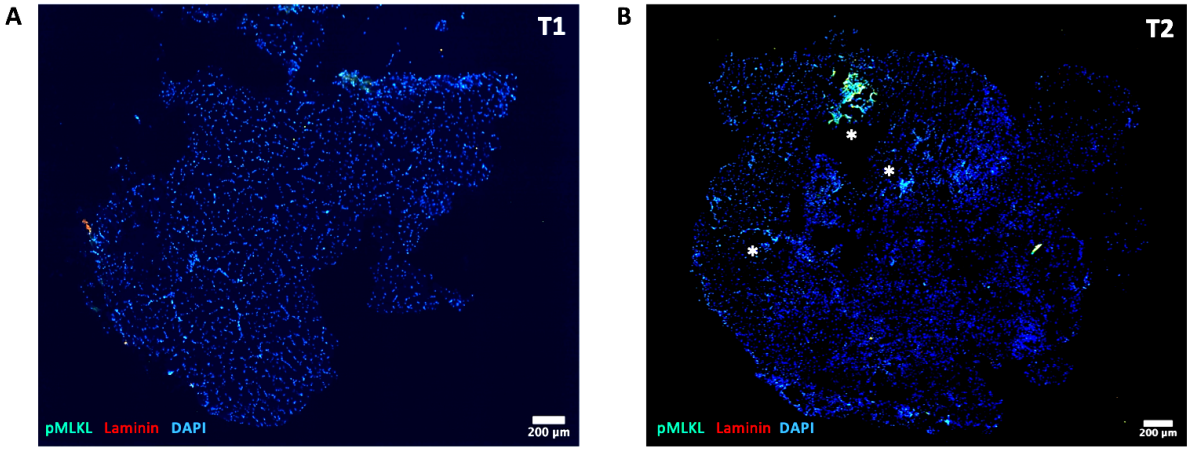


Figure 6-17. Wide field microscopy of necrotic human skeletal muscle during critical illness.

Skeletal muscle immunohistochemistry demonstrating absence of pMLKL at T1. However, at T2 there are multi-focal areas of skeletal muscle with positive for pMLKL (indicated by *). Stitched images of multiple fields of view taken on a spinning disc confocal microscope at 20x magnification. Scale bars shown in bottom right of each image.

6.6.5.2 Translocation of pMLKL during critical illness

In two NEC patients, additional day 3 muscle biopsies were available to study the translocation of pMLKL. In both biopsy series, confocal microscopy demonstrated that at T1, pMLKL appears to be predominantly based within the sarcoplasm. Conversely, at T2 there is marked interstitial pMLKL suggesting necrolysis of the myofibre. Between these two time points, at day 3, pMLKL is again present in the cytoplasm but there appeared to be an increased concentration of sarcolemma bound pMLKL (Figure 6-18).

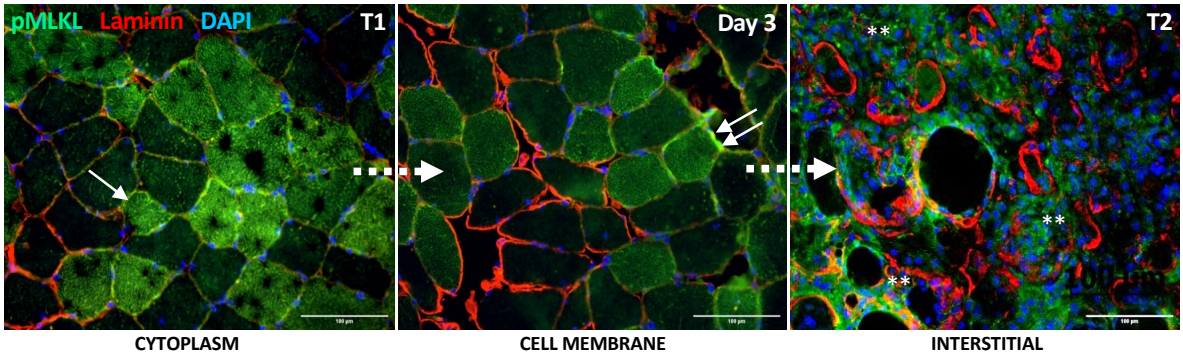


Figure 6-18. Translocation of pMLKL in human skeletal muscle during critical illness.

At T1, pMLKL is concentrated within the cytoplasm (single white arrow), moving towards the cell membrane at day 3 (double white arrow). At T2, there is marked interstitial pMLKL (**) suggesting myofibre necrolysis. Each image is a single field of view taken on a wide field microscope at 20x magnification.

6.6.5.3 RIPK3 co-localises with pMLKL in necrotic muscle

To support the findings of the translocation of pMLKL, I sought to determine if pMLKL was co-localising with RIPK3 within the muscle fibre. Due to both primary antibodies sharing the same host species, co-localisation analysis was performed on serial sections with the same myofibres identified visually using local landmarks and fibre morphology identified via laminin immunostaining. Myofibres expressing pMLKL were found to have co-localised RIPK3 that followed a similar cytoplasmic to membrane to interstitium translocation as pMLKL in NEC but not in NONEC (Figure 6-19).

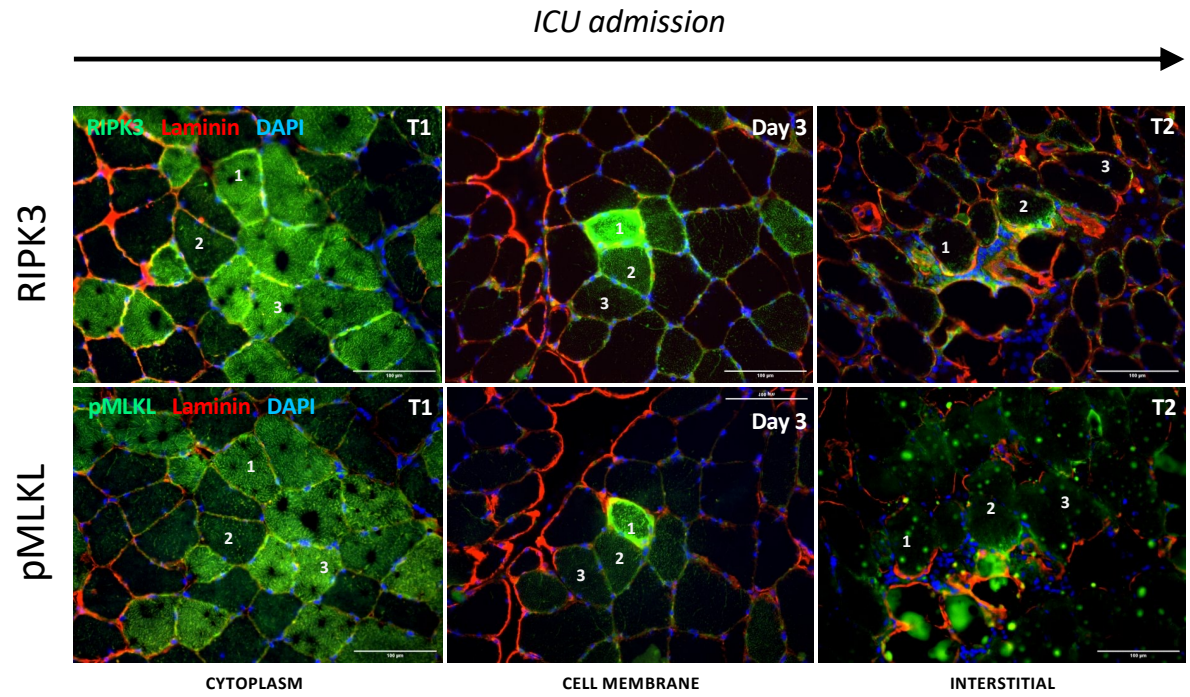


Figure 6-19. Co-localisation of RIPK3 and pMLKL in necrotic human skeletal muscle.

Co-localisation of RIPK3 and pMLKL during critical illness associated muscle wasting. The top row of images represents admission (T1), day 3 and day 7-10 (T2) skeletal muscle of a NEC patient and immunostained for RIPK3. The bottom row of images represents admission (T1), day 3 and day 7-10 (T2) skeletal muscle of a NEC patient and stained for pMLKL. Individual muscle myofibres have been labelled (1,2,3) for direct comparison between antibody staining. Each image is a single field of view taken on a wide field microscope at 20x magnification. All scale bars shown represent 100µm.

6.6.6 Systemic inflammation as predictors of myonecrosis

Given the prevalence of pMLKL in necrotic skeletal muscle and suggestion of necroptosis activation, I sought to determine whether circulating inflammatory cytokines and markers of necrosis can differentiate distinct 'inflammatory phenotypes'. Serum and intramuscular concentrations of 8 analytes (IL-1β, IL-6, IL-8, IL-10, IFN-γ, TNF-α, TNFR1 and VEGF) were reproduced with permission (Appendix **9**-**1**).

6.6.6.1 Serum cytokines do not reliably predict underlying myonecrosis

At baseline (T1), concentrations of IL-1β, IL-6, IL-8, IL-10, TNF-α, TNFR1 and IFN-γ were not significantly different between NONEC and NEC groups (Figure 6-20). Levels of VEGF were significantly higher in NEC patients at T1 (NONEC: 68.7ng/L (IQR 26.3-104.8) vs. NEC: 135.0ng/L (IQR 96.1-193.7), p=0.002).

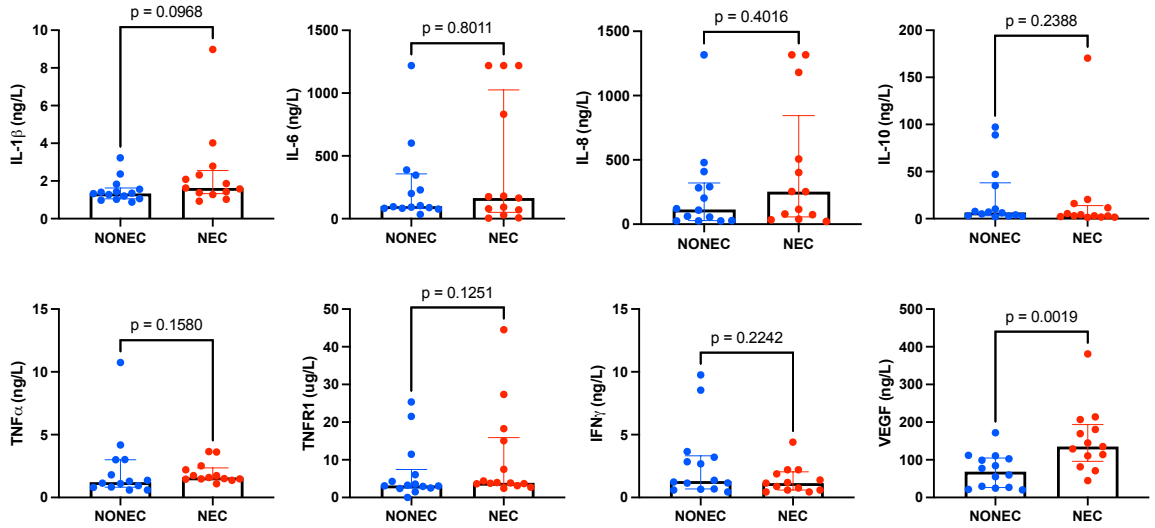


Figure 6-20. Baseline levels of systemic cytokines in non-necrotic and necrotic patients

Comparison of serum concentration of inflammatory mediators in patients with myonecrosis (NEC) and without myonecrosis (NONEC) at baseline (T1). Differences between groups analysed using Mann-Whitney test.

In the NONEC patients, there was no difference in IL-1β, IL-6, IL-8, IL-10, IFN-γ, TNF-α, and TNFR1 concentration between T1 and T2 (Figure 6-21). However, there was a significantly higher concentration of VEGF at T2 (T1: 84.3ng/L (IQR 25.8-111.3) vs. T2: 209.4ng/L (IQR 130.5-305.9, p=0.008) (Figure 6-21, Appendix **9**-**24**).

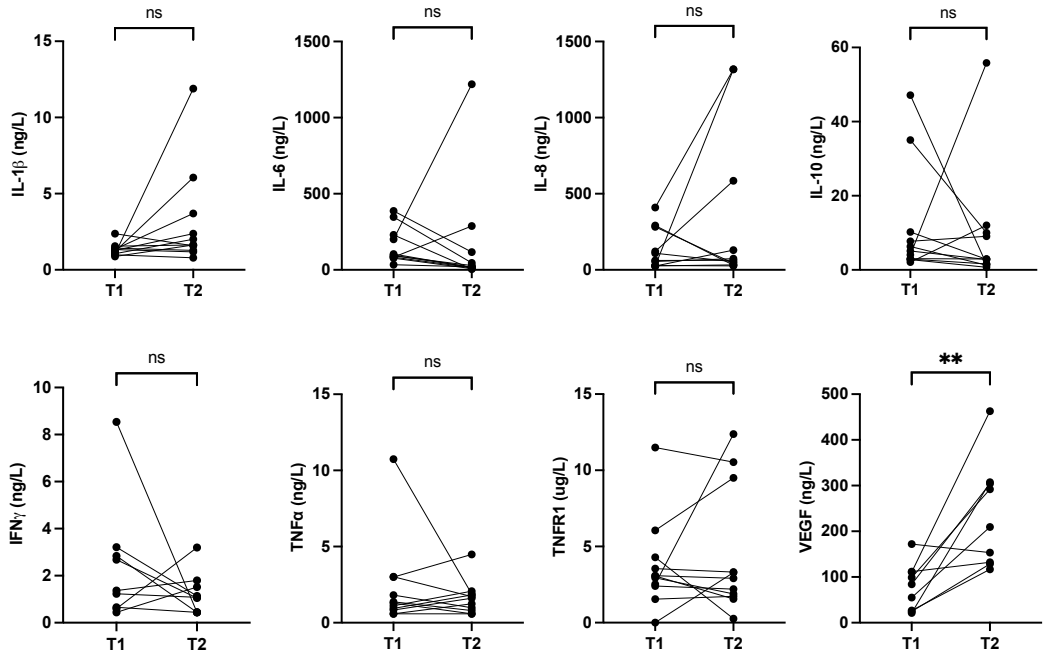


Figure 6-21. Systemic inflammatory mediators in non-necrotic patients.

Serum concentrations of inflammatory mediators at day 1 (T1) and day 7-10 (T2) in patients without histological evidence of myonecrosis at T2 (NONEC). Differences between groups analysed using Mann-Whitney test. ** p<0.01.

In NEC patients, there were significantly higher concentrations of IL-1β, IL-6, IL-8 and Il-10 at T1 compared to T2 (Appendix **9**-**24**) suggesting a greater degree of inflammation in patients with eventual myonecrosis. Concentration of VEGF was significantly higher at T2 (140.0 (IQR 111.5-200.3) vs. 233.6 ng/L (IQR 150.6-469.1) , p=0.0005) in NEC patients.

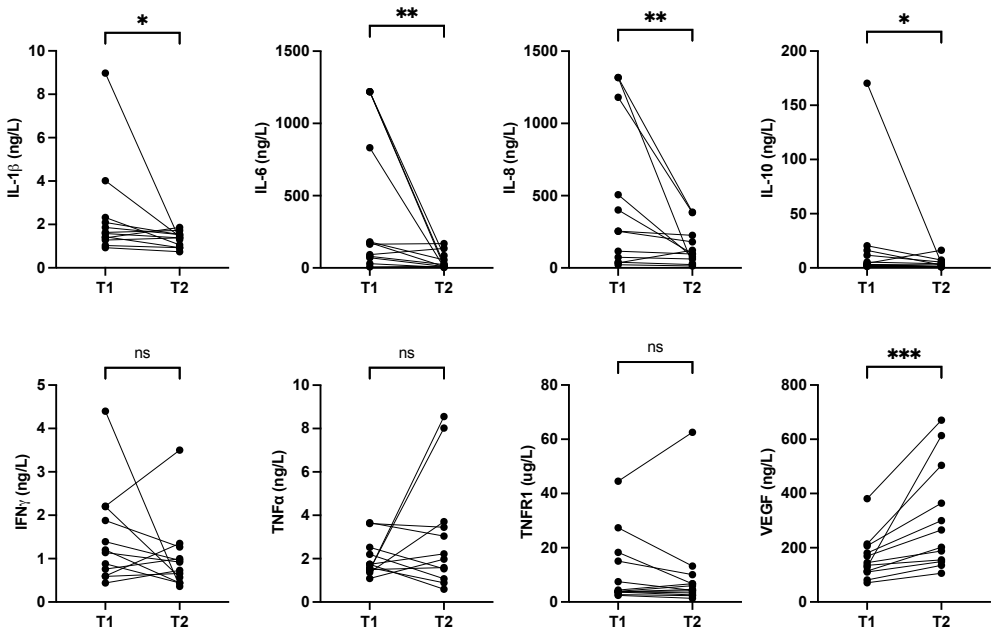


Figure 6-22. Systemic inflammatory mediators in necrotic patients.

Serum concentrations of inflammatory mediators at day 1 (T1) and day 7-10 (T2) in patients with histological evidence of myonecrosis at T2 (NEC). Differences between groups analysed using Mann-Whitney test. * p<0.05, ** p<0.01, *** p<0.001, ns = p>0.05.

6.6.7 Intramuscular inflammatory mediators do not differentiate underlying myonecrosis

Intramuscular concentrations of the same 8 inflammatory mediators were then studied. At baseline, there was no significant difference in baseline concentration of IL-1β, IL-6, IL-8, IL-10, IFN-γ, TNFR1 and VEGF between NONEC and NEC groups (Figure 6-23). Intramuscular concentration of TNFα was higher at T1 in NONEC patients when compared to NEC patients (NONEC: 32.0ng/L (IQR 16.7-68.3) vs. NEC: 20.8ng/L (IQR 0.6-23.4), p=0.039).

In the NONEC group, there was no significant differences between the concentrations at T1 and T2 (Figure 6-24). In the NEC group, T2 concentrations of TNFR1 were significantly higher compared to T1 (T1: 0.3 (IQR 0.0-0.7) vs. T2: 1.5 μg/L (IQR 0.1-3.3), p=0.048) (Figure 6-25). The remaining 7 analytes did not show any significant changes between T1 and T2.

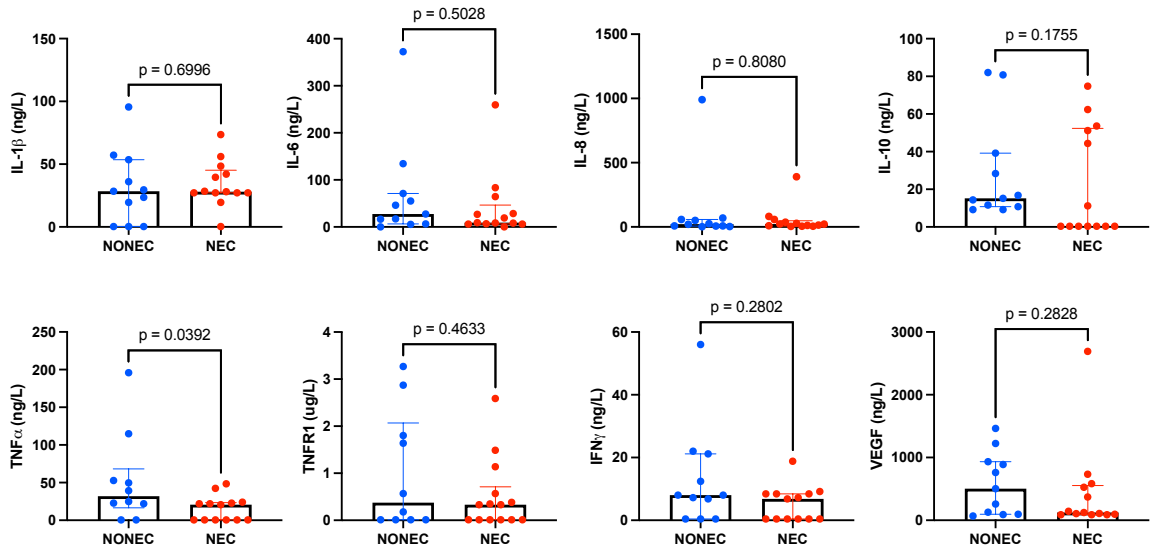


Figure 6-23. Baseline levels of intramuscular cytokines in non-necrotic and necrotic patients

Comparison of intramuscular concentration of inflammatory mediators in patients with myonecrosis (NEC) and without myonecrosis (NONEC) at baseline (T1). Differences between groups analysed using Mann-Whitney test.

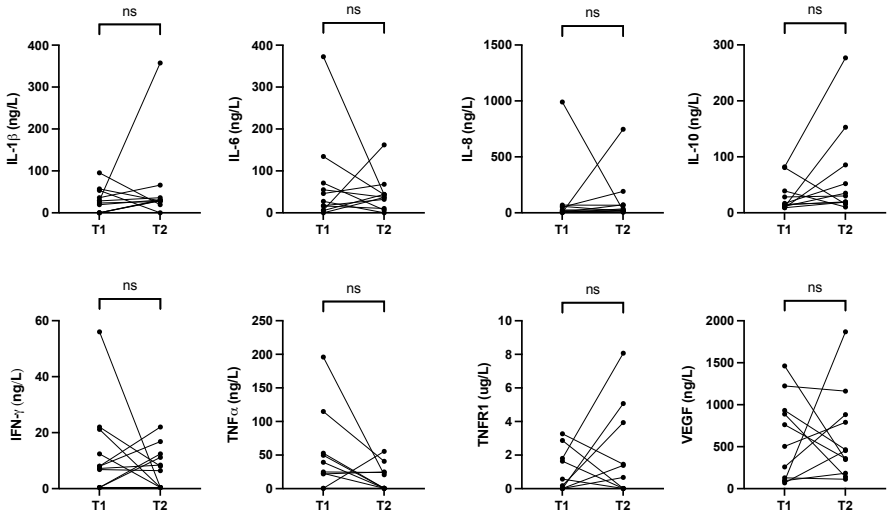


Figure 6-24. Intramuscular concentration of inflammatory cytokines in non-necrotic muscle.

Intramuscular inflammatory mediators at day 1 (T1) and day 7-10 (T2) in patients without histological evidence of myonecrosis at T2. ns = not statistically different. Differences between groups analysed using Mann-Whitney test.

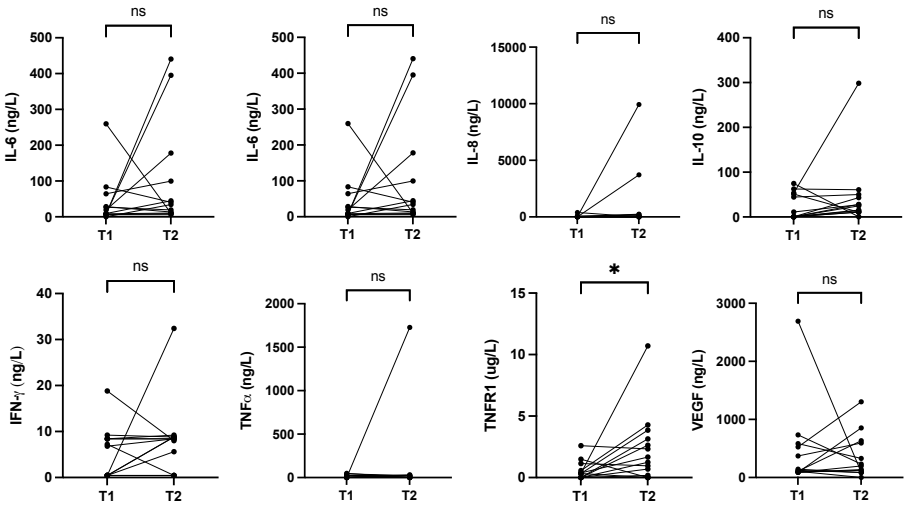


Figure 6-25. Intramuscular concentration of inflammatory cytokines in necrotic muscle.

Intramuscular inflammatory mediators at day 1 (T1) and day 7-10 (T2) in patients with histological evidence of myonecrosis at T2. ns = not statistically different, *p<0.05. Differences between groups analysed using Mann-Whitney test.

6.6.7.1 Systemic markers of necrosis do not differentiate patients with myonecrosis

Given the suggestion that necroptosis is activated in myonecrosis during critical illness I studied serum concentration of RIPK3 and cleaved cytokeratin 18 (CCK18) as systemic markers of necrosis using standalone ELISA. Levels of TNFR1, the most common implicated death receptor, were obtained on fresh ELISA assays. In addition, day 3 and day 10 samples for some patients were made available to illustrate early and longitudinal changes over the ICU admission.

Baseline levels of RIPK3 were lower in the NEC group but not statistically significant (Table 6-3). At day 3, 7 and 10, levels of RIPK3 were higher in the NEC group but not statistically different at T1 (NEC: 2215.9 pg/ml (IQR 798.11-9367.9) vs NONEC: 4434.0 pg/ml (IQR 2293.7-6658.4), p=0.511) or at T2 (NEC: 5004.28 pg/ml (IQR 2673.4-16881.9) vs. NONEC: 3546.0 pg/ml (IQR 2037.3-13827.0, p=0.401). In addition, CCK-18 levels were not significantly different between groups at T1 (NEC: 535.3 IU/L (IQR 268.2-768.1) vs. NONEC: 576.1 IU/L (IQR 226.0-1566.5), p>0.05) or at T2 (NEC: 537.7 IU/L (IQR 316.8-906.0) vs. NONEC: 858.3 IU/L (IQR 310.8-2096.8), p=0.511). Longitudinally, levels of TNFR1, RIPK3 and

CCK18 were not different between NEC and NONEC patients at any timepoint (Figure 6-26). Overall, systemic markers of necrosis could not differentiate patients with and without underlying myonecrosis.

Analyte	Myonecrosis (n=14)	No myonecrosis (n=14)	P value
TNFR1			
Day 1	3.4 (2.0-12.0)	1.9 (1.1-5.9)	0.104
Day 3	4.0 (2.7-13.19	1.9 (1.3-4.8)	0.068
Day 7	3.5 (2.1-6.3)	2.2 (2.0-7.0)	0.540
Day 10	3.3 (2.3-5.6)	2.0 (1.6-6.1)	0.238
RIPK3			
Day 1	2215.9 (798.1-7367.9)	4434.0 (2293.7-6658.4)	0.511
Day 3	7603.6 (2120.0-12860.8)	2419.8 (1429.9-5797.4)	0.161
Day 7	5004.3 (2673.4-16881.9)	3546.0 (2037.3-13827.0)	0.401
Day 10	6636 (3694.6-12676.5)	2421.9 (580.0-7961.6)	0.131
CCK-18			
Day 1	535.3 (268.2-768.1)	576.1 (226.0-1566.5)	0.999
Day 3	775.4 (178.1-2138.2)	451.9 (256.8-505.8)	0.682
Day 7	537.7 (316.8-905.1)	858.3 (310.8-2096.8)	0.511
Day 10	350.0 (180.2-1024.5)	380.8 (272.9-1493.7)	0.305

Table 6-3. Systemic markers of necrosis in non-necrotic and necrotic patients.

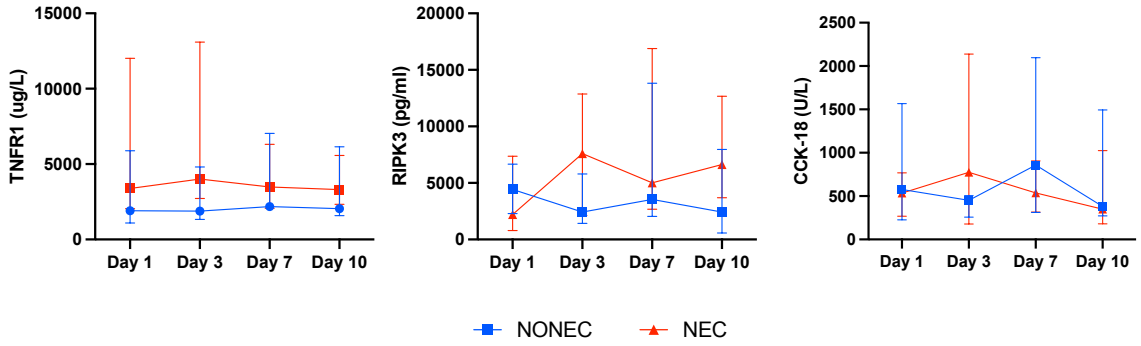


Figure 6-26. Systemic markers of necrosis in non-necrotic and necrotic patients

Serum levels of TNFR1, RIPK3 and CCK18 in patients with myonecrosis (NEC) and without myonecrosis (NONEC). There were no significant differences between day of ICU admission and concentration of systemic necrosis analyte. Columns and error bars displayed as median and IQR respectively. Comparisons between groups and time-points analysed using Sidak's multiple comparisons test.

6.7 Discussion

The data presented in this chapter show for the first time in man that necroptosis machinery is upregulated in critical illness-associated skeletal muscle wasting and myonecrosis. In some patients with pre-determined necrotic features, there is significantly higher expression of the terminal effector protein pMLKL in early critical illness compared to those without necrotic features. I corroborated this finding by localising pMLKL in myofibres in NEC patients but not in NONEC patients. I could not determine significant associations between the presence of myonecrosis and systemic mediators of inflammation and necrosis.

The identification of pMLKL in skeletal muscle tissue does provide a degree of mechanistic specificity regardless of the underlying myopathy appearances. However, to further confirm the biological nature of necroptosis activation in skeletal muscle, I also show the co-localisation of pMLKL within RIPK3 positive myofibres. This supports formation of the necrosome complex,[299,300] but also the progressive movement in early critical illness of RIPK3 and pMLKL expression from the intracellular compartment to cell membrane and extracellular compartments and gives some indication of the time-course of necroptosis in acutely inflamed human muscle. However, the possibility of RIPK3 and pMLKL originating from cellular interstitial infiltrate rather than from myofibre lysis also needs further exploration. Pin-pointing the exact timing of cell lysis through daily or more frequent muscle biopsies in critically ill patients carries significant risk and unlikely to be supported from an ethical perspective. Further mechanistic data has suggested that phosphorylation of MLKL in the absence of RIPK3 is also sufficient to activate necroptosis[301] and cytosolic necrosome formation can indirectly activate necroptosis after phosphorylation of MLKL.[302] Thus, identification of pMLKL seems the more reliable marker of necroptosis activation. Currently, RIPK3 and pMLKL remain the most commonly utilised markers of necroptosis in a variety of non-critical illness states including non-alcoholic steatohepatitis, pancreatitis, multiple sclerosis and ischaemia-reperfusion injury.[298]

I utilised semi-quantitative methods to detect pMLKL and whilst detection of the necrosome by techniques such as co-immunoprecipitation may provide further evidence of oligomer formation as the complex expands,[224,297] such quantification of the necrosome is currently challenging with respect to quantification of the protein of interest .[303] Phosphorylation of MLKL leading to oligomerisation is another well described terminal stage of necroptosis.[304] In our Western blot data, I did not detect significant protein bands at high molecular weight that would suggest pMLKL oligomerisation. However, there is a degree of equipoise surrounding optimum oligomer size in activated necroptosis.[297]

Immunohistochemistry in NEC patients showed multi-focal, non-homogenous distribution of pMLKL. It has been shown that heterogenous pro-inflammatory infiltrates of macrophage origin exist in histological specimens of critical illness myopathy[14] but it is unclear as to which inflammatory mechanisms lead to necrotising myopathy,[199] or whether different descriptions are simply earlier manifestations of a common pathway leading to necrosis. Hund and Latronico *et al.,* describe three distinct histological entities of myopathy during critical illness.[200,201] In addition to acute necrotising myopathy, myopathy with selective loss of myosin filaments and critical illness myopathy (CIM) have different biochemical and physiological characteristics. For example, in CIM, whilst there is muscle fibre atrophy and variation in fibre size, there can be single fibre necrosis and fatty degeneration of fibres. What is notable in this sub-type, is that inflammatory changes are often absent.[200] Necrotising myopathy has more prominent features of necrosis with vacuolisation and phagocytosis of fibres. Myopathy with selective loss of myosin filaments is rare and often associated with corticosteroid use with or without neuromuscular blockade and this may ultimately progress to more familiar necrotising myopathy. However, the chronology of this process is poorly understood and warrants further research.

Minimising risk factors for critical illness induced muscle wasting do not seem to prevent its onset and is often not possible. For example, critically ill patients requiring mechanical ventilation often need high levels of sedation with or without neuromuscular blockade and thus have little potential for passive or active rehabilitation or trials of spontaneous breathing. Therefore, early identification of necrotic histology coupled with minimisation of the individual risks may lead to tailored management strategies in the prevention of muscle wasting during critical illness. Despite accounting for patient heterogeneity, chronic disease and critical illness severity, myonecrosis is difficult to predict.[14] Furthermore, there is a lack of currently accepted, non-volitional methods[21] meaning the diagnosis is often made once the patient regains consciousness – by which point ICUAW and muscle wasting are well established in as many as 40% of patients.[21] Whilst, acquiring muscle tissue for histological assessment is invasive, early identification of necroptosis activation may help develop clinical use of necroptosis inhibitors and potentially reduce and/or prevent the onset of severe muscle wasting and weakness. This is particularly important as not only are ICU-related outcomes influenced by muscle wasting, but also long-term physical outcomes in those that survive.[10,11,18] However, this study did not investigate the impact of myonecrosis on longer-term morbidity.

Whilst systemic mediators of inflammation are commonly implicated and predispose an individual to loss of muscle mass and protein catabolism during critical illness,[305] there remains a lack of specific circulating biomarkers in the determination of programmed myonecrosis activation and even more so in clinically significant skeletal muscle wasting during critical illness.[306] TNF receptor activation in muscle has been widely implicated to induce myositis and functional impairment.[193] Our observations of high intramuscular TNFR1 concentrations at T2 could be explained through a number of mechanisms as pro-inflammatory cytokines often having pleiotropic effects in anabolic and catabolic pathways.[20,187] Firstly, TNFR1 receptor upregulation and subsequent shedding in myofibres may occur during early critical illness after TNF-α binding and death complex formation. Alternatively, immunohistochemistry in NEC patients has previously shown multi-focal, non-homogenous

distribution of CD68 positive, pro-inflammatory infiltrate[14] in areas of necrotising myopathy and the soluble TNF receptors could also originate from inflammatory macrophages during this activation.[307] Indeed, the soluble TNF receptors may also act as decoy receptors in an attempt to reduce further inflammatory/cell death activation at the cell surface whilst quenching soluble TNF-α itself. I show that concentrations of systemic mediators of inflammation and necrosis do not correlate with those seen in skeletal muscle and poorly characterise those with and without underlying myonecrosis. This is likely to be confounded by the small and heterogenous patient cohort. Systemic and intramuscular concentrations of pro-inflammatory cytokines differ with only significant elevations of TNFR1 seen in the original study.[295]

Persistent hypoxia alongside critical illness may partially explain elevated levels of VEGF in our cohort.[14] Skeletal muscle tissue represents the largest quantity of intracellular VEGF (compared to that of the extracellular space) per weight of tissue.[308] In our study, baseline levels of serum VEGF were significantly higher in NEC patients compared to NONEC patients. However, baseline intramuscular levels of VEGF were significantly lower in NEC patients. There is little data available for the significance of varying VEGF in human skeletal muscle during critical illness, however data in inherited muscular disease suggest a role of VEGF in promoting myoblast proliferation, myofibre regeneration and eventual repair and recovery.[309] Thus, one hypothesis would be that the failure to upregulate VEGF in early critical illness (or T2 in this instance) leads to cell death through ischaemic conditioning of the muscle. Furthermore, in exercise models, there is upregulation of expression with increasing levels of physicial activity.[310] During early critical illness, patients are largely immobile and unable to engage in active rehabilitation. These findings need further exploration in both in-vitro and in-vivo human models.

Larger patient numbers and controlling for confounders would be required to detect any potential difference between NEC and NONEC states and was not the scope of this study. Currently, combining

molecular techniques such as immunohistochemistry, electron microscopy and protein assays serve as the most reliable in determining necrotic cell death.

The quadricep muscles, namely rectus femoris and vastus lateralis, are highly accessible for biopsy even in challenging circumstances such as critical illness.[199,311] There is an assumption that programmed necrosis detected in the vastus lateralis muscle biopsies in this study are representative of other muscle groups, including those in the upper limbs and trunk. However, different muscle groups may be more sensitive to loading and unloading, and I cannot extrapolate our findings to all muscle groups. To reduce the possibility of missing potential necrotic features through single site biopsy approach, I performed large field of view microscopy incorporating multiple fields of view. These confirmed areas of normal muscle architecture interspersed with areas of marked pMLKL infiltrate and myonecrosis. This supported the stratification of initial muscle samples with necrotic features and reliably suggesting necroptosis activation. Given that necroptosis requires a pro-inflammatory stimulus which is often systemic in nature, acquisition of multi-site biopsies is not required nor ethical in these high-risk patients. Therefore, adequately sized biopsies should be representative of the entire muscle and the likelihood of completely missing 'more inflamed' areas of muscle with little pMLKL infiltrate is low. However, from a technical perspective, I determined pMLKL upregulation after protein loading titration (Figure 2-13, Figure 2-14) and found that protein loading of 50μg provided a balance of protein signal and minimisation of non-specific bands. Secondly, preservation of phosphorylation status in homogenised muscle samples were optimised by using phosphatase and protease inhibitors, suitably blocked membranes and minimisation of delay in transferring and loading samples in Western blot experiments.

Given the exploratory nature of this work, I utilised samples that remained after initial analyses by the MUSCLE-UK group. It is possible that some of these samples may have undergone a freeze-thaw cycle,

but I made efforts to use aliquots that had not been previously used by studying the starting volume of sample against the sample log.

In this study I assume that T1 samples represent a histological 'baseline' for each patient – i.e. before the onset of critical illness. In fact, a specific onset point is difficult to accurately ascertain and whilst patients were admitted to the ICU promptly, the underlying illness (and inflammatory process) may have started before acquiring skeletal muscle at T1. However, the length of hospital stay before ICU admission was 1 day (IQR 1-3) in the NEC group and 2 days (IQR 1-3) in the NONEC group (p=0.620) and I found no differences in pMLKL at T1 between NEC and NONEC patients. Importantly, no patients were found to have necrotic histology at T1. Immunohistochemistry of one NONEC patient showed a low sarcoplasmic pMLKL signal at T2 which may suggest late-onset necroptosis activation. Indeed, recurrent and/or persistent pro-inflammatory drivers likely exist across the length of an individual's critical care stay and hence there is potential for necroptosis activation at a later stage. This was described by Helliwell *et al.* where the percentage of myofibre necrosis increased with length of stay on the ICU in a range of underlying presentations.[199]

Another limitation in this study was that our patient cohort (n=16) was sampled from an original study of 38 patients. Of these, 20 were found to have necrotic features but only 10 of these patients were included in the current study due to sample availability. Therefore, 10 patients were not assessed and thus the incidence of necroptosis activation may be underestimated in the current study. To reduce false positives, iatrogenic necrosis was also screened by excluding muscle samples with sharply circumscribed groups of necrotic and/or regenerating fibres. Furthermore, in NONEC patients, despite evidence of morphological myofibrillar disruption in terms of circular fibres and disruption to the connective tissue, there was no evidence of sarcolemma rupture, interstitial pMLKL staining or infiltration of nuclei into the muscle tissue, supporting the absence of necrolysis.

It is important to remember that cell death pathways are often interconnected[312], particularly apoptosis and necroptosis where death complexes II and III are similar in structural components.[216] The scope of this study was to determine if terminal effector proteins of necroptosis were present within muscle of critically ill patients due to the consistently reported high prevalence of myonecrosis. Our work highlights the clear need for cell death mechanisms to be further investigated in critical illness related muscle wasting.

In conclusion, this study demonstrates the first evidence of necroptosis activation in human skeletal muscle during early critical illness. Mechanisms of myonecrosis during critical illness are poorly described and systemic markers are not yet sensitive or specific to utilise despite the devastating long-term impact of muscle weakness and wasting in those who survive critical illness. There is a lack of histological studies of human skeletal muscle in critical illness and there is a clear need to better understand muscle level changes during critical illness as identification of necroptosis activation offers potential for therapeutic blockade. There has been a surge in healthcare utilisation, particular with critical care services, due to the COVID19 worldwide pandemic, which has led to a greater proportion of ICU admissions requiring mechanical ventilation, prolonged hospital stays and ultimately at risk of ICUAW and long-term functional dependence in those who survive. Further research is warranted to investigate skeletal muscle cell death mechanisms and their role in myonecrosis during critical illness. Thus, there is a clear need to better understand muscle level changes, such as necroptosis activation, that offers the potential for therapeutic blockade.

Chapter 7: Discussion

7.1 Overview

Skeletal and respiratory muscle wasting occurs acutely and continuously in early critical illness. There is a lack of applied interventions to prevent not only the severity of wasting, but also the physical restriction that occurs during and after critical illness. Despite a plethora of research looking at diagnostic application of radiology in muscle wasting assessment, there remains a lack of consensus regarding methodology in a critical care cohort. Muscle weakness and atrophy is continually reported in survivors of critical illness up to five years later and represents a public health issue. Furthermore, the impact of COVID19 on critical care associated muscle wasting is yet to be described and thus, there is a need to develop research focus and strategies in musculoskeletal diagnostics and intervention to manage likely upsurge in survivors of critical illness with significant physical restriction.

This thesis focussed on the diagnostic ability of freely available imaging modalities to longitudinally describe and quantify the severity of peripheral and respiratory muscle wasting. I assessed the reliability and feasibility of CT and ultrasound techniques and detail robust protocols for each to support the incorporation of these techniques into everyday clinical practice. In this regard, I then provide the first prospective description of non-invasive parasternal muscle strain measurement in the context of critical illness and its use as a dynamic and quantitative measure of mechanical loading during invasive mechanical ventilation.

Given the consistent findings of muscle atrophy and reduction in muscle quality (increased echogenicity), I investigated whether the suggestions of underlying myonecrosis was programmed. Using qualitative and semi-quantitative techniques I show that terminal effector proteins of programmed necrosis are consistently present in necrotic but not non-necrotic skeletal muscle. I also provide evidence and describe of the evolution of myonecroptosis in early critical illness.

7.2 Summary of main findings

In chapter 3 I describe the incidence of low muscle mass and muscle quality as well as acute muscle wasting in a sub-cohort in those with severe respiratory failure and acute respiratory distress syndrome. In its severe form, these patients have an associated mortality of around 40%, which has not significantly improved despite the depth of ARDS-related research over the last 20 years. I studied CT imaging acquired during routine care and quantified skeletal muscle loss in multiple axial muscle groups. In addition, I utilised and tested specialist software to provide qualitative description of muscle change using skeletal muscle density and degree of intra-muscular adipose tissue. I rigorously tested methods of imaging analysis and compared two software platforms with an excellent evidence base and consistently achieved an ICC>0.9 and CoV<7.5%. The study cohort included patients with COVID19 in the early phases of the pandemic.

In 346 critically ill patients with severe respiratory failure and ARDS, I found a low muscle mass state (as given by admission SMI) in 28% and low muscle quality (as given by admission SMD) of 25%. This is lower than previously reported in critical care studies using similar methodology,[165,171,172] and perhaps reflect the younger age of patients selected for extracorporeal support at our tertiary centre. However, a large meta-analysis of body composition in patients specifically with COVID19 related critical illness showed a large variation in prevalence of SMI (22-90%) and SMD (11-85%)[313] and our data found no differences in muscle wasting patterns between patients with COVID19 disease and without. Overall, longitudinal assessment in patients with a second CT image (n=164) demonstrated a loss in L3-SkM_{CSA} of 10.8% (IQR -18.0--3.0), a loss in SMD of -13.7% (IQR -24.3--3.4) with an image interval of 12 days (IQR 6-19) which represents an acceptable interval for measuring acute muscle wasting. Furthermore, I show that change in SMD at a second time point was associated with higher baseline levels of C-reactive protein and the requirement for extracorporeal support. This highlights and supports the role of inflammation and severity of illness as a contributing factor for muscle wasting. Further assessment of muscle changes in a third CT image had a wide interval from intubation

(22 days (IQR 14-33). Whilst the data confirms the severity of muscle wasting, there is little control over timing of imaging and as such would be limited to retrospective observational studies as performing CT studies outside of clinical care poses ethical concerns mainly from additional radiation exposure. The utilisation of CT imaging and quantification of axial skeletal muscle does however have potential for automated technology to quantify muscle groups prospectively and in a timely fashion.

In chapter 4 and 5 I utilised ultrasonography as a prospective, portable, and pragmatic method of musculoskeletal imaging. One of the primary aims was to concurrently compare different muscle groups during early critical illness. Whilst rectus femoris changes are now well described and the methodology the subject of much variation, I detailed and adopted robust methodology with excellent reliability data (ICC>0.9). This approach was extended to the diaphragm and parasternal muscle with similar results. The musculoskeletal ultrasound protocol was challenging and intensive but allowed large data sets to be collected and analysed offline. This included functional measures of respiratory muscle function – DIA_{TF} and PSM_{TF} and PSM_{ε}. Utilisation of muscle strain in respiratory muscle has not been described in a critical care cohort. Parasternal muscle strain offers potential as a measure of respiratory muscle load which may help guide mechanical ventilator strategy and weaning. I provide the first description of PSM strain in various mechanical ventilation modes and longitudinally during ICU admission. I show that PSM_{ε} is high even in the context of high degree of muscle atrophy, thus suggesting that absolute loss of mass does not equate to loss of function. However, it is important to note that I did not look at the level of ventilatory advantage associated with greater PSM_{ε}. In chapter 5, I developed more complex modelling of muscle measurements to determine clinical associations including the impact of advanced respiratory support in the form of ultra-protective mechanical ventilation during vvECMO. I show that changes in diaphragm and PSM muscle are similar and equally active during ICU admission. Parasternal muscle function and activity during mechanical ventilation may provide a non-invasive method of assessing respiratory muscle load, and thus may help tailor

ventilatory strategies in patients to reduce atrophy through 'over-support' and under-loading leading to recruitment of accessory muscles.

Whilst absolute reduction in muscle mass is severe, qualitative changes may shed light on functional aspects and help predict those at risk and prompt timely intervention. In chapters 3, 4 and 5 I addressed qualitative measurements of muscle to infer degree of muscle quality. Using CT imaging Hounsfield units were used to determine muscle density and thus quality. Through logistic regression analyses, I found that SMI (per 10 cm^2) (OR 0.787 (0.616-1.005), p=0.055) , SMD (per 10 HU) (OR 0.640 (0.482-0.851), p=0.002), APACHE II score (OR 1.059 (1.006-1.114), p=0.029) and pre-ICU length of stay (OR 1.068 (1.019-1.120), p=0.007) were all significantly associated with ICU mortality in univariate regression analysis and included in the primary model. When adjusted for SMI (per 10 cm^2), APACHE II and pre-ICU length of stay, SMD (per 10 HU) remained significantly associated with ICU mortality (OR 0.666 (0.488-0.909), p=0.010). Similarly, when adjusted for SMI (per 10 cm^2), SMD (per 10 HU) and APACHE II, pre-ICU length of stay remained significantly associated with ICU mortality (OR 1.064 (1.014-1.117), p=0.011). Therefore, a decrease in muscle density of 10 HU was associated with an increase in ICU mortality by a factor of 1.5. (95% CI 1.10-2.05). Similarly, an additional day in hospital before ICU admission increased the ICU mortality by a factor of 1.06 (95% CI 1.01-1.12). Utilisation of routine admission CT imaging to determine muscle quality may serve to identify clinical risk in certain patients and thus prompt earlier intervention. Qualitative measurements using ultrasound were in the form of echogenicity which has been found to be associated with the presence of underlying myonecrosis. I focussed on the echogenicity of the PSM and RF muscles and found significant rises at day 7 of ICU admission – suggesting loss of muscle quality as well as atrophy. However, the cause of the changes in quality were unclear. CT data suggested higher proportion of intramuscular adipose tissue as a possible factor. Currently literature concerning qualitative ultrasound suggests that high echogenicity may predict underlying myonecrosis. Furthermore, following on from the findings of higher C-reactive protein levels in those with significant loss of SMD, chapter 4 investigated pro-

inflammatory cytokine profiles alongside changes in muscle mass in a variety of patient groups. No distinct inflammatory phenotypes were identified when comparing high and low wasting states, ARDS and non-ARDS patients and COVID and non-COVID patients. However, in the ARDS group, I saw higher levels of RIPK3 and CCK18 throughout the ICU admission but not statistically different at the defined study time points. Whilst these two analytes have been used as circulating markers of necrosis, reliable systemic markers are lacking. Thus, in chapter 6, I sought to evaluate skeletal muscle tissue for potentially programmed pathways of necrosis.

I utilised human skeletal muscle biopsies from the UK-MUSCLE study to evaluate whether there was evidence of programmed necrosis activation. The original study identified 54% of patients with underlying histological necrosis features which warranted exploration to ascertain whether programmed pathways exist. Using Western blotting, I identified higher expression of pMLKL in necrotic muscle compared to non-necrotic. I compared the skeletal muscle expression of pMLKL at ICU admission to a small sample of healthy muscle tissue and found that absolute expression was not significant different. Most notably, I observed differences using immunohistochemistry. I describe the significantly greater change in pMLKL at T2 (day 7-10 of ICU admission) in necrotic muscle (NEC: 9.1 fold change from T1 (IQR 3.9-22.3) vs. NONEC: 0.9 (IQR 0.6-1.1) and then corroborated this finding with IHC once more. In necrotic muscle, pMLKL expression was multi-focal and non-homogenous in distribution and in a smaller sample, demonstrated translocation from the cytoplasm to the sarcolemma and the interstitial space after necrolysis. To further support its activation, I found that RIPK3 was co-localised providing evidence of necrosome formation. These data are the first description of programmed necrosis in acute skeletal muscle wasting in a critical care cohort. The identification of programmed necrotic pathways may suggest that pro-inflammatory triggers and subsequent coordinated necrosis represents a crucial process in the onset of acute skeletal muscle wasting in critical illness.

7.3 Limitations

Defining the onset of critical illness is a frequent challenge in critical care research. Patients are admitted acutely and sometimes managed in an environment external to the ICU before eventual admission. In our tertiary centre, patients can be admitted electively, acutely or retrieved from referring hospitals for specialist respiratory failure management. Patients retrieved with severe respiratory failure were intubated at a median of 5 days (IQR 3-9) following hospital admission compared to those within the hospital who were admitted at a median of 1 day (IQR 0-4) ($p<0.01$). Furthermore, in our prospective study cohort, patients with respiratory failure had musculoskeletal ultrasound performed at a median of 9 days (IQR 6-13) following presentation, compared to a median of 3 days (IQR 1-6) ($p<0.01$) in patients admitted within our hospital. Thus, the onset of critical illness and indeed the muscle atrophy is likely to have begun before enrolment in the study. Despite this, marked muscle atrophy was still found at baseline with progressive decline.

Patient recruitment was certainly affected by the COVID19 pandemic which halted all recruitment for the WAVE study for 6 months. However, commencement of the DeVENT study in our tertiary centre (as a COVID19 prioritised study) allowed ongoing recruitment but with different inclusion/exclusion criteria as well as different patient population (WAVE: cardiac surgery vs. DeVENT: ARDS). Furthermore, 26/28 (and 26/44 of the whole patient cohort) received vvECMO. This often led to physical restrictions to access anatomical sites for imaging studies. However, this cohort of patients have a paucity of data describing the longitudinal changes in muscle and the impact of ultra-protective ventilation and extracorporeal support on respiratory muscle mass and activity is poorly described.

Single side and level PSM were measured throughout this study. I assume that PSM changes at the 3rd intercostal space were representative for all PSM at all levels. I chose anterior muscles for accessibility and 3rd intercostal space to avoid commonly placed dressings and drains I seen on our ICU. Furthermore, PSM shortening occurs in all intercostal spaces, but the absolute decline reduces from

the 2nd to the 5th ICS. Diaphragm and PSM activity were not verified with so-called gold-standard techniques due to their invasive nature. I utilised thickening fraction as a measure of inspiratory effort rather than concurrent measurement of other physiological parameters requiring invasive monitoring.

In chapter 6, samples were restricted by availability from the original study. I studied 16 patients with skeletal muscle tissue (10 NEC and 6 NONEC) from a possible 38. This may have underreported the incidence of programmed necrosis in the overall cohort. There is a clear need to better understand muscle level changes in critical illness to determine the onset of programmed necrosis and whether these changes persist through to recovery as well as the long-term impact on function and physical health. I focussed on a critical care cohort to study muscle histology. Currently, programmed necrosis has only been found to occur in patients with hereditary muscle disease. Thus, it is not clear whether prolonged admission in patients with acute illness but without critical illness, can lead to programmed myonecrosis.

7.4 Future work and direction

7.4.1 Formalising methodology of musculoskeletal ultrasound in the ICU

Our data has meticulously described imaging approach, data capture and image analysis for three different muscle groups. I urge future work to follow strict adherence to thorough reporting of methods such that comparisons can be made across multiple studies. I have published our techniques in peer reviewed journals and specialist texts to promote a consensus approach to musculoskeletal imaging in the ICU and look to contribute to national guidance.

7.4.2 Developing parasternal strain protocol and clinical application

PSM_{ε} measurement requires further research. Determining normal ranges of PSM strain by gender, age, BMI etc is unlikely to yield any clinically significant information. For example, I show that with

variable degrees of muscle atrophy, PSM strain increased. Therefore, the effect of muscle atrophy may be patient specific and not determined by a minimum percentage loss. This is supported by the fact that significant strain is muscle specific and load dependent due the mathematical relationship between stress, force and area. I quantified PSM_{ε} in a small cohort of healthy volunteers during tidal volume breathing. The effects at maximal lung capacity and during increased resistance on this measurement was not tested. Furthermore, effects of MV on PSM_{ε} and standardised levels of MV support in critically ill patients are required (i.e. titration of pressure support/PEEP). Thus, respiratory muscle loading during varying levels of support and prior to extubation trials or spontaneous breathing trials are also required to determine utility in predicting successful SBT and extubation. A proof-of-concept study in the first instance comparing PSM_{ε} using ultrasound against PSM electromyography is also warranted to assess correlation and reliability in neural output measurements against the current gold standard.

7.4.3 Long-term effect of PSM atrophy on physical function

The prospective recruitment of patients into clinical studies was limited due to the COVID19 pandemic. This was compounded by the restriction in conducting formal study follow up with repeat PSM imaging and functional measures such as 6MWT and lung function to study associations. As alluded to above, it is also currently unclear as to what degree of PSM atrophy constitutes a significant change, thus exploring associations with physical restriction may help to elucidate a significant level and support the observed changes in PSM strain.

7.4.4 Confirming activation of programmed myonecrosis

Chapter 6 highlights the clear need for a prospective clinical trial evaluating skeletal muscle changes during critical illness. Whilst I detected the upregulation of pMLKL at day 7-10 in the majority of necrotic skeletal muscle, it is entirely plausible that myonecrosis may occur much earlier and I show evidence of pMLKL translocation at day 3. It is also cannot be inferred that activation of necroptosis

occurs in respiratory muscle. However, the suitability to perform respiratory muscle biopsy may pose far greater risk to the patient and biopsy may be limited to patients undergoing thoracic surgery (where diaphragm and accessory muscle biopsies can be performed under direct vision) or from post-mortem samples. Whilst the upstream stimulus of necroptosis is driven by systemic pro-inflammatory cytokine binding to death receptors such as TNFR1, it also cannot be inferred that respiratory and non-respiratory muscle follow the same programmed death pathway. Therefore, it is pragmatically more favourable to confirm findings from chapter 6 in fresh human skeletal muscle. A control group consisting of acute but non-critical illness may serve to ascertain whether myonecrosis is specific to those with significant critical illness and multi-organ failure rather than in general acute illness requiring hospitalisation.

7.4.5 Developing in-vitro models of programmed necrosis in human skeletal muscle

Finally, in-vitro models of necroptosis in primary human skeletal muscle cell culture have not been described. Our preliminary findings and evidence of necroptosis activation in skeletal muscle demonstrate the need to investigate whether this pathway is amenable to selective inhibition by targeted therapeutics. It is therefore prudent to investigate whether human myoblasts and myofibres are amenable to programmed cell death following a pro-inflammatory stimulus and whether subsequent cell death complexes can be inhibited. Determining the extent of interconnecting cell death pathways requires carefully controlled in vitro assay studies to ascertain the extent of each pathway following a pro-inflammatory stimulus. Following reliable induction of necroptosis, reversibility, and rescue of this cell phenotype with necroptosis inhibitors such as necrostatin-1 (RIPK-1 inhibitor) and necrosulfonamide (pMLKL inhibitor) are required. Induction of necroptosis in a primary skeletal muscle culture has not been reported. To-date, induction of necroptosis in in-vitro skeletal muscle studies are limited to murine models of inherited skeletal muscle disease and myocardium studies.

Chapter 8: References

1. What 'critical care' means | Information for the public | Rehabilitation after critical illness in adults | Guidance | NICE. https://www.nice.org.uk/guidance/cg83/ifp/chapter/what-critical-care-means.
2. Intensive Care National Audit & Research Centre. ICNARC – Summary Statistics 2013-2018. https://www.icnarc.org/Our-Audit/Audits/Cmp/Reports/Summary-Statistics.
3. ICNARC – Admission Summary Statistics. https://www.icnarc.org/Our-Audit/Audits/Cmp/Reports/Summary-Statistics.
4. Group, T. R. C. Dexamethasone in Hospitalized Patients with Covid-19. *https://doi.org/10.1056/NEJMoa2021436* **384**, 693–704 (2020).
5. Abani, O. *et al.* Tocilizumab in patients admitted to hospital with COVID-19 (RECOVERY): a randomised, controlled, open-label, platform trial. *Lancet* **397**, 1637–1645 (2021).
6. Acute Respiratory Distress Syndrome Network *et al.* Ventilation with lower tidal volumes as compared with traditional tidal volumes for acute lung injury and the acute respiratory distress syndrome. *N. Engl. J. Med.* **342**, 1301–8 (2000).
7. Papazian, L. *et al. Neuromuscular Blockers in Early Acute Respiratory Distress Syndrome*. *n engl j med* vol. 12 (2010).
8. Guérin, C. *et al.* Prone Positioning in Severe Acute Respiratory Distress Syndrome. *NEJM.org. N Engl J Med* **23**, 2159–68 (2013).
9. Peek, G. J. *et al.* Efficacy and economic assessment of conventional ventilatory support versus extracorporeal membrane oxygenation for severe adult respiratory failure (CESAR): a multicentre randomised controlled trial. *Lancet* **374**, 1351–1363 (2009).
10. Herridge, M. S. *et al.* One-year outcomes in survivors of the acute respiratory distress syndrome. *N. Engl. J. Med.* **348**, 683–93 (2003).
11. Herridge, M. S. *et al.* Functional Disability 5 Years after Acute Respiratory Distress Syndrome. *N. Engl. J. Med.* **364**, 1293–1304 (2011).
12. Poulsen, J. B., Møller, K., Kehlet, H. & Perner, A. Long-term physical outcome in patients with septic shock. *Acta Anaesthesiol. Scand.* **53**, 724–30 (2009).
13. National Institute for Health and Care Excellence (NICE). NICE Guidance - Rehabilitation After Critical Illness in Adults. https://www.nice.org.uk/guidance/cg83 (2009).
14. Puthucheary, Z. A. *et al.* Acute Skeletal Muscle Wasting in Critical Illness. *JAMA* **310**, 1591 (2013).
15. Levine, S. *et al.* Rapid Disuse Atrophy of Diaphragm Fibers in Mechanically Ventilated Humans. *N. Engl. J. Med.* **358**, 1327–1335 (2008).
16. De Jonghe, B. *et al.* Respiratory weakness is associated with limb weakness and delayed weaning in critical illness. *Crit. Care Med.* **35**, 2007–15 (2007).
17. Ali, N. A. *et al.* Acquired Weakness, Handgrip Strength, and Mortality in Critically Ill Patients. *Am. J. Respir. Crit. Care Med.* **178**, 261–268 (2008).
18. Herridge, M. S. *et al.* The RECOVER Program: Disability Risk Groups and 1-Year Outcome after 7 or More Days of Mechanical Ventilation. *Am. J. Respir. Crit. Care Med.* **194**, 831–844 (2016).
19. Hermans, G. & Van den Berghe, G. Clinical review: intensive care unit acquired weakness. *Crit. Care* **19**, 274 (2015).
20. Friedrich, O. *et al.* The Sick and the Weak: Neuropathies/Myopathies in the Critically Ill. *Physiol. Rev.* **95**, 1025–109 (2015).
21. Fan, E. *et al.* An official american thoracic society clinical practice guideline: The diagnosis of intensive care unit-acquired weakness in adults. *Am. J. Respir. Crit. Care Med.* **190**, (2014).
22. MS, D. & EFM, W. The clinical management of neuromuscular disorders in intensive care. *Neuromuscul. Disord.* **29**, 85–96 (2019).
23. Stevens, R. D. *et al.* A framework for diagnosing and classifying intensive care unit-acquired weakness. *Crit. Care Med.* **37**, S299-308 (2009).

24. Latronico, N. & Bolton, C. F. Critical illness polyneuropathy and myopathy: A major cause of muscle weakness and paralysis. *The Lancet Neurology* (2011) doi:10.1016/S1474-4422(11)70178-8.
25. Dres, M. *et al.* Coexistence and impact of limb muscle and diaphragm weakness at time of liberation from mechanical ventilation in medical intensive care unit patients. *Am. J. Respir. Crit. Care Med.* **195**, (2017).
26. Heunks, L. M. & van der Hoeven, J. G. Clinical review: the ABC of weaning failure--a structured approach. *Crit. Care* **14**, 245 (2010).
27. Boles, J.-M. *et al.* Weaning from mechanical ventilation. *Eur. Respir. J.* **29**, 1033–56 (2007).
28. Larsson, L. & Friedrich, O. Critical Illness Myopathy (CIM) and Ventilator-Induced Diaphragm Muscle Dysfunction (VIDD): Acquired myopathies affecting contractile proteins. *Compr. Physiol.* **7**, 105–112 (2017).
29. Batt, J., Dos Santos, C. C., Cameron, J. I. & Herridge, M. S. Intensive care unit-acquired weakness clinical phenotypes and molecular mechanisms. *Am. J. Respir. Crit. Care Med.* **187**, 238–246 (2013).
30. Petrof, B. J. Diaphragm Weakness in the Critically Ill: Basic Mechanisms Reveal Therapeutic Opportunities. *Chest* (2018) doi:10.1016/j.chest.2018.08.1028.
31. De Jonghe, B. *et al.* Paresis acquired in the intensive care unit: a prospective multicenter study. *JAMA* **288**, 2859–67 (2002).
32. Mayer, K. P. *et al.* Acute skeletal muscle wasting and dysfunction predict physical disability at hospital discharge in patients with critical illness. *Crit. Care* **24**, 1–12 (2020).
33. Patel, S., Bear, D., Patel, B. & Puthucheary, Z. Clinical Application of Ultrasound in Intensive Care Unit-Acquired Weakness. *Ultraschall Med.* **41**, 244–266 (2020).
34. Puthucheary, Z. *et al.* S141 Tumour Necrosis Factor Receptor 1 Shedding Is Related To Acute Skeletal Muscle Wasting In Critical Illness. *Thorax* **69**, A75–A75 (2014).
35. Puthucheary, Z. A. *et al.* Rectus Femoris Cross-Sectional Area and Muscle Layer Thickness: Comparative Markers of Muscle Wasting and Weakness. *Am. J. Respir. Crit. Care Med.* **195**, 136–138 (2017).
36. Wischmeyer, P. E., Puthucheary, Z., Millán, I. S., Butz, D. & Grocott, M. P. W. Muscle mass and physical recovery in ICU: Innovations for targeting of nutrition and exercise. *Curr. Opin. Crit. Care* **23**, 269–278 (2017).
37. Vanhorebeek, I., Latronico, N. & Van den Berghe, G. ICU-acquired weakness. *Intensive Care Med.* **46**, 637–653 (2020).
38. Roberson, A. R., Starkweather, A., Grossman, C., Acevedo, E. & Salyer, J. Influence of muscle strength on early mobility in critically ill adult patients: Systematic literature review. *Heart Lung* **47**, 1–9 (2018).
39. Corner, E. J., Soni, N., Handy, J. M. & Brett, S. J. Construct validity of the Chelsea critical care physical assessment tool: an observational study of recovery from critical illness. (2014) doi:10.1186/cc13801.
40. Jolley, S. E., Bunnell, A. E. & Hough, C. L. ICU-Acquired Weakness. *Chest* **150**, 1129–1140 (2016).
41. Hermans, G., De Jonghe, B., Bruyninckx, F. & Van den Berghe, G. Clinical review: Critical illness polyneuropathy and myopathy. *Critical care (London, England)* vol. 12 238 (2008).
42. Frontera, W. R. & Ochala, J. Skeletal Muscle: A Brief Review of Structure and Function. *Behav. Genet.* **45**, 183–195 (2015).
43. Relaix, F. & Zammit, P. S. Satellite cells are essential for skeletal muscle regeneration: the cell on the edge returns centre stage. *Development* **139**, 2845–56 (2012).
44. Hawke, T. J. & Garry, D. J. Myogenic satellite cells: physiology to molecular biology. *J. Appl. Physiol.* **91**, 534–551 (2001).
45. Nijholt, W., Scafoglieri, A., Jager-Wittenaar, H., Hobbelen, J. S. M. & van der Schans, C. P. The reliability and validity of ultrasound to quantify muscles in older adults: a systematic review. *J. Cachexia. Sarcopenia Muscle* **8**, 702–712 (2017).

46. Cartwright, M. S. *et al.* Quantitative neuromuscular ultrasound in the intensive care unit. *Muscle Nerve* **47**, 255–259 (2013).
47. Parry, S. M. *et al.* Ultrasonography in the intensive care setting can be used to detect changes in the quality and quantity of muscle and is related to muscle strength and function. *J. Crit. Care* **30**, 1151.e9-1151.e14 (2015).
48. De Troyer, A. & Boriek, A. M. Mechanics of the respiratory muscles. *Compr. Physiol.* **1**, 1273–1300 (2011).
49. Moore, K. L. & Agur, A. M. R. *Essential clinical anatomy*. (Lippincott Williams & Wilkins, 2002).
50. Wilcox, P. *et al.* Phrenic nerve function and its relationship to atelectasis after coronary artery bypass surgery. *Chest* **93**, 693–8 (1988).
51. DeVita, M. A., Robinson, L. R., Rehder, J., Hattler, B. & Cohen, C. Incidence and Natural History of Phrenic Neuropathy Occurring During Open Heart Surgery. *Chest* **103**, 850–856 (1993).
52. Esposito, R. A. & Spencer, F. C. The effect of pericardial insulation on hypothermic phrenic nerve injury during open-heart surgery. *Ann. Thorac. Surg.* **43**, 303–8 (1987).
53. McCool, F. D. & Tzelepis, G. E. Dysfunction of the Diaphragm. *N. Engl. J. Med.* **366**, 932–942 (2012).
54. Cohn, D., Benditt, J. O., Eveloff, S. & McCool, F. D. Diaphragm thickening during inspiration. *J. Appl. Physiol.* **83**, 291–296 (1997).
55. DiNino, E., Gartman, E. J., Sethi, J. M. & McCool, F. D. Diaphragm ultrasound as a predictor of successful extubation from mechanical ventilation. *Thorax* **69**, 423–7 (2014).
56. Ueki, J., De Bruin, P. F. & Pride, N. B. In vivo assessment of diaphragm contraction by ultrasound in normal subjects. *Thorax* **50**, 1157–61 (1995).
57. Matamis, D. *et al.* Sonographic evaluation of the diaphragm in critically ill patients. Technique and clinical applications. *Intensive Care Med.* **39**, 801–810 (2013).
58. Goligher, E. C. *et al.* Mechanical ventilation-induced diaphragm atrophy strongly impacts clinical outcomes. *Am. J. Respir. Crit. Care Med.* **197**, 204–213 (2018).
59. De Troyer, A., Kirkwood, P. A. & Wilson, T. A. Respiratory action of the intercostal muscles. *Physiological Reviews* vol. 85 717–756 (2005).
60. De Troyer, A., Legrand, A., Gevenois, P. A. & Wilson, T. A. Mechanical advantage of the human parasternal intercostal and triangularis sterni muscles. *J. Physiol.* **513**, 915–925 (1998).
61. Jackman, R. W. & Kandarian, S. C. The molecular basis of skeletal muscle atrophy. *Am. J. Physiol. - Cell Physiol.* **287**, (2004).
62. Bloch, S., Polkey, M. I., Griffiths, M. & Kemp, P. Molecular mechanisms of intensive care unit-acquired weakness. *Eur. Respir. J.* **39**, 1000–11 (2012).
63. Glass, D. J. Skeletal muscle hypertrophy and atrophy signaling pathways. *Int. J. Biochem. Cell Biol.* **37**, 1974–1984 (2005).
64. Shrikrishna, D. *et al.* Quadriceps wasting and physical inactivity in patients with COPD. *Eur. Respir. J.* **40**, 1115–1122 (2012).
65. Ceco, E., Weinberg, S. E., Chandel, N. S. & Sznajder, J. I. Metabolism and Skeletal Muscle Homeostasis in Lung Disease. *Am. J. Respir. Cell Mol. Biol.* **57**, 28–34 (2017).
66. Cohen, S., Nathan, J. A. & Goldberg, A. L. Muscle wasting in disease: molecular mechanisms and promising therapies. *Nat. Rev. Drug Discov.* **14**, 58–74 (2015).
67. Fearon, K. C. H., Glass, D. J. & Guttridge, D. C. Cancer Cachexia: Mediators, Signaling, and Metabolic Pathways. *Cell Metab.* **16**, 153–166 (2012).
68. Baracos, V. E., Martin, L., Korc, M., Guttridge, D. C. & Fearon, K. C. H. Cancer-associated cachexia. *Nat. Rev. Dis. Prim. 2018 41* **4**, 1–18 (2018).
69. Aldridge, K., Donnelly, K. & Johnston, A. Permissive underfeeding or standard enteral feeding in critically ill adults. *Journal of the Intensive Care Society* vol. 16 (2015).
70. Harvey, S. E. *et al.* Trial of the Route of Early Nutritional Support in Critically Ill Adults. *N. Engl. J. Med.* **371**, 1673–1684 (2014).
71. Wischmeyer, P. E. Are we creating survivors…or victims in critical care? Delivering targeted

nutrition to improve outcomes. *Curr. Opin. Crit. Care* **22**, 279–284 (2016).
72. Stanojcic, M., Finnerty, C. C. & Jeschke, M. G. Anabolic and anticatabolic agents in critical care. *Curr. Opin. Crit. Care* **22**, 325–331 (2016).
73. Knaus, W. A., Draper, E. A., Wagner, D. P. & Zimmerman, J. E. APACHE II: a severity of disease classification system. *Crit. Care Med.* **13**, 818–29 (1985).
74. JL, V. *et al.* The SOFA (Sepsis-related Organ Failure Assessment) score to describe organ dysfunction/failure. On behalf of the Working Group on Sepsis-Related Problems of the European Society of Intensive Care Medicine. *Intensive Care Med.* **22**, 707–710 (1996).
75. Carney, N. *et al.* Guidelines for the Management of Severe Traumatic Brain Injury 4th Edition. (2016).
76. JM, F. *et al.* Neuromuscular blocking agents decrease inflammatory response in patients presenting with acute respiratory distress syndrome. *Crit. Care Med.* **34**, 2749–2757 (2006).
77. SA, B. *et al.* Treatment of comatose survivors of out-of-hospital cardiac arrest with induced hypothermia. *N. Engl. J. Med.* **346**, 557–563 (2002).
78. F, A. *et al.* Complication profiles of adult asthmatics requiring paralysis during mechanical ventilation. *Intensive Care Med.* **27**, 1729–1736 (2001).
79. Behbehani, N. A., Al-Mane, F., D'yachkova, Y., Paré, P. & FitzGerald, J. M. Myopathy following mechanical ventilation for acute severe asthma: the role of muscle relaxants and corticosteroids. *Chest* **115**, 1627–31 (1999).
80. Jakob, S. M. *et al.* Dexmedetomidine vs Midazolam or Propofol for Sedation During Prolonged Mechanical Ventilation. *JAMA* **307**, 1151 (2012).
81. Reade, M. C. *et al.* Effect of Dexmedetomidine Added to Standard Care on Ventilator-Free Time in Patients With Agitated Delirium. *JAMA* **315**, 1460 (2016).
82. Reade, M. C. & Finfer, S. Sedation and Delirium in the Intensive Care Unit. *N. Engl. J. Med.* **370**, 444–454 (2014).
83. Shehabi, Y. *et al.* The SPICE III study protocol and analysis plan: a randomised trial of early goaldirected sedation compared with standard care in mechanically ventilated patients. *Crit. Care Resusc.* **19**, 318–326 (2017).
84. Kortebein, P., Ferrando, A., Lombeida, J., Wolfe, R. & Evans, W. J. Effect of 10 days of bed rest on skeletal muscle in healthy older adults. *JAMA* **297**, 1772–4 (2007).
85. NM, H. *et al.* Physical inactivity rapidly induces insulin resistance and microvascular dysfunction in healthy volunteers. *Arterioscler. Thromb. Vasc. Biol.* **27**, 2650–2656 (2007).
86. T, S., T, M. & P, T. A protocol of no sedation for critically ill patients receiving mechanical ventilation: a randomised trial. *Lancet (London, England)* **375**, 475–480 (2010).
87. Macfarlane, I. A. & Rosenthal, F. D. Severe myopathy after status asthmaticus. *Lancet (London, England)* **2**, 615 (1977).
88. Pereira, R. M. R. & Freire de Carvalho, J. Glucocorticoid-induced myopathy. *Jt. bone spine* **78**, 41–44 (2011).
89. Evans, L. *et al.* Surviving sepsis campaign: international guidelines for management of sepsis and septic shock 2021. *Intensive Care Med.* (2021) doi:10.1007/S00134-021-06506-Y.
90. Venkatesh, B. *et al.* Adjunctive Glucocorticoid Therapy in Patients with Septic Shock. *http://dx.doi.org/10.1056/NEJMoa1705835* **378**, 797–808 (2018).
91. Nanas, S. *et al.* Predisposing factors for critical illness polyneuromyopathy in a multidisciplinary intensive care unit. *Acta Neurol. Scand.* **118**, 175–181 (2008).
92. Sprung, C. L. *et al.* Hydrocortisone therapy for patients with septic shock. *N. Engl. J. Med.* **358**, 111–124 (2008).
93. De Letter, M. A. C. J. *et al.* Critical illness polyneuropathy and myopathy (CIPNM): evidence for local immune activation by cytokine-expression in the muscle tissue. *J. Neuroimmunol.* **106**, 206–213 (2000).
94. Finfer, S. *et al.* Intensive versus Conventional Glucose Control in Critically Ill Patients. *N. Engl. J. Med.* **360**, 1283–1297 (2009).

95. Brower, R. G. Consequences of bed rest. *Crit. Care Med.* **37**, (2009).
96. Bloomfield, S. A. Changes in musculoskeletal structure and function with prolonged bed rest. *Med. Sci. Sports Exerc.* **29**, 197–206 (1997).
97. Allen, C., Glasziou, P. & Del Mar, C. Bed rest: A potentially harmful treatment needing more careful evaluation. *Lancet* **354**, 1229–1233 (1999).
98. Parry, S. M. & Puthucheary, Z. A. The impact of extended bed rest on the musculoskeletal system in the critical care environment. *Extrem. Physiol. Med.* **4**, 16 (2015).
99. Winkelman, C. Bed rest in health and critical illness: a body systems approach. *AACN Adv. Crit. Care* **20**, 254–266 (2009).
100. Truong, A. D., Fan, E., Brower, R. G. & Needham, D. M. Bench-to-bedside review: mobilizing patients in the intensive care unit--from pathophysiology to clinical trials. *Crit. Care* **13**, 216 (2009).
101. Maffiuletti, N. A. Physiological and methodological considerations for the use of neuromuscular electrical stimulation. *Eur. J. Appl. Physiol.* **110**, 223–234 (2010).
102. Parry, S. M. *et al.* Functional electrical stimulation with cycling in the critically ill: a pilot case-matched control study. *J. Crit. Care* **29**, 695.e1-695.e7 (2014).
103. Parry, S. M. *et al.* Electrical muscle stimulation in the intensive care setting: a systematic review. *Crit. Care Med.* **41**, 2406–2418 (2013).
104. Cases in the UK | Coronavirus in the UK. https://coronavirus.data.gov.uk/details/cases.
105. (ICNARC), I. C. N. A. & R. C. ICNARC – COVID19 Reports: COVID19 Admissions up to 31st August 2020.
106. Chen, G. *et al.* Clinical and immunological features of severe and moderate coronavirus disease 2019. *J. Clin. Invest.* **130**, 2620–2629 (2020).
107. Guan, W. *et al.* Clinical characteristics of coronavirus disease 2019 in China. *N. Engl. J. Med.* **382**, 1708–1720 (2020).
108. Richards-Belle, A. *et al.* COVID-19 in critical care: epidemiology of the first epidemic wave across England, Wales and Northern Ireland. *Intensive Care Med.* (2020) doi:10.1007/s00134-020-06267-0.
109. Evans, R. A. *et al.* Physical, cognitive, and mental health impacts of COVID-19 after hospitalisation (PHOSP-COVID): a UK multicentre, prospective cohort study. *Lancet Respir. Med.* **9**, 1275–1287 (2021).
110. Giraudo, C. *et al.* Reduced muscle mass as predictor of intensive care unit hospitalization in COVID-19 patients. *PLoS One* **16**, e0253433 (2021).
111. Aerde, N. Van, Berghe, G. Van Den, Wilmer, A., Gosselink, R. & Hermans, G. Intensive care unit acquired muscle weakness in COVID-19 patients. **30**, 10–12 (2020).
112. Vassilakopoulos, T. & Petrof, B. J. Ventilator-induced diaphragmatic dysfunction. *Am. J. Respir. Crit. Care Med.* **169**, 336–41 (2004).
113. Hooijman, P. E. *et al.* Diaphragm muscle fiber weakness and ubiquitin-proteasome activation in critically ill patients. *Am. J. Respir. Crit. Care Med.* **191**, (2015).
114. Goligher, E. C. *et al.* Evolution of Diaphragm Thickness during Mechanical Ventilation. Impact of Inspiratory Effort. *Am. J. Respir. Crit. Care Med.* **192**, 1080–8 (2015).
115. Goligher, E. C. *et al.* Diaphragmatic myotrauma: a mediator of prolonged ventilation and poor patient outcomes in acute respiratory failure. *Lancet Respir. Med.* (2018) doi:10.1016/S2213-2600(18)30366-7.
116. Jaber, S. *et al.* Rapidly progressive diaphragmatic weakness and injury during mechanical ventilation in humans. *Am. J. Respir. Crit. Care Med.* **183**, 364–371 (2011).
117. Picard, M. *et al.* Mitochondrial dysfunction and lipid accumulation in the human diaphragm during mechanical ventilation. *Am. J. Respir. Crit. Care Med.* **186**, 1140–1149 (2012).
118. Esteban, A., Alía, I., Ibañez, J., Benito, S. & Tobin, M. J. Modes of mechanical ventilation and weaning. A national survey of Spanish hospitals. The Spanish Lung Failure Collaborative Group. *Chest* **106**, 1188–93 (1994).

119. Beduneau, G. *et al.* Epidemiology of weaning outcome according to a new definition the WIND study. *Am. J. Respir. Crit. Care Med.* **195**, 772–783 (2017).
120. Esteban, A. *et al.* A Comparison of Four Methods of Weaning Patients from Mechanical Ventilation. *N. Engl. J. Med.* **332**, 345–350 (1995).
121. Kim, W. Y., Suh, H. J., Hong, S.-B., Koh, Y. & Lim, C.-M. Diaphragm dysfunction assessed by ultrasonography: Influence on weaning from mechanical ventilation*. *Crit. Care Med.* **39**, 2627–2630 (2011).
122. Dres, M. *et al.* Dyspnoea and respiratory muscle ultrasound to predict extubation failure. *Eur. Respir. J.* **58**, 2100002 (2021).
123. Ninane, V., Farkas, G. A., Baer, R. & De Troyer, A. Mechanism of rib cage inspiratory muscle recruitment in diaphragmatic paralysis. *Am. Rev. Respir. Dis.* **139**, 146–149 (1989).
124. Goligher, E. C. *et al.* Lung- and Diaphragm-Protective Ventilation. *Am. J. Respir. Crit. Care Med.* **202**, 950–961 (2020).
125. Goligher, E. C., Ferguson, N. D. & Brochard, L. J. Clinical challenges in mechanical ventilation. *Lancet* **387**, 1856–1866 (2016).
126. Seymour, J. M. *et al.* Ultrasound measurement of rectus femoris cross-sectional area and the relationship with quadriceps strength in COPD. *Thorax* **64**, 418–23 (2009).
127. Wild, J. J. & Neal, D. Use of high-frequency ultrasonic waves for detecting changes of texture in living tissues. *Lancet (London, England)* **1**, 655–7 (1951).
128. Heckmatt, J. Z., Dubowitz, V. & Leeman, S. Detection of pathological change in dystrophic muscle with B-scan ultrasound imaging. *Lancet (London, England)* **1**, 1389–90 (1980).
129. Scheibe, N., Sosnowski, N., Pinkhasik, A., Vonderbank, S. & Bastian, A. Sonographic evaluation of diaphragmatic dysfunction in COPD patients. *Int. J. COPD* **10**, 1925–1930 (2010).
130. Vivier, E. *et al.* Diaphragm ultrasonography to estimate the work of breathing during non-invasive ventilation. *Intensive Care Med.* **38**, 796–803 (2012).
131. Cala, S. J. *et al.* Respiratory Ultrasonography of Human Parasternal Intercostal Muscle In Vivo. *Ultrasound Med. Biol.* **24**, 313–326 (1998).
132. de Bruin, P. F., Ueki, J., Watson, A. & Pride, N. B. Size and strength of the respiratory and quadriceps muscles in patients with chronic asthma. *Eur. Respir. J.* **10**, 59–64 (1997).
133. Puthucheary, Z. A. *et al.* Qualitative Ultrasound in Acute Critical Illness Muscle Wasting. *Crit. Care Med.* **43**, 1603–11 (2015).
134. Pillen, S. Skeletal muscle ultrasound. *Eur. J. Transl. Myol.* **20**, 145 (2010).
135. Pillen, S. *et al.* Quantitative gray-scale analysis in skeletal muscle ultrasound: A comparison study of two ultrasound devices. *Muscle Nerve* **39**, 781–786 (2009).
136. Paris, M. & Mourtzakis, M. Assessment of skeletal muscle mass in critically ill patients: Considerations for the utility of computed tomography imaging and ultrasonography. *Curr. Opin. Clin. Nutr. Metab. Care* **19**, 125–130 (2016).
137. Mourtzakis, M., Parry, S., Connolly, B. & Puthucheary, Z. Skeletal muscle ultrasound in critical care: A tool in need of translation. *Ann. Am. Thorac. Soc.* **14**, 1495–1503 (2017).
138. Boussuges, A., Gole, Y. & Blanc, P. Diaphragmatic motion studied by m-mode ultrasonography: methods, reproducibility, and normal values. *Chest* **135**, 391–400 (2009).
139. Dubé, B. P. *et al.* Ultrasound evaluation of diaphragm function in mechanically ventilated patients: Comparison to phrenic stimulation and prognostic implications. *Thorax* **72**, 811–818 (2017).
140. Connolly, B. *et al.* Ultrasound for the assessment of peripheral skeletal muscle architecture in critical illness: A systematic review. *Crit. Care Med.* **43**, 897–905 (2015).
141. Frich, L. H., Lambertsen, K. L., Hjarbaek, J., Dahl, J. S. & Holsgaard-Larsen, A. Musculoskeletal application and validation of speckle-tracking ultrasonography. *BMC Musculoskelet. Disord.* **20**, 1–8 (2019).
142. Bloch, S. A. A. *et al.* MiR-181a: a potential biomarker of acute muscle wasting following elective high-risk cardiothoracic surgery. *Crit. Care* **19**, 147 (2015).

143. Sarwal, A. *et al.* Interobserver Reliability of Quantitative Muscle Sonographic Analysis in the Critically Ill Population. *J. Ultrasound Med.* **34**, 1191–1200 (2015).
144. Reimers, K., Reimers, C. D., Wagner, S., Paetzke, I. & Pongratz, D. E. Skeletal muscle sonography: a correlative study of echogenicity and morphology. *J. Ultrasound Med.* **12**, 73–77 (1993).
145. Pillen, S., Scholten, R. R., Zwarts, M. J. & Verrips, A. Quantitative skeletal muscle ultrasonography in children with suspected neuromuscular disease. *Muscle Nerve* **27**, 699–705 (2003).
146. Fukumoto, Y. *et al.* Skeletal muscle quality assessed from echo intensity is associated with muscle strength of middle-aged and elderly persons. *Eur. J. Appl. Physiol.* **112**, 1519–1525 (2012).
147. Grimm, A. *et al.* Muscle ultrasound for early assessment of critical illness neuromyopathy in severe sepsis. *Crit. Care* **17**, R227 (2013).
148. De Troyer, A., Kelly, S., Macklem, P. T. & Zin, W. A. Mechanics of intercostal space and actions of external and internal intercostal muscles. *J. Clin. Invest.* **75**, 850–857 (1985).
149. Hershenson, M. B., Kikuchi, Y., Tzelepis, G. E. & McCool, F. D. Preferential fatigue of the rib cage muscles during inspiratory resistive loaded ventilation. *https://doi.org/10.1152/jappl.1989.66.2.750* **66**, 750–754 (1989).
150. Yoshida, R. *et al.* Measurement of intercostal muscle thickness with ultrasound imaging during maximal breathing. *J. Phys. Ther. Sci.* **31**, 340–343 (2019).
151. Formenti, P., Umbrello, M., Dres, M. & Chiumello, D. Ultrasonographic assessment of parasternal intercostal muscles during mechanical ventilation. *Ann. Intensive Care* **10**, (2020).
152. Goligher, E. C. *et al.* Measuring diaphragm thickness with ultrasound in mechanically ventilated patients: feasibility, reproducibility and validity. *Intensive Care Med.* **41**, 642–9 (2015).
153. Umbrello, M. & Formenti, P. Ultrasonographic Assessment of Diaphragm Function in Critically Ill Subjects. *Respir. Care* **61**, 542–555 (2016).
154. Nakanishi, N. *et al.* Monitoring of muscle mass in critically ill patients: Comparison of ultrasound and two bioelectrical impedance analysis devices. *J. Intensive Care* **7**, (2019).
155. Umbrello, M. *et al.* Oesophageal pressure and respiratory muscle ultrasonographic measurements indicate inspiratory effort during pressure support ventilation. *Br. J. Anaesth.* **125**, e148–e157 (2020).
156. Dres, M. *et al.* Usefulness of Parasternal Intercostal Muscle Ultrasound during Weaning from Mechanical Ventilation. *Anesthesiology* **132**, 1114–1125 (2020).
157. Collier, P., Phelan, D. & Klein, A. A Test in Context: Myocardial Strain Measured by Speckle-Tracking Echocardiography. *Journal of the American College of Cardiology* (2017) doi:10.1016/j.jacc.2016.12.012.
158. Goutman, S. A. *et al.* Speckle tracking as a method to measure hemidiaphragm excursion. *Muscle and Nerve* **55**, 125–127 (2017).
159. Orde, S. R., Boon, A. J., Firth, D. G., Villarraga, H. R. & Sekiguchi, H. Diaphragm assessment by two dimensional speckle tracking imaging in normal subjects. *BMC Anesthesiol.* **16**, 43 (2015).
160. Oppersma, E. *et al.* Functional assessment of the diaphragm by speckle tracking ultrasound during inspiratory loading. *J. Appl. Physiol.* **123**, 1063–1070 (2017).
161. Winter, D. Kinesiological Electromyography. in *Biomechanics and Motor Control of Human Movement* (University of Waterloo, 2009).
162. Hernandez-Suarez, D. F. & López-Candales, A. Strain Imaging Echocardiography: What Imaging Cardiologists Should Know. *Curr. Cardiol. Rev.* **13**, 118 (2017).
163. Dandel, M., Lehmkuhl, H., Knosalla, C., Suramelashvili, N. & Hetzer, R. Strain and Strain Rate Imaging by Echocardiography – Basic Concepts and Clinical Applicability. *Curr. Cardiol. Rev.* **5**, 133 (2009).
164. Goodpaster, B. H., Kelley, D. E., Thaete, F. L., He, J. & Ross, R. Skeletal muscle attenuation determined by computed tomography is associated with skeletal muscle lipid content. *J. Appl.*

Physiol. **89**, 104–110 (2000).
165. Looijaard, W. G. P. M. *et al.* Skeletal muscle quality as assessed by CT-derived skeletal muscle density is associated with 6-month mortality in mechanically ventilated critically ill patients. *Crit. Care* **20**, 386 (2016).
166. Gomez-Perez, S. L. *et al.* Measuring Abdominal Circumference and Skeletal Muscle From a Single Cross-Sectional Computed Tomography Image: A Step-by-Step Guide for Clinicians Using National Institutes of Health ImageJ. *JPEN. J. Parenter. Enteral Nutr.* **40**, 308–18 (2016).
167. Irving, B. A. *et al.* NIH ImageJ and Slice-O-Matic computed tomography imaging software to quantify soft tissue. *Obesity* **15**, 370–376 (2007).
168. Van Der Werf, A. *et al.* Percentiles for skeletal muscle index, area and radiation attenuation based on computed tomography imaging in a healthy Caucasian population. *Eur. J. Clin. Nutr.* **72**, 288–296 (2018).
169. Prado, C. M. *et al.* Prevalence and clinical implications of sarcopenic obesity in patients with solid tumours of the respiratory and gastrointestinal tracts: a population-based study. *Lancet Oncol.* **9**, 629–635 (2008).
170. Martin, L. *et al.* Cancer cachexia in the age of obesity: Skeletal muscle depletion is a powerful prognostic factor, independent of body mass index. *J. Clin. Oncol.* **31**, 1539–1547 (2013).
171. Weijs, P. J. M. *et al.* Low skeletal muscle area is a risk factor for mortality in mechanically ventilated critically ill patients. *Crit. Care* **18**, 1–7 (2014).
172. Moisey, L. L. *et al.* Skeletal muscle predicts ventilator-free days, ICU-free days, and mortality in elderly ICU patients. *Crit. Care* **17**, R206 (2013).
173. Reinders, I. *et al.* Muscle Quality and Myosteatosis: Novel Associations with Mortality Risk. *Am. J. Epidemiol.* **183**, 53–60 (2016).
174. Bear, D. E. *et al.* Relationship Between Skeletal Muscle Area and Density and Clinical Outcome in Adults Receiving Venovenous Extracorporeal Membrane Oxygenation. *Crit. Care Med.* **Publish Ah**, 1–10 (2021).
175. Fred, H. L. Drawbacks and limitations of computed tomography: Views from a medical educator. *Texas Heart Institute Journal* vol. 31 345–348 (2004).
176. Netea, M. G. *et al.* A guiding map for inflammation. *Nature Immunology* vol. 18 826–831 (2017).
177. Kany, S., Vollrath, J. T. & Relja, B. Cytokines in Inflammatory Disease. *Int. J. Mol. Sci.* **20**, 6008 (2019).
178. Dinarello, C. A. Proinflammatory Cytokines. *Chest* **118**, 503–508 (2000).
179. Hranjec, T. *et al.* Diagnosis-dependent relationships between cytokine levels and survival in patients admitted for surgical critical care. *J. Am. Coll. Surg.* **210**, 833–44, 845–6 (2010).
180. MERA, S. *et al.* Multiplex cytokine profiling in patients with sepsis. *APMIS* **119**, 155–163 (2011).
181. Deshmane, S. L., Kremlev, S., Amini, S. & Sawaya, B. E. Monocyte Chemoattractant Protein-1 (MCP-1): An Overview. *J. Interf. Cytokine Res.* **29**, 313 (2009).
182. Pedersen, B. K. & Febbraio, M. A. Muscle as an Endocrine Organ: Focus on Muscle-Derived Interleukin-6. *Physiol. Rev.* **88**, 1379–1406 (2008).
183. Lang, C. H., Silvis, C., Deshpande, N., Nystrom, G. & Frost, R. A. Endotoxin stimulates in vivo expression of inflammatory cytokines tumor necrosis factor alpha, interleukin-1beta, -6, and high-mobility-group protein-1 in skeletal muscle. *Shock* **19**, 538–46 (2003).
184. Schulze, P. C. *et al.* Muscular levels of proinflammatory cytokines correlate with a reduced expression of insulinlike growth factor-I in chronic heart failure. *Basic Res. Cardiol.* **98**, 267–274 (2003).
185. Borrelli, E. *et al.* Plasma concentrations of cytokines, their soluble receptors, and antioxidant vitamins can predict the development of multiple organ failure in patients at risk. *Crit. Care Med.* **24**, 392–7 (1996).
186. Adams, V. *et al.* Induction of MuRF1 Is Essential for TNF-α-Induced Loss of Muscle Function in Mice. *J. Mol. Biol.* (2008) doi:10.1016/j.jmb.2008.08.087.

187. Spate, U. & Schulze, P. C. Proinflammatory cytokines and skeletal muscle. *Curr. Opin. Clin. Nutr. Metab. Care* **7**, 265–269 (2004).
188. Jatoi, A. *et al.* A placebo-controlled double blind trial of etanercept for the cancer anorexia/weight loss syndrome. *Cancer* **110**, 1396–1403 (2007).
189. Bayliss, T. J., Smith, J. T., Schuster, M., Dragnev, K. H. & Rigas, J. R. A humanized anti-IL-6 antibody (ALD518) in non-small cell lung cancer. *Expert Opin. Biol. Ther.* **11**, 1663–1668 (2011).
190. Li, Y.-P. & Reid, M. B. NF-κB mediates the protein loss induced by TNF-α in differentiated skeletal muscle myotubes. *Am. J. Physiol. Integr. Comp. Physiol.* **279**, R1165–R1170 (2000).
191. Gomes, M. D., Lecker, S. H., Jagoe, R. T., Navon, A. & Goldberg, A. L. Atrogin-1, a muscle-specific F-box protein highly expressed during muscle atrophy. *Proc. Natl. Acad. Sci. U. S. A.* **98**, 14440–14445 (2001).
192. Foletta, V. C., White, L. J., Larsen, A. E., Léger, B. & Russell, A. P. The role and regulation of MAFbx/atrogin-1 and MuRF1 in skeletal muscle atrophy. *Pflügers Arch. - Eur. J. Physiol.* **461**, 325–335 (2011).
193. Reid, M. B. & Li, Y. P. Tumor necrosis factor-alpha and muscle wasting: a cellular perspective. *Respir. Res.* **2**, 269–72 (2001).
194. Sandri, M. Protein breakdown in muscle wasting: Role of autophagy-lysosome and ubiquitin-proteasome. *Int. J. Biochem. Cell Biol.* **45**, 2121–2129 (2013).
195. Saghizadeh, M., Ong, J. M., Garvey, W. T., Henry, R. R. & Kern, P. A. The expression of TNFα by human muscle: Relationship to insulin resistance. *J. Clin. Invest.* **97**, 1111–1116 (1996).
196. Bonaldo, P. & Sandri, M. Cellular and molecular mechanisms of muscle atrophy. *Dis. Model. Mech.* **6**, 25–39 (2013).
197. LN, van K. & AJ, B. Effect of tumor necrosis factor alpha on electrically induced calcium transients elicited in C2C12 skeletal myotubes. *Muscle Nerve* **35**, 251–253 (2007).
198. Reid, M. B., Lännergren, J. & Westerblad, H. Respiratory and limb muscle weakness induced by tumor necrosis factor-alpha: involvement of muscle myofilaments. *Am. J. Respir. Crit. Care Med.* **166**, 479–84 (2002).
199. Helliwell, T. R. *et al.* Necrotizing myopathy in critically-ill patients. *J. Pathol.* **164**, 307–314 (1991).
200. Hund, E. Myopathy in critically ill patients. *Crit. Care Med.* **27**, 2544–2547 (1999).
201. Latronico, N. *et al.* Critical illness myopathy and neuropathy. *Lancet (London, England)* **347**, 1579–82 (1996).
202. Vandenabeele, P., Galluzzi, L., Vanden Berghe, T. & Kroemer, G. Molecular mechanisms of necroptosis: an ordered cellular explosion. *Nat. Rev. Mol. Cell Biol.* **11**, 700–714 (2010).
203. Tonnus, W. *et al.* The pathological features of regulated necrosis. *J. Pathol.* **247**, 697–707 (2019).
204. Moreno-Gonzalez, G., Vandenabeele, P. & Krysko, D. V. Necroptosis: A novel cell death modality and its potential relevance for critical care medicine. *Am. J. Respir. Crit. Care Med.* **194**, 415–428 (2016).
205. Luedde, M. *et al.* RIP3, a kinase promoting necroptotic cell death, mediates adverse remodelling after myocardial infarction. *Cardiovasc. Res.* **103**, 206–216 (2014).
206. Linkermann, A. *et al.* Rip1 (Receptor-interacting protein kinase 1) mediates necroptosis and contributes to renal ischemia/reperfusion injury. *Kidney Int.* **81**, 751–761 (2012).
207. Oerlemans, M. I. F. J. *et al.* Inhibition of RIP1-dependent necrosis prevents adverse cardiac remodeling after myocardial ischemia–reperfusion in vivo. *Basic Res. Cardiol.* **107**, 270 (2012).
208. Laster, S. M., Wood, J. G. & Gooding, L. R. Tumor necrosis factor can induce both apoptic and necrotic forms of cell lysis. *J. Immunol.* **141**, 2629–34 (1988).
209. Holler, N. *et al.* Fas triggers an alternative, caspase-8–independent cell death pathway using the kinase RIP as effector molecule. *Nat. Immunol.* **1**, 489–495 (2000).
210. Vercammen, D. *et al.* Dual signaling of the Fas receptor: initiation of both apoptotic and necrotic cell death pathways. *J. Exp. Med.* **188**, 919–30 (1998).

211. Kelliher, M. A. *et al.* The death domain kinase RIP mediates the TNF-induced NF-kappaB signal. *Immunity* **8**, 297–303 (1998).
212. Hsu, H., Huang, J., Shu, H. B., Baichwal, V. & Goeddel, D. V. TNF-dependent recruitment of the protein kinase RIP to the TNF receptor-1 signaling complex. *Immunity* **4**, 387–96 (1996).
213. Christofferson, D. E., Li, Y. & Yuan, J. Control of Life-or-Death Decisions by RIP1 Kinase. *Annu. Rev. Physiol.* **76**, 129–150 (2014).
214. Wang, L., Du, F. & Wang, X. TNF-α Induces Two Distinct Caspase-8 Activation Pathways. *Cell* **133**, 693–703 (2008).
215. Micheau, O. & Tschopp, J. Induction of TNF receptor I-mediated apoptosis via two sequential signaling complexes. *Cell* **114**, 181–90 (2003).
216. Pasparakis, M. & Vandenabeele, P. Necroptosis and its role in inflammation. *Nature* **517**, 311–320 (2015).
217. Grootjans, S., Vanden Berghe, T. & Vandenabeele, P. Initiation and execution mechanisms of necroptosis: an overview. *Cell Death Differ.* **24**, 1184–1195 (2017).
218. Zhang, D.-W. *et al.* RIP3, an Energy Metabolism Regulator That Switches TNF-Induced Cell Death from Apoptosis to Necrosis. *Science (80-.).* **325**, 332–336 (2009).
219. Li, J. *et al.* The RIP1/RIP3 necrosome forms a functional amyloid signaling complex required for programmed necrosis. *Cell* **150**, 339–50 (2012).
220. He, S. *et al.* Receptor Interacting Protein Kinase-3 Determines Cellular Necrotic Response to TNF-α. *Cell* **137**, 1100–1111 (2009).
221. Cho, Y. *et al.* Phosphorylation-Driven Assembly of the RIP1-RIP3 Complex Regulates Programmed Necrosis and Virus-Induced Inflammation. *Cell* **137**, 1112–1123 (2009).
222. Sun, L. *et al.* Mixed Lineage Kinase Domain-like Protein Mediates Necrosis Signaling Downstream of RIP3 Kinase. *Cell* **148**, 213–227 (2012).
223. Samson, A. L. *et al.* MLKL trafficking and accumulation at the plasma membrane control the kinetics and threshold for necroptosis. *Nat. Commun.* **11**, 1–17 (2020).
224. Wang, H. *et al.* Mixed Lineage Kinase Domain-like Protein MLKL Causes Necrotic Membrane Disruption upon Phosphorylation by RIP3. *Mol. Cell* **54**, 133–146 (2014).
225. Dondelinger, Y. *et al. MLKL Compromises Plasma Membrane Integrity by Binding to Phosphatidylinositol Phosphates*. *Cell Reports* vol. 7 (2014).
226. Kaczmarek, A., Vandenabeele, P. & Krysko, D. V. Necroptosis: The Release of Damage-Associated Molecular Patterns and Its Physiological Relevance. *Immunity* **38**, 209–223 (2013).
227. Kim, E. H., Wong, S. W. & Martinez, J. Programmed Necrosis and Disease:We interrupt your regular programming to bring you necroinflammation. *Cell Death Differ.* 25–40 (2018) doi:10.1038/s41418-018-0179-3.
228. Eigenbrod, T., Park, J.-H., Harder, J., Iwakura, Y. & Núñez, G. Cutting edge: critical role for mesothelial cells in necrosis-induced inflammation through the recognition of IL-1 alpha released from dying cells. *J. Immunol.* **181**, 8194–8 (2008).
229. Tonnus, W. & Linkermann, A. The in vivo evidence for regulated necrosis. *Immunol. Rev.* **277**, 128–149 (2017).
230. Tonnus, W. *et al.* The clinical relevance of necroinflammation—highlighting the importance of acute kidney injury and the adrenal glands. *Cell Death Differ.* **26**, 68–82 (2019).
231. Shashaty, M. G. S. *et al.* Plasma Levels of Receptor Interacting Protein Kinase-3 (RIP3), an Essential Mediator of Necroptosis, are Associated with Acute Kidney Injury in Critically Ill Trauma Patients. *SHOCK* **46**, 139–143 (2016).
232. Qing, D. Y. *et al.* Red Blood Cells Induce Necroptosis of Lung Endothelial Cells and Increase Susceptibility to Lung Inflammation. *Am. J. Respir. Crit. Care Med.* **190**, 1243–1254 (2014).
233. Ma, K. C. *et al.* Circulating RIPK3 levels are associated with mortality and organ failure during critical illness. *JCI insight* **3**, 0–10 (2018).
234. Siempos, I. I. *et al.* RIPK3 mediates pathogenesis of experimental ventilator-induced lung injury. *JCI insight* **3**, 1–12 (2018).

235. Moriwaki, K. & Chan, F. K.-M. RIP3: a molecular switch for necrosis and inflammation. *Genes Dev.* **27**, 1640–9 (2013).
236. Moriwaki, K. & Chan, F. K. M. Necrosis-dependent and independent signaling of the RIP kinases in inflammation. *Cytokine Growth Factor Rev.* **25**, 167–174 (2014).
237. Mandal, P. *et al.* RIP3 induces apoptosis independent of pronecrotic kinase activity. *Mol. Cell* **56**, 481–95 (2014).
238. Lawlor, K. E. *et al.* RIPK3 promotes cell death and NLRP3 inflammasome activation in the absence of MLKL. *Nat. Commun.* **6**, 6282 (2015).
239. Szobi, A. *et al.* Analysis of necroptotic proteins in failing human hearts. *J. Transl. Med.* **15**, 1–7 (2017).
240. Mourtzakis, M. *et al.* A practical and precise approach to quantification of body composition in cancer patients using computed tomography images acquired during routine care. *Appl. Physiol. Nutr. Metab.* **33**, 997–1006 (2008).
241. Patel, S. & Puthucheary, Z. *Point-of-Care Ultrasound in Critical Care*. (Scion Publishing Ltd, 2022).
242. Pasero, D. *et al.* Improving ultrasonic measurement of diaphragmatic excursion after cardiac surgery using the anatomical M-mode: a randomized crossover study. *Intensive Care Med.* **41**, 650–656 (2015).
243. Wallbridge, P. *et al.* Parasternal intercostal muscle ultrasound in chronic obstructive pulmonary disease correlates with spirometric severity. *Sci. Rep.* **8**, 15274 (2018).
244. Arts, I. M., Overeem, S., Pillen, S., Schelhaas, H. J. & Zwarts, M. J. Muscle ultrasonography to predict survival in amyotrophic lateral sclerosis. *J. Neurol. Neurosurg. Psychiatry* **82**, 552–554 (2011).
245. Zaidman, C. M., Holland, M. R., Anderson, C. C. & Pestronk, A. Calibrated quantitative ultrasound imaging of skeletal muscle using backscatter analysis. *Muscle Nerve* **38**, 893–898 (2008).
246. Reed, G. F., Lynn, F. & Meade, B. D. Use of coefficient of variation in assessing variability of quantitative assays. *Clin. Diagn. Lab. Immunol.* **9**, 1235–1239 (2002).
247. Dietrichson, P. *et al.* Conchotome and needle percutaneous biopsy of skeletal muscle. *J. Neurol. Neurosurg. Psychiatry* **50**, 1461–1467 (1987).
248. Bradford, M. A Rapid and Sensitive Method for the Quantitation of Microgram Quantities of Protein Utilizing the Principle of Protein-Dye Binding. *Anal. Biochem.* **72**, 248–254 (1976).
249. Bass, J. J. *et al.* An overview of technical considerations for Western blotting applications to physiological research. *Scand. J. Med. Sci. Sport.* **27**, 4–25 (2017).
250. Walter, S. D., Eliasziw, M. & Donner, A. Sample size and optimal designs for reliability studies. *Stat. Med.* **17**, 101–10 (1998).
251. Bellani, G. *et al.* Epidemiology, Patterns of Care, and Mortality for Patients With Acute Respiratory Distress Syndrome in Intensive Care Units in 50 Countries. *JAMA* **315**, 788 (2016).
252. Cho, W. H. *et al.* Prognostic Value of Sarcopenia for Long-Term Mortality in Extracorporeal Membrane Oxygenation for Acute Respiratory Failure. *ASAIO J.* 1 (2019) doi:10.1097/mat.0000000000001006.
253. Schweitzer, L. *et al.* What is the best reference site for a single MRI slice to assess whole body skeletal muscle and adipose tissue volumes in healthy adults? *Am. J. Clin. Nutr.* **102**, 58–65 (2015).
254. Derstine, B. A. *et al.* Skeletal muscle cutoff values for sarcopenia diagnosis using T10 to L5 measurements in a healthy US population. *Sci. Rep.* **8**, 1–8 (2018).
255. Patel, S. *et al.* Decline in skeletal muscle mass during veno-venous extracorporeal membrane oxygenation. *Intensive Care Med. Exp.* **7**, 000958 (2019).
256. Xiong, J., Zhang, L. & Bao, L. Complications and mortality of venovenous extracorporeal membrane oxygenation in the treatment of neonatal respiratory failure: A systematic review and meta-analysis. *BMC Pulm. Med.* **20**, (2020).

257. Thiolliere, F. *et al.* Intensive care-related loss of quality of life and autonomy at 6 months post-discharge: Does COVID-19 really make things worse? *Crit. Care 2022 261* **26**, 1–8 (2022).
258. Karagiannidis, C. *et al.* Complete countrywide mortality in COVID patients receiving ECMO in Germany throughout the first three waves of the pandemic. *Crit. Care* **25**, 1–2 (2021).
259. Henry, B. M. & Lippi, G. Poor survival with extracorporeal membrane oxygenation in acute respiratory distress syndrome (ARDS) due to coronavirus disease 2019 (COVID-19): Pooled analysis of early reports. *J. Crit. Care* **58**, 27 (2020).
260. van der Werf, A. *et al.* Skeletal muscle analyses: agreement between non-contrast and contrast CT scan measurements of skeletal muscle area and mean muscle attenuation. *Clin. Physiol. Funct. Imaging* **38**, 366–372 (2018).
261. Póvoa, P. *et al.* Early identification of intensive care unit-acquired infections with daily monitoring of C-reactive protein: a prospective observational study. *Crit. Care* **10**, (2006).
262. Zhang, Z. & Ni, H. C-reactive protein as a predictor of mortality in critically ill patients: a meta-analysis and systematic review. *Anaesth. Intensive Care* **39**, 854–861 (2011).
263. Zhou, J., Liu, B., Liang, C., Li, Y. & Song, Y. H. Cytokine Signaling in Skeletal Muscle Wasting. *Trends Endocrinol. Metab.* **27**, 335–347 (2016).
264. Doorduin, J., Van Hees, H. W. H., Van Der Hoeven, J. G. & Heunks, L. M. A. Monitoring of the respiratory muscles in the critically Ill. *Am. J. Respir. Crit. Care Med.* **187**, 20–27 (2013).
265. Demoule, A. *et al.* Diaphragm dysfunction on admission to the intensive care unit: Prevalence, risk factors, and prognostic impact - A prospective study. *Am. J. Respir. Crit. Care Med.* **188**, 213–219 (2013).
266. Mills, G. H. *et al.* Tracheal tube pressure change during magnetic stimulation of the phrenic nerves as an indicator of diaphragm strength on the intensive care unit. *Br. J. Anaesth.* **87**, 876–84 (2001).
267. Schepens, T., Dres, M., Heunks, L. & Goligher, E. C. Diaphragm-protective mechanical ventilation. *Curr. Opin. Crit. Care* **25**, 77–85 (2019).
268. Lerolle, N. *et al.* Ultrasonographic diagnostic criterion for severe diaphragmatic dysfunction after cardiac surgery. *Chest* **135**, 401–407 (2009).
269. Andrade-Junior, M. C. de *et al.* Skeletal Muscle Wasting and Function Impairment in Intensive Care Patients With Severe COVID-19. *Front. Physiol.* **0**, 207 (2021).
270. Formenti, P. *et al.* Respiratory and peripheral muscular ultrasound characteristics in ICU COVID 19 ARDS patients. *J. Crit. Care* **67**, 14–20 (2022).
271. Nakanishi, N. *et al.* Change in diaphragm and intercostal muscle thickness in mechanically ventilated patients: A prospective observational ultrasonography study. *J. Intensive Care* **7**, 1–10 (2019).
272. Grosu, H. B. *et al.* Diaphragm Muscle Thinning in Subjects Receiving Mechanical Ventilation and Its Effect on Extubation. *Respir. Care* **62**, (2017).
273. Schepens, T. *et al.* The course of diaphragm atrophy in ventilated patients assessed with ultrasound: a longitudinal cohort study. *Crit. Care* **19**, 422 (2015).
274. Supinski, G. S. & Ann Callahan, L. Diaphragm weakness in mechanically ventilated critically ill patients. *Crit. Care* **17**, (2013).
275. Jolley, C. J. *et al.* Neural respiratory drive in healthy subjects and in COPD. *Eur. Respir. J.* **33**, 289–297 (2009).
276. Murphy, P. B. *et al.* Neural respiratory drive as a physiological biomarker to monitor change during acute exacerbations of COPD. *Thorax* **66**, 602–608 (2011).
277. Walterspacher, S. *et al.* Activation of respiratory muscles during weaning from mechanical ventilation. *J. Crit. Care* **38**, 202–208 (2017).
278. Suh, E. S. *et al.* Neural respiratory drive predicts clinical deterioration and safe discharge in exacerbations of COPD. *Thorax* **70**, 1123–1130 (2015).
279. Moldoveanu, B. *et al.* Inflammatory mechanisms in the lung. *J. Inflamm. Res.* **2**, 1–11 (2009).
280. Bos, L. D. *et al.* Identification and validation of distinct biological phenotypes in patients with

acute respiratory distress syndrome by cluster analysis. *Thorax* **72**, 876–883 (2017).
281. Ranieri, V. M. *et al.* Effect of Mechanical Ventilation on Inflammatory Mediators in Patients With Acute Respiratory Distress Syndrome. *JAMA* **282**, 54 (1999).
282. Ebihara, S. *et al.* Mechanical ventilation protects against diaphragm injury in sepsis: interaction of oxidative and mechanical stresses. *Am. J. Respir. Crit. Care Med.* **165**, 221–228 (2002).
283. Coiffard, B. *et al.* Diaphragm echodensity in mechanically ventilated patients: a description of technique and outcomes. *Crit. Care* **25**, 64 (2021).
284. Goligher, E. C. *et al.* Clinical strategies for implementing lung and diaphragm-protective ventilation: avoiding insufficient and excessive effort. *Intensive Care Med.* **46**, 2314–2326 (2020).
285. Goligher, E. C. *et al.* Mechanical Ventilation–induced Diaphragm Atrophy Strongly Impacts Clinical Outcomes. *Am. J. Respir. Crit. Care Med.* **197**, 204–213 (2018).
286. Combes, A. *et al.* Extracorporeal Membrane Oxygenation for Severe Acute Respiratory Distress Syndrome. *N. Engl. J. Med.* **378**, 1965–1975 (2018).
287. Gea, J., Ausín, P., Martínez-Llorens, J. M. & Barreiro, E. Respiratory muscle senescence in ageing and chronic lung diseases. *Eur. Respir. Rev.* **29**, 1–8 (2020).
288. Millar, J. E., Fanning, J. P., McDonald, C. I., McAuley, D. F. & Fraser, J. F. The inflammatory response to extracorporeal membrane oxygenation (ECMO): a review of the pathophysiology. *Crit. Care* **20**, 387 (2016).
289. Sommers, J. *et al.* Feasibility of Exercise Testing in Patients Who Are Critically Ill: A Prospective, Observational Multicenter Study. *Arch. Phys. Med. Rehabil.* **100**, 239–246 (2019).
290. Welch, J. F., Kipp, S. & Sheel, A. W. Respiratory muscles during exercise: mechanics, energetics, and fatigue. *Curr. Opin. Physiol.* **10**, 102–109 (2019).
291. Sklar, M. C. *et al.* Association of Low Baseline Diaphragm Muscle Mass With Prolonged Mechanical Ventilation and Mortality Among Critically Ill Adults. *JAMA Netw. open* **3**, e1921520 (2020).
292. Parthasarathy, S., Jubran, A., Laghi, F. & Tobin, M. J. Sternomastoid, rib cage, and expiratory muscle activity during weaning failure. *J. Appl. Physiol.* **103**, 140–147 (2007).
293. Güerri, R. *et al.* Mass of intercostal muscles associates with risk of multiple exacerbations in COPD. *Respir. Med.* **104**, 378–88 (2010).
294. Duiverman, M. L. *et al.* Reproducibility and responsiveness of a noninvasive EMG technique of the respiratory muscles in COPD patients and in healthy subjects. *J. Appl. Physiol.* **96**, 1723–1729 (2004).
295. Puthucheary, Z. A. *et al.* Metabolic phenotype of skeletal muscle in early critical illness. *Thorax* **73**, 926–935 (2018).
296. Jouan-Lanhouet, S. *et al.* Necroptosis, in vivo detection in experimental disease models. *Semin. Cell Dev. Biol.* **35**, 2–13 (2014).
297. Chen, X. *et al.* Translocation of mixed lineage kinase domain-like protein to plasma membrane leads to necrotic cell death. *Cell Res.* **24**, 105–121 (2014).
298. Zhang, J., Yang, Y., He, W. & Sun, L. Necrosome core machinery: MLKL. *Cell. Mol. Life Sci.* **73**, 2153–2163 (2016).
299. Degterev, A., Zhou, W., Maki, J. L. & Yuan, J. *Assays for Necroptosis and activity of RIP kinases*. *Methods in Enzymology* vol. 545 (Elsevier Inc., 2014).
300. Chan, F. K.-M., Luz, N. F. & Moriwaki, K. Programmed Necrosis in the Cross Talk of Cell Death and Inflammation. *Annu. Rev. Immunol.* **33**, 79–106 (2014).
301. Chen, J., Kos, R., Garssen, J. & Redegeld, F. Molecular Insights into the Mechanism of Necroptosis: The Necrosome as a Potential Therapeutic Target. *Cells* **8**, 1486 (2019).
302. Weber, K., Roelandt, R., Bruggeman, I., Estornes, Y. & Vandenabeele, P. Nuclear RIPK3 and MLKL contribute to cytosolic necrosome formation and necroptosis. *Commun. Biol. 2018 11* **1**, 1–13 (2018).
303. Anderson, N. G. Co-Immunoprecipitation. *Methods Mol. Biol.* **88**, 35–45 (1998).

304. Petrie, E. J., Hildebrand, J. M. & Murphy, J. M. Insane in the membrane: a structural perspective of MLKL function in necroptosis. *Immunol. Cell Biol.* **95**, 152–159 (2017).
305. Langhans, C. *et al.* Inflammation-Induced Acute Phase Response in Skeletal Muscle and Critical Illness Myopathy. *PLoS One* **9**, e92048 (2014).
306. Vanlangenakker, N., Vanden Berghe, T. & Vandenabeele, P. Many stimuli pull the necrotic trigger, an overview. *Cell Death Differ.* **19**, 75–86 (2012).
307. Peterson, J. M., Feeback, K. D., Baas, J. H. & Pizza, F. X. Tumor necrosis factor-alpha promotes the accumulation of neutrophils and macrophages in skeletal muscle. *J. Appl. Physiol.* **101**, 1394–1399 (2006).
308. Kut, C., Mac Gabhann, F. & Popel, A. S. Where is VEGF in the body? A meta-analysis of VEGF distribution in cancer. *Br. J. Cancer 2007 977* **97**, 978–985 (2007).
309. Deasy, B. M. *et al.* Effect of VEGF on the Regenerative Capacity of Muscle Stem Cells in Dystrophic Skeletal Muscle. *Mol. Ther.* **17**, 1788–1798 (2009).
310. Hoier, B. & Hellsten, Y. Exercise-induced capillary growth in human skeletal muscle and the dynamics of VEGF. *Microcirculation* **21**, 301–314 (2014).
311. Morgan, J. E. *et al.* Necroptosis mediates myofibre death in dystrophin-deficient mice. *Nat. Commun.* **9**, 3655 (2018).
312. Bertheloot, D., Latz, E. & Franklin, B. S. Necroptosis, pyroptosis and apoptosis: an intricate game of cell death. *Cell. Mol. Immunol. 2021 185* **18**, 1106–1121 (2021).
313. Montes-Ibarra, M. *et al.* Prevalence and clinical implications of abnormal body composition phenotypes in patients with COVID-19: a systematic review. *Am. J. Clin. Nutr.* (2023) doi:10.1016/j.ajcnut.2023.04.003.

Chapter 9: Appendix

Appendix 9-1. Permission to use MUSCLE-UK samples in thesis

Queen Mary University of London
Barts & The London

Queen Mary University of London
Critical Care and Perioperative Medicine Group
Centre for Translational Medicine and Therapeutics
William Harvey Research Institute
London E1 4NS

RE: SAMPLES FROM MUSCLE-UK (NCT01106300)

To Whom It May Concern:

Samples (serum and whole muscle tissue and homogenate) from the above study were offered for further analysis by Dr Sunil Patel towards his higher degree.

Zudin Puthucheary MBBS B.Med.Sci D.UHM PGCME EDICM FRCP FHEA
FFICM PhD Clinical Senior Lecturer, William Harvey Research Institute,
Barts and The London School of Medicine & Dentistry, Queen Mary University of London
Consultant in Intensive Care, Royal London Hospital, Barts Health NHS Trust

Appendix 9-2. Raw data from musculoskeletal ultrasound reliability studies

Operator 1 (SP); intra-observer. Healthy volunteers

INTRA-OBSERVER					
DIA-INSP	SP1	SP2	Mean	SD	CoV
Healthy					
1	0.25	0.25	0.25	0.00	0.94%
2	0.21	0.21	0.21	0.00	1.13%
3	0.25	0.25	0.25	0.00	0.95%
5	0.17	0.19	0.18	0.01	7.71%
6	0.18	0.18	0.18	0.00	0.00%
7	0.25	0.25	0.25	0.00	0.00%
8	0.29	0.30	0.29	0.01	2.42%
9	0.29	0.28	0.28	0.00	1.66%
10	0.21	0.22	0.21	0.00	2.21%
11	0.22	0.22	0.22	0.00	0.00%
12	0.29	0.30	0.30	0.01	2.40%
13	0.23	0.22	0.23	0.01	3.10%
			0.24	**0.00**	**1.82%**

INTRA-OBSERVER					
PSM-INSP	SP1	SP2	Mean	SD	CoV
Healthy					
1	0.49	0.51	0.50	0.01	2.83%
2	0.35	0.37	0.36	0.01	3.29%
3	0.46	0.45	0.46	0.00	0.52%
5	0.32	0.31	0.32	0.01	2.98%
6	0.37	0.35	0.36	0.01	2.62%
7	0.35	0.33	0.34	0.01	4.20%
8	0.42	0.43	0.43	0.01	1.66%
9	0.39	0.40	0.40	0.00	1.19%
10	0.31	0.31	0.31	0.00	0.00%
11	0.47	0.47	0.47	0.00	0.00%
12	0.46	0.48	0.47	0.02	4.01%
13	0.26	0.27	0.26	0.01	2.70%
			0.39	**0.01**	**2.12%**

INTRA-OBSERVER					
DIA-EXP	SP1	SP2	Mean	SD	CoV
Healthy					
1	0.20	0.21	0.21	0.00	2.28%
2	0.19	0.18	0.19	0.01	3.82%
3	0.21	0.21	0.21	0.00	0.00%
5	0.13	0.15	0.14	0.01	10.10%
6	0.15	0.15	0.15	0.00	3.14%
7	0.23	0.21	0.22	0.01	5.40%
8	0.20	0.20	0.20	0.00	0.00%
9	0.20	0.18	0.19	0.01	4.96%
10	0.17	0.17	0.17	0.00	2.77%
11	0.17	0.17	0.17	0.00	0.00%
12	0.24	0.24	0.24	0.00	1.96%
13	0.17	0.17	0.17	0.00	0.00%
			0.19	**0.01**	**2.71%**

INTRA-OBSERVER					
PSM-EXP	SP1	SP2	Mean	SD	CoV
Healthy					
1	0.49	0.47	0.48	0.02	3.45%
2	0.35	0.35	0.35	0.00	1.35%
3	0.44	0.43	0.44	0.00	0.54%
5	0.32	0.30	0.31	0.01	3.78%
6	0.36	0.35	0.36	0.00	0.66%
7	0.33	0.32	0.33	0.01	2.89%
8	0.40	0.41	0.41	0.00	0.58%
9	0.39	0.40	0.39	0.00	1.20%
10	0.31	0.30	0.31	0.01	2.32%
11	0.47	0.47	0.47	0.00	0.50%
12	0.46	0.48	0.47	0.01	2.52%
13	0.26	0.26	0.26	0.00	0.00%
			0.38	**0.01**	**1.65%**

INTRA-OBSERVER					
DIA-TF	SP1	SP2	Mean	SD	CoV
Healthy					
1	0.25	0.19	0.22	0.04	17.96%
2	0.09	0.17	0.13	0.06	43.89%
3	0.16	0.17	0.16	0.01	6.73%
5	0.33	0.29	0.31	0.03	10.10%
6	0.20	0.25	0.22	0.04	17.25%
7	0.09	0.17	0.13	0.06	46.47%
8	0.41	0.46	0.43	0.03	8.00%
9	0.46	0.53	0.49	0.05	10.00%
10	0.26	0.25	0.26	0.01	2.77%
11	0.25	0.25	0.25	0.00	0.00%
12	0.19	0.27	0.23	0.05	23.34%
13	0.35	0.29	0.32	0.04	12.86%
			0.26	**0.04**	**13.40%**

INTRA-OBSERVER					
PSM-CSA	SP1	SP2	Mean	SD	CoV
Healthy					
1	1.37	1.24	1.30	0.09	6.79%
2	0.92	0.98	0.95	0.04	4.23%
3	1.07	1.06	1.06	0.01	0.67%
5	0.92	0.88	0.90	0.03	3.14%
6	0.96	0.89	0.92	0.05	5.11%
7	0.84	0.76	0.80	0.05	6.79%
8	0.87	0.89	0.88	0.02	1.88%
9	0.98	0.99	0.98	0.01	0.72%
10	1.00	1.05	1.03	0.04	3.45%
11	0.93	0.91	0.92	0.02	1.80%
12	1.38	1.28	1.33	0.07	5.33%
13	0.73	0.69	0.71	0.03	4.65%
			0.98	**0.04**	**3.77%**

INTRA-OBSERVER					
DIA-EXC	SP1	SP2	Mean	SD	CoV
Healthy					
1	2.82	2.87	2.85	0.04	1.32%
2	2.10	1.90	2.00	0.14	7.08%
3	2.11	2.00	2.05	0.08	3.90%
5	1.26	1.91	1.59	0.46	29.00%
6	2.11	1.97	2.04	0.10	4.85%
7	2.51	2.33	2.42	0.13	5.25%
8	2.55	2.67	2.61	0.08	3.16%
9	2.11	2.18	2.15	0.05	2.20%
10	1.96	2.04	2.00	0.06	2.95%
11	4.01	3.39	3.70	0.44	11.86%
12	2.35	2.17	2.26	0.13	5.74%
13	2.24	1.90	2.07	0.24	11.63%
			2.31	**0.16**	**7.01%**

INTRA-OBSERVER					
RF-CSA	SP1	SP2	Mean	SD	CoV
Healthy					
1	742.33	752.67	747.50	7.31	0.98%
2	370.33	371.67	371.00	0.94	0.25%
3	651.67	654.67	653.17	2.12	0.32%
5	496.00	500.00	498.00	2.83	0.57%
6	644.33	647.33	645.83	2.12	0.33%
7	605.00	610.67	607.83	4.01	0.66%
8	611.33	612.67	612.00	0.94	0.15%
9	407.33	410.33	408.83	2.12	0.52%
10	590.67	601.33	596.00	7.54	1.27%
11	794.00	810.33	802.17	11.55	1.44%
12	663.33	650.00	656.67	9.43	1.44%
13	485.33	490.33	487.83	3.54	0.72%
			590.57	**4.54**	**0.77%**

Operator 3 (RH); intra-observer. healthy volunteers

INTRA-OBSERVER					
DIA-INSP	RH1	RH2	Mean	SD	CoV
Healthy					
1	0.22	0.23	0.22	0.01	4.22%
2	0.21	0.21	0.21	0.00	1.13%
3	0.25	0.24	0.25	0.00	1.91%
5	0.16	0.16	0.16	0.00	0.00%
6	0.18	0.19	0.19	0.00	1.27%
7	0.24	0.24	0.24	0.00	0.00%
8	0.28	0.30	0.29	0.01	4.09%
9	0.28	0.28	0.28	0.00	0.84%
10	0.20	0.21	0.21	0.00	1.15%
11	0.22	0.21	0.22	0.00	1.10%
12	0.29	0.23	0.26	0.04	16.11%
13	0.24	0.23	0.23	0.00	2.02%
			0.23	**0.01**	**3.08%**

INTRA-OBSERVER					
PSM-INSP	RH1	RH2	Mean	SD	CoV
Healthy					
1	0.50	0.51	0.50	0.01	1.18%
2	0.35	0.36	0.36	0.01	1.97%
3	0.43	0.46	0.44	0.02	4.25%
5	0.34	0.38	0.36	0.03	8.55%
6	0.36	0.36	0.36	0.00	0.00%
7	0.34	0.33	0.33	0.00	1.41%
8	0.41	0.42	0.42	0.00	1.13%
9	0.41	0.39	0.40	0.01	2.93%
10	0.30	0.32	0.31	0.01	3.78%
11	0.48	0.48	0.48	0.00	0.49%
12	0.50	0.48	0.49	0.01	1.92%
13	0.27	0.26	0.27	0.01	3.54%
			0.39	**0.01**	**2.47%**

INTRA-OBSERVER					
DIA-EXP	RH1	RH2	Mean	SD	CoV
Healthy					
1	0.18	0.19	0.18	0.01	3.26%
2	0.16	0.18	0.17	0.02	9.61%
3	0.22	0.21	0.22	0.01	3.29%
5	0.16	0.15	0.15	0.00	3.07%
6	0.15	0.15	0.15	0.00	3.14%
7	0.22	0.22	0.22	0.00	0.00%
8	0.21	0.24	0.22	0.02	10.55%
9	0.18	0.19	0.19	0.01	3.82%
10	0.15	0.15	0.15	0.00	1.59%
11	0.17	0.16	0.17	0.01	4.20%
12	0.24	0.18	0.21	0.04	21.16%
13	0.18	0.17	0.18	0.00	2.67%
			0.18	**0.01**	**5.84%**

INTRA-OBSERVER					
PSM-EXP	RH1	RH2	Mean	SD	CoV
Healthy					
1	0.47	0.49	0.48	0.01	2.95%
2	0.35	0.34	0.35	0.00	0.68%
3	0.43	0.43	0.43	0.00	1.10%
5	0.32	0.35	0.34	0.02	6.33%
6	0.36	0.35	0.35	0.00	1.33%
7	0.33	0.33	0.33	0.00	0.72%
8	0.41	0.42	0.41	0.00	1.14%
9	0.41	0.39	0.40	0.01	2.36%
10	0.30	0.31	0.31	0.01	3.07%
11	0.48	0.47	0.48	0.00	0.99%
12	0.50	0.46	0.48	0.02	4.91%
13	0.26	0.26	0.26	0.00	0.90%
			0.38	**0.01**	**2.25%**

INTRA-OBSERVER					
DIA-TF	RH1	RH2	Mean	SD	CoV
Healthy					
1	0.23	0.24	0.23	0.01	5.07%
2	0.29	0.15	0.22	0.10	47.30%
3	0.14	0.16	0.15	0.02	10.72%
5	0.04	0.09	0.07	0.03	49.85%
6	0.20	0.27	0.23	0.05	23.27%
7	0.12	0.12	0.12	0.00	0.00%
8	0.35	0.24	0.30	0.08	28.41%
9	0.57	0.47	0.52	0.07	13.55%
10	0.36	0.41	0.38	0.04	9.90%
11	0.25	0.31	0.28	0.04	14.27%
12	0.21	0.30	0.25	0.06	25.60%
13	0.31	0.33	0.32	0.01	2.67%
			0.26	**0.04**	**17.03%**

INTRA-OBSERVER					
PSM-CSA	RH1	RH2	Mean	SD	CoV
Healthy					
1	1.29	1.30	1.29	0.01	0.55%
2	1.01	0.98	1.00	0.02	1.89%
3	1.07	1.05	1.06	0.01	1.33%
5	0.99	1.04	1.02	0.04	3.48%
6	0.91	0.96	0.94	0.04	3.78%
7	0.78	0.77	0.77	0.00	0.61%
8	0.87	0.92	0.90	0.04	4.21%
9	1.03	1.00	1.02	0.02	1.63%
10	0.95	0.99	0.97	0.02	2.43%
11	0.96	0.96	0.96	0.00	0.49%
12	1.29	1.34	1.32	0.04	3.05%
13	0.74	0.74	0.74	0.00	0.32%
			1.00	**0.02**	**2.01%**

INTRA-OBSERVER					
DIA-EXC	RH1	RH2	Mean	SD	CoV
Healthy					
1	2.86	2.33	2.59	0.37	14.36%
2	1.88	1.86	1.87	0.02	0.88%
3	1.84	1.80	1.82	0.03	1.43%
5	1.94	1.93	1.93	0.01	0.49%
6	1.95	2.08	2.02	0.09	4.44%
7	1.99	2.77	2.38	0.55	23.09%
8	2.78	2.90	2.84	0.09	3.07%
9	2.04	2.28	2.16	0.17	7.97%
10	1.96	2.15	2.06	0.14	6.65%
11	2.60	3.70	3.15	0.78	24.78%
12	2.32	2.12	2.22	0.14	6.26%
13	2.12	2.08	2.10	0.03	1.46%
			2.26	**0.20**	**8.88%**

INTRA-OBSERVER					
RF-CSA	RH1	RH2	Mean	SD	CoV
Healthy					
1	755.33	762.00	758.67	4.71	0.62%
2	393.67	415.67	404.67	15.56	3.84%
3	651.33	649.00	650.17	1.65	0.25%
5	515.67	509.00	512.33	4.71	0.92%
6	663.67	644.00	653.83	13.91	2.13%
7	608.33	613.00	610.67	3.30	0.54%
8	608.67	601.67	605.17	4.95	0.82%
9	431.33	420.33	425.83	7.78	1.83%
10	628.67	616.00	622.33	8.96	1.44%
11	813.67	824.00	818.83	7.31	0.89%
12	664.67	674.67	669.67	7.07	1.06%
13	517.67	477.00	497.33	28.76	5.78%
			602.46	**9.05**	**1.50%**

Operator 1 (SP); intra-observer. ICU patients

INTRA-OBSERVER					
DIA-INSP	SP1	SP2	Mean	SD	CoV
Round 1					
1	0.46	0.48	0.47	0.02	3.50%
2	0.41	0.46	0.43	0.03	7.61%
3	0.33	0.36	0.35	0.02	6.15%
5	0.23	0.22	0.23	0.01	3.14%
6	0.37	0.37	0.37	0.00	0.63%
7	0.47	0.45	0.46	0.02	4.10%
8	0.20	0.23	0.22	0.02	9.72%
9	0.25	0.23	0.24	0.02	6.83%
10	0.15	0.15	0.15	0.00	1.55%
11	0.35	0.35	0.35	0.00	0.67%
12	0.19	0.19	0.19	0.00	1.23%
13	0.33	0.34	0.33	0.01	2.83%
			0.32	**0.01**	**4.04%**

INTRA-OBSERVER					
DIA-EXP	SP1	SP2	Mean	SD	CoV
Round 1					
1	0.33	0.33	0.33	0.00	0.71%
2	0.33	0.38	0.36	0.03	8.63%
3	0.28	0.30	0.29	0.01	4.93%
5	0.20	0.19	0.20	0.01	3.63%
6	0.28	0.30	0.29	0.01	4.93%
7	0.38	0.38	0.38	0.00	0.00%
8	0.20	0.22	0.21	0.02	7.92%
9	0.21	0.18	0.19	0.02	11.07%
10	0.11	0.11	0.11	0.00	0.00%
11	0.23	0.23	0.23	0.00	0.00%
12	0.12	0.13	0.13	0.00	1.89%
13	0.28	0.29	0.28	0.00	1.66%
			0.25	**0.01**	**3.79%**

INTRA-OBSERVER					
DIA-TF	SP1	SP2	Mean	SD	CoV
Round 1					
1	0.38	0.46	0.42	0.06	14.17%
2	0.23	0.21	0.22	0.01	5.63%
3	0.19	0.21	0.20	0.01	7.21%
5	0.15	0.16	0.15	0.01	3.63%
6	0.34	0.26	0.30	0.06	18.73%
7	0.23	0.17	0.20	0.05	24.60%
8	0.03	0.06	0.05	0.02	39.97%
9	0.23	0.30	0.26	0.05	20.39%
10	0.44	0.41	0.42	0.02	5.24%
11	0.51	0.50	0.51	0.01	1.99%
12	0.54	0.53	0.53	0.01	1.89%
13	0.17	0.19	0.18	0.01	7.77%
			0.29	**0.03**	**9.46%**

INTRA-OBSERVER					
DIA-EXC	SP1	SP2	Mean	SD	CoV
Round 1					
1	1.09	1.12	1.10	0.02	1.71%
2	2.68	2.60	2.64	0.06	2.23%
3	1.70	1.53	1.61	0.12	7.30%
5	1.70	1.72	1.71	0.01	0.55%
6	2.23	2.41	2.32	0.12	5.38%
7	0.70	0.77	0.74	0.05	6.40%
8	1.39	1.56	1.47	0.12	8.00%
9	1.49	1.49	1.49	0.00	0.00%
10	0.95	1.27	1.11	0.22	20.14%
11	4.22	4.21	4.22	0.01	0.28%
12					
13	1.44	1.45	1.45	0.01	0.65%
			1.81	**0.07**	**3.73%**

INTRA-OBSERVER					
PSM-INSP	SP1	SP2	Mean	SD	CoV
Round 1					
1	0.72	0.70	0.71	0.01	2.00%
2	0.44	0.44	0.44	0.00	0.53%
3	0.69	0.68	0.68	0.00	0.69%
5	0.67	0.65	0.66	0.01	2.14%
6	0.36	0.34	0.35	0.01	3.35%
7	0.74	0.73	0.73	0.01	0.97%
8	0.26	0.26	0.26	0.00	1.81%
9	0.39	0.37	0.38	0.01	3.09%
10	0.23	0.23	0.23	0.00	0.00%
11	0.56	0.56	0.56	0.00	0.84%
12	0.57	0.57	0.57	0.00	0.41%
13	0.45	0.46	0.46	0.00	0.52%
			0.50	**0.01**	**1.33%**

INTRA-OBSERVER					
PSM-EXP	SP1	SP2	Mean	SD	CoV
Round 1					
1	0.67	0.65	0.66	0.02	2.51%
2	0.39	0.40	0.40	0.01	2.98%
3	0.61	0.63	0.62	0.01	2.28%
5	0.63	0.62	0.62	0.01	1.14%
6	0.32	0.32	0.32	0.00	1.47%
7	0.71	0.66	0.68	0.03	4.83%
8	0.25	0.25	0.25	0.00	0.94%
9	0.36	0.36	0.36	0.00	0.00%
10	0.23	0.22	0.23	0.00	2.08%
11	0.45	0.46	0.46	0.00	1.03%
12	0.48	0.48	0.48	0.00	0.98%
13	0.45	0.45	0.45	0.00	0.00%
			0.46	**0.01**	**1.88%**

INTRA-OBSERVER					
PSM-CSA	SP1	SP2	Mean	SD	CoV
Round 1					
1	1.06	1.08	1.07	0.01	0.88%
2	0.82	0.80	0.81	0.01	1.74%
3	1.06	0.97	1.01	0.07	6.51%
5	0.95	0.95	0.95	0.00	0.00%
6	0.61	0.63	0.62	0.01	2.28%
7	0.96	0.94	0.95	0.01	1.24%
8	0.84	0.78	0.81	0.04	4.66%
9	0.48	0.49	0.49	0.01	2.43%
10	0.69	0.68	0.68	0.00	0.69%
11	0.79	0.80	0.79	0.00	0.59%
12	0.80	0.79	0.80	0.01	1.48%
13	0.56	0.57	0.57	0.00	0.83%
			0.80	**0.02**	**2.00%**

INTRA-OBSERVER					
RF-CSA	SP1	SP2	Mean	SD	CoV
Round 1					
1	2.74	2.77	2.76	0.02	0.68%
2	3.62	3.47	3.55	0.10	2.86%
3	1.82	1.80	1.81	0.02	0.91%
5	1.45	1.43	1.44	0.02	1.15%
6	4.86	4.80	4.83	0.04	0.93%
7	2.09	2.03	2.06	0.04	2.18%
8	3.78	3.69	3.73	0.06	1.64%
9	2.67	2.68	2.68	0.01	0.26%
10	5.29	5.24	5.27	0.03	0.58%
11	5.87	5.80	5.83	0.05	0.89%
12	4.49	4.59	4.54	0.07	1.56%
13	3.35	3.36	3.36	0.00	0.14%
			3.49	**0.04**	**1.12%**

Operator 2 (SS); intra-observer. ICU patients

INTRA-OBSERVER					
DIA-INSP	SS1	SS2	Mean	SD	CoV
Round 1					
1	0.42	0.52	0.47	0.07	14.49%
2	0.45	0.46	0.46	0.01	2.06%
3	0.34	0.33	0.34	0.01	2.80%
5	0.22	0.23	0.23	0.00	2.08%
6	0.37	0.39	0.38	0.01	2.48%
7	0.47	0.46	0.46	0.01	1.53%
8	0.20	0.21	0.20	0.01	4.64%
9	0.27	0.27	0.27	0.00	1.75%
10	0.17	0.15	0.16	0.01	7.44%
11	0.36	0.36	0.36	0.00	0.66%
12	0.19	0.19	0.19	0.00	1.25%
13	0.30	0.33	0.32	0.02	5.24%
			0.32	**0.01**	**4.07%**

INTRA-OBSERVER					
DIA-EXP	SS1	SS2	Mean	SD	CoV
Round 1					
1	0.32	0.38	0.35	0.04	12.12%
2	0.34	0.36	0.35	0.01	2.69%
3	0.30	0.26	0.28	0.03	9.32%
5	0.19	0.20	0.20	0.01	6.04%
6	0.27	0.28	0.28	0.01	2.57%
7	0.38	0.39	0.39	0.00	1.22%
8	0.18	0.19	0.19	0.01	3.75%
9	0.24	0.21	0.23	0.02	8.32%
10	0.10	0.11	0.10	0.00	4.56%
11	0.23	0.25	0.24	0.01	5.89%
12	0.12	0.13	0.13	0.00	1.89%
13	0.26	0.28	0.27	0.02	6.07%
			0.25	**0.01**	**5.52%**

INTRA-OBSERVER					
DIA-TF	SS1	SS2	Mean	SD	CoV
Round 1					
1	0.32	0.37	0.35	0.03	9.31%
2	0.31	0.30	0.30	0.01	2.69%
3	0.16	0.27	0.21	0.08	37.11%
5	0.20	0.13	0.16	0.05	28.18%
6	0.38	0.38	0.38	0.00	0.33%
7	0.22	0.17	0.19	0.03	16.92%
8	0.07	0.09	0.08	0.01	11.99%
9	0.14	0.25	0.19	0.08	40.41%
10	0.67	0.41	0.54	0.18	34.33%
11	0.55	0.44	0.50	0.08	15.81%
12	0.54	0.47	0.51	0.05	9.32%
13	0.17	0.15	0.16	0.01	6.07%
			0.30	**0.05**	**16.98%**

INTRA-OBSERVER					
DIA-EXC	SS1	SS2	Mean	SD	CoV
Round 1					
1	1.14	1.14	1.14	0.00	0.00%
2	2.45	2.72	2.58	0.19	7.48%
3	1.60	1.63	1.61	0.02	1.46%
5	1.66	1.73	1.70	0.05	2.78%
6	2.50	2.02	2.26	0.34	14.90%
7	0.74	0.72	0.73	0.01	1.62%
8	1.39	1.40	1.39	0.01	0.68%
9	1.53	1.49	1.51	0.03	2.03%
10	1.35	1.29	1.32	0.04	3.21%
11	4.32	4.26	4.29	0.04	0.99%
12					
13	1.44	1.57	1.51	0.09	6.09%
			1.82	**0.08**	**4.14%**

INTRA-OBSERVER					
PSM-INSP	SS1	SS2	Mean	SD	CoV
Round 1					
1	0.68	0.70	0.69	0.02	2.39%
2	0.45	0.40	0.42	0.04	8.91%
3	0.72	0.78	0.75	0.04	5.68%
5	0.66	0.66	0.66	0.00	0.36%
6	0.38	0.38	0.38	0.00	1.24%
7	0.70	0.71	0.71	0.00	0.33%
8	0.22	0.28	0.25	0.04	16.14%
9	0.37	0.49	0.43	0.09	20.36%
10	0.24	0.24	0.24	0.00	0.99%
11	0.54	0.55	0.55	0.00	0.86%
12	0.56	0.57	0.57	0.01	1.25%
13	0.47	0.47	0.47	0.00	0.50%
			0.51	**0.02**	**4.09%**

INTRA-OBSERVER					
PSM-EXP	SS1	SS2	Mean	SD	CoV
Round 1					
1	0.63	0.64	0.64	0.00	0.37%
2	0.40	0.37	0.39	0.02	5.51%
3	0.69	0.74	0.71	0.04	5.29%
5	0.63	0.62	0.62	0.01	1.14%
6	0.33	0.33	0.33	0.00	1.43%
7	0.68	0.69	0.68	0.01	1.04%
8	0.22	0.28	0.25	0.05	18.86%
9	0.36	0.48	0.42	0.08	20.36%
10	0.23	0.23	0.23	0.00	0.00%
11	0.46	0.46	0.46	0.00	0.51%
12	0.49	0.51	0.50	0.01	2.85%
13	0.47	0.46	0.47	0.01	1.52%
			0.47	**0.02**	**4.14%**

INTRA-OBSERVER					
PSM-CSA	SS1	SS2	Mean	SD	CoV
Round 1					
1	1.07	1.08	1.08	0.01	1.10%
2	0.84	0.83	0.84	0.00	0.28%
3	0.98	1.02	1.00	0.02	2.36%
5	0.92	0.94	0.93	0.01	1.27%
6	0.64	0.64	0.64	0.00	0.00%
7	0.97	0.96	0.96	0.01	0.98%
8	0.76	0.82	0.79	0.04	5.39%
9	0.48	0.51	0.50	0.02	3.80%
10	0.69	0.70	0.70	0.00	0.34%
11	0.77	0.78	0.78	0.01	1.52%
12	0.81	0.80	0.80	0.01	0.88%
13	0.55	0.56	0.56	0.01	1.27%
			0.80	**0.01**	**1.55%**

INTRA-OBSERVER					
RF-CSA	SS1	SS2	Mean	SD	CoV
Round 1					
1	2.70	2.69	2.69	0.01	0.35%
2	3.66	3.72	3.69	0.04	1.02%
3	1.64	1.64	1.64	0.00	0.29%
5	1.56	1.41	1.48	0.11	7.16%
6	4.85	4.80	4.83	0.04	0.78%
7	2.34	2.30	2.32	0.03	1.12%
8	3.60	3.69	3.64	0.07	1.81%
9	2.76	2.80	2.78	0.02	0.89%
10	5.20	5.27	5.23	0.05	0.90%
11	5.76	5.77	5.77	0.01	0.12%
12	4.64	4.59	4.62	0.04	0.77%
13	3.36	3.21	3.29	0.11	3.23%
			3.50	**0.04**	**1.21%**

Operator 1 (SP) vs. Operator 3 (RH); inter-observer. healthy volunteers

INTER-OBSERVER					
DIA-INSP	SP	RH	Mean	SD	CoV
Round 1					
1	0.25	0.22	0.24	0.03	11.03%
2	0.21	0.21	0.21	0.00	0.00%
3	0.25	0.25	0.25	0.00	0.95%
5	0.17	0.16	0.17	0.01	4.20%
6	0.18	0.18	0.18	0.00	0.00%
7	0.25	0.24	0.25	0.00	0.96%
8	0.29	0.28	0.28	0.00	1.66%
9	0.29	0.28	0.29	0.00	0.83%
10	0.21	0.20	0.21	0.00	2.28%
11	0.22	0.22	0.22	0.00	0.00%
12	0.29	0.29	0.29	0.00	0.81%
13	0.23	0.24	0.24	0.00	1.00%
			0.23	**0.00**	**1.93%**
Round 2					
1	0.25	0.23	0.24	0.01	5.89%
2	0.21	0.21	0.21	0.00	0.00%
3	0.25	0.24	0.25	0.00	1.91%
4	0.19	0.16	0.18	0.02	11.90%
6	0.18	0.19	0.19	0.00	1.27%
7	0.25	0.24	0.25	0.00	0.96%
9	0.30	0.30	0.30	0.00	0.00%
10	0.28	0.28	0.28	0.00	0.00%
11	0.22	0.21	0.21	0.01	3.34%
12	0.22	0.21	0.22	0.00	1.10%
13	0.30	0.23	0.27	0.05	17.68%
14	0.22	0.23	0.23	0.00	2.08%
			0.23	**0.01**	**3.79%**

INTER-OBSERVER					
DIA-EXP	SP	RH	Mean	SD	CoV
Round 1					
1	0.20	0.18	0.19	0.02	9.92%
2	0.19	0.16	0.18	0.02	12.12%
3	0.21	0.22	0.22	0.00	2.18%
5	0.13	0.16	0.14	0.02	13.16%
6	0.15	0.15	0.15	0.00	0.00%
7	0.23	0.22	0.22	0.01	3.19%
8	0.20	0.21	0.21	0.00	1.15%
9	0.20	0.18	0.19	0.01	6.26%
10	0.17	0.15	0.16	0.01	7.44%
11	0.17	0.17	0.17	0.00	0.00%
12	0.24	0.24	0.24	0.00	0.00%
13	0.17	0.18	0.18	0.00	2.67%
			0.19	**0.01**	**4.51%**
Round 2					
1	0.21	0.19	0.20	0.02	8.95%
2	0.18	0.18	0.18	0.00	1.30%
3	0.21	0.21	0.21	0.00	1.11%
4	0.15	0.15	0.15	0.00	0.00%
6	0.15	0.15	0.15	0.00	0.00%
7	0.21	0.22	0.21	0.00	2.21%
9	0.20	0.24	0.22	0.03	11.70%
10	0.18	0.19	0.19	0.00	2.53%
11	0.17	0.15	0.16	0.02	11.79%
12	0.17	0.16	0.17	0.01	4.20%
13	0.24	0.18	0.21	0.04	19.23%
14	0.17	0.17	0.17	0.00	0.00%
			0.18	**0.01**	**5.58%**

INTER-OBSERVER					
DIA-TF	SP	RH	Mean	SD	CoV
Round 1					
1	0.25	0.23	0.24	0.01	5.83%
2	0.09	0.29	0.19	0.14	76.02%
3	0.16	0.14	0.15	0.01	9.61%
5	0.33	0.04	0.19	0.21	109.40%
6	0.20	0.20	0.20	0.00	0.00%
7	0.09	0.12	0.11	0.02	23.32%
8	0.41	0.35	0.38	0.04	10.17%
9	0.46	0.57	0.52	0.08	15.96%
10	0.26	0.36	0.31	0.07	21.95%
11	0.25	0.25	0.25	0.00	0.00%
12	0.19	0.21	0.20	0.01	4.88%
13	0.35	0.31	0.33	0.02	6.71%
			0.25	**0.05**	**20.45%**
Round 2					
1	0.19	0.24	0.22	0.04	17.21%
2	0.17	0.15	0.16	0.01	9.61%
3	0.17	0.16	0.17	0.01	5.62%
4	0.29	0.09	0.19	0.14	74.87%
6	0.25	0.27	0.26	0.02	6.15%
7	0.17	0.12	0.15	0.04	24.48%
9	0.46	0.24	0.35	0.16	45.35%
10	0.53	0.47	0.50	0.04	7.57%
11	0.25	0.41	0.33	0.11	34.14%
12	0.25	0.31	0.28	0.04	14.27%
13	0.27	0.30	0.28	0.02	7.20%
14	0.29	0.33	0.31	0.03	8.84%
			0.27	**0.05**	**20.45%**

INTER-OBSERVER					
DIA-EXC	SP	RH	Mean	SD	CoV
Round 1					
1	2.82	2.87	2.85	0.04	1.32%
2	2.10	1.90	2.00	0.14	7.08%
3	2.11	2.00	2.05	0.08	3.90%
5	1.26	1.91	1.59	0.46	29.00%
6	2.11	1.97	2.04	0.10	4.85%
7	2.51	2.33	2.42	0.13	5.25%
8	2.55	2.67	2.61	0.08	3.16%
9	2.11	2.18	2.15	0.05	2.20%
10	1.96	2.04	2.00	0.06	2.95%
11	4.01	3.39	3.70	0.44	11.86%
12	2.35	2.17	2.26	0.13	5.74%
13	2.24	1.90	2.07	0.24	11.63%
			2.31	**0.16**	**7.01%**
Round 2					
1	2.86	2.33	2.59	0.37	14.36%
2	1.88	1.86	1.87	0.02	0.88%
3	1.84	1.80	1.82	0.03	1.43%
4	1.94	1.93	1.93	0.01	0.49%
6	1.95	2.08	2.02	0.09	4.44%
7	1.99	2.77	2.38	0.55	23.09%
9	2.78	2.90	2.84	0.09	3.07%
10	2.04	2.28	2.16	0.17	7.97%
11	1.96	2.15	2.06	0.14	6.65%
12	2.60	3.70	3.15	0.78	24.78%
13	2.32	2.12			
14	2.12	2.08	2.10	0.03	1.46%
			2.26	**0.21**	**9.11%**

INTER-OBSERVER					
PSM-INSP	SP	RH	Mean	SD	CoV
Round 1					
1	0.49	0.50	0.49	0.00	0.96%
2	0.35	0.35	0.35	0.00	0.67%
3	0.46	0.43	0.44	0.02	4.25%
5	0.32	0.34	0.33	0.01	2.86%
6	0.37	0.36	0.37	0.00	0.65%
7	0.35	0.34	0.34	0.01	2.07%
8	0.42	0.41	0.42	0.00	1.13%
9	0.39	0.41	0.40	0.01	2.93%
10	0.31	0.30	0.31	0.01	2.29%
11	0.47	0.48	0.48	0.00	0.99%
12	0.46	0.50	0.48	0.03	5.93%
13	0.26	0.27	0.27	0.01	4.45%
			0.39	**0.01**	**2.42%**
Round 2					
1	0.51	0.51	0.51	0.00	0.70%
2	0.37	0.36	0.37	0.00	0.65%
3	0.45	0.46	0.46	0.00	0.52%
4	0.31	0.38	0.35	0.05	14.35%
6	0.35	0.36	0.36	0.01	1.97%
7	0.33	0.33	0.33	0.00	0.72%
9	0.43	0.42	0.43	0.01	1.66%
10	0.40	0.39	0.40	0.00	1.19%
11	0.31	0.32	0.32	0.00	1.49%
12	0.47	0.48	0.48	0.00	0.50%
13	0.48	0.48	0.48	0.00	0.00%
14	0.27	0.26	0.26	0.00	1.79%
			0.39	**0.01**	**1.92%**

INTER-OBSERVER					
PSM-EXP	SP	RH	Mean	SD	CoV
Round 1					
1	0.49	0.47	0.48	0.02	3.45%
2	0.35	0.35	0.35	0.00	1.35%
3	0.44	0.43	0.44	0.00	0.54%
5	0.32	0.30	0.31	0.01	3.78%
6	0.36	0.35	0.36	0.00	0.66%
7	0.33	0.32	0.33	0.01	2.89%
8	0.40	0.41	0.41	0.00	0.58%
9	0.39	0.40	0.39	0.00	1.20%
10	0.31	0.30	0.31	0.01	2.32%
11	0.47	0.47	0.47	0.00	0.50%
12	0.46	0.48	0.47	0.01	2.52%
13	0.26	0.26	0.26	0.00	0.00%
			0.38	**0.01**	**1.65%**
Round 2					
1	0.47	0.49	0.48	0.02	3.45%
2	0.35	0.34	0.35	0.01	2.03%
3	0.43	0.43	0.43	0.00	0.00%
4	0.30	0.35	0.33	0.03	10.10%
6	0.35	0.35	0.35	0.00	0.67%
7	0.32	0.33	0.32	0.00	1.46%
9	0.41	0.42	0.41	0.01	1.72%
10	0.40	0.39	0.40	0.00	0.60%
11	0.30	0.31	0.31	0.01	3.07%
12	0.47	0.47	0.47	0.00	0.50%
13	0.48	0.46	0.47	0.01	2.01%
14	0.26	0.26	0.26	0.00	0.00%
			0.38	**0.01**	**2.06%**

INTER-OBSERVER					
PSM-CSA	SP	RH	Mean	SD	CoV
Round 1					
1	1.37	1.29	1.33	0.06	4.27%
2	0.92	1.01	0.97	0.06	6.59%
3	1.07	1.07	1.07	0.00	0.44%
5	0.92	0.99	0.96	0.05	5.18%
6	0.96	0.91	0.93	0.03	3.54%
7	0.84	0.78	0.81	0.04	5.26%
8	0.87	0.87	0.87	0.00	0.27%
9	0.98	1.03	1.00	0.04	3.53%
10	1.00	0.95	0.98	0.03	3.38%
11	0.93	0.96	0.95	0.02	2.49%
12	1.38	1.29	1.33	0.06	4.78%
13	0.73	0.74	0.74	0.00	0.32%
			0.99	**0.03**	**3.44%**
Round 2					
1	1.24	1.30	1.27	0.04	3.07%
2	0.98	0.98	0.98	0.00	0.48%
3	1.06	1.05	1.06	0.00	0.22%
4	0.88	1.04	0.96	0.11	11.79%
6	0.89	0.96	0.93	0.05	5.35%
7	0.76	0.77	0.77	0.01	0.92%
9	0.89	0.92	0.91	0.02	2.60%
10	0.99	1.00	1.00	0.01	1.18%
11	1.05	0.99	1.02	0.04	4.40%
12	0.91	0.96	0.93	0.04	3.79%
13	1.28	1.34	1.31	0.05	3.60%
14	0.69	0.74	0.71	0.04	5.29%
			0.99	**0.03**	**3.52%**

INTER-OBSERVER					
RF-CSA	SP	RH	Mean	SD	CoV
Round 1					
1	742.33	755.33	748.83	9.19	1.23%
2	370.33	393.67	382.00	16.50	4.32%
3	651.67	651.33	651.50	0.24	0.04%
5	496.00	515.67	505.83	13.91	2.75%
6	644.33	663.67	654.00	13.67	2.09%
7	605.00	608.33	606.67	2.36	0.39%
8	611.33	608.67	610.00	1.89	0.31%
9	407.33	431.33	419.33	16.97	4.05%
10	590.67	628.67	609.67	26.87	4.41%
11	794.00	813.67	803.83	13.91	1.73%
12	663.33	664.67	664.00	0.94	0.14%
13	485.33	517.67	501.50	22.86	4.56%
			596.43	**11.61**	**1.95%**
Round 2					
1	752.67	762.00	757.33	6.60	0.87%
2	371.67	415.67	393.67	31.11	7.90%
3	654.67	649.00	651.83	4.01	0.61%
4	500.00	509.00	504.50	6.36	1.26%
6	647.33	644.00	645.67	2.36	0.37%
7	610.67	613.00	611.83	1.65	0.27%
9	612.67	601.67	607.17	7.78	1.28%
10	410.33	420.33	415.33	7.07	1.70%
11	601.33	616.00	608.67	10.37	1.70%
12	810.33	824.00	817.17	9.66	1.18%
13	650.00	674.67	662.33	17.44	2.63%
14	490.33	477.00	483.67	9.43	1.95%
			596.60	**9.49**	**1.59%**

Operator 1 (SP) vs. Operator 2 (SS); inter-observer. ICU patients

INTER-OBSERVER					
DIA-INSP	SP	SS	Mean	SD	CoV
Round 1					
1	0.46	0.42	0.44	0.03	5.87%
2	0.41	0.45	0.43	0.03	6.58%
3	0.33	0.34	0.34	0.01	2.80%
5	0.23	0.22	0.23	0.00	2.08%
6	0.37	0.37	0.37	0.00	0.63%
7	0.47	0.47	0.47	0.00	1.00%
8	0.20	0.20	0.20	0.00	2.36%
9	0.25	0.27	0.26	0.01	5.37%
10	0.15	0.17	0.16	0.01	5.89%
11	0.35	0.36	0.36	0.00	0.66%
12	0.19	0.19	0.19	0.00	0.00%
13	0.33	0.30	0.32	0.02	5.24%
			0.31	**0.01**	**3.26%**
Round 2					
1	0.48	0.52	0.50	0.03	5.17%
2	0.46	0.46	0.46	0.00	1.02%
3	0.36	0.33	0.35	0.02	6.15%
4	0.22	0.23	0.23	0.01	3.14%
6	0.37	0.39	0.38	0.01	2.48%
7	0.45	0.46	0.45	0.01	1.57%
9	0.23	0.21	0.22	0.02	7.44%
10	0.23	0.27	0.25	0.03	10.44%
11	0.15	0.15	0.15	0.00	0.00%
12	0.35	0.36	0.36	0.01	1.99%
13	0.19	0.19	0.19	0.00	2.48%
14	0.34	0.33	0.33	0.01	2.83%
			0.32	**0.01**	**3.60%**

INTER-OBSERVER					
DIA-EXP	SP	SS	Mean	SD	CoV
Round 1					
1	0.33	0.32	0.33	0.01	2.89%
2	0.33	0.34	0.34	0.01	2.09%
3	0.28	0.30	0.29	0.01	4.93%
5	0.20	0.19	0.19	0.01	4.88%
6	0.28	0.27	0.27	0.00	1.72%
7	0.38	0.38	0.38	0.00	0.00%
8	0.20	0.18	0.19	0.01	4.96%
9	0.21	0.24	0.22	0.02	10.55%
10	0.11	0.10	0.10	0.00	4.56%
11	0.23	0.23	0.23	0.00	1.02%
12	0.12	0.12	0.12	0.00	0.00%
13	0.28	0.26	0.27	0.01	5.24%
			0.25	**0.01**	**3.36%**
Round 2					
1	0.33	0.38	0.36	0.04	9.96%
2	0.38	0.36	0.37	0.01	3.86%
3	0.30	0.26	0.28	0.03	9.32%
4	0.19	0.20	0.20	0.01	4.79%
6	0.30	0.28	0.29	0.01	4.09%
7	0.38	0.39	0.39	0.00	1.22%
9	0.22	0.19	0.21	0.02	9.12%
10	0.18	0.21	0.20	0.03	13.30%
11	0.11	0.11	0.11	0.00	0.00%
12	0.23	0.25	0.24	0.01	4.88%
13	0.13	0.13	0.13	0.00	0.00%
14	0.29	0.28	0.29	0.00	0.83%
			0.25	**0.01**	**5.28%**

INTER-OBSERVER					
DIA-TF	SP	SS	Mean	SD	CoV
Round 1					
1	0.38	0.32	0.35	0.04	11.48%
2	0.23	0.31	0.27	0.06	21.10%
3	0.19	0.16	0.18	0.03	14.33%
5	0.15	0.20	0.17	0.03	18.95%
6	0.34	0.38	0.36	0.03	8.91%
7	0.23	0.22	0.23	0.01	5.44%
8	0.03	0.07	0.05	0.03	51.50%
9	0.23	0.14	0.18	0.06	33.70%
10	0.44	0.67	0.55	0.16	29.35%
11	0.51	0.55	0.53	0.03	4.84%
12	0.54	0.54	0.54	0.00	0.00%
13	0.17	0.17	0.17	0.00	0.00%
			0.30	**0.04**	**13.29%**
Round 2					
1	0.46	0.37	0.42	0.07	16.34%
2	0.21	0.30	0.26	0.06	23.97%
3	0.21	0.27	0.24	0.04	16.33%
4	0.16	0.13	0.14	0.02	13.09%
6	0.26	0.38	0.32	0.09	27.10%
7	0.17	0.17	0.17	0.00	2.41%
9	0.06	0.09	0.07	0.02	24.66%
10	0.30	0.25	0.28	0.04	13.30%
11	0.41	0.41	0.41	0.00	0.00%
12	0.50	0.44	0.47	0.04	9.03%
13	0.53	0.47	0.50	0.04	7.44%
14	0.19	0.15	0.17	0.02	13.81%
			0.29	**0.04**	**12.68%**

INTER-OBSERVER					
DIA-EXC	SP	SS	Mean	SD	CoV
Round 1					
1	1.09	1.14	1.12	0.04	3.17%
2	2.68	2.45	2.57	0.17	6.52%
3	1.70	1.60	1.65	0.07	4.29%
5	1.70	1.66	1.68	0.03	1.68%
6	2.23	2.50	2.37	0.19	7.97%
7	0.70	0.74	0.72	0.02	3.27%
8	1.39	1.39	1.39	0.00	0.17%
9	1.49	1.53	1.51	0.03	2.03%
10	0.95	1.35	1.15	0.28	24.35%
11	4.22	4.32	4.27	0.07	1.55%
12					
13	1.44	1.44	1.44	0.00	0.16%
			1.81	**0.08**	**4.51%**
Round 2					
1	1.12	1.14	1.13	0.02	1.46%
2	2.60	2.72	2.66	0.08	3.19%
3	1.53	1.63	1.58	0.07	4.48%
4	1.72	1.73	1.72	0.01	0.55%
6	2.41	2.02	2.22	0.27	12.33%
7	0.77	0.72	0.75	0.04	4.75%
9	1.56	1.40	1.48	0.11	7.49%
10	1.49	1.49	1.49	0.00	0.00%
11	1.27	1.29	1.28	0.01	1.10%
12	4.21	4.26	4.23	0.04	0.84%
13					
14	1.45	1.57	1.51	0.08	5.61%
			1.82	**0.07**	**3.67%**

INTER-OBSERVER					
PSM-INSP	SP	SS	Mean	SD	CoV
Round 1					
1	0.72	0.68	0.70	0.03	3.71%
2	0.44	0.45	0.45	0.01	1.59%
3	0.69	0.72	0.70	0.02	3.02%
5	0.67	0.66	0.67	0.01	1.06%
6	0.36	0.38	0.37	0.02	4.44%
7	0.74	0.70	0.72	0.02	3.27%
8	0.26	0.22	0.24	0.03	10.88%
9	0.39	0.37	0.38	0.02	4.36%
10	0.23	0.24	0.24	0.00	1.00%
11	0.56	0.54	0.55	0.01	1.71%
12	0.57	0.56	0.57	0.01	1.25%
13	0.45	0.47	0.46	0.01	2.55%
			0.50	**0.01**	**2.89%**
Round 2					
1	0.70	0.70	0.70	0.00	0.67%
2	0.44	0.40	0.42	0.03	7.86%
3	0.68	0.78	0.73	0.07	9.38%
4	0.65	0.66	0.65	0.00	0.72%
6	0.34	0.38	0.36	0.02	6.55%
7	0.73	0.71	0.72	0.01	1.97%
9	0.26	0.28	0.27	0.01	3.49%
10	0.37	0.49	0.43	0.08	19.11%
11	0.23	0.24	0.24	0.00	1.99%
12	0.56	0.55	0.56	0.01	1.69%
13	0.57	0.57	0.57	0.00	0.41%
14	0.46	0.47	0.47	0.01	2.53%
			0.51	**0.02**	**4.40%**

INTER-OBSERVER					
PSM-EXP	SP	SS	Mean	SD	CoV
Round 1					
1	0.67	0.63	0.65	0.03	3.98%
2	0.39	0.40	0.39	0.01	2.40%
3	0.61	0.69	0.65	0.05	8.36%
5	0.63	0.63	0.63	0.00	0.00%
6	0.32	0.33	0.33	0.01	3.63%
7	0.71	0.68	0.69	0.02	3.07%
8	0.25	0.22	0.23	0.02	10.10%
9	0.36	0.36	0.36	0.00	0.66%
10	0.23	0.23	0.23	0.00	1.02%
11	0.45	0.46	0.46	0.00	1.03%
12	0.48	0.49	0.48	0.01	1.47%
13	0.45	0.47	0.46	0.01	2.55%
			0.46	**0.01**	**3.14%**
Round 2					
1	0.65	0.64	0.64	0.01	1.10%
2	0.40	0.37	0.39	0.02	6.10%
3	0.63	0.74	0.69	0.08	11.35%
4	0.62	0.62	0.62	0.00	0.00%
6	0.32	0.33	0.33	0.00	0.73%
7	0.66	0.69	0.67	0.02	2.80%
9	0.25	0.28	0.27	0.02	7.91%
10	0.36	0.48	0.42	0.08	19.72%
11	0.22	0.23	0.23	0.01	3.10%
12	0.46	0.46	0.46	0.00	0.51%
13	0.48	0.51	0.50	0.02	3.33%
14	0.45	0.46	0.46	0.00	1.03%
			0.47	**0.02**	**4.67%**

INTER-OBSERVER					
PSM-CSA	SP	SS	Mean	SD	CoV
Round 1					
1	1.06	1.07	1.07	0.00	0.22%
2	0.82	0.84	0.83	0.01	1.14%
3	1.06	0.98	1.02	0.05	5.31%
5	0.95	0.92	0.94	0.02	2.52%
6	0.61	0.64	0.63	0.02	3.76%
7	0.96	0.97	0.96	0.01	0.98%
8	0.84	0.76	0.80	0.06	7.10%
9	0.48	0.48	0.48	0.00	0.98%
10	0.69	0.69	0.69	0.00	0.68%
11	0.79	0.77	0.78	0.02	2.12%
12	0.80	0.81	0.81	0.00	0.29%
13	0.56	0.55	0.56	0.01	1.69%
			0.80	**0.02**	**2.27%**
Round 2					
1	1.08	1.08	1.08	0.00	0.44%
2	0.80	0.83	0.82	0.02	2.59%
3	0.97	1.02	0.99	0.04	3.57%
4	0.95	0.94	0.95	0.01	1.25%
6	0.63	0.64	0.64	0.01	1.48%
7	0.94	0.96	0.95	0.01	1.24%
9	0.78	0.82	0.80	0.02	2.95%
10	0.49	0.51	0.50	0.01	2.35%
11	0.68	0.70	0.69	0.01	1.71%
12	0.80	0.78	0.79	0.01	1.19%
13	0.79	0.80	0.79	0.01	0.89%
14	0.57	0.56	0.57	0.01	1.25%
			0.80	**0.01**	**1.73%**

INTER-OBSERVER					
RF-CSA	SP	SS	Mean	SD	CoV
Round 1					
1	2.74	2.70	2.72	0.03	1.13%
2	3.62	3.66	3.64	0.03	0.91%
3	1.82	1.64	1.73	0.12	7.21%
5	1.45	1.56	1.50	0.08	5.02%
6	4.86	4.85	4.86	0.00	0.10%
7	2.09	2.34	2.21	0.17	7.88%
8	3.78	3.60	3.69	0.13	3.45%
9	2.67	2.76	2.72	0.06	2.26%
10	5.29	5.20	5.24	0.06	1.17%
11	5.87	5.76	5.82	0.08	1.34%
12	4.49	4.64	4.57	0.11	2.32%
13	3.35	3.36	3.36	0.00	0.14%
			3.50	**0.07**	**2.10%**
Round 2					
1	2.77	2.69	2.73	0.06	2.16%
2	3.47	3.72	3.60	0.17	4.79%
3	1.80	1.64	1.72	0.11	6.59%
4	1.43	1.41	1.42	0.01	1.00%
6	4.80	4.80	4.80	0.00	0.05%
7	2.03	2.30	2.16	0.19	8.93%
9	3.69	3.69	3.69	0.00	0.00%
10	2.68	2.80	2.74	0.08	2.88%
11	5.24	5.27	5.26	0.02	0.31%
12	5.80	5.77	5.78	0.02	0.33%
13	4.59	4.59	4.59	0.00	0.00%
14	3.36	3.21	3.29	0.11	3.23%
			3.48	**0.06**	**1.85%**

Appendix 9-3. Ultrasonographic changes in respiratory and skeletal muscle

	Non-ARDS (n=16)	**ARDS (n=28)**	**p value**
Change in RF_{CSA} (Day 3)	-5.6 (-10.9--1.88)	-7.1 (-9.4--4.3)	0.772
Change in RF_{CSA} (Day 7)	-13.1 (-18.3--8.1)	-16.0 (-20.7--10.3)	0.368
Change in RF_{CSA} (Day 14)	-23.4 (-30.5--18.0)	-23.4 (-30.7--16.8)	0.914
Change in DIA_{EXP} (Day 3)	0.0 (-18.8-4.9)	-4.2 (-10.3-0.0)	0.945
Change in DIA_{EXP} (Day 7)	-5.6 (-15.4-3.8)	-10.8 (-15.3-0.0)	0.549
Change in DIA_{EXP} (Day 14)	-15.8 (-30.2-2.0)	-11.6 (-22--4.6)	0.759
Change in PSM_{EXP} (Day 3)	0.0 (-5.4-4.5)	-5.8 (-7.7--2.1)	0.008
Change in PSM_{EXP} (Day 7)	-6.1 (-18.9-0.0)	-10.7 (-12.4--4.1)	0.903
Change in PSM_{EXP} (Day 14)	-9.4 (-16.0--1.7)	-10.5 (-15.6--4.9)	0.780
Change in PSM_{CSA} (Day 3)	-7.8 (-17.6--4.1))	-7.0 (-11.4--3.4)	0.493
Change in PSM_{CSA} (Day 7)	-7.8 (-23.6--6.8)	-12.3 (-14.8--7.8)	0.948
Change in PSM_{CSA} (Day 14)	-23.2 (-30.0--2.5)	-16.0 (-20.3--12.4)	0.558

Appendix 9-4. Systemic inflammatory mediators in high and low wasting patients

	All Patients (n=40)	Low Waster (<1.4%/day) (n=12)	High Waster (≥1.4%/day) (n=28)	p value
TNFR1 (pg/ml)				
Day 0	4086.0 (2698.0-9448.0)	2817.0 (2645.1-5704.5)	4910.1 (2725.6-11301.4)	0.995
Day 3	5439.0 (3344.0-7863.0)	4141.1 (3169.0-8256.2)	5789.4 (3583.4-7892.7)	0.726
Day 7	4668.0 (3397.0-10554.0)	4394.3 (3502.7-5337.1)	5132.4 (3362.4-14299.9)	0.227
Day 14	4622 (3810-9277)	4792.9 (3864.2-6781.0)	4570.3 (3738.6-15142.3)	0.325
TNF-α				
Day 0	50.5 (23.3-89.5)	34.0 (22.3-49.5)	68.1 (28.3-104.9)	0.104
Day 3	59.4 (42.3-79.7)	60.8 (33.5-65.6)	58.4 (42.8-92.8)	0.841
Day 7	61.3 (41.2-90.4)	54.2 (38.2-71.3)	67.4 (43.4-99.0)	0.926
Day 14	53.0 (37.0-80.5)	56.3 (37.3-102.8)	53.0 (36.2-68.9)	0.992
IL-6 (pg/ml)				
Day 0	28.8 (9.6-95.3)	22.7 (8.0-87.7)	42.3 (9.6-102.4)	0.623
Day 3	19.3 (8.0-40.2)	21.4 (4.1-51.8)	19.2 (8.4-40.3)	0.938
Day 7	19.5 (7.9-34.2)	12.4 (4.9-28.4)	21.9 (10.1-34.3)	0.893
Day 14	11.4 (7.0-18.4)	13.9 (6.3-16.9)	9.6 (7.1-27.3)	0.818
IL-8 (pg/ml)				
Day 0	30.2 (13.6-54.5)	15.0 (8.6-50.6)	35.4 (17.2-62.5)	0.925
Day 3	22.3 (15.8-37.6)	21.8 (14.9-34.7)	22.4 (15.8-38.6)	0.998
Day 7	21.3 (14.4-44.6)	19.9 (16.0-35.5)	23.1 (14.1-49.1)	0.996
Day 14	21.0 (14.0-31.0)	23.3 (17.1-165.4)	210. (14.0-31.3)	0.893
IL-10 (pg/ml)				
Day 0	85.2 (50.8-146.3)	53.0 (37.6-86.2)	100.9 (58.0-157.6)	0.984
Day 3	56.7 (30.5-100.0)	47.7 (20.9-181.9)	65.1 (30.6-99.1)	0.879
Day 7	13.1 (9.0-51.4)	67.1 (39.3-206.3)	10.6 (7.1-14.2)	0.069
Day 14	56.8 (44.8-120.9)	62.1 (41.7-205.2)	53.5 (43.6-110.8)	0.906
IFN-γ (pg/ml)				
Day 0	8.6 (2.2-33.4)	6.5 (1.8-35.2)	13.2 (2.6-37.6)	0.387
Day 3	8.8 (3.8-34.5)	5.7 (4.4-54.4)	8.2 (3.0-32.3)	0.801
Day 7	11.0 (6.7-15.3)	12.4 (4.9-28.4)	10.6 (7.1-14.2)	0.999
Day 14	10.8 (3.2-19.1)	9.3 (2.5-22.7)	10.8 (3.5-18.9)	0.924
MCP-1 (pg/ml)				
Day 0	384.6 (190.0-905.1)	318.4 (172.3-616.9)	479.1 (162.4-1057.1)	0.600
Day 3	315.3 (214.7-579.0)	344 (218.7-609.5)	315.3 (204.5-574.5)	0.999
Day 7	284.7 (226.3-471.8)	315 (248.8-523.4)	281.8 (173.7-458.2)	0.747
Day 14	248.4 (159.4-477.0)	236.4 (164.1-584.1)	248.4 (145.7-438.3)	0.994
RIPK-3 (pg/ml)				
Day 0	22289.0 (11600-42787)	11692.3 (8212.4-47222.1)	24069.1 (12482.9-41308.8)	0.968
Day 3	24740.0 (11531-45259)	26302.1 (9341.5-41824.8)	22405.4 (13160-46177.7)	0.993
Day 7	19293.0 (11946-35949)	12159.2 (8517.8-25530.0)	22199.8 (15637.7-39172.3)	0.199
Day 14	19429.0 (9765-36351)	9654.1 (6256.5-34019.1)	22220.3 (15020.6-36890.5)	0.885
CCK-18 (IU/L)				
Day 0	1166.0 (498.7-1741.0)	820.0 (121.8-1391.5)	1248.3 (560.1-1812.4)	0.355
Day 3	890.7 (468.3-1630.0)	433.5 (299.5-1154.4)	1026.8 (712.9-1897.2)	0.391
Day 7	768.1 (404.2-1344.0)	593.6 (332.1-1527.0)	840.6 (538.9-1282.4)	0.895
Day 14	534.9 (391.9-755.5)	560.3 (380.1-944.0)	532.7 (404.6-726.5)	0.990
TRAIL (pg/ml)				
Day 0	37.5 (19.7-65.9)	35.8 (18.3-91.3)	38.7 (24.5-65.9)	0.999
Day 3	73.9 (46.1-107.1)	89.3 (48.3-129.1)	73.1 (45.6-107.5)	0.891
Day 7	74.1 (54.2-99.7)	86.9 (57.7-131.2)	67.6 (46.5-85.0)	0.644
Day 14	82.3 (50.6-111.4)	61.9 (51.4-115.	88.3 (44.7-109.8)	0.946

Between group comparisons and study point performed using 2-way ANOVA, or mixed-effects model (when missing values present).

Appendix 9-5. Systemic inflammatory mediators in ARDS and non-ARDS patients

	All Patients (n=44)	Non-ARDS (n=16)	ARDS (n=28)	p value
TNFR1 (pg/ml)				
Day 0	3765.0 (2711.0-9849.0)	4998.7 (2758.5-13703.6)	3662.1 (2395.3-6832.7)	0.460
Day 3	5318.0 (3244.0-7952.0)	6665.7 (3392.8-14520.3)	5010.2 (3012.0-6906.9)	0.962
Day 7	4616.0 (3380.0-11663.0)	6983.2 (4123.9-17356.5)	4201.7 (3361.0-5685.1)	0.849
Day 14	4724.0 (3986.0-9761.0)	5254.5 (4504.2-16774.4)	4621.5 (3646.8-8271.3)	0.999
TNF-α				
Day 0	50.5 (24.1-99.2)	37.0 (22.8-51.8)	68.2 (31.1-108.9)	0.152
Day 3	58.9 (43.0-71.2)	46.3 (33.2-58.9)	63.2 (53.1-105.7)	**0.009**
Day 7	62.5 (44.3-79.6)	52.1 (32.8-84.3)	66.2 (49.2-83.9)	0.470
Day 14	56.9 (37.7-81.4)	43.5 (37.7-52.2)	66.7 (40.4-98.6)	0.086
IL-6 (pg/ml)				
Day 0	28.8 (9.6-102.4)	43.9 (19.2-126.2)	16.1 (6.0-102.4)	0.473
Day 3	18.2 (7.9-40.2)	15.7 (7.9-27.6)	24.0 (6.9-41.1)	0.384
Day 7	19.5 (7.9-34.2)	12.3 (4.3-25.3)	22.2 (11.4-34.8)	0.983
Day 14	13.5 (7.1-18.5)	14.3 (5.0-27.3)	12.4 (7.9-17.9)	0.999
IL-8 (pg/ml)				
Day 0	30.6 (14.9-62.5)	40.9 (14.9-73.7)	28.9 (13.6-52.3)	0.933
Day 3	21.6 (15.9-37.7)	20.5 (15.9-33.4)	24.8 (16.7-39.3)	0.999
Day 7	23.9 (16.3-53.9)	18.8 (12.0-67.5)	26.4 (18.5-51.9)	0.996
Day 14	22.8 (14.1-39.3)	18.4 (13.1-31.2)	24.2 (17.9-42.8)	0.604
IL-10 (pg/ml)				
Day 0	86.2 (53.0-132.8)	54.4 (32.6-108.6)	90.1 (68.9-167.9)	**0.045**
Day 3	56.8 (30.7-100.1)	43.4 (22.4-65.1)	73.5 (31.0-131.3)	0.901
Day 7	62.5 (37.3-122.2)	73.3 (33.2-165.3)	60.2 (37.3-87.1)	0.999
Day 14	60.9 (46.1-131.0)	48.4 (38.6-110.8)	67.6 (49.9-131.4)	0.608
IFN-γ (pg/ml)				
Day 0	7.2 (1.9-31.6)	2.6 (1.2-6.8)	21.5 (2.9-78.9)	**0.041**
Day 3	6.8 (3.5-29.3)	6.2 (2.2-19.2)	8.9 (3.8-42.2)	0.358
Day 7	10.8 (7.1-32.9)	9.5 (6.6-29.5)	11.0 (7.6-34.6)	0.976
Day 14	10.8 (2.9-19.4)	6.6 (2.9-18.6)	11.6 (2.7-24.0)	0.945
MCP-1 (pg/ml)				
Day 0	384.6 (226.2-905.1)	348.2 (171.8-678.2)	529.0 (228.4-1286.1)	0.200
Day 3	318.1 (220.8-581.2)	309.6 (213.3-416.1)	350.3 (227.5-634.4)	0.376
Day 7	312.5 (229.0-504.0)	261.6 (210.1-328.9)	395.5 (241.8-533.5)	0.950
Day 14	254.3 (162.0-438.3)	166.5 (145.7-247.7)	283.3 (239.5-531.6)	0.325
RIPK-3 (pg/ml)				
Day 0	23561.0 (11692.0-41309.0)	15347.8 (9452.2-27771.7)	30462 (12413.3-46281.3)	0.420
Day 3	22470.0 (11403.0-43207.0)	15810.9 (9215.3-24468.9)	27953.8 (12406.3-45259.0)	0.422
Day 7	19199.0 (9411.0-33558.0)	14048 (8356.5-18379.4)	24504 (14124.8-38819.2)	0.095
Day 14	19532 (10830.0-36891.0)	9654.1 (6737.1-19634.4)	24806 (18051.6-41800.8)	**0.059**
CCK-18 (IU/L)				
Day 0	1171.0 (531.5-1599.0)	551.6 (167.6-1351.6)	1244.6 (846.3-1741.0)	0.777
Day 3	899.1 (523.7-1575.0)	516.0 (272.9-925.0)	1200.1 (715.9-1897.2)	0.100
Day 7	834.0 (444.9-1500.0)	599.4 (372.1-1499.9)	845.5 (559.4-1578.8)	0.786
Day 14	547.6 (388.6-881.9)	914.4 (453.7-1145.9)	530.6 (320.6-674.9)	0.518
TRAIL (pg/ml)				
Day 0	38.7 (19.8-96.3)	22.2 (12.0-121.6)	52.3 (35.6-121.6)	**0.001**
Day 3	73.7 (45.9-107.4)	49.1 (30.2-67.8)	89.8 (52.6-111.4)	0.166
Day 7	70.9 (53.0-105.3)	59.1 (33.4-72.4)	78.0 (61.6-132.1)	**0.007**
Day 14	69.3 (49.1-109.8)	52.1 (44.3-69.3)	88.5 (53.7-119.0)	0.093

Between group comparisons and study point performed using 2-way ANOVA, or mixed-effects model (when missing values present).

Appendix 9-6. Systemic inflammatory mediators in COVID19 and non-COVID19 patients

	All Patients (n=43)	Non-COVID19 ARDS	COVID19 ARDS (n=)	p value
TNFR1 (pg/ml)				
Day 0	3765.0 (2711.0-9849.0)	3676.3 (2621.1-11718.1)	3854.6 (2778.2-6063.9)	0.807
Day 3	5318 (3244.0-7952.0)	5789.4 (3246.2-14485.0)	5198.2 (3235.8-6928.8)	0.782
Day 7	4616 (3380.0-11663.0)	4730.6 (3346.9-16463.1)	4300.8 (3539.9-7588.4)	0.967
Day 14	4724.0 (3986.0-9761.0)	4792.9 (4102.4-10246.0)	4654.5 (3809.5-12741.4)	0.803
TNF-α (pg/ml)				
Day 0	50.5 (24.1-99.2)	32.7 (23.0-66.5)	80.4 (54.0-115.9)	0.182
Day 3	58.9 (43.0-71.4)	46.3 (31.5-60.7)	65.3 (58.1-131.2)	**0.042**
Day 7	62.5 (44.3-79.6)	50.6 (40.9-76.0)	70.6 (59.0-107.6)	0.674
Day 14	56.9 (37.7-81.4)	46.4 (37.4-57.0)	66.7 (46.1-103.7)	0.094
IL-6 (pg/ml)				
Day 0	28.8 (9.6-102.4)	28.7 (8.4-113.9)	32.4 (10.1-215.3)	0.980
Day 3	18.2 (7.9-40.2)	15.7 (7.9-32.1)	28.6 (8.1-48.5)	0.435
Day 7	19.5 (7.8-34.2)	13.6 (5.2-34.2)	22.4 (12.6-36.1)	0.995
Day 14	13.5 (7.1-18.5)	15.4 (5.0-29.5)	11.3 (8.2-16.5)	0.785
IL-8 (pg/ml)				
Day 0	30.6 (14.9-62.5)	36.2 (14.0-73.1)	27.7 (16.3-42.8)	0.895
Day 3	21.6 (15.9-37.7)	21.6 (15.8-44.6)	26.4 (17.6-37.6)	0.816
Day 7	23.9 (16.3-53.9)	20.6 (13.1-54.6)	28.2 (18.9-51.3)	0.999
Day 14	22.8 (14.1-39.4)	19.7 (13.3-30.5)	26.7 (16.4-51.6)	0.605
IL-10 (pg/ml)				
Day 0	86.2 (53.0-132.8)	80.7 (40.1-110.7)	122.7 (60.9-198.1)	0.499
Day 3	56.8 (30.7-100.1)	50.8 (29.8-87.8)	68.5 (30.6-136.4)	0.874
Day 7	62.5 (37.3-122.2)	76.6 (38.6-173.3)	58.8 (29.8-76.2)	0.917
Day 14	60.9 (46.1-131.0)	49.0 (38.0-126.2)	71.7 (52.1-131.3)	0.962
IFN-γ (pg/ml)				
Day 0	7.2 (1.9-31.6)	2.5 (1.7-6.9)	30.6 (17.6-98.6)	0.132
Day 3	6.8 (3.4-29.3)	5.0 (2.2-21.7)	9.3 (5.9-43.1)	0.581
Day 7	10.8 (7.1-33.0)	9.8 (7.2-15.3)	12.2 (9.0-42.3)	0.977
Day 14	10.8 (2.9-19.4)	10.4 (2.7-27.4)	10.8 (3.0-19.1)	0.995
MCP-1 (pg/ml)				
Day 0	384.6 (226.2-905.1)	338.9 (151.2-655.7)	722.7 (343.1-1518.8)	**0.031**
Day 3	318.1 (220.8-581.2)	287.1 (189.5-480.8)	380.8 (244.0-976.8)	0.135
Day 7	312.5 (229.0-504.0)	255.1 (203.5-444.8)	413.3 (284.7-613.2)	0.751
Day 14	254.3 (162.0-438.3)	164.3 (135.2-314.7)	289.0 (251.4-543.3)	0.331
RIPK-3 (pg/ml)				
Day 0	23561.0 (11692.0-41309.0)	21700.7 (10456.2-45476.3)	24069.1 (12346.8-41308.8)	0.977
Day 3	22470.0 (11403.0-43207.0)	10562.7 (5547.6-22309.8)	26136.4 (13616.1-31468.3)	0.254
Day 7	19199.0 (9411.0-33558)	16542.7 (8926.8-44778.1)	21022.7 (11113.1-33314.7)	0.891
Day 14	19532.0 (10830.0-36891.0)	19634.4 (7886.8-35271.4)	19090.6 (15547.4-41787.0)	0.993
CCK-18 (IU/L)				
Day 0	1171.0 (531.5-1599.0)	824.4 (298.5-1325.6)	1246.8 (1154.1-1784.0)	0.898
Day 3	899.1 (523.7-1575.0)	715.9 (299.5-1241.2)	1200.1 (812.8-1637.5)	0.999
Day 7	834.0 (444.9-1500.0)	622.3 (384.2-1860.0)	980.5 (706.1-1374.7)	0.999
Day 14	547.6 (388.6-881.9)	725.3 (422.9-1145.9)	534.9 (259.4-674.9)	0.334
TRAIL (pg/ml)				
Day 0	38.7 (19.7-96.3)	24.5 (14.4-42.1)	104.6 (45.4-143.2)	**0.001**
Day 3	77.7 (45.9-107.4)	51.6 (32.9-91.6)	106.2 (68.3 (130.4)	0.088
Day 7	70.9 (53.0-49.1)	62.9 (38.6-80.8)	80.3 (64.3-140.6)	0.140
Day 14	69.3 (49.1-109.8)	52.6 (42.5-92.5)	88.3 (53.9-125.9)	0.231

Between group comparisons and study point performed using 2-way ANOVA, or mixed-effects model (when missing values present).

Appendix 9-7. Linear mixed effects models of parasternal muscle thickness

Dependent variable: Parasternal muscle end-expiratory thickness (natural logarithm of measured value).

Fixed Effects	**Random Effects**
• Day of mechanical ventilation • Age(years) • Sex • SOFA score • Neuromuscular blockers • Level of sedation	Subject (intercepts and slopes) <u>*Pre-specified Rationale for Model Variable Selection*</u> • Day of mechanical ventilation – this variable was employed to assess the effect of time on parasternal muscle thickness (i.e. to establish the magnitude and rate of atrophy) • Age – this variable was deemed *a priori* to be a potentially important determinant of parasternal muscle thickness and atrophy • Sex – this variable was deemed *a priori* to be a potentially important determinant of parasternal muscle thickness and atrophy • Daily SOFA score (average over first 7 days) - based on previous observations regarding the effect of multiple organ failure on muscle function and injury during critical illness, this variable was deemed *a priori* to be a potentially important determinant of parasternal muscle thickness and atrophy • Neuromuscular blocker use – this variable was deemed *a priori* to be a potentially important determinant of parasternal muscle thickness and atrophy • Level of sedation (average RASS first 7 days) – this variable was deemed *a priori* to be a potentially important determinant of parasternal muscle thickness and atrophy

Appendix 9-8. Linear mixed effects models of parasternal contractile activity

Dependent variable: Parasternal muscle thickening fraction or strain

Fixed Effects	**Random Effects**
• Day of mechanical ventilation • Tidal volume • PEEP • Neuromuscular blockers • Level of sedation	Subject (intercepts and slopes) <u>*Pre-specified Rationale for Model Variable Selection*</u> • Day of mechanical ventilation – this variable was employed to assess the effect of • time on parasternal muscle contractile activity (i.e. to establish the magnitude and rate of change) • Tidal volume – as per IBW, average over first 3 days, increasing tidal volume during pressure targeted ventilation can suggest an increase in ventilatory motor output • PEEP - average over first 3 days - higher values of PEEP result in greater end- expiratory intrathoracic volume and diaphragm lengthening. This may impact measurements of diaphragm thickening during mechanical ventilation. • Neuromuscular blocker use – this variable was deemed *a priori* to be a potentially important determinant

Appendix 9-9. Linear mixed effects models of diaphragm end-expiratory thickness

Dependent variable: Diaphragm muscle thickness (natural logarithm of measured value)

Before examining the effect of diaphragm contractile activity on PSM thickness, I repeated the model of Gohlighter *et al.,*[114] to attempt to replicate and establish the relationship between diaphragm thickness and diaphragm contractile activity in our study cohort.

Fixed Effects	**Random Effects**
• Day of mechanical ventilation • Age (years) • Sex • SOFA score • Neuromuscular blockers • Level of sedation	Subject (intercepts and slopes) *Pre-specified Rationale for Model Variable Selection* •

Appendix 9-10. Linear mixed effects modelling: PSM thickness over ICU admission

Model Variable	**Beta coefficient (95% CI)**	**P-value**
Day of ICU admission (days)	-0.009 (-0.013– -0.006)	<0.001
Age (years)	0.000 (-0.003– 0.004)	0.814
Sex (=male)	0.188 (0.084– 0.290)	0.001
SOFA score^	-0.001 (-0.018– 0.016)	0.914
Neuromuscular use in first 3 days (=yes)	0.043 (-0.071– 0.157)	0.452
Level of sedation[$]	0.029 (-0.005– 0.063)	0.096

Dependent variable Parasternal muscle thickness (natural logarithm of measured value). Random intercepts and random slopes. ^Average over first 7 days of ICU admission. [$]Average RASS over first 7 days of ICU admission. ICU - intensive care unit, SOFA - sequential organ failure assessment score

Subsequent models were extensions of the primary linear mixed effects model of PSM thickness over time. In studies with available parasternal muscle thickening fraction and strain measurements I repeated the primary model of parasternal muscle thickness to examine the effect of contractile activity over time using interaction terms. The coefficients for these interaction terms represent the magnitude by which the exposures modified the variation in parasternal muscle thickness over time.

Appendix 9-11. PSM thickness over ICU admission and effect of PSM thickening fraction

Model Variable	**Beta coefficient (95% CI)**	**P-value**
Day of ICU admission (days)	-0.010 (-0.014– -0.006)	<0.001
Age (years)	0.000 (-0.005– 0.003)	0.659
Sex (=male)	0.228 (0.098– 0.359)	0.001
SOFA score^	-0.001 (-0.043– 0.023)	0.544
Neuromuscular use in first 3 days (=yes)	-0.095 (-0.263– 0.073)	0.258
Level of sedation$	-0.077 (-0.157– 0.003)	0.059
Parasternal muscle thickening fraction#	0.003 (-0.002–0.007)	0.241
Day of ICU admission* Parasternal muscle thickening fraction	0.000 (0.000–0.000)	0.953

Dependent variable Parasternal muscle thickness (natural logarithm of measured value). Random intercepts and random slopes. ^Average over first 7 days of ICU admission. $Average RASS over first 7 days of ICU admission. #Time-varying measurement of parasternal muscle thickening fraction. ICU - intensive care unit, SOFA - sequential organ failure assessment score

Appendix 9-12. PSM thickness over ICU admission and effect of PSM strain

Model Variable	**Beta coefficient (95% CI)**	**P-value**
Day of ICU admission (days)	-0.008 (-0.014– -0.006)	<0.001
Age (years)	0.001 (-0.006– 0.003)	0.583
Sex (=male)	0.201 (0.068– 0.333)	0.004
SOFA score^	0.002 (-0.030– 0.031)	0.988
Neuromuscular use in first 3 days (=yes)	-0.078 (-0.248– 0.092)	0.359
Level of sedation$	-0.052 (-0.132– 0.029)	0.200
Parasternal muscle strain#	0.005 (-0.007–0.017)	0.399
Day of ICU admission* Parasternal muscle strain	0.000 (-0.001–0.001)	0.666

Dependent variable Parasternal muscle thickness (natural logarithm of measured value). Random intercepts and random slopes. ^Average over first 7 days of ICU admission. $Average RASS over first 7 days of ICU admission. # Time-varying measurement of parasternal muscle strain. ICU - intensive care unit, SOFA - sequential organ failure assessment score.

Appendix 9-13. Parasternal muscle thickness and rectus femoris cross-sectional area

Model Variable	**Beta coefficient (95% CI)**	**P-value**
Day of ICU admission (days)	0.001 (-0.011– 0.013)	0.834
Age (years)	0.002 (-0.001– 0.005)	0.233
Sex (=male)	0.130 (0.022– 0.243)	0.020
SOFA score^	0.000 (-0.015– 0.017)	0.833
Neuromuscular use in first 3 days (=yes)	0.029 (-0.083– 0.141)	0.607
Level of sedation[$]	0.033 (0.000– 0.066)	0.059
Rectus femoris CSA[#]	0.168 (0.042– 0.295)	0.009
Rectus femoris CSA * day of ICU admission	-0.005 (-0.014– 0.003)	0.214

Dependent variable parasternal muscle thickness (natural logarithm of measured value). Random intercepts and random slopes. ^Average over first 7 days of ICU admission. *[$]Average RASS over first 7 days of ICU admission. #Rectus femoris CSA (natural logarithm of measured value in cm) ICU - intensive care unit, SOFA - sequential organ failure assessment score, CSA - cross-sectional area.*

Appendix 9-14. PSM thickness and association with diaphragm thickness over ICU admission

Model Variable	**Beta coefficient (95% CI)**	**P-value**
Day of ICU admission (days)	0.012 (-0.005– 0.028)	0.163
Age (years)	-0.002 (-0.006– 0.002)	0.401
Sex (=male)	0.192 (0.061– 0.323)	0.005
SOFA score^	0.002 (-0.028– 0.032)	0.896
Neuromuscular use in first 3 days (=yes)	-0.095 (-0.263– 0.074)	0.262
Level of sedation[$]	-0.061 (-0.140– 0.018)	0.125
Diaphragm thickness (mm)	0.035 (-0.032– 0.103)	0.300
Diaphragm thickness * day of ICU admission	-0.009 (-0.016– -0.002)	0.014

Dependent variable parasternal muscle thickness (natural logarithm of measured value). Random intercepts and random slopes. ^Average over first 7 days of ICU admission. [$]Average RASS over first 7 days of ICU admission. ICU - intensive care unit, SOFA - sequential organ failure assessment score.

Appendix 9-15. Diaphragm thickening fraction over ICU admission

Model Variable	**Beta coefficient (95% CI)**	**P-value**
Day of ICU admission (days)	0.793 (0.309– 1.278)	0.015
Sex (male)	-0.940 (-7.337– 5.479)	0.766
Sofa score^	0.459 (-0.767– 1.686)	0.457
Neuromuscular use in first 3 days (=yes)	-6.840 (-12.727– -0.952)	0.024

Dependent variable diaphragm thickening fraction. Random intercepts and random slopes. ^Average over first 7 days of ICU admission. ICU - intensive care unit.

Appendix 9-16. Diaphragm thickness and association with diaphragm thickening fraction

Dependent variable: Diaphragm muscle thickness (natural logarithm of measured value)

Random Effects: Subject (intercepts and slopes)

Fixed Effects: day of mechanical ventilation, age (years), sex, SOFA score, neuromuscular blockers, level of sedation.

Model Variable	**Beta coefficient (95% CI)**	**P-value**
Day of ICU admission (days)	-0.010 (-0.014– -0.006)	<0.001
Age (years)	0.001 (-0.003– 0.005)	0.681
Sex (=male)	0.110 (-0.021– 0.241)	0.097
SOFA score^	0.010 (-0.023– 0.043)	0.539
Neuromuscular use in first 3 days (=yes)	0.074 (-0.089– 0.238)	0.362
Level of sedation$	-0.029 (-0.120– 0.052)	0.467
Diaphragm thickening fraction (%)	-0.004 (-0.006– -0.001)	0.300
Diaphragm thickening fraction * day of ICU admission	0.0002 (0.0000– 0.0004)	0.005

Dependent variable diaphragm muscle thickness (natural logarithm of measured value). Random intercepts and random slopes. ^Average over first 7 days of ICU admission. $Average RASS over first 7 days of ICU admission. ICU - intensive care unit, SOFA - sequential organ failure assessment score.

Appendix 9-17. PSM thickness and association with diaphragm thickening fraction

Model Variable	**Beta coefficient (95% CI)**	**P-value**
Day of ICU admission (days)	-0.010 (-0.014– -0.007)	<0.001
Age (years)	-0.001 (-0.005– 0.004)	0.778
Sex (=male)	0.244 (0.108– 0.380)	0.001
SOFA score^	-0.013 (-0.048– 0.021)	0.437
Neuromuscular use in first 3 days (=yes)	-0.114 (-0.286– 0.057)	0.184
Level of sedation[$]	-0.087 (-0.170– -0.004)	0.040
Diaphragm thickening fraction (%)	0.000 (-0.002– 0.002)	0.974
Diaphragm thickening fraction * day of ICU admission	0.000 (0.000– 0.000)	0.305

Dependent variable parasternal muscle thickness (natural logarithm of measured value). Random intercepts and random slopes. ^Average over first 7 days of ICU admission. [$]Average RASS over first 7 days of ICU admission. ICU - intensive care unit, SOFA - sequential organ failure assessment score.

Appendix 9-18. Diaphragm thickness and association with PSM strain and thickening fraction

Model Variable	**Beta coefficient (95% CI)**	**P-value**
Day of ICU admission (days)	-0.001 (-0.012– -0.004)	<0.001
Age (years)	0.001 (-0.003– 0.005)	0.655
Sex (=male)	0.093 (-0.036– 0.222)	0.152
SOFA score^	0.013 (-0.017– 0.042)	0.390
Neuromuscular use in first 3 days (=yes)	0.073 (-0.091– 0.238)	0.370
Level of sedation$	0.006 (-0.071– 0.084)	0.868
PSM strain	0.017 (0.002– 0.031)	0.020
PSM strain * day of ICU admission	-0.001 (-0.002– 0.000)	0.054

Model Variable	**Beta coefficient (95% CI)**	**P-value**
Day of ICU admission (days)	-0.008 (-0.011– -0.004)	<0.001
Age (years)	0.000 (-0.003– 0.004)	0.913
Sex (=male)	0.091 (-0.032– 0.214)	0.143
SOFA score^	0.022 (-0.008– 0.052)	0.156
Neuromuscular use in first 3 days (=yes)	0.097 (-0.060– 0.253)	0.220
Level of sedation$	-0.009 (-0.084– 0.066)	0.807
PSM thickening fraction	-0.006 (-0.012– 0.001)	0.089
PSM thickening * day of ICU admission	0.000 (0.000– 0.001)	0.091

Dependent variable diaphragm thickness (natural logarithm of measured value). Random intercepts and random slopes. ^Average over first 7 days of ICU admission. $Average RASS over first 7 days of ICU admission. ICU - intensive care unit, SOFA - sequential organ failure assessment score.

Appendix 9-19. Parasternal muscle thickening fraction and strain and ventilation strategy

Model Variable	Beta coefficient (95% CI)	P-value
Day of ICU admission (days)	0.430 (0.156– 0.717)	0.003
Tidal volume* (ml)	0.009 (0.001– 0.017)	0.036
PEEP$^{\$}$ (cmH_2O)	-0.096 (-0.461– 0.268)	0.596
Neuromuscular use in first 3 days (=yes)	-2.13 (-4.481– 0.219)	0.074

PSM thickening fraction over ICU admission.

*Dependent variable Parasternal muscle thickening fraction. Random intercepts and random slopes. *Average over first 3 days of ICU admission. $^{\$}$Average over first 3 days of ICU admission. ICU - intensive care unit, PEEP - positive end expiratory pressure.*

Model Variable	Beta coefficient (95% CI)	P-value
Day of ICU admission (days)	-0.150 (-0.225– -0.761)	<0.001
Tidal volume* (ml)	-0.003 (-0.006– 0.001)	0.115
PEEP$^{\$}$ (cmH_2O)	0.081 (-0.080– 0.242)	0.315
Neuromuscular use in first 3 days (=yes)	0.936 (-0.101– 1.972)	0.076

PSM strain over ICU admission.

*Dependent variable parasternal muscle strain. Random intercepts and random slopes. *Average over first 3 days of ICU admission. $^{\$}$Average over first 3 days of ICU admission. ICU - intensive care unit, PEEP - positive end expiratory pressure.*

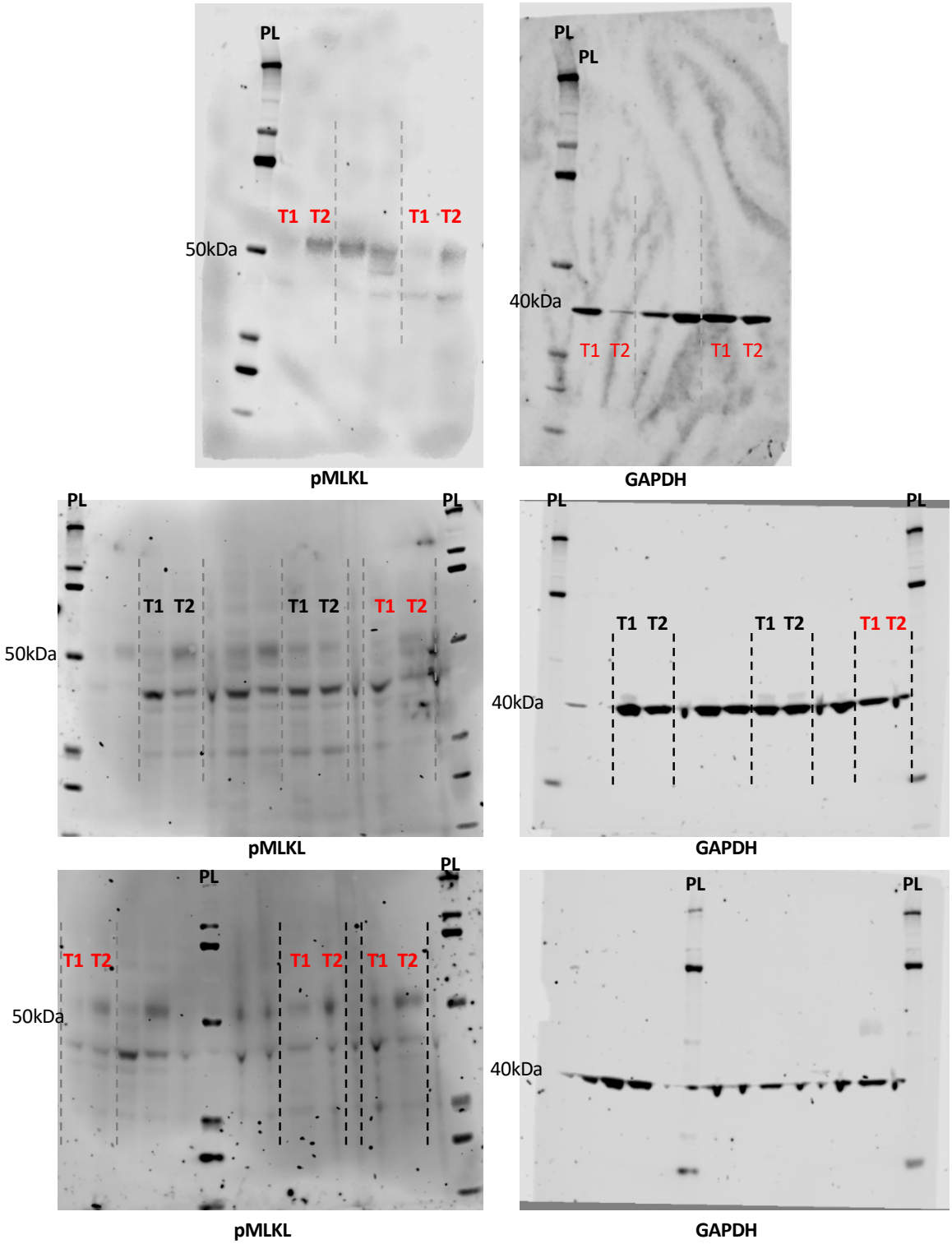
Appendix 9-20. Effect of vvECMO on parasternal, diaphragm, and rectus femoris muscle

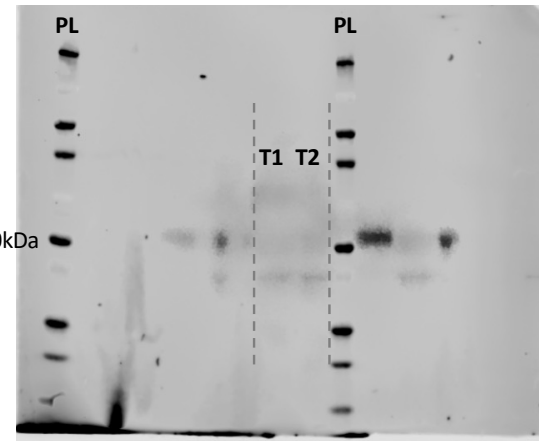
Model	PSM thickness (n=67)	P-value	PSM thickening fraction (n=40)	P-value	PSM Strain (n=41)	P-value	Diaphragm thickness (n=41)	P-value	Rectus femoris CSA (n= 66)	P-value
Day	-0.010 (-0.016–-0.006)	<0.001	0.926 (0.509 – 1.343)	<0.001	-0.171 (-0.305– -0.037)	0.013	-0.008 (-0.014–-0.002)	0.006	-0.030 (-0.036–-0.024)	<0.001
ECMO (=yes)	0.083 (-0.018–0.184)	0.107	-2.655 (-4.717–0.593)	0.013	1.602 (0.717–2.489)	<0.001	0.068 (-0.043–0.179)	0.226	0.224 (0.057–0.392)	0.009
ECMO * day of ICU admission	0.003 (-0.004–0.011)	0.478	-0.778 (-1.295–-0.264)	0.003	0.029 (-0.132 –0.191)	0.714	0.001 (-0.006–0.007)	0.883	0.010 (0.002–0.018)	0.013

Table S15. *Effect of vvECMO on changes in parasternal (PSM), diaphragm (DIA), and rectus femoris (RF) muscle.*

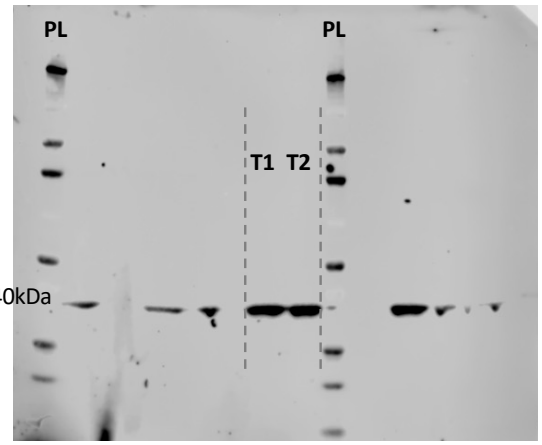
PSM thickness, diaphragm thickness, and rectus femoris use log transformation of measured value. All unadjusted models include random intercepts and slopes.

Appendix 9-21. Original Western blots from MUSCLE-UK skeletal muscle protein

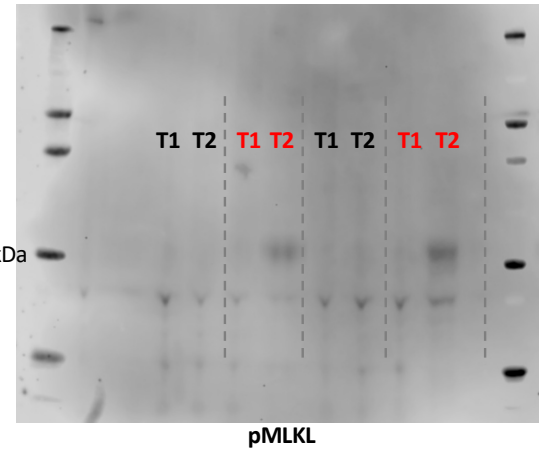




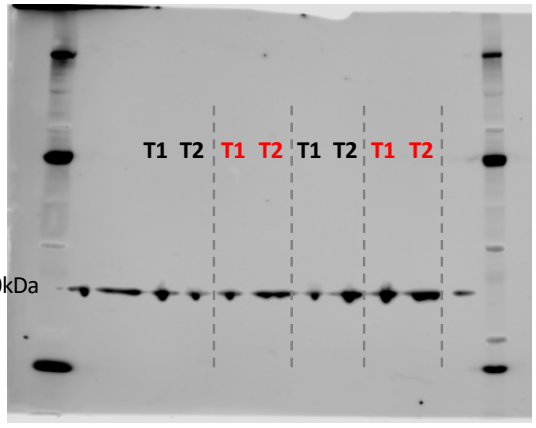
pMLKL



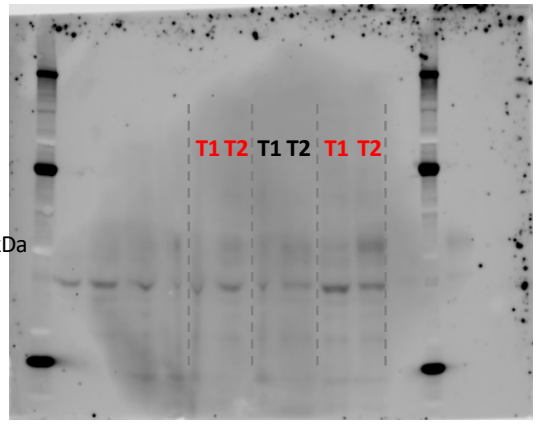
GAPDH



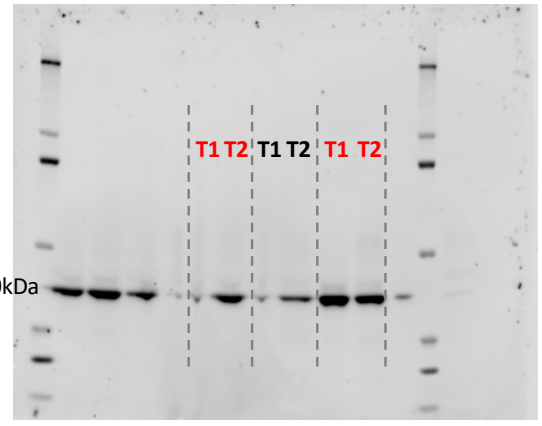
pMLKL



GAPDH



pMLKL

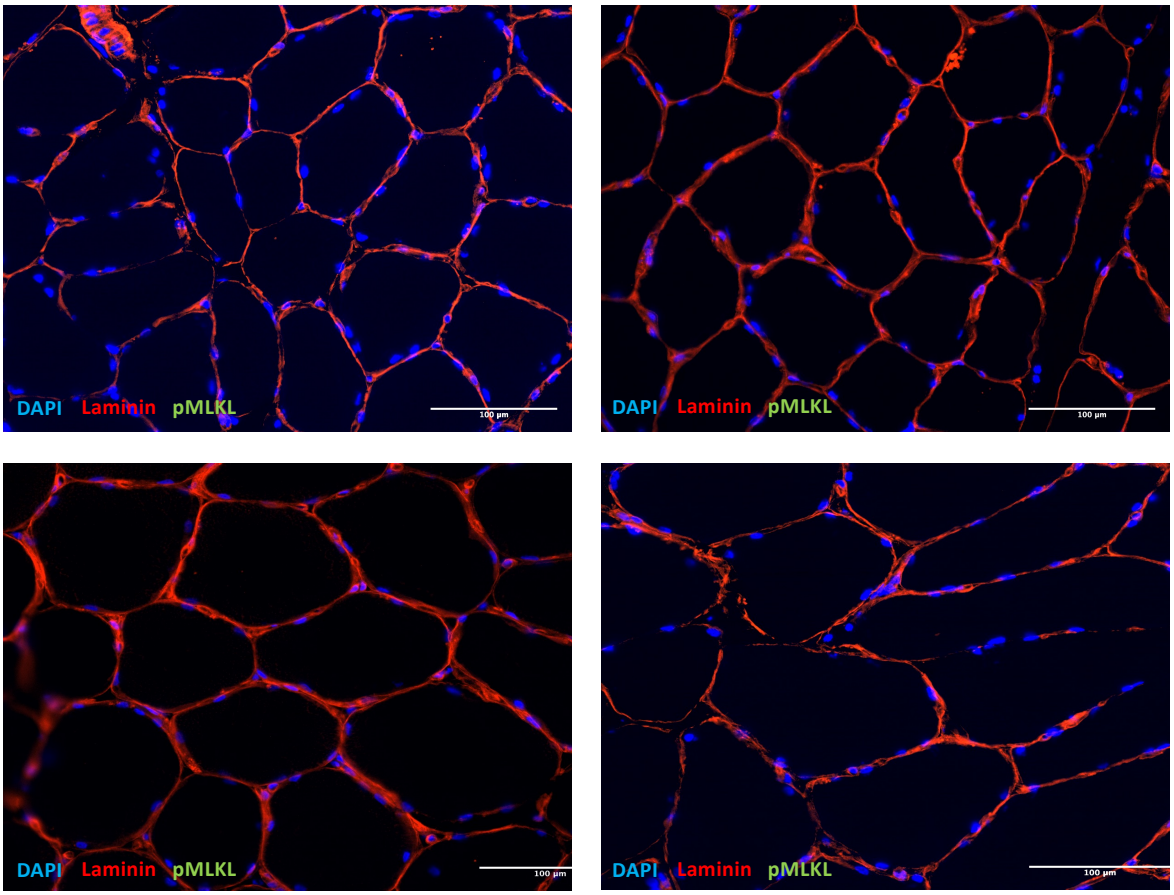


GAPDH

Appendix 9-22. Acquiring healthy human skeletal muscle biopsies

Samples utilising healthy volunteer skeletal muscle were kindly provided by Professor Steve Harridge (Centre for Human & Applied Physiological Sciences, Faculty of Life Sciences & Medicine, King's College London) as part of the research and ethics committee approved study 12/LO/0457 and subsequent experiments were conducted at Centre for Human & Applied Physiological Sciences, Faculty of Life Sciences & Medicine, King's College London.

Appendix 9-23. Immunohistochemistry of health human skeletal muscle



Immunohistochemistry of healthy volunteer skeletal muscle. Each panel represents a separate volunteer biopsy. There is preserved morphology amongst the samples and no evidence of cytoplasmic, cell membrane or interstitial pMLKL. All imaging captured at 20x magnification and error bars displayed are 100µm.

Appendix 9-24. Serum concentration of inflammatory cytokines and circulating markers of necrosis in necrotic and non-necrotic patients

Analyte	NEC (n=14)	NONEC (n=14)	P value
IL-1β			
Day 1	1.6 (1.3-2.3)*	1.3 (1.0-1.4)	0.053
Day 7	1.4 (1.0-1.5)	1.6 (1.3-3.7)	**0.042**
IL-6			
Day 1	169.9 (73.1-1122.2)*	95.4 (83.1-229.9)	0.740
Day 7	17.6 (9.6-78.2)	19.5 (14.4-116.8)	0.486
IL-8			
Day 1	254.2 (48.2-1012.5)*	61.6 (26.0-283.0)	0.130
Day 7	96.9 (37.4-214.3)	62.9 (33.2-585.2)	0.999
IL-10			
Day 1	3.7 (2.4-15.0)*	5.1 (2.9-10.3)	0.740
Day 7	2.7 (1.2-5.2)	2.9 (1.6-10.0)	0.422
TNF-α			
Day 1	1.7 (1.5-2.4)	1.3 (0.8-3.0)	0.173
Day 7	2.1 (1.2-3.6)	1.6 (0.8-1.9)	0.169
TNFR1			
Day 1	3.9 (3.7-16.7)	3.1 (2.4-4.3)	**0.026**
Day 7	4.6 (3.0-8.41)	2.9 (1.7-9.15)	0.134
VEGF			
Day 1	140.0 (111.5-200.3)	84.3 (25.8-111.3)	**0.007**
Day 7	233.6 (150.6-469.1)***	209.4 (130.5-305.9)**	0.508
RIPK3			
Day 1	2215.9 (798.1-7367.9)	4434.0 (2293.7-6658.4)	0.511
Day 7	5004.3 (2673.4-16881.9)	3546.0 (2037.3-13827.0)	0.401
CCK-18			
Day 1	535.3 (268.2-768.1)	576.1 (226.0-1566.5)	0.999
Day 7	537.7 (316.8-905.1)	858.3 (310.8-2096.8)	0.511

NEC and NONEC denote necrotic and non-necrotic patients respectively. Data presented as median (inter-quartile range). Interleukin-1-beta (IL-1β), interleukin-6 (IL-6), interleukin-8 (IL-8), interleukin-10 (IL-10), interferon-gamma (IFN-γ), tumour necrosis factor alpha (TNF-α), tumour necrosis factor receptor 1 (TNFR1), vascular endothelial growth factor (VEGF), receptor interacting protein kinase 3 (RIPK3), cleaved cytokeratin 18 (CCK18). * or *** denote significant differences between day 1 and day 7 of that group. *p<0.05, **p<0.01, ***p<0.001. All data kindly provided by the MUSCLE-UK study group.

Appendix 9-25. Intramuscular concentration of inflammatory cytokines in necrotic and non-necrotic patients

Analyte	NEC (n=14)	NONEC (n=14)	P value
IL-1β			
Day 1	28 (27.2-45.2)	28.4 (0.3-53.6)	0.700
Day 7	30.8 (26.4-44.0)	29.6 (27.2-36.0)	0.898
IL-6			
Day 1	9.2 (6.4-46.4)	27.6 (6.4-71.2)	0.503
Day 7	34.3 (10.2-138.8)	37.2 (10.4-44.0)	0.809
IL-8			
Day 1	21.6 (7.4-47.8)	20.4 (7.2-58.0)	0.808
Day 7	56.8 (9.0-232.6)	26.4 (15.6-72.4)	0.865
IL-10			
Day 1	0.4 (0.4-52.4)	15.2 (10.8-39.2)	0.175
Day 7	24.8 (11.0-46.6)	30.0 (18.8-85.6)	0.310
IFN-γ			
Day 1	6.8 (0.4-8.4)	8.0 (0.4-21.2)	0.280
Day 7	8.4 (3.0-8.8)	8.0 (0.4-12.4)	0.895
TNF-α			
Day 1	20.8 (0.6-23.4)	32.0 (16.7-68.3)	0.039
Day 7	0.6 (0.6-23)	10.7 (0.6-28.8)	0.707
TNFR1			
Day 1	0.3 (0.0-0.7)	0.4 (0.0-2.1)	0.463
Day 7	1.5 (0.1-3.3)	1.0 (0.0-4.2)	0.662
VEGF			
Day 1	123.2 (92.0-554.8)	504.8 (95.2-933.2)	0.283
Day 7	198.8 (87.0-612.8)	454.4 (184.4-882.8)	0.103

NEC and NONEC denote necrotic and non-necrotic patients respectively. Data presented as median (inter-quartile range). Interleukin-1-beta (IL-1β), interleukin-6 (IL-6), interleukin-8 (IL-8), interleukin-10 (IL-10), interferon-gamma (IFN-γ), tumour necrosis factor alpha (TNF-α), tumour necrosis factor receptor 1 (TNFR1), vascular endothelial growth factor (VEGF). * or *** denote significant differences between day 1 and day 7 of that group. *p<0.05, ***p<0.001. All data kindly provided by the MUSCLE-UK study group. Original intramuscular data adapted with permission for current study cohort.

Appendix 9-26. Parasternal muscle strain reliability study

Operator SO	Study ID	Study Day	Attempt 1	Attempt 2	Attempt 3	Average
	INF001	D7	-1.828	-2.007	-2.568	-2.134
	INF008	D1	-9.632	-6.033	-7.584	-7.750
	INF016	D7	-2.936	-2.886	-3.807	-3.210
	HV1		-7.332	-6.223	-6.521	-6.692
	DEV002	D0	-0.367	-0.573	-0.395	-0.445
	DEV005	D3	-0.314	-0.318	-0.342	-0.325
	DEV010	D7	-0.833	-0.834	-0.552	-0.740
	DEV012	D0	-0.240	-0.142	-0.251	-0.211
	DEV013	D21	-0.799	-2.332	-1.790	-1.640
	DEV016	D7	-0.947	-0.686	-0.820	-0.818
	DEV020	D0	-0.678	-0.720	-0.381	-0.593
	DEV023	D14	-3.809	-2.922	-3.010	-3.247
Operator EA	**Study ID**	**Study Day**	**Attempt 1**	**Attempt 2**	**Attempt 3**	**Average**
	INF001	D7	-2.237	-1.930	-2.340	-2.169
	INF008	D1	-6.329	-4.162	-5.230	-5.240
	INF016	D7	-2.831	-2.890	-2.101	-2.607
	HV1		-7.848	-6.175	-7.934	-7.319
	DEV002	D0	-0.431	-0.384	-0.327	-0.381
	DEV005	D3	-0.381	-0.263	-0.226	-0.290
	DEV010	D7	-0.487	-1.295	-0.987	-0.923
	DEV012	D0	-0.319	-0.313	-0.202	-0.278
	DEV013	D21	-0.643	-0.939	-1.098	-0.893
	DEV016	D7	-0.893	-1.011	-1.002	-0.969
	DEV020	D0	-0.615	-0.576	-0.433	-0.541
	DEV023	D14	-1.547	-1.922	-1.748	-1.739

Appendix 9-27. Clinical and ultrasound data from RWH study

Study ID	Study Day	PSM-thick (mm)	PSM-csa (cm^2)	RF-csa (cm^2)	Mode of MV
k01	1	3.3	1.2	4.3	Spontaneous
k01	3	3.1	1.3	2.7	Spontaneous
k01	5	3.4	1.6	3.0	Spontaneous
k01	7	4.0	1.4	2.5	Spontaneous
k02	1	3.9	1.6	3.8	Mandatory
k02	3	3.5	1.6	3.5	Mandatory
k02	5	3.4	1.5	2.8	Mandatory
k02	7	3.5	1.7	2.5	Mandatory
k02	10	2.9	1.6	2.6	Mandatory
k02	23	4.1	1.3	2.3	Mandatory
k02	33		1.0	2.6	Mandatory
k03	1	3.1	1.1	5.5	Mandatory
k03	3	3.2	1.6	5.2	Mandatory
k03	5	2.6	1.5	5.3	Mandatory
k03	7	2.5	1.1	4.4	Mandatory
k03	10	2.5	0.9	4.5	Mandatory
k03	15	2.6	0.7	3.9	Mandatory
k04	1	2.6	0.8	3.9	Spontaneous
k04	3	2.5	0.8	3.7	Spontaneous
k04	5	2.6	0.8	3.7	Spontaneous
k04	7	2.5	0.9	3.3	Spontaneous
k04	10	2.0	0.8	2.7	Spontaneous
k04	18	1.8	0.6	1.9	Spontaneous
k05	1	5.3	1.2	3.4	Spontaneous
k05	3	4.2	1.2	3.2	Spontaneous
k05	5	2.6	0.8	2.4	Spontaneous
k05	6	5.0	0.9	2.5	Spontaneous
k06	1	5.2	1.1	3.8	Spontaneous
k06	3	4.9	1.3	3.7	Spontaneous
k06	5	4.9	0.9	3.1	Spontaneous
k06	7	5.8	1.0	2.8	Spontaneous
k06	10	4.0	1.0	2.2	Spontaneous
k06	44	4.1	0.6	2.1	Spontaneous
k07	1	4.1	1.3	3.2	Mandatory
k07	3	2.8	1.0	3.4	Mandatory
k07	7	1.8	0.7	2.7	Mandatory
k07	10	2.0	1.1	2.5	Mandatory

k07	54	2.3	1.1	1.4	Mandatory
k08	1	3.3	0.7	3.3	Mandatory
k08	3	4.3	0.8	2.5	Mandatory
k08	5	4.0	0.8	2.9	Mandatory
k08	7	3.8	0.8	2.1	Mandatory
k08	10	4.3	0.9	2.3	Mandatory
k09	1	3.8	0.7	5.0	Spontaneous
k09	3	3.8	0.8	4.2	Spontaneous
k09	5	4.3	0.8	3.8	Spontaneous
k09	7	4.6	0.8	3.9	Spontaneous
k09	8	4.0	0.9	4.0	Spontaneous
k10	1	3.1	0.6	4.3	Spontaneous
k10	3	2.8	0.6	3.0	Spontaneous
k10	5	3.2	1.1	3.0	Spontaneous
k10	7	3.3	0.8	3.0	Spontaneous
k10	10	3.1	0.8	2.9	Spontaneous
k10	15	3.4	1.3	1.6	Spontaneous
k11	1	3.6	0.8	4.3	Spontaneous
k11	3	3.4	0.8	3.9	Spontaneous
k11	5	3.9	0.9	3.7	Spontaneous
k11	7	4.0	0.9	3.6	Spontaneous
k11	10	4.0	0.9	3.0	Spontaneous
k12	1	4.9	1.2	4.3	Spontaneous
k12	3	4.9	1.2	4.3	Spontaneous
k12	5	4.8	1.3	4.1	Spontaneous
k12	7	4.8	1.2	4.0	Spontaneous
k16	1	4.0	1.1	5.1	Spontaneous
k16	3	3.5	1.2	5.5	Spontaneous
k16	7	2.9	1.1	4.7	Spontaneous
k16	10	3.5	0.8	4.7	Spontaneous
k16	12	3.3	1.0	3.5	Spontaneous
k17	1	3.4	1.0	2.9	Mandatory
k17	3	3.1	1.0	2.8	Mandatory
k17	5	3.7	1.0	3.2	Mandatory
k17	7	2.4	0.6	2.5	Mandatory
k17	10	2.2	1.0	2.7	Mandatory
k17	46	3.5	1.1	2.0	Mandatory
k19	1	4.3	1.0	8.0	Mandatory
k19	3	4.3	1.1	7.7	Mandatory
k19	5	4.0	0.8	8.4	Mandatory
k19	7	3.7	1.0	7.3	Mandatory
k19	10	3.6	1.2	7.6	Mandatory

k19	33	4.2	1.1	6.7	Mandatory
k20	1	4.9	1.4	3.3	Spontaneous
k20	3	4.7	1.6	2.6	Spontaneous
k20	5	2.9	0.9	3.0	Spontaneous
k21	1	5.1	1.5	7.7	Mandatory
k21	3	4.7	1.6	6.7	Mandatory
k21	5	3.8	1.6	6.1	Mandatory
k21	10	3.5	1.7	3.9	Mandatory
k22	1	5.1	1.4	4.4	Mandatory
k22	3	5.2	1.3	4.2	Mandatory
k23	1	4.7	0.9	7.2	Spontaneous
k23	3	5.7	0.9	6.4	Spontaneous
k23	5	5.6	1.2	6.4	Spontaneous
k23	10	5.1	0.8	4.4	Spontaneous
k24	1	5.7	1.5	5.6	Mandatory
k24	3	5.6	1.2	4.8	Mandatory
k24	7	5.3	0.9	4.8	Mandatory
k24	17	5.0	0.9	4.6	Mandatory
k25	1	4.2	0.7	4.6	Spontaneous
k25	5	3.5	0.9	4.2	Spontaneous
k25	7	4.0	0.9	3.7	Spontaneous
k25	29	5.5	1.3	1.7	Spontaneous
k26	1	4.6	1.2	3.9	Mandatory
k26	3	4.3	0.8	3.7	Mandatory
k26	7	4.0	1.0	3.4	Mandatory
k28	1	4.9	1.4	2.8	Mandatory
k28	3	4.8	1.3	2.3	Mandatory
k29	1	5.6	0.9	4.0	Spontaneous
k29	3	5.6	0.9	4.0	Spontaneous
k29	7	5.8	1.3	3.4	Spontaneous
k29	10	5.4	0.8	3.5	Spontaneous
k31	1	3.2	0.7	2.6	Spontaneous
k31	3	3.3	0.8	3.1	Spontaneous
k31	5	3.2	0.7	2.8	Spontaneous
k31	7	3.2	0.7	2.7	Spontaneous
k31	10	3.4	0.7	2.0	Spontaneous
k31	15	3.2	0.6	2.0	Spontaneous
k32	1	3.7	0.7	7.4	Mandatory
k32	3	3.0	0.6	7.2	Mandatory
k32	5	3.0	0.7	5.8	Mandatory
k32	7	3.3	0.7	5.6	Mandatory